A Proteomics Investigation of Anchored PKA-RI Signaling

Duangnapa Kovanich

2013

A Proteomics Investigation of Anchored PKA-RI Signaling

Duangnapa Kovanich

Dissertation, Utrecht university, The Netherlands

ISBN: 978-90-393-5951-8

E-mail: kovanich@hotmail.com

Cover and layout designed by : www.DayDreamingTeam.com / Saksin Punyaratabandhu

Printed by: B.V.S Service

A Proteomics Investigation of Anchored PKA-RI Signaling

Een Proteomics Onderzoek naar Geankerde PKA-RI Signaal Transductie
(met een samenvatting in het Nederlands)

Proefschrift

ter verkrijging van de graad van doctor aan de Universiteit Utrecht op gezag van de rector magnificus, prof. dr. G.J. van der Zwaan, ingevolge het besluit van het college voor promoties in het openbaar te verdedigen op maandag 13 mei 2013 des middags te 12.45 uur

door

Duangnapa Kovanich
geboren op 26 juni 1982, te Chonburi, Thailand

Promotor: Prof. dr. A.J.R. Heck
Co-promotoren: Dr. A. Scholten
Dr. M.A.G. van der Heyden

Table of Contents

Chapter 1 An introduction to cAMP signaling 7

I cAMP signaling events at cellular level 8
II BCL-2 family proteins and apoptosis 22
III Scope and outline of this thesis 28

Chapter 2 Applications of Stable Isotope Dimethyl Labeling in Quantitative Proteomics 41

Chapter 3 Probing the Specificity of Protein-Protein Interactions by Quantitative Chemical Proteomics 69

Chapter 4 Sphingosine kinase interacting protein is an A-kinase anchoring protein specific for type I cAMP-dependent protein kinase 85

Chapter 5 A BH3 domain in the A-kinase anchoring protein SPHKAP provides a link between cAMP signaling and mitochondrial-mediated apoptosis 103

Chapter 6 136

Summary 138
Outlook 140
References 144
Samenvatting 146

Acknowledgements 149

Curriculum Vitae 152

Chapter 1
An introduction to cAMP signaling

Duangnapa Kovanich
Arjen Scholten
Albert J.R. Heck

Biomolecular Mass Spectrometry and Proteomics,
Utrecht Institute for Pharmaceutical Sciences and Bijvoet Center for Biomolecular Research ,
Utrecht University, Padualaan 8, 3584 CH, Utrecht, The Netherlands

I cAMP Signaling Events at Cellular Level
II BCL-2 Family Proteins and Apoptosis
III Scope and Outline of this Thesis

I cAMP Signaling Events at Cellular Level

I.1 cAMP signaling pathway

cAMP was identified more than 50 years ago as an intracellular secondary messenger produced in response to hormone action (1). cAMP signaling is initiated when G protein-coupled receptors (GPCRs), a large family of integral plasma membrane proteins, are activated by a plethora of different hormones and neurotransmitters. The ligand-bound GPCR undergoes conformational changes, which allow it to act as a guanine nucleotide exchange factor (GEF). Its GEF activity can then catalyze the exchange of GDP for GTP on the α-subunit of the associated heterotrimeric G protein, resulting in the activation of the α-subunit and together with the bound GEF, its dissociation from the βγ dimer. The dissociated α -subunit is then activated by adenylyl cyclases (ACs), a family of enzymes that synthesize cAMP from ATP, resulting in an intracellular increase in the levels of cAMP. The intracellular concentration of cAMP is controlled by the counterbalancing activities of two enzymes: ACs and cAMP-phosphodiesterases (PDEs). While ACs produce cAMP, the degradation is regulated by PDEs. In mammalian systems both are present in a large number of variants including 9 AC isoforms and a large superfamily of more than 40 different PDE isozymes (Figure 1).

cAMP was initially identified as a diffusible molecule with a radius of action of around 220 μm (2). However, live-cell imaging and fluorescence resonance energy transfer (FRET) have visualized several distinct micro-domains with a high concentration of cAMP with a range of action as small as ~1 μm (3, 4), indicating that cAMP accumulates at specific locations in the cell rather than diffusing freely throughout the cell. cAMP mediates its effects through several protein targets including PDEs, cAMP-regulated guanine nucleotide-exchange proteins (EPACs), cyclic-nucleotide-gated channels and its principal target, the cAMP-dependent protein kinase, also called protein kinase A (PKA) (Figure 1).

I.2 cAMP-dependent protein kinase (PKA)

The PKA holo-enzyme is a heterotetramer consisting of two identical regulatory (R) sub-units and two identical catalytic (C) sub-units. The kinase is held in an inactive state when the catalytic (C) sub-units are associated with the R dimer. In mammals there are three C isoforms (Cα, β, γ), which have practically identical kinetic and physiological properties. In contrast, four different genes encode in mammals for four R subunits, RIα, RIβ, RIIα and RIIβ, which each exhibit different cAMP binding affinities, cellular localization, and tissue distribution. All different R's can form holoenzymes with all different C-subunits.

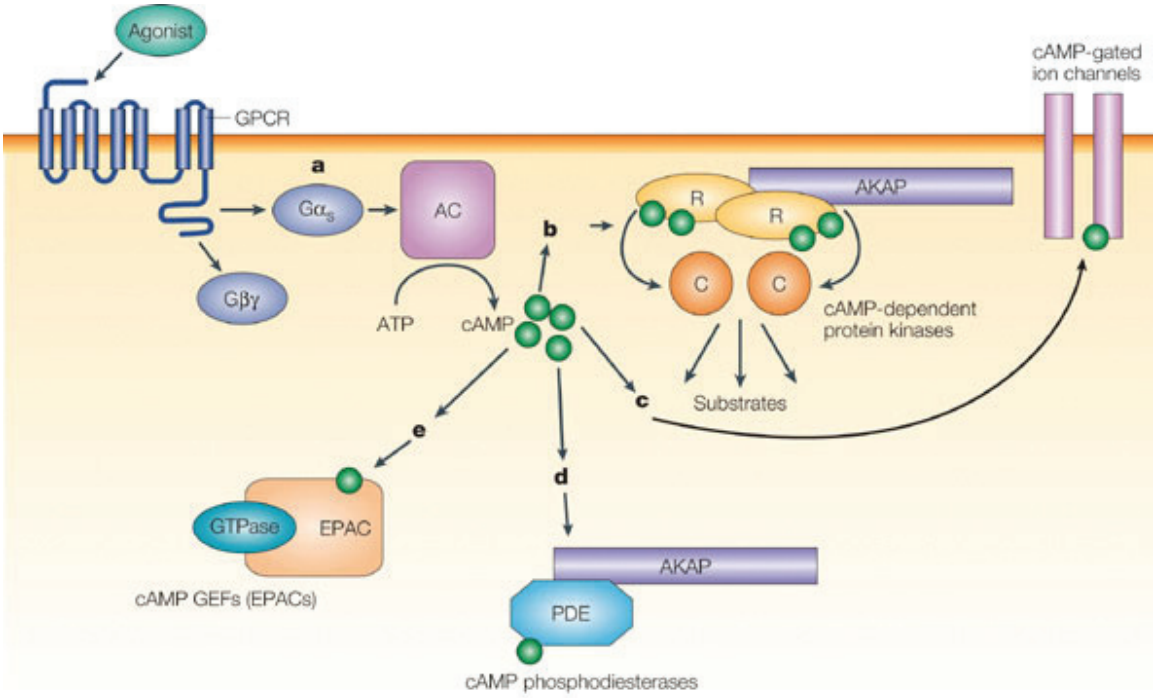

Figure 1 > General cAMP signaling pathway

Stimulation of a G-protein-coupled receptor (GPCR) by its extracellular ligand results in a conformational change in the receptor that is transmitted to an attached heterotrimeric G protein complex. a) The alpha subunit (Gα) is then released from the G protein complex and activates the enzyme adenylyl cyclase (AC), which catalyses the production of cAMP from ATP. b) The principle target of cAMP is protein kinase A (PKA). cAMP binds to the regulatory (R) subunits of PKA, resulting in the release of active catalytic (C) subunits, which can then phosphorylate nearby substrates. Besides PKA, cAMP can mediate its effects through several other protein targets including c) cyclic-nucleotide-gated channels , d) phosphodiesterases (PDEs) and e) guanine nucleotide-exchange factors (GEFs), also known as exchange proteins activated by cAMP (EPACs) (Adapted from ref (5)).

PKA RI based holo-enzymes are more sensitive to cAMP with an activation constant (Ka) of 50-100 nM cAMP and are considered predominantly cytosolic. PKA RII mainly associates with cellular structures and organelles and presents a Ka of 200-400 nM by cAMP (6). Structurally, PKA- R is composed of a dimerization/docking (D/D) domain at the N-terminus followed by a linker containing an auto-inhibitory site for C and two tandem cAMP-binding domains (A and B) (7). PKA RI and RII display high sequence homology in the D/D domain and cAMP-binding domains (8), whereas the linker regions are highly variable in length and sequence (9).

When the level of cAMP is elevated, 2 molecules of cAMP bind to each regulatory subunit, resulting in the release of active C subunits. The C subunits are broad-spectrum serine/threonine kinases that could potentially phosphorylate numerous proteins, predominantly within the substrate sequence context of [R/K][R/K]-X-[S/T], [R/K]-X-X-[S/T], in which the canonical R [R/K]-X-[S/T] is the most abundant consensus sequence (as reviewed in(10)). It is now known that the differences in cAMP affinity and localization between the two PKA isoforms contribute to the specificity of cAMP signaling. Therein, subcellular localization of PKA is of the utmost importance and is obtained by anchoring of PKA-R to the large family of A-kinase anchoring proteins (AKAPs).

I.3 A-kinase-anchoring proteins (AKAPs)

Since PKA is involved in a multitude of signaling events and physiological responses, spatial and temporal specificity is very important. PKA achieves this through intracellular targeting and compartmentalization. This is mediated through association of the kinase with AKAPs. AKAPs are a group of structurally-diverse but functionally-related proteins. Up to date, more than 50 AKAPs, including splice variants, have been classified by their ability to interact directly with one of the PKA-R subunits (as reviewed in (11)). However, the functional importance further involves targeting PKA to specific subcellular compartments where they form multivalent signal transduction complexes with other signaling proteins including phosphatases, other kinases, PDEs and local PKA substrates. Through this major role in the spatial and temporal integration of effectors and substrates, AKAPs provide a high level of specificity to many parallel cAMP signaling pathways. Table 1 presents an overview of confirmed AKAPs to date, annotated by their official name (Gene name). Synonyms are provided to prevent confusion from earlier annotations of different splice variants of the same gene.

Table 1 > Overview of characterized mammalian AKAPs; nomenclature, subcellular localization, and identified binding partners

Official name	Common name	Alternate names and Spliced variants	Cell localization	Proteins in complex	Ref.
AKAP 1	D-AKAP1	sAKAP84, AKAP121, AKAP149	Mitochondrial outer membrane, ER	P90 (RSK1), PP2A, PP1, PTPD1, Src, AMY-1, AAT-1, Siah2	(12-18)
AKAP2	AKAP-KL	PALM2-AKAP2	Plasma membrane	AQP0	(19, 20)
AKAP3	AKAP110	FSP95, CT82, SOB1	Sperm fibrous sheath	Ropporin, ASP, PDE4A, CABYR	(21-23)
AKAP4	AKAP4	AKAP82, p82, FSC1, CT99	Sperm fibrous sheath	AKAP3, FSIP1, FSIP2	(24)
AKAP5	AKAP79 (human)	AKAP150 (rat/mouse), AKAP75 (bovine)	Plasma membrane	PKC, PP2B (Calcineurin), PP1, CaM (calmodulin), Calden-drin, neuronal LTCC (CaV1.2), KCNQ2, GluR1, SAP97,ADRB1, ADRB2, GABA(A)	(25-34)
AKAP6	mAKAP	AKAP100, mAKAPα, mAKAPβ	Sarcoplasmic reticulum, nuclear membrane	Nesprin-1α, RyR2, PDE4D3, PP2A, PP2B,ERK5, MEK5, Epac1, AC5, PLCε, RSK3, HIF-1, PHD2, PHD3, pVHL, Siah2, MEFs, PDK1	(35-41)
AKAP7	AKAP18	AKAP18α (AKAP15), AKAP18β, AKAP18γ, AKAP18δ	Cytoplasm (γ), plasma mem-brane (α, β, δ), nucleus (γ)	cardiac LTCC (CaV1.2), Na^+ channel (Nav1.2), SERCA2, PLN (δ)	(42-45)
AKAP8	AKAP95		Nucleus	Eg7, p68, AMY-1, MCM2, D-type cyclins, Caspase 3, Fidgetin	(46-53)

Official name	Common name	Alternate names and Spliced variants	Cell localization	Proteins in complex	Ref.
AKAP9	Yotiao	AKAP350, AKAP450, CG-NAP	Cytoskeleton, centrosome, Golgi	KCNQ1, PDE4D3, AC9, Epac1, NMDA receptor, InsP(3) receptor 1, PKN, PP1, PP2A, PKCδ, PKCε, CK1δ, CK1ε, CaM, Pericentrin, γ-tubulin, GCP2, Cyclin E, CDK2, LFA-1, Dynactin, Dynein, G alpha-13, Ran, TACC3, TACC4, CLIC, CCAR1, Caprin-1, TRAX	(54-71)
AKAP10	D-AKAP2		Cytoplasmic, Mitochondria	Rab4, Rab11	(72)
AKAP11	AKAP220		Cytoplasm, Centrosome, Cytoskeleton, Peroxisome	GABAC-receptor	(73-75)
AKAP12	Gravin	AKAP250, SSeCKS, GAG12, AKAP12α, AKAP12β, AKAP12γ	Plasma and vesicle membrane, cytoskeleton	PKC, Src, PDE4D, CaM, Cyclins, β4galT1, β-adrenegic receptor, Actin, PFN1, PKM2, POF1B, PPIA, SC-9c5.12, SPRR2E, TF, VCP	As reviewed in (76)
AKAP13	AKAP-Lbc	Ht31, BRX	Cytoplasm	PKC (α, η), PKD, G alpha- 12, Rho, 14-3-3 proteins (β, ε, ζ), LC3, KSR-1, RAF, MEK-1, PKNα, MLTK, MKK3, p38α, Hsp20, Shp2, IKKβ	(77-85)
AKAP14	AKAP28	T-AKAP80	Sperm fibrous sheath		(86)
AKAP17A	SFRS17A	XE7	Nucleus (splicing factor compartment)	ZNF265, ASF/SF2	(87, 88)

Official name	Common name	Alternate names and Spliced variants	Cell localization	Proteins in complex	Ref.
EZR	Ezrin	AKAP78, Villin 2	Plasma membrane, cytoplasm, cytoskeleton	Radixin, Moesin, Merlin, Epac1, Sky, Hamarin, E3KAPP, A2b receptor, β-actin, ACAP4, Rho GDI, CD43, CD44, CD95, E-cadherin, β-catenin, CFTR, CLIC5, EBP50, SAP97, ICAM-1, ICAM-2, V-CAM1, FAK, S100P, Syndecan-2, L-selectin, PSGL-1, NGX6, WWOX	As reviewed in (89), (90-109)
WASF1	WAVE-1	SCAR	cytoplasm, cytoskeleton, mitochondria	Arp2, Arp3, Abl, WRP, Abi1, Cdk5, Nap1, PIR121, Nap125, HSPC300, Giα, Tuba, p47phox, BAD, PP1, Glucokinase,	(110-120)
ACBD3	PAP7	GOLPH1, GOCAP1, GCP60	Golgi	PBR, Golgin-160, Gigantin, PI4KB , DMT1	(121-125)
NF2	Merlin	Neurofibromin 2, Schwannomin	Cytoskeleton	Ezrin, Pak1, βII-spectrin, NHE-RF, SCHIP-1	(91, 126-130)
PCNT	Pericentrin	Pericentrin-B, Kendrin	Cytoskeleton, centrosome	AKAP9, γ-tubulin, GCP2, PCM-1, Cep55, DISC1, CHD3, CHD4, LIC1-containing dynein	(62, 131-136)
MAP2	MAP2	MAP2A, MAP2B, MAP2C, MAP2D, AKAP80	Cytoskeleton	B-actin, ApoE3, Fyn, c-Src, Grb2, myosin VII, plectin, β-Dystroglycan	(137-144)
RAB32	RAB32		Mitochondria, ER	Rab38, BLOC-2, AP-3, AP-1, Varp	(145-148)
ARFGEF2	BIG2		Golgi, endosome	PP1γ, PDE3A, TNRF1, Exo70, GABA(A) receptor, AMY-1, FLNA	(149-156)

Official name	Common name	Alternate names and Spliced variants	Cell localization	Proteins in complex	Ref.
CMYA5	Myospryn	SPRYD2, TRIM76, sr553, Genethonin-3	Perinuclear, lysosome, sarcoplasmic reticulum	Dysbindin-1, α-actinin, Desmin, Dystrophin, Titin, CAPN3	As reviewed in (157), (158, 159)
SYNM	Synemin	A-synemin, β-synemin, Desmuslin	Cytoskeleton	α-dystrobrevin Desmin, Dystrophin, Utrophin, Vinculin, Zyxin, PP2A	(160-164)
PDE4DIP	Myomegalin	CMYA2	Cytoplasm, Golgi, centrosome	PDE4D, cMyBPC, cTNI, ENO1, ENO3, CARP, COMMD4,	(165, 166)
MYO7A	Myosin VIIA	USH1B, DFNB2, DFNA11, NSRD2	Cytoskeleton	CaM, MAP-2B, Harmonin, Vezatin, Cadherin, Catenins, Keap1, Slac2-c, MyRIP,	(142, 167-172)
CBFA2T3	MTG16b	MTGR2, ZMYND4,	Golgi	Plexin A1, Plexin A3	(173)
GSKIP	GSKIP	HSPC210	Cytoplasm	GSK3β	(174)
OPA1	OPA1	MGM1	Lipid droplets, Mitochondria	Perilipin	(175)
SPHKAP	SPHKAP	SKIP	Cytoplasm, Mitochondria	CHCHD3	(176-178)
smAKAP	smAKAP	MGC13057	Plasma membrane		(179)

As mentioned earlier, from all knowledge gathered so far, PKA type II is mainly confined to subcellular structures and compartments by anchoring to AKAPs, which explains the fact that the majority of AKAPs identified to date bind PKA RII (as reviewed in (11)). Several AKAPs such as D-AKAP1 (180) and D-AKAP2 (181) were identified as dual-specific AKAPs as they also strongly bind PKA type I. The first evidence of RI binding to an AKAP was shown by Miki and Eddy who identified RIα-specific and dual-specificity anchoring domains on FSC1/AKAP82 (182). However, it is worth noting that, at the start of my thesis work, AKAP-CE was the only AKAP identified to bind specifically to the RI-like regulatory subunit of C. elegans PKA (183).

Early on, deletion mapping studies on MAP2, the first protein shown to co-purify with PKA RII, identified a region that mediates association with PKA RII (137, 184). Subsequent in silico secondary-structural analysis on MAP2 and another 3 RII-anchoring sequences identified common regions of approximately just 14 residues, which display a high probability to form an amphipathic helix with opposing hydrophilic, charged residues aligned along one face and hydrophobic residues along the other face (185). To probe the role of the amphipathic helix proline substitution, which disrupts the helicity of the region, was used and shown to disrupt binding to PKA (185).

Since then, binding of the AKAP amphiphatic helix to R subunits has been characterized by biochemical and structural approaches. Peptide arrays have been used extensively to design R-isoform-specific AKAP helices to disrupt the PKA:AKAP interaction (186-189). The data gained from such peptide arrays can also be used to understand the specificity requirements for binding to RI and RII. D-AKAP2 has been used as a starting point for such studies as it binds with high affinity to both RII and RI (KD = 2 and 48 nM, respectively) (190). A 27-amino-acid peptide encompassing the A-kinase binding (AKB) domain was evaluated by N- and C-terminal truncation arrays to identify the minimal sequence required for binding each R isoform (187). The data indicated that the hydrophobic contact surface between the docking surface of RIα and the AKAP was larger than that for RIIα interaction. Only 12 residues were required for binding to RIIα, while at least 14 residues, which extended the length of the helix, were required for binding to RIα (Figure 2A). Peptide substitution arrays also indicated that RIIα/AKAP interactions are sensitive for bulky amino acids (Trp, Phe, Tyr). Several substitutions of hydrophobic aliphatic-chain residues with aromatic-chain residues effected in a considerable reduction in affinity to RIIα, but dramatically enhanced binding to RIα (187). Peptide arrays were also used as a tool to develop the RIα-specific disrupting peptide, RIAD (188) and the RII preferring superAKAP-IS (186) . In the absence of RI specific AKAPs, for RIAD, 5 anchoring domains from known dual-specific AKAPs were used as a template and by introduction of acidic amino acids into the positions that make up the hydrophilic face of the helix, the affinity to RIIα was diminished and RIAD exhibited a 50-fold selectivity for RIα over RIIα (188). It is worth mentioning that RIAD also contains a bulky residue, tyrosine which is selective for RIα in the peptide (Figure 2B and C). Peptide array data by Alto et al. and Gold et al. which led to the development of a highly selective RIIα-specific peptide also indicated that AKAP-RII interactions were not compatible with bulky residues in the positions that make up a hydrophobic face of the helix (186, 189).

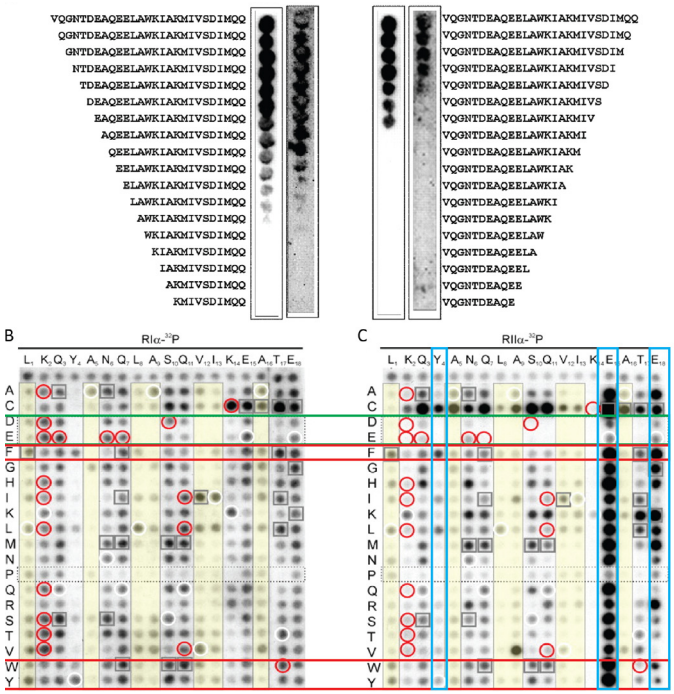

Figure 2 > Peptide arrays as a tool to understand the specificity requirements for binding to RI and RII.

A) *N-terminal (left) and C-terminal (right) truncations of the 27-residue AKB domain of D-AKAP2 to determine the size of hydrophobic contact surface between RIα-D-AKAP2 and RIIα-D-AKAP2. Only 12 residues were required for binding to RIIα, while at least 14 residues which extended the length of the helix were required for binding to RIα.* **B and C)** *Two-dimensional peptide substitution array of the template AKB peptide derived from known dual specificity AKAPs. All 18 amino acids (left side of the blot) were substituted into each position along the AKB peptide (top of the blot). Red boxes highlight those substitutions of hydrophobic aliphatic-chain residues with aromatic-chain residues (F, W, Y). The introduction of aromatic-chain residues has an effect on binding to RIIα. A green box indicates the introduction of acidic amino acids (D, E), which has a drastic effect on binding to RIIα. Blue boxes indicate the substitutions of aromatic-chain residue (Y) and acidic amino acid (E) in the starting AKB peptide with other residues. By removing the Y and E from the starting AKB peptide, its binding to RIIα is dramatically improved. (Adapted from Ref (187, 188))*

In addition to data gathered by using peptide arrays, structural approaches have shed light on the binding of AKAPs to RI and RII. The initial reports established a structural basis for the AKAP binding to the D/D domain. NMR analysis and X-ray crystallography were performed to determine structures of RIIα D/D and RIα D/D (189, 191-197). The data have demonstrated that RII subunits dimerize their N-terminus through their D/D domain, which is necessary for AKAP docking. The RIIα D/D domain consists of an antiparallel dimer of two polypeptide chains in a helix-turn-helix motif, forming an X-type four-helix bundle that serves as a docking surface for the AKAP helix. The N-terminus of RIIα can be divided into two regions: residues 1-23, which form the AKAP-binding surface and residues 24-44, which cover the majority of the dimer contacts. RIα subunits dimerize in a similar manner, however, the monomer has an additional N-terminal helical extension that is cross-linked to the other monomer by disulfide bonds, making the RIα dimer a more compact module. The AKAP binding site of RIα D/D is shifted further from the N-terminus and covers residues 12-61. Another difference is the AKAP-docking surface topology. The surface of the RIIα D/D presents a shallow hydrophobic groove for the AKAP helix to lie across. However, the shallow groove of RIIα becomes a deep cleft in RIα D/D, providing it a unique ability to accommodate the earlier mentioned bulky aromatic residues. The surface charges are also different for RI and RII. The RII D/D surface consists solely of hydrophobic residues, whereas the RI D/D contains several charged residues, which reduce the hydrophobic nature of the surface (193) (Figure 3).

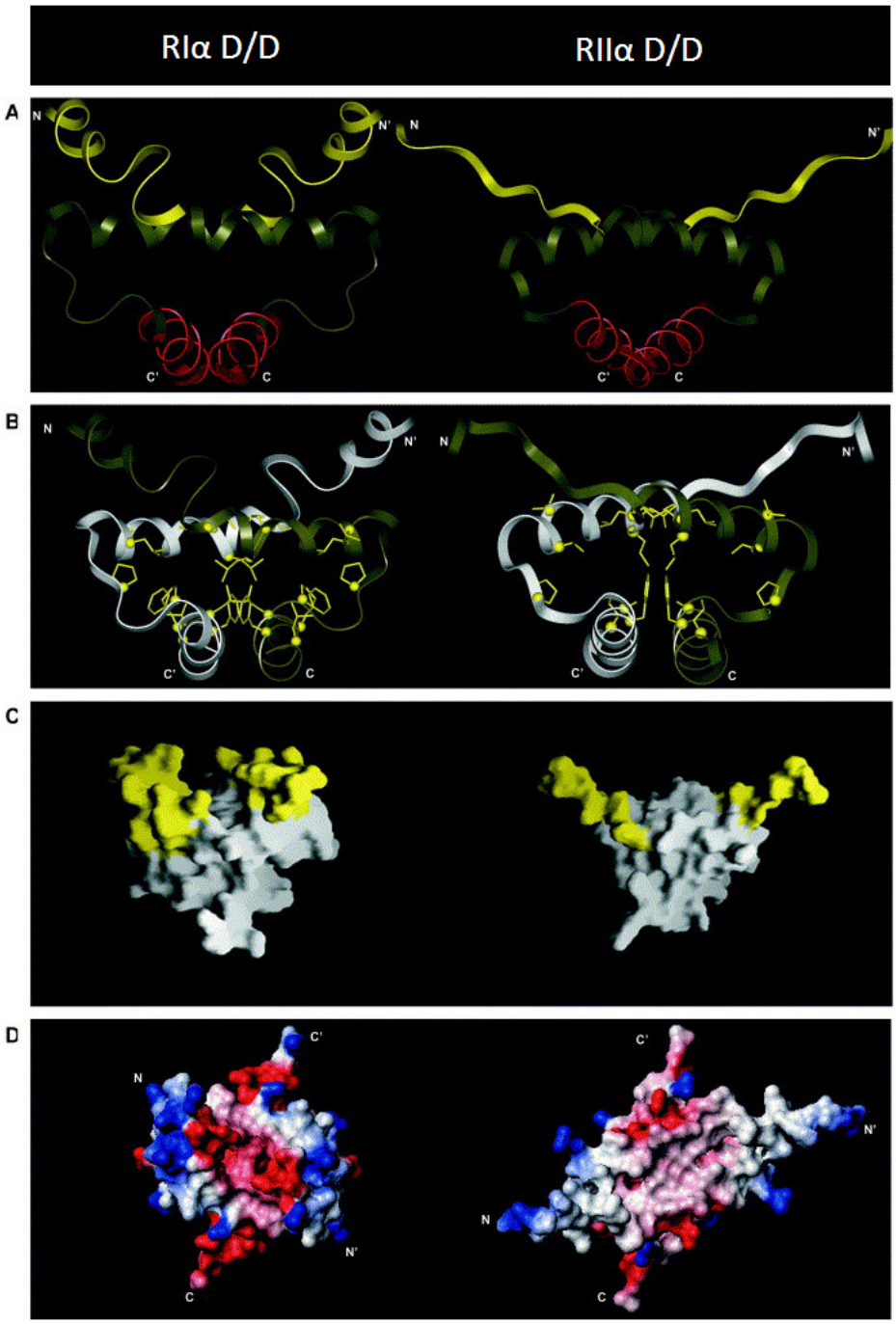

Figure 3 > Comparison of AKAP binding to the RIα and RIIα D/D domains.

A) *Ribbon representation of bovine RIα (residues 12–61) (left) and rat RIIα (residues 1–44) (right). The D/D domains consist of an antiparallel dimer of two polypeptide chains in a helix-turn-helix motif, forming an X-type four-helix bundle (as labeled in grey and red) that serves as a docking surface for an AKAP. The isoform specific N-terminal region is shown in yellow.* **B)** *Key residues mediating interactions for dimer contacts in RIα and RIIα are shown.* **C)** *Surface representation of the AKAP binding surface in RIα and RIIα. The surface of the RIIα D/D presents a shallow hydrophobic groove while the surface of RIα D/D presents a deep cleft.* **D)** *Electrostatic surface potential representation of RIα and RIIα. Acidic residues are red; basic residues are blue. Their surface charges are different. The RI D/D contains several charged residues which reduce the hydrophobic nature of the surface (Adapted from ref (193)).*

Later on, crystal structures of RIIα D/D with the D-AKAP2 anchoring domain and with a RII-selective peptide, superAKAP-IS were determined to further understand the molecular basis of AKAP anchoring (189, 194). The amphipathic helices bind diagonally across the D/D domain and induce a pronounced asymmetry in the monomers. Interestingly, the N-terminus of one monomer is ordered and makes critical interactions with the helix through two essential isoleucines, Ile3 and Ile 5, while the N-terminus of another monomer is disordered (189, 194). Recently, the crystal structure of RIα with the same D-AKAP2 anchoring domain has been solved (198). Overall, the core D/D domains align well with each other including the angle of binding to the AKAP. However, in the complex, RIα D/D is oxidized (disulfide bridge) and the N-terminal helices of both monomers are ordered by virtue of the inter-monomer disulfide bonds. Another significant difference between the two isoforms is the size of interaction surface. There are 4 main pockets, I-IV, at the docking surface of RIα D/D, whereas the surface of RIIα D/D presents only 2 pockets, I and II, which are structurally equivalent to the RIα pockets I and II. The 4 helix turns of the D-AKAP2 amphipathic peptide have interaction with 4 corresponding pockets of RIα D/D while only 2 helix turns are required to fill the two pockets of RIIα D/D. It is also worth noting that the D-AKAP2 helix bound to the RIIα structure is shifted toward the N-terminus by a complete helical turn. While the pocket I of RIα D/D is filled by D-AKAP2 residues 634 and 635, the equivalent pocket of RIIα D/D is occupied by residues 637 and 638 from the next helical turn. The same goes also for pocket II (Figure 4) (194, 198).

When comparing the two structures, it becomes clear that the residues of the D/D domain lining the pockets define which amino acids can or cannot fit in the pockets. In other words, the sequence of the AKAP anchoring domain determines its PKA-R isoform specificity. For example, in the pocket I of RIα D/D, any hydrophobic residue can fit at position 634 while an alanine residue at position 635 is the only unique fit as it is tightly packed in space and any other residue will be sterically occluded and disrupt binding. However for RIIα, pocket I can only weakly tolerate a bulky hydrophobic residue (198).

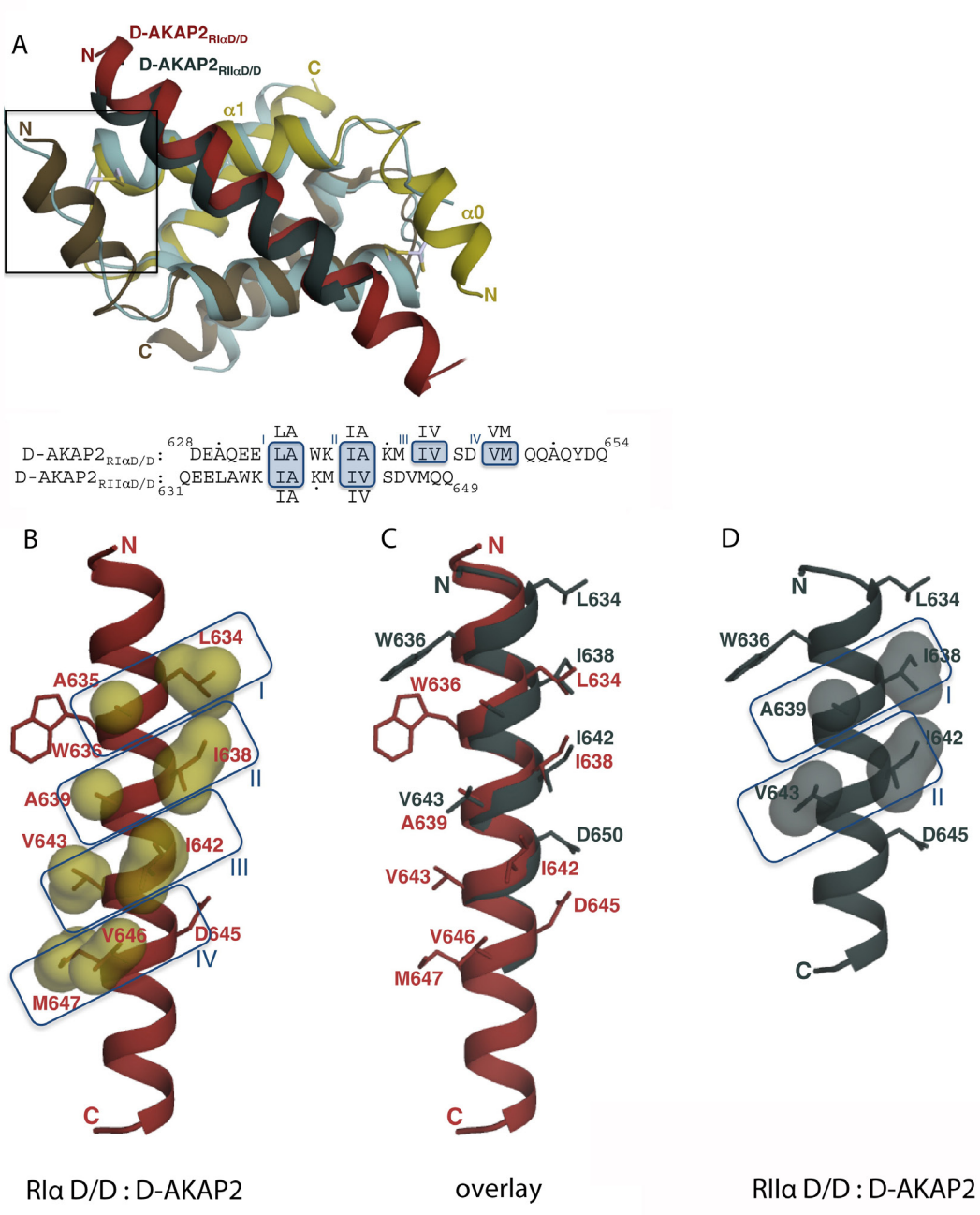

Figure 4 > Comparison of RIα D/D-D-AKAP2 and RIIα D/D-D-AKAP2 structures.

A) *Structural overlay of the D-AKAP2 AKB-helix bound to RIα D/D (in red) and to RIIα D/D (in teal). Overall, the core D/D domains of the two isoforms align well including the angle of binding to the AKAP. The D-AKAP2 helix bound to RIα D/D* **(B)**, *to RIIα D/D* **(C)** *and the overlay* **(D)** *are shown. The RIα D/D presents 4 pockets, I-IV, at the docking surface, whereas RIIα D/D presents only 2 pockets, I and II, which are structurally equivalent to RIα pocket I and II. Pocket residues are also labeled. 4 helix turns of the D-AKAP2 helix make an interaction with 4 pockets of RIα D/D while only 2 helix turns are required to make an interaction with the pockets I and II of the RIIα D/D. The D-AKAP2 helix bound to the RIα D/D is shifted from the N terminus by a complete helical turn. The pocket I of RIα D/D is filled by D-AKAP2 residues 634 and 635 and the equivalent pocket of RIIα D/D is filled by residues 637 and 638 from the next helical turn. The same goes also for pocket II which is filled by D-AKAP2 residues 638 and 639 for RIα D/D and by residues 642 and 643 for RIIα D/D. Structure-based alignment of the D-AKAP2 helix bound to RIα D/D and RIIα D/D is also shown. Binding pockets are boxed and labeled (Adapted from ref (198)).*

I.4 AKAPs in cardiac physiology and pathophysiology

To date, knowledge about the physiological roles of a number of AKAPs stems predominantly from studies into cardiac function. In the heart, an important cAMP signaling route is regulated through the β-adrenegic receptors, a class of GPCRs that are targets of the catecholamine hormones, especially epinephrine (adrenaline) and norepinephrine (noradrenaline). The binding of the hormone to the receptor will generally cause a sympathetic ("fight-or-flight") response, which leads to an increase in both heart rate and force of contracting and relaxation of the cardiac muscle. PKA RIα is believed to play a role in cardiac function as it is the predominant isoform associated with the cardiomyocyte plasma membrane (sarcolemma) (199) and mutations in the RIα gene have been shown to be associate with familial cardiac tumors (myxomas) and Carney complex (200, 201). However, very little is known about PKA RI-specific AKAPs in general, so also not in the heart. In contrast to RIα, several AKAPs targeting type II PKA have been characterized in the heart. Each plays a critical role in regulating localized phosphorylation events to regulate specific parts of cardiac function. In particular, mAKAP, yotiao (AKAP9), AKAP15/18 (AKAP7), AKAP79/150 (AKAP5), AKAP-Lbc (AKAP13), synemin, and myospryn, all being R II AKAPs, are well characterized to have physiological functions in the heart, as well as the dual specificity AKAP, D-AKAP2 (as reviewed in (202-204)).

One of the most prominent roles of AKAPs in the heart is to coordinate $Ca2^+$ handling, which is heavily intertwined with primary physiological responses such as contractility and conduction. Numerous cardiac PKA substrates involved in $Ca2^+$ handling have been identified including the L-type $Ca2^+$ channel (LTCC), the $Ca2^+$-activated $Ca2^+$ channel ryanodine receptor (RyR), the cardiac sarcoplasmic reticulum $Ca2^+$ -ATPase (SERCA2), and phospholamban (PLN). The muscle AKAP (mAKAP) is highly expressed in cardiac tissue and localized both to RyR2 embedded in the sacroplasmic reticulum (SR) as well as at the nuclear membrane in cardiac myocytes. mAKAP serves as a scaffold for a wide range of enzymes such as besides PKA, the phosphodiesterase PDE4D3, the phosphatases PP2A and PP2B (calcineurin), the MAP kinase signaling components, ERK5 and MEK5 and Epac1. While the function of the nuclear RyR2 is less clear, the SR-embedded RyR2 is responsible for calcium release from SR into cytosol. The resulting increase in calcium concentration then triggers the cardiac muscle to contract. PKA phosphorylation of RyR2 increases its calcium sensitivity as well as open probability. mAKAP has been shown to associate with the SR pool of RyR2 and facilitate the PKA-induced opening of the receptor. Tight regulation of cardiac contractility is critical for function of the heart and mAKAP plays a role in this by tethering PKA and PDE4D3 to the same complex to rapidly hydrolyze localized cAMP pool, resulting in the attenuation of PKA activity and restoring the kinase as well as the receptor back to its inactive state. Interestingly, phosphorylation of the PDE4D3 has been shown to increase both its cAMP hydrolysis activity and its association to the complex. In addition to a role in mediating cardiac contractility, mAKAP function is also implicated in the cardiac myocyte for full activation of the calcineurin/NFAT transcription factor pathway and cardiac hypertrophy. A model wherein mAKAP serves as a master integrator of cAMP signaling in $Ca2^+$ handling was described in a review by Dodge-Kafka and Kapillof (35).

Another AKAP playing a major role in $Ca2^+$ handling is AKAP18α (AKAP15, AKAP7). The name AKAP18 refers to a family of splice variants arising from the AKAP7 gene. The first identified target of AKAP18α was the LTCC (205). LTCC is the major voltage-gated calcium channel in the heart. AKAP18α scaffolds PKA RII and LTCC to facilitate PKA phosphorylation of the channel to enhance its opening and activity (42). Disruption of the LTCC and AKAP18α association blocked β-adrenergic stimulation of the channel in myocytes and the transgenic mice expressing only the

truncated channel, in which regulation by PKA is abolished, also suffer from cardiac hypertrophy (42, 206). Another isoform of AKAP18, AKAP 18δ has been shown to regulate cardiac $Ca2^{+}$ handling through the cardiac sarcoplasmic reticulum $Ca2^{+}$ -ATPase (SERCA2) and its negative regulator phospholamban (PLN). SERCA2 has a crucial role in controlling $Ca2^{+}$ re-uptake into the SR. PLN is a negative regulator of SERCA2 and in its dephosphorylated state, PLN binds SERCA2 and suppresses its activity. Upon β-adrenegic stimulation AKAP18δ coordinates PKA-mediated phosphorylation at serine 16 of PLN, by scaffolding SERCA2, PLN and PKA in the same complex, thereby providing accurate control of SERCA2 activity and $Ca2^{+}$ re-uptake (43).

Potassium handling in the heart is also partly regulated by AKAPs. The regulation of the duration of cardiac action potential (APD) requires PKA-mediated phosphorylation of the α-subunit (KCNQ1) of the slowly activating potassium channel (IKs). Yotiao regulates APD by recruiting PKA RII, phosphatase PP1, PDE4D3 and adenylyl cyclase 9 (AC9) to KCNQ1 (54) to dynamically modulate its phosphorylation state and activity. A prevalent single nucleotide polymorphism (SNP) in Yotiao changes the amino acid at position 1570 from serine to leucine. This variation disrupts the interaction between Yotiao and KCNQ1, thereby reducing cAMP-induced phosphorylation of the channel to cause prolonged action potential duration and hence long-QT syndrome (207, 208).

Another AKAP's involvement in cardiac function was identified from a SNP found in the AKAP10 gene (D-AKAP2). Although the exact function of D-AKAP2 in the heart is unknown, these genetic studies suggest that the I646V variant, which is in the PKA-binding domain is associated with the shortening of the electrocardiogram PR interval of the cardiac cycle. The I646V variant binds with a 3-fold higher affinity to PKA-RIα and also alters RIα subcellular localization (209). In line with this, a subsequent study by Tingley et al. showed that D-AKAP2-mutant mice lacking the PKA-binding domain suffer from cardiac arrhythmia and die in the first year of life (210).

Our knowledge about the extensive AKAP family has rapidly expanded over the last decades. The studies to date depict an integral role of AKAPs in cardiac function. In past years, functional characterization of AKAPs has been mainly studied in isolated cardiomyocytes (42, 43). However, more efforts have been put into the development of knock-out animals for individual AKAPs as a genetic model to study its role in cardiac physiology as well as pathophysiology such as hypertrophy and arrhythmia (206, 210, 211). The combined application of knock-out animals with proteomics and imaging techniques could shed light on how AKAPs regulate the spatial and temporal organization of cardiac signaling in healthy and diseased hearts. Moreover, genome-wide association studies on SNPs will also be useful to determine AKAP genes that are associated with known cardiac diseases. The complete understanding of the cAMP signaling pathway will dramatically help us to define the molecular basis of several cardiac diseases as well as the identification of novel drug targets.

II BCL-2 Family Proteins and Apoptosis

During the work presented in this thesis we uncovered a putative role of SPHKAP in apoptosis, and worked on a hypothesis that SPHKAP may do so through a domain resembling those present in the BCL-2 family of proteins, that are well known for their role in apoptosis. Therefore, I here concisely summarize the current literature about apoptosis and the BCL-2 family of proteins.

Apoptosis, or programmed cell death, is pivotal for development, normal aging and tissue homeostasis. Aberrations in apoptotic signaling are implicated in numerous diseases, including cancer and degenerative disorders such as Alzheimer's and Parkinson's disease (as reviewed in (212, 213)). Apoptotic signaling can initiate from outside the cell via death receptors at the plasma membrane (referred to as the extrinsic pathway) or through stress from inside the cells (referred to as the intrinsic or mitochondrial pathway). The extrinsic pathway is activated when pro-apoptotic ligands such as TNFα or FAS bind to their receptors, which directly lead to the activation of caspases, the aspartate-specific cysteine proteases responsible for cleaving a number of cellular proteins and inducing apoptotic phenotypes such as DNA laddering, loss of plasma membrane asymmetry, and membrane blebbing. The intrinsic pathway is triggered by intracellular stress such as DNA damage, hypoxia, and growth factor withdrawal. The intrinsic pathway is regulated through the BCL-2 (B-cell lymphoma 2) family proteins. In general, the protein-protein interactions among members of the BCL-2 protein family, along with transcriptional and post-translational regulations of individual members, regulate the mitochondrial-related apoptosis process by maintaining mitochondrial integrity (as reviewed in (214)). When the cell is under stress, anti-apoptotic BCL-2 family proteins become functionally inhibited, while pro-apoptotic BCL-2 family members become active. The latter ones destroy the outer mitochondrial membrane (OMM) to promote mitochondrial outer membrane permeabilization (MOMP). As a consequence of MOMP, mitochondrial inner membrane space proteins such as cytochrome c and SMAC/DIABLO are released into the cytosol, where they activate caspases and induce apoptosis (Figure 5). MOMP represents the commitment step at the point-of-no return to apoptosis. Although these two pathways are completely different, there are situations of cross-talk where the extrinsic pathway promotes apoptosis through the intrinsic pathway and vice versa. In these situations, the BCL-2 family of proteins are also the central players (Figure 5).

The BCL-2 family of proteins

The landmark discovery that BCL-2 was a functional homolog of the C. elegans cell survival protein CED-9 and could prevent apoptosis (215) has led to the characterization of numerous pro- and anti-apoptotic family members, which are essential for an array of apoptosis programs. The role of the BCL-2 family of proteins in coordinating apoptosis is extremely well conserved in metazoans, with a single family member in each of the anti- and pro-apoptotic sub-group in the worm and multiple pro- and anti-apoptotic members in higher animals. Although the BCL-2 family is conserved among animals, its role in regulating the integrity of the OMM has been shown only in vertebrates. In C. elegans, CED-9 does not function in maintaining the integrity of OMM, but instead inhibits apoptosis by sequestering the APAF-1 homolog, CED-4 (as reviewed in (216)). Up to date, more than 20 members of BCL-2 protein family have been identified in mammals (as reviewed in (217)). Proteins of the BCL-2 family are characterized by the presence of one of the four conserved Bcl-2 homology (BH) domains, designated as BH1, BH2, BH3, and BH4. Proteins which contain BH1-4 domains are generally anti-apoptotic. Other members of the family are pro-apoptotic and are divided between multi-domain proteins, which contain a BH1-3 domains (BAK and BAX) and BH3-only proteins (BOPs).

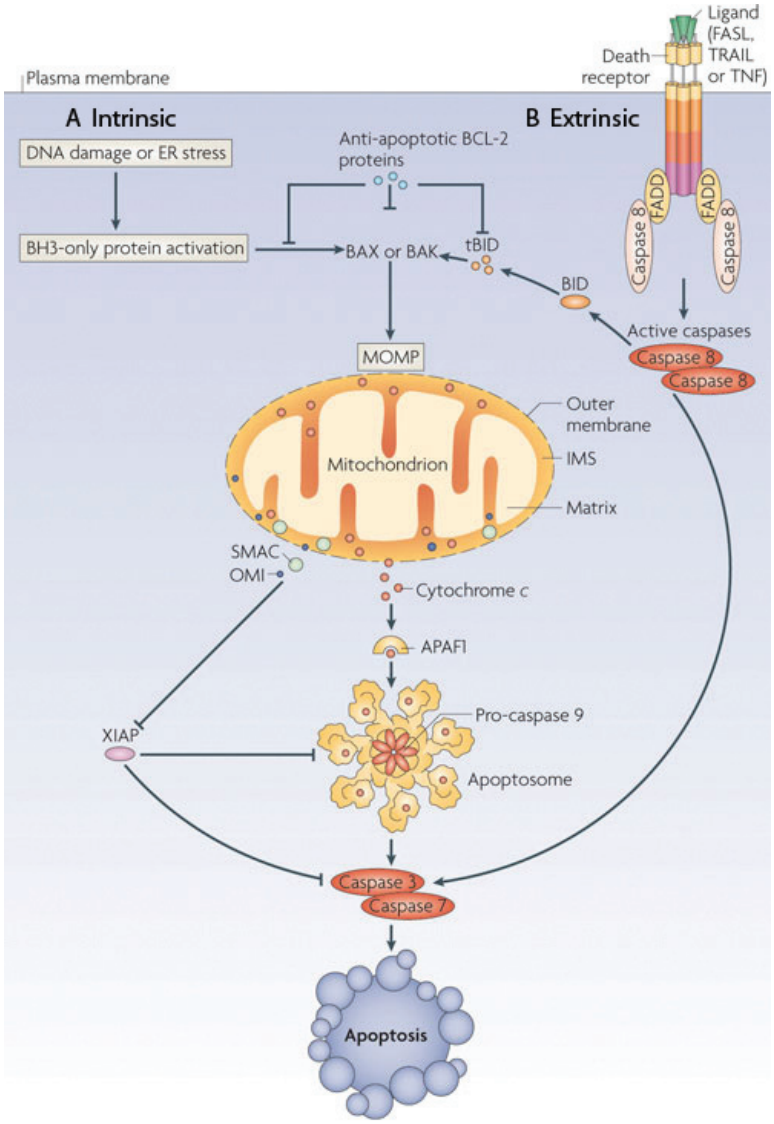

Figure 5 > Regulation of apoptosis by BCL-2 family proteins via the intrinsic and extrinsic pathways.

A) *Intrinsic apoptotic stimuli, such as DNA damage or endoplasmic reticulum (ER) stress, lead to the transcriptional up-regulation and/or activation of pro-apoptotic BH3-only proteins (BOPs), which can then promote BAK and BAX oligomerization and mitochondrial outer membrane permeabilization (MOMP). Anti-apoptotic BCL-2 family proteins prevent MOMP by binding BOPs and prevent them to activate BAK and BAX. As a consequence of MOMP, release of various proteins from the mitochondrial intermembrane space (IMS) activates caspases and apoptosis. Cytochrome c binds apoptotic protease-activating factor 1 (APAF1), inducing its oligomerization and thereby forming a structure termed the apoptosome that recruits and activates an initiator caspase, caspase 9. Caspase 9 cleaves and activates executioner caspases, caspase 3 and caspase 7, leading to apoptosis. Mitochondrial release of SMAC/ DIABLO and OMI inhibits the caspase inhibitory function of XIAP.*
B) *The extrinsic apoptotic pathway is activated by extracellular death ligands, including FASL/CD95L, TRAIL and TNFα. Binding of these ligands to their receptors leads to the recruitment of adaptor molecules such as FAS-associated death domain protein (FADD) and then caspase 8. This results in the dimerization and activation of caspase 8, which can then directly activate caspase 3 and caspase 7, leading to apoptosis. Crosstalk between the extrinsic and intrinsic pathways occurs through caspase 8 cleavage and activation of the BH3-only protein, BID. the product of the cleavage, truncated BID (tBID) is required to initiate the intrinsic apoptotic pathway (Adapted from (215)).*

Anti-apoptotic Bcl-2 proteins

The anti-apoptotic Bcl-2 proteins are responsible for maintaining the integrity of OMM. The members of this subfamily include BCL-2, BCL-xL, BCL-W, MCL-1, and A1. Even though they can be found at the endoplasmic reticulum (ER) and in the cytosol, their primary site for action is at the OMM. The anti-apoptotic BCL-2 proteins protect OMM by directly binding to pro-apoptotic BCL-2 family proteins, thereby neutralizing their ability to promote MOMP. The anti-apoptotic proteins share a conserved "BCL-2 core" structure consisting of two central hydrophobic α-helices surrounded by 6 or 7 amphiphatic α-helices of varying lengths. The three functionally important BH1-3 regions are in close spatial proximity and form an elongated hydrophobic groove. The groove is present on the surface of the proteins and is used as a docking site for the BH3 domains of pro-apoptotic binding partners (as reviewed in (218)). Although the BCL-2 core is conserved in sequence and structure among the anti-apoptotic members, slight variations within the groove provide unique binding profiles between the anti- and pro-apoptotic proteins (Figure 6A).

Pro-apoptotic BCL-2 effector proteins

The effector proteins are BCL-2 family members, which contain BH 1-3 domains. There are two well-characterized members: BCL-2 antagonist killer 1 (BAK) and BCL-2-associated X (BAX) protein. Both of them can independently permeabilize the OMM to promote MOMP. Although BAK and BAX have a redundant ability to promote MOMP, they are different in their subcellular localizations prior to pro-apoptotic stimulation. BAK is primarily attached to the OMM via a C-terminal transmembrane domain, while BAX is cytosolic and re-localizes to the OMM under apoptotic condition. Under normal conditions, BAK and BAX exist as monomers, however, under apoptotic stimulation, BAK and BAX are activated which leads to their homo-oligomerization into protein permeable pores at the OMM (Figure 7A). BAK and BAX are the essential gateway for MOMP to proceed, as bak –/– and bax –/– double homozygous knock-outs, but not the single knock-outs are completely resistant to apoptotic stimuli (219, 220).

Pro-apoptotic BH3-only proteins (BOPs)

The BH3-only proteins are the major sentinels for cellular stress, and diverse signaling pathways converge upon these proteins. The BH3-only proteins share little sequence homology with only a single BH3 domain, which may explain the variety of mechanisms capable of regulating their functions. The BH3 domain is a variable 13-residue sequence motif, Φ1ΣXXΦ2XXΦ3ΣDZΦ4Γ, that contains a conserved leucine at hydrophobic position Φ2 and an aspartic acid residue (D) at position 10 (221). X represents any residue and Σ represents small residue (G, A, S, or C). Z represents any acidic residue and Γ is occupied by a hydrophilic residue (N, H, D, or Y), although there seems to be no strict conservation (Figure 6B). This short motif forms an amphiphatic α-helix where the four hydrophobic residues, Φ1–Φ4, reside on one side of the helix to interact with the hydrophobic groove on anti-apoptotic proteins. Structural analyses revealed that only the most conserved leucine and aspartic amino acid residues appear to be more important for the interaction between pro-apoptotic BCL-family and BH3-only proteins. The leucine is buried in the binding pocket and packs against conserved residues provided by the anti-apoptotic proteins, whereas the aspartic acid is solvent-exposed and forms an ionic interaction with a conserved arginine in the BH1 domain of the pro-survival protein. Other binding interactions arise from three other hydrophobic residues that project into the binding pocket (221).

Well characterized members of the sub-family include BID, BAD, BIM, BMF, BNIP1, Beclin1, PUMA, Hrk, and Noxa, although, several other proteins were reported to contain BH3 domains and possess the ability to induce apoptosis or interact with anti-apoptotic BCL-2 family proteins. They

include p193, MAP-1, Spike, Sphk2, BRCC2, TG2, MULE/ ARF-BP1, Apol6, ApoL1, ERRBB4/ HER4 and ERBB2/ HER-2 (as reviewed in (217)). However, very little is known about the integration of these proteins in apoptosis-signaling pathways.

BOPs can be divided into two groups, depending on their ability to interact with the anti-apoptotic and effector proteins. The first subgroup is termed the direct activators. Direct activators are able to bind the anti-apoptosis BCL-2 family proteins, but also directly engage with BAX and BAK, allowing them to homo-oligomerize and promote MOMP (Figure 7B). The well-characterized direct activators include BID and BIM. PUMA may also demonstrate direct activation potential, however, the role of PUMA as a direct activator is still conflicting as its ability to promote BAK/ BAX activation may not be direct (223). It was recently shown that BID, BIM, and PUMA are essential for BAK/ BAX activation as triple knockout mice showed no homo-oligomerization of BAX and BAK, despite the presence of other BH3-only molecules (224).

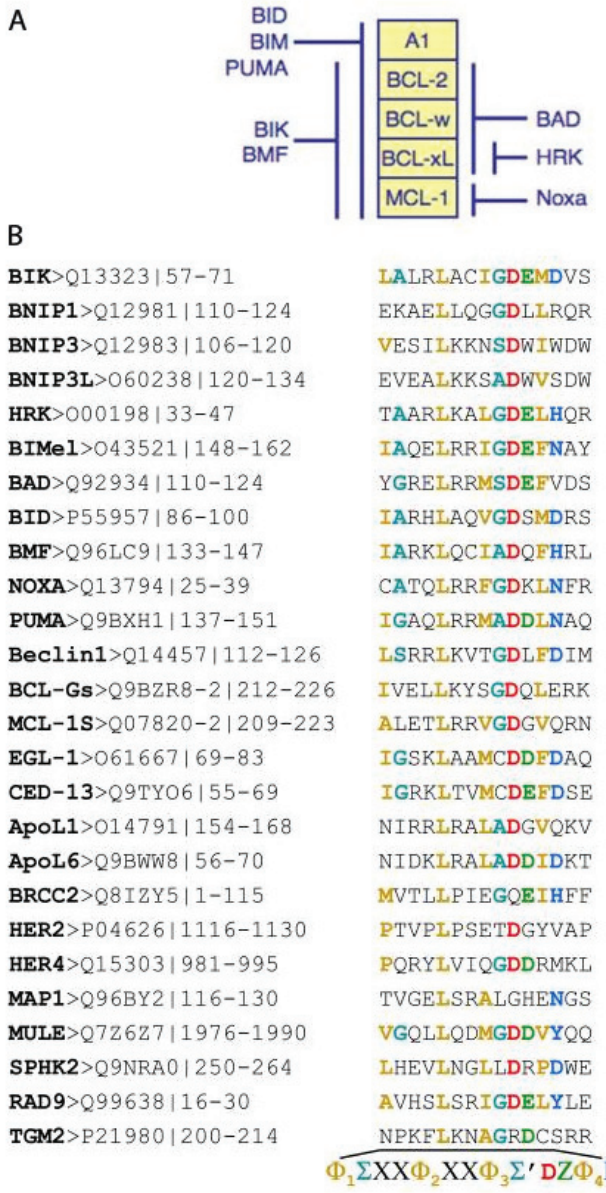

Figure 6 >

A) *Unique binding profiles between the anti-apoptotic BCL-2 proteins and the BH3-only proteins. Although BID, BIM, and PUMA are able to bind all 5 members of anti-apoptotic BCL-2 proteins, other BH3-only proteins are selective within the anti-apoptotic BCL-2 repertoire.* **B)** *Amino acid sequences of BH3 domains from various BH3-only proteins. Their accession numbers and amino acid coordinates are indicated. The consensus sequence of the BH3 domain is shown at the bottom. Φ represents a hydrophobic residue (Φ2 is usually leucine). Σ is a small residue (G, A, S, C) and Z represents an acidic residue. Γ is a hydrophilic residue (N, H, D or Y) (Adapted from (217, 222))*

The second group is the sensitizers and the de-repressors. The terms “sensitizer” and “de-repressor” are used to indicate the two distinct mechanisms that promote BAK/BAX activation: sensitization and de-repression. This group of BOPs lacks the ability to directly engage BAK and BAK, however, they bind and inhibit the anti-apoptotic BCL-2 network to promote MOMP. The well-characterized sensitizers/ de-repressors include BAD, BMF, Hrk, Noxa and PUMA (225-228). For the de-repression mechanism, a direct activator is sequestered by an anti-apoptotic BCL-2 protein, and a subsequent BOP releases the direct activator to promote MOMP (Figure 7C). For example, cellular stress can induce BIM function, but its activity is inhibited by the anti-apoptotic BCL-2 protein repertoire and the cell survives. However, if a de-repressor BOP is induced while the direct activator is sequestered, the latter can compete BIM for binding to the anti-apoptotic BCL-2 proteins and subsequently release BIM to promote MOMP. This is referred to as “de-repression”. The de-repression mechanism of NOXA is shown in figure 3C. In contrast, sensitizers lower the threshold or “sensitize” the cells for BAK and BAX activation and MOMP, but do not cause apoptosis themselves. In this scenario, an anti-apoptotic protein is in complex with a sensitizer BOP, which prevents the inhibition of subsequent direct activators. For example, if anti-apoptotic BCL-2 members are associated with BAD, any future induction of BIM is not inhibited and MOMP proceeds. In the absence of BAD, BIM would be sequestered by the anti-apoptotic members and the cell may survive (Figure 7D). It is worth noting that although direct activators: BID, BIM, and PUMA are able to bind all the anti-apoptotic BCL-2 members, each sensitizer/de-repressor BH3-only protein has a unique binding profile for the anti-apoptotic repertoire, which was primarily determined by using BH3 peptides (as reviewed in (222)). Therefore, it is likely that the combined interactions between the anti-apoptotic BCL-2 repertoire and BOPs establish the threshold and trigger apoptosis (Figure 7).

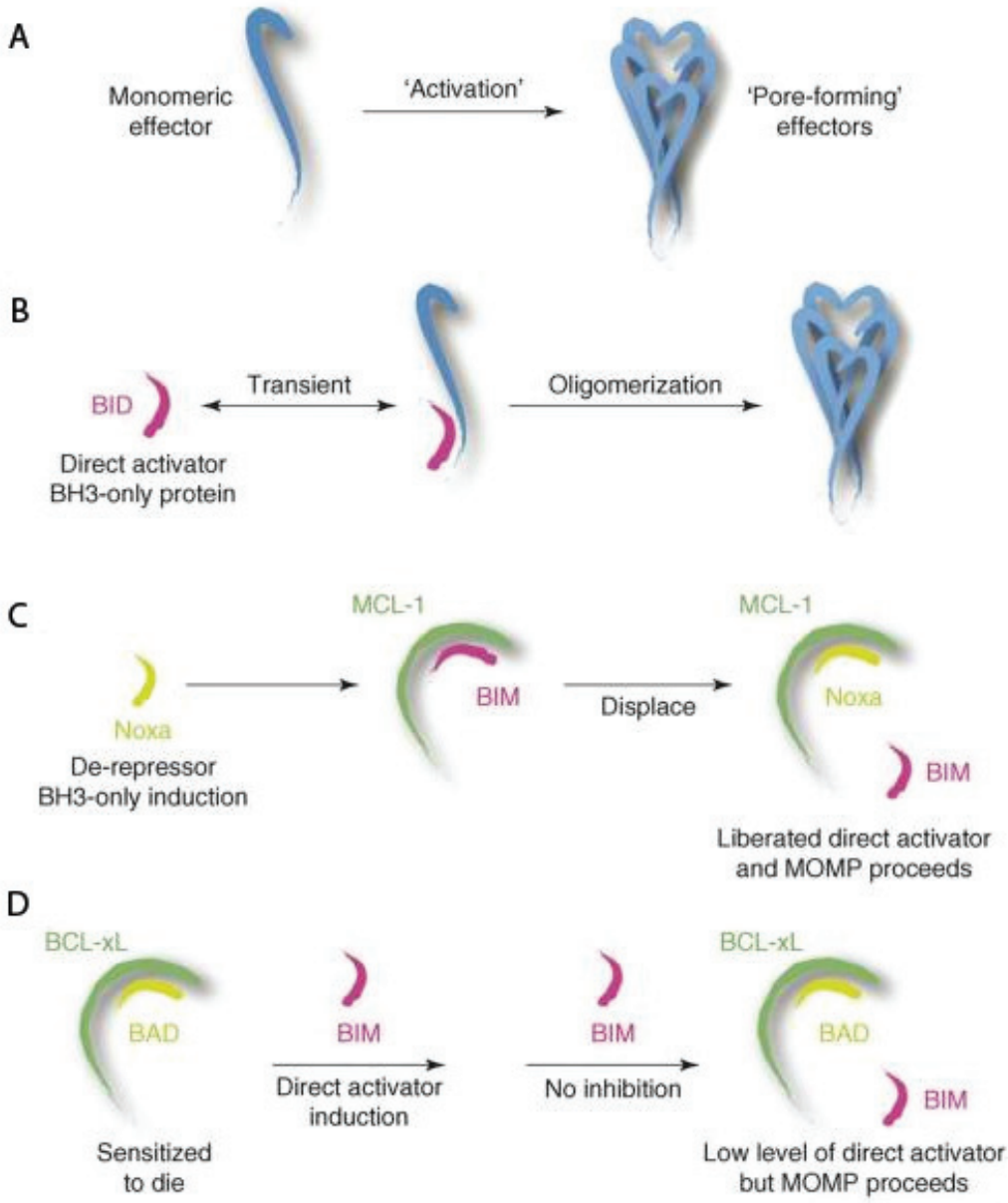

Figure 7 > Mechanisms of pro-apoptotic effector activation by BH3-only proteins.

A) *Central to MOMP is the activation and oligomerization of BAX or BAK. Once activated by a BH3-only protein, BAK and BAX create pores in OMM and promote MOMP.* **B)** *Direct activator BH3-only proteins (e.g. BID and BIM) induce the oligomerization of BAK and BAX directly.* **C)** *A subset of BH3-only proteins, the de-repressors cannot directly induce the activation of BAX or BAK. In this scenario, a direct activator is sequestered by an anti-apoptotic BCL-2 protein under healthy conditions. Following stress, a de-repressor BH3-only protein is induced, either by transcriptional up-regulation or by post-translational modification, and then binds to an anti-apoptotic BCL-2 protein, promoting the release of a sequestered, direct activator. For example, the direct activator BIM is sequestered by MCL-1, and the induction of Noxa enables the release of BIM to promote MOMP. This is referred to as "de-repression".* **D)** *Cells are sensitized to undergo MOMP when BH3-only proteins are constitutively inhibiting anti-apoptotic BCL-2 proteins, and any future induction of BID or BIM cannot be tolerated. This scenario is referred to as 'sensitized for death'. In this example, BCL-xL is inhibited by BAD, and the induction of BIM engages MOMP; in the absence of BAD expression, the MOMP signal would have been inhibited by BCL-xL (Adapted from (229).*

III Scope and Outline of this Thesis

The starting point for my thesis was the finding in our laboratory, in a previous chemical proteomics experiment targeting proteins binding to cAMP/PKA, that the in cardiac tissue highly expressed protein Sphingosine kinase-1 interacting protein (SPHKAP or SKIP) could be a novel AKAP (176, 230). With this result in mind, the aim of this thesis was to study the molecular function of the SPHKAP in the heart using proteomics technology complemented with classical biochemistry and cell biology. The first part of **Chapter 1** reviews the diverse protein family of AKAPs, which establish spatial and temporal specificity for many parallel cAMP signaling pathways. A comprehensive list of AKAPs identified to date is provided, together with an overview of AKAPs role in cardiac physiology. In the following section, work performed on the structural basis of different PKA-R isoforms and AKAPs are reviewed. As in chapter 5 we reveal a putative role of SPHKAP in apoptosis, the remainder part of the introduction chapter 1 describes the basics of apoptosis with the focus on the role of BCL-2 family proteins in apoptosis.

In chapter 2 and 3 two key proteomics methodologies applied in this thesis are described in detail. **Chapter 2** provides an extensive overview of stable isotope dimethyl labeling in proteomics application. This isotope labeling strategy is fast and efficient as well as economically attractive. Its increasing popularity has spurred many proteomics laboratories to adopt these labels for quantitative proteomics applications. The chapter starts by outlining the basic concepts and software packages available for dimethyl labeling-based analysis. Subsequently, the application of the technique in expression proteomics, PTM studies and interaction proteomics is described. Examples of experimental setups for the three types of studies are provided.

Chapter 3 depicts how cAMP-based affinity purification using a variety of differentially coupled cAMP-analogs can be exploited to build an effective tool to screen for PKA-R/AKAP specificity directly in any cell or tissue sample. This chemical proteomics methodology can be combined with stable isotope dimethyl labeling for effective mass spectrometric read-out.

Chapter 4 describes the initial characteristics of SPHKAP by using a variety of biochemical and proteomics methods. We show that SPHKAP is the first mammalian PKA-type I specific AKAP, both in vitro and in vivo. Closer inspection of SPHKAP's AKB domain matched perfectly to all reviewed structural determinants reviewed in chapter 1.

In **Chapter 5**, we aimed to continue evaluating other characteristics of SPHKAP. Confocal microscopy and subcellular fractionation were used to show that SPHKAP localizes both in mitochondria, as well as in the cytosolic fraction. To characterize SPHKAP's molecular environment and identify its binding partners, we performed affinity pull-downs with GFP-tagged SPHKAP revealing many putative mitochondrial partners. Failure to create a cell line, stably expressing SPHKAP hinted already at a potential enhancing role in apoptosis. With this in mind we identified a putative BH3 domain on SPHKAP, further suggesting a role of SPHKAP in apoptosis. Further experiments using immuno-affinity purifications revealed SPHKAP 's interaction with pro-survival proteins BCL-2 and BCL-xL via its BH3 domain to lay the foundation for SPHKAP's function in apoptosis.All these chapters are summarized and discussed in **Chapter 6**.

References

1. E.W. Sutherland, T. W. Rall, Fractionation and characterization of a cycle adenine ribonucleotide formed by tissue particles. J Biol Chem 232, 1077 (1958).
2. H. Kasai, O.H. Petersen, Spatial dynamics of second messengers: IP3 and cAMP as long-range and associative messengers. Trends Neurosci 17, 95 (1994).
3. B.J. Bacskai et al., Spatially resolved dynamics of cAMP and protein kinase A subunits in Aplysia sensory neurons. Science 260, 222 (1993).
4. M. Zaccolo, T. Pozzan, Discrete Microdomains with High Concentration of cAMP in Stimulated Rat Neonatal Cardiac Myocytes. Science 295, 1711 (2002).
5. W. Wong, J.D. Scott, AKAP signalling complexes: focal points in space and time. Nat Rev Mol Cell Biol 5, 959 (2004).
6. WR. Dostmann, S.S. Taylor, Identifying the molecular switches that determine whether (Rp)-cAMPS functions as an antagonist or an agonist in the activation of cAMP- dependent protein kinase I. Biochemistry 30, 8710 (1991).
7. W.T. Heller et al., C subunits binding to the protein kinase A RIα dimer induce a large conformational change. J Biol Chem 279, 19084 (2004).
8. J.M. Canaves, S.S. Taylor, Classification and phylogenetic analysis of the cAMP dependent protein kinase regulatory subunit family. J Mol Evol 54, 17 (2002).
9. D. Vigil et al., conformational differences among solution structures of the type Iα, IIα and IIβ protein kinase A regulatory subunit homodimers: role of the linker regions. J Mol Biol 337, 1183 (2004).
10. J.B. Shabb, Physiological substrates of cAMP-dependent protein kinase. Chem Rev 101, 2381 (2001).
11. G. Pidoux, K. Taskén, Specificity and spatial dynamics of protein kinase A signaling organized by A-kinase-anchoring proteins. J Mol Endocrinol 44, 271 (2010).
12. D. Chaturvedi, M. S. Cohen, J. Taunton, T. B. Patel, The PKARIα subunit of protein kinase A modulates the activation of p90RSK1 and its Function. J Biol Chem 284, 23670 (2009).
13. D. Bridges, J.A. MacDonald, B. Wadzinski, G.B.G. Moorhead, Identification and characterization of D-AKAP1 as a major adipocyte PKA and PP1 binding protein. Biochem Biophys Res Commun 346, 351 (2006).
14. L.J. Huang et al., NH2-Terminal targeting motifs direct dual specificity A-kinase-anchoring protein 1 (D-AKAP1) to either mitochondria or endoplasmic reticulum. J Cell Biol 145, 951 (1999).
15. M. Furusawa, T. Ohnishi, T. Taira, S.M.M. Iguchi-Ariga, H. Ariga, AMY-1, a c-Myc-binding protein, is localized in the mitochondria of sperm by association with S-AKAP84, an anchor protein of cAMP-dependent protein kinase. J Biol Chem 276, 36647 (2001).
16. L. Cardone et al., mitochondrial AKAP121 binds and targets protein tyrosine phosphatase D1, a novel positive regulator of src signaling. Mol Cell Biol 24, 4613 (2004).
17. H. Yukitake, M. Furusawa, T. Taira, S.M.M. Iguchi-Ariga, H. Ariga, AAT-1, a novel testis-specific AMY-1-binding protein, forms a quaternary complex with AMY-1, A-kinase anchor protein 84, and a regulatory subunit of cAMP-dependent protein kinase and is phosphorylated by its kinase. J Biol Chem 277, 45480 (2002).
18. A. Carlucci et al., Proteolysis of AKAP121 regulates mitochondrial activity during cellular hypoxia and brain ischaemia. EMBO J 27, 1073 (2008).
19. M.G. Gold et al., AKAP2 anchors PKA with aquaporin-0 to support ocular lens transparency. EMBO Mol Med 4, 15 (2012).
20. B.Hu,N.G.Copeland, D.J. Gilbert, N.A.Jenkins,M.W. Kilimann, The paralemmin protein family: identification of paralemmin-2, an isoform differentially spliced to AKAP2/AKAP-KL, and of palmdelphin, a more distant cytosolic relative. Biochem BiophysRes Commun 285, 1369 (2001).
21. D.W. Carr et al., Identification of sperm-specific proteins that interact with A-kinase anchoring proteins in a manner similar to the type II regulatory subunit of PKA. J Biol Chem 276, 17332 (2001).
22. M. Bajpai et al., AKAP3 selectively binds PDE4A isoforms in bovine spermatozoa. Biol Reprod 74, 109 (2006).
23. Y.-F. Li et al., CABYR binds to AKAP3 and Ropporin in the human sperm fibrous sheath. Asian J Androl 13, 266 (2011).

24. P.R. Brown, K. Miki, D.B. Harper, E.M. Eddy, A-Kinase anchoring protein 4 binding proteins in the fibrous sheath of the sperm flagellum. Biol Reprod 68, 2241 (2003).

25. T.M. Klauck et al., Coordination of three signaling enzymes by AKAP79, a mammalian scaffold protein. Science 271, 1589 (1996).

26. S.F. Oliveria, M. L. Dell'Acqua, W. A. Sather, AKAP79/150 anchoring of calcineurin controls neuronal L-Type $Ca2^{+}$ channel activity and nuclear signaling. Neuron 55, 261 (2007).

27. M.L. Dell'Acqua, M.C. Faux, J. Thorburn, A. Thorburn, J.D. Scott, Membrane-targeting sequences on AKAP79 bind phosphatidylinositol-4,5-bisphosphate. EMBO J 17, 2246 (1998).

28. S.J. Tavalin et al., Regulation of GluR1 by the A-kinase anchoring protein 79 (AKAP79)signaling complex shares properties with long-term depression. J Neurosci 22, 3044 (2002).

29. N.J.Brandon et al., A-kinase anchoring protein 79/150 facilitates the phosphorylation of GABAA receptors by cAMP-dependent protein kinase via selective interaction with receptor β subunits. Mol Cell Neurosci 22, 87 (2003).

30. X.Gorny et al., AKAP79/150 interacts with the neuronal calcium-binding protein caldendrin. J Neurochem 122, 714 (2012).

31. A.V.Le,S.J. Tavalin, K.L. Dodge-Kafka, Identification of AKAP79 as a protein phosphatase 1 catalytic binding protein. Biochemistry 50, 5279 (2011).

32. L.A. Gardner, A. P. Naren, S. W. Bahouth, Assembly of an SAP97-AKAP79-cAMP-dependent protein kinase scaffold at the type 1 PSD-95/DLG/ZO1 motif of the human β1-adrenergic receptor generates a receptosome involved in receptor recycling and networking. J Biol Chem 282, 5085 (2007).

33. I.D.C. Fraser et al., Assembly of an A kinase-anchoring protein–β2-adrenergic receptor complex facilitates receptor phosphorylation and signaling. Curr Biol 10, 409 (2000).

34. N.Hoshi et al., AKAP150 signaling complex promotes suppression of the M-current by muscarinic agonists. Nat Neurosci 6, 564 (2003).

35. K.L. Dodge-Kafka, M. S. Kapiloff, The mAKAP signaling complex: integration of cAMP, calcium, and MAP kinase signaling pathways. Eur J Cell Biol 85, 593 (2006).

36. M.S. Kapiloff et al., An adenylyl cyclase-mAKAPβ signaling complex regulates cAMP levels in cardiac myocytes. J Biol Chem 284, 23540 (2009).

37. W.Wong, A.S. Goehring, M.S. Kapiloff, L.K. Langeberg, J.D. Scott, mAKAP compartmentalizes oxygen-dependent control of HIF-1α. Sci. Signal. 1, ra18 (2008).

38. J. Li et al., Anchored p90 ribosomal S6 kinase 3 is required for cardiac myocyte hypertrophy. Circ Res, (2012).

39. M.A.X. Vargas, J.S. Tirnauer, N. Glidden, M.S. Kapiloff, K.L. Dodge-Kafka, Myocyte enhancer factor 2 (MEF2) tethering to muscle selective A-kinase anchoring protein (mAKAP) is necessary for myogenic differentiation. Cell Signal 24, 1496 (2012).

40. L.Zhang, S.Malik, G.G. Kelley, M.S. Kapiloff, A.V. Smrcka, Phospholipase C epsilon scaffolds to muscle-specific A kinase anchoring protein (mAKAPβ) and integrates multiple hypertrophic stimuli in cardiac myocytes. J Biol Chem 286, 23012 (2011).

41. J.J. Carlisle Michel et al., spatial restriction of PDK1 activation cascades by anchoring to mAKAPα. Mol Cell 20, 661 (2005).

42. J.T. Hulme, T.W.-C. Lin, R.E. Westenbroek, T. Scheuer, W.A. Catterall, β-Adrenergic regulation requires direct anchoring of PKA to cardiac CaV1.2 channels via a leucine zipper interaction with A kinase-anchoring protein 15. Proc Natl Acad Sci U S A 100, 13093 (2003).

43. B. Lygren et al., AKAP complex regulates $Ca2^{+}$ re-uptake into heart sarcoplasmic reticulum. EMBO Rep 8, 1061 (2007).

44. A.R. Cantrell et al., Molecular mechanism of convergent regulation of brain Na^{+} channels by protein kinase C and protein kinase A anchored to AKAP-15. Mol Cell Neurosci 21, 63 (2002).

45. R.L. Brown, S.L. August, C.J. Williams, S.B. Moss, AKAP7γ is a nuclear RI-binding AKAP. Biochem Biophys Res Commun 306, 394 (2003).

46. P. Collas, K. Le Guellec, K. Taskén, The A-kinase anchoring protein AKAP95 is a multivalent protein with a key role in chromatin condensation at mitosis. J Cell Biol 147, 1167 (1999).

47. L. Akileswaran, J.W. Taraska, J. A. Sayer, J.M.Gettemy, V.M. Coghlan, A-kinase anchoring protein AKAP95 is targeted to the nuclear matrix and associates with p68 RNA helicase. J Biol Chem 276, 17448 (2001).

48. S. Kamada, U. Kikkawa, Y. Tsujimoto, T. Hunter, A-kinase-anchoring protein 95 functions as a potential carrier for the nuclear translocation of active caspase 3 through an enzyme-substrate-like association. Mol Cell Biol 25, 9469 (2005).

49. T. Arsenijevic, C. Degraef, J.E. Dumont, P. P. Roger, I. Pirson, A novel partner for D-type cyclins: protein kinase A-anchoring protein AKAP95. Biochem J 378, 673 (2004).

50. T. Eide et al., Protein kinase A-anchoring protein AKAP95 interacts with MCM2, a regulator of DNA replication. J Biol Chem 278, 26750 (2003).

51. M. Furusawa, T. Taira, S.M.M. Iguchi-Ariga, H. Ariga, AMY-1 interacts with S-AKAP84 and AKAP95 in the cytoplasm and the nucleus, respectively, and inhibits cAMP-dependent protein kinase activity by preventing binding of its catalytic subunit to A-kinase-anchoring Protein (AKAP) complex. J Biol Chem 277, 50885 (2002).

52. T. Arsenijevic, C. Degraef, J.E. Dumont, P.P. Roger, I. Pirson, G1/S cyclins interact with regulatory subunit of PKA via A-kinase anchoring protein, AKAP95. Cell Cycle 5, 1217 (2006).

53. Y. Yang, C.L. Mahaffey, N. Bérubé, W.N. Frankel, Interaction between fidgetin and protein kinase A-anchoring protein AKAP95 is critical for palatogenesis in the mouse. J Biol Chem 281, 22352 (2006).

54. Y. Li, L. Chen, R.S. Kass, C.W. Dessauer, The A-kinase anchoring protein Yotiao facilitates complex formation between adenylyl cyclase type 9 and the IKs potassium channel in heart. J Biol Chem 287, 29815 (2012).

55. M. Takahashi et al., Characterization of a novel giant scaffolding protein, CG-NAP, that anchors multiple signaling enzymes to centrosome and the Golgi apparatus. J Biol Chem 274, 17267 (1999).

56. R.S. Westphal et al., Regulation of NMDA receptors by an associated phosphatase-kinase signaling complex. Science 285, 93 (1999).

57. M. Suzuki et al., A novel A-kinase anchoring protein in the heart interacts with Gα13. Jpn Heart J 40, 199 (1999).

58. M.Takahashi, H. Mukai, K. Oishi, T. Isagawa, Y. Ono, Association of immature hypophosphorylated protein kinase Cε with an anchoring protein CG-NAP. J Biol Chem 275, 34592 (2000).

59. B.T. Steadman, P.H. Schmidt, R.A. Shanks, L.A. Lapierre, J.R. Goldenring, Transforming acidic coiled-coil-containing protein 4 interacts with centrosomal AKAP350 and the mitotic spindle apparatus. J Biol Chem 277, 30165 (2002).

60. J.D. Bray, V.M. Chennathukuzhi, N.B. Hecht, Identification and characterization of cDNAs encoding four novel proteins that interact with translin associated factor-X. Genomics 79, 799 (2002).

61. R.A. Shanks et al., AKAP350 at the Golgi apparatus. J Biol Chem 277, 40973 (2002).

62. M.Takahashi, A. Yamagiwa, T. Nishimura, H. Mukai, Y. Ono, Centrosomal proteins CG-NAP and kendrin provide microtubule nucleation sites by anchoring γ-tubulin ring complex. Mol Biol Cell 13, 3235 (2002).

63. J.E. Sillibourne, D.M. Milne, M. Takahashi, Y. Ono, D.W. Meek, Centrosomal Anchoring of the Protein Kinase CK1δ Mediated by Attachment to the Large, Coiled-coil Scaffolding Protein CG-NAP/AKAP450. J Mol Biol 322, 785 (2002).

64. G. Keryer et al., Part of Ran Is Associated with AKAP450 at the Centrosome: Involvement in Microtubule-organizing Activity. Mol Biol Cell 14, 4260 (2003).

65. M.A. Berryman, J.R. Goldenring, CLIC4 is enriched at cell-cell junctions and colocalizes with AKAP350 at the centrosome and midbody of cultured mammalian cells. Cell Motil Cytoskeleton 56, 159 (2003).

66. H. Tu, T.-S. Tang, Z. Wang, I. Bezprozvanny, Association of Type 1 Inositol 1,4,5- Trisphosphate Receptor with AKAP9 (Yotiao) and Protein Kinase A. J Biol Chem 279, 19375 (2004).

67. T. Nishimura, M. Takahashi, H.-S. Kim, H. Mukai, Y. Ono, Centrosome-targeting region of CG-NAP causes centrosome amplification by recruiting cyclin E-cdk2 complex. Genes Cells 10, 75 (2005).

68. B.S.E.D. El Homasany et al., The Scaffolding Protein CG-NAP/AKAP450 Is a Critical Integrating Component of the LFA-1-Induced Signaling Complex in Migratory T Cells. J Immunol 175, 7811 (2005).

69. H.S.Kim, M. Takahashi, K. Matsuo, Y. Ono, Recruitment of CG-NAP to the Golgi apparatus through interaction with dynein–dynactin complex. Genes Cells 12, 421 (2007).

70. E. Kolobova et al., Microtubule-dependent association of AKAP350A and CCAR1 with RNA stress granules. Exp Cell Res 315, 542 (2009).

71. S. Sehrawat et al., AKAP9 regulation of microtubule dynamics promotes Epac1-induced endothelial barrier properties. Blood 117, 708 (2011).

72. C.T. Eggers, J.C. Schafer, J.R. Goldenring, S.S. Taylor, D-AKAP2 Interacts with Rab4 and Rab11 through Its RGS Domains and Regulates Transferrin Receptor Recycling. J Biol Chem 284, 32869 (2009).

73. L.B. Lester, V. M. Coghlan, B. Nauert, J.D. Scott, Cloning and Characterization of a Novel A-kinase Anchoring Protein: AKAP 220, Association with testicular peroxisomes. J Biol Chem 271, 9460 (1996).

74. N. Reinton et al., Localization of a Novel Human A-Kinase-Anchoring Protein, hAKAP220, during Spermatogenesis. Dev Biol 223, 194 (2000).

75. L. Yang, Y. Nakayama, N. Hattori, B. Liu, C. Inagaki, GABAC-Receptor Stimulation Activates cAMP-Dependent Protein Kinase via A-Kinase Anchoring Protein 220. J Pharmacol Sci 106, 578 (2008).

76. I.H. Gelman, Emerging Roles for SSeCKS/Gravin/AKAP12 in the Control of Cell Proliferation, Cancer Malignancy, and Barriergenesis. Genes Cancer 1, 1147 (2010).

77. D. Diviani, J. Soderling, J.D. Scott, AKAP-Lbc Anchors Protein Kinase A and Nucleates Gα12-selective Rho-mediated Stress Fiber Formation. J Biol Chem 276, 44247 (2001).

78. G.K. Carnegie, F.D. Smith, G. McConnachie, L.K. Langeberg, J.D. Scott, AKAP-Lbc Nucleates a Protein Kinase D Activation Scaffold. Mol Cell 15, 889 (2004).

79. D. Diviani, L. Abuin, S. Cotecchia, L. Pansier, Anchoring of both PKA and 14-3-3 inhibits the Rho-GEF activity of the AKAP-Lbc signaling complex. EMBO J 23, 2811 (2004).

80. L. Baisamy, S. Cavin, N. Jurisch, D. Diviani, The Ubiquitin-like Protein LC3 Regulates the Rho-GEF Activity of AKAP-Lbc. J Biol Chem 284, 28232 (2009).

81. F.D. Smith et al., AKAP-Lbc enhances cyclic AMP control of the ERK1/2 cascade. Nat Cell Biol 12, 1242 (2010).

82. L. Cariolato, S. Cavin, D. Diviani, A-Kinase Anchoring Protein (AKAP)-Lbc Anchors a PKN-based Signaling Complex Involved in α1-Adrenergic Receptor-induced p38 Activation. J Biol Chem 286, 7925 (2011).

83. H.V. Edwards, J.D. Scott, G.S. Baillie, The A-kinase-anchoring protein AKAP-Lbc facilitates cardioprotective PKA phosphorylation of Hsp20 on Ser16. Biochem J 446, 437 (2012).

84. B.T. Burmeister, D.M. Taglieri, L. Wang, G.K. Carnegie, SH2 domain-containing phosphatase 2 (Shp2) is a component of the AKAP-Lbc complex and is inhibited by protein kinase A (PKA) under pathological hypertrophic conditions in the heart. J Biol Chem 287, 40535 (2012).

85. C.D. del Vescovo, S. Cotecchia, D. Diviani, AKAP-LBC anchors IKKβ to support interlukin-6-mediated cardiomyocyte hypertrophy. Mol Cell Biol 33,14 (2013).

86. X. Mei, I.S. Singh, J. Erlichman, G.A. Orr, Cloning and Characterization of a Testis-Specific, Developmentally Regulated A-Kinase-Anchoring Protein (Takap-80) Present on the Fibrous Sheath of Rat Sperm. Eur J Biochem 246, 425 (1997).

87. E. Jarnæss et al., Splicing Factor Arginine/Serine-rich 17A (SFRS17A) Is an A-kinase Anchoring Protein That Targets Protein Kinase A to Splicing Factor Compartments. J Biol Chem 284, 35154 (2009).

88. A. H. Mangs et al., XE7: A novel splicing factor that interacts with ASF/SF2 and ZNF265. Nucleic Acids Res 34, 4976 (2006).

89. A.L. Neisch, R.G. Fehon, Ezrin, Radixin and Moesin: key regulators of membrane–cortex interactions and signaling. Curr Opin Cell Biol 23, 377 (2011).

90. D.T. Dransfield et al., Ezrin is a cyclic AMP-dependent protein kinase anchoring protein. EMBO J 16, 35 (1997).

91. M. Gronholm et al., Homotypic and heterotypic interaction of the neurofibromatosis 2 tumor suppressor protein merlin and the ERM protein ezrin. J Cell Sci 112, 895 (1999).

92. S.V. Sitaraman et al., The Adenosine 2b Receptor Is Recruited to the Plasma Membrane and Associates with E3KARP and Ezrin upon Agonist Stimulation. J Biol Chem 277, 33188 (2002).

93. F. Sun, M.J. Hug, N.A. Bradbury, R.A. Frizzell, Protein Kinase A Associates with Cystic Fibrosis Transmembrane Conductance Regulator via an Interaction with Ezrin. J Biol Chem 275, 14360 (2000).

94. A. Urzainqui et al., ITAM-Based Interaction of ERM Proteins with Syk Mediates Signaling by the Leukocyte Adhesion Receptor PSGL-1. Immunity 17, 401 (2002).

95. R.F. Lamb et al., The TSC1 tumour suppressor hamartin regulates cell adhesion through ERM proteins and the GTPase Rho. Nat Cell Biol 2, 281 (2000).

96. K. Takahashi et al., Direct Interaction of the Rho GDP Dissociation Inhibitor with Ezrin/Radixin/Moesin Initiates the Activation of the Rho Small G Protein. J Biol Chem 272, 23371 (1997).

97. S. Hiscox, W. G. Jiang, Ezrin regulates cell-cell and cell-matrix adhesion, a possible role with E-cadherin/beta-catenin. J Cell Sci 112, 3081 (1999).

98. M. Berryman, A. Bretscher, Identification of a Novel Member of the Chloride Intracellular Channel Gene Family (CLIC5) That Associates with the Actin Cytoskeleton of Placental Microvilli. Mol Biol Cell 11, 1509 (2000).

99. V.L. Bonilha, E. Rodriguez-Boulan, Polarity and Developmental Regulation of Two PDZ Proteins in the Retinal Pigment Epithelium. Invest Ophthalmol Vis Sci 42, 3274 (2001).

100. F. Lozupone et al., Identification and Relevance of the CD95-binding Domain in the N-terminal Region of Ezrin. J Biol Chem 279, 9199 (, 2004).

101. L. Heiska et al., Association of Ezrin with Intercellular Adhesion Molecule-1 and -2 (ICAM-1 and ICAM-2): regulation by phosphatidylinositol-4,5-bisphosphate. J Biol Chem 273, 21893 (1998).

102. P. Poullet et al., Ezrin Interacts with Focal Adhesion Kinase and Induces Its Activation Independently of Cell-matrix Adhesion. J Biol Chem 276, 37686 (2001).

103. J. Austermann, A.R. Nazmi, C. Müller-Tidow, V. Gerke, Characterization of the $Ca2^{+}$-regulated Ezrin-S100P Interaction and Its Role in Tumor Cell Migration. J Biol Chem 283, 29331 (2008).

104. F. Granes, J.M. Urena, N. Rocamora, S. Vilaro, Ezrin links syndecan-2 to the cytoskeleton. J Cell Sci 113, 1267 (2000).

105. A. Ivetic, J. Deka, A. Ridley, A. Ager, The Cytoplasmic Tail of L-selectin Interacts with Members of the Ezrin-Radixin-Moesin (ERM) Family of Proteins: cell activation-dependent binding of Moesin but not Erzin. J Biol Chem 277, 2321 (2002).

106. J.M. Serrador et al., CD43 Interacts With Moesin and Ezrin and Regulates Its Redistribution to the Uropods of T Lymphocytes at the Cell-Cell Contacts. Blood 91, 4632 (1998).

107. S. Peng et al., The expression of ezrin in NPC and its interaction with NGX6, a novel candidate suppressor. Cancer Sci 98, 341 (2007).

108. C. Jin et al., PKA-mediated protein phosphorylation regulates ezrin–WWOX interaction. Biochem Biophys Res Commun 341, 784 (2006).

109. O. Barreiro et al., Dynamic interaction of VCAM-1 and ICAM-1 with moesin and ezrin in a novel endothelial docking structure for adherent leukocytes. J Cell Biol 157, 1233 (2002).

110. R.S. Westphal, S.H. Soderling, N.M. Alto, L.K. Langeberg, J.D. Scott, Scar/WAVE-1, a Wiskott-Aldrich syndrome protein, assembles an actin-associated multi-kinase scaffold. EMBO J 19, 4589 (2000).

111. S.H. Soderling et al., The WRP component of the WAVE-1 complex attenuates Rac-mediated signalling. Nat Cell Biol 4, 970 (2002).

112. M. Innocenti et al., Abi1 is essential for the formation and activation of a WAVE2 signalling complex. Nat Cell Biol 6, 319 (2004).

113. S. Suetsugu, H. Miki, T. Takenawa, Identification of Two Human WAVE/SCAR Homologues as General Actin Regulatory Molecules Which Associate with the Arp2/3 Complex. Biochem Biophys Res Commun 260, 296 (1999).

114. N.N. Danial et al., BAD and glucokinase reside in a mitochondrial complex that integrates glycolysis and apoptosis. Nature 424, 952 (2003).

115. S. Eden, R. Rohatgi, A. V. Podtelejnikov, M. Mann, M. W. Kirschner, Mechanism of regulation of WAVE1-induced actin nucleation by Rac1 and Nck. Nature 418, 790 (2002).

116. Y. Kim et al., Phosphorylation of WAVE1 regulates actin polymerization and dendritic spine morphology. Nature 442, 814 (2006).

117. M.A. Salazar et al., Tuba, a Novel Protein Containing Bin/Amphiphysin/Rvs and Dbl Homology Domains, Links Dynamin to Regulation of the Actin Cytoskeleton. J Biol Chem 278, 49031 (2003).

118. K.S. Song et al., Identification and characterization of a G-protein regulatory motif in WAVE1. FEBS Letters 580, 1993 (2006).

119. R.F. Wu, Y. Gu, Y.C. Xu, F.E. Nwariaku, L.S. Terada, Vascular Endothelial Growth Factor Causes Translocation of p47phox to Membrane Ruffles through WAVE1. J Biol Chem 278, 36830 (2003).

120. S. Tsukita, K. Oishi, N. Sato, J. Sagara, A. Kawai, ERM family members as molecular linkers between the cell surface glycoprotein CD44 and actin-based cytoskeletons. J Cell Biol 126, 391 (1994).

121. H. Li et al., Identification, Localization, and Function in Steroidogenesis of PAP7: A Peripheral-Type Benzodiazepine Receptor- and PKA (RIα)-Associated Protein. Mol Endocrinol 15, 2211 (2001).

122. J.I. Sbodio, S. W. Hicks, D. Simon, C.E. Machamer, GCP60 Preferentially Interacts with a Caspase-generated Golgin-160 Fragment. J Biol Chem 281, 27924 (2006).

123. J. Sasaki, K. Ishikawa, M. Arita, K. Taniguchi, ACBD3-mediated recruitment of PI4KB to picornavirus RNA replication sites. EMBO J 31, 754 (2012).

124. Y. Okazaki et al., DMT1 (IRE) expression in intestinal and erythroid cells is regulated by peripheral benzodiazepine receptor-associated protein 7. Am J Physiol Gastrointest Liver Physiol 302, G1180 (2012).

125. M. Sohda et al., Identification and Characterization of a Novel Golgi Protein, GCP60, That Interacts with the Integral Membrane Protein Giantin. J Biol Chem 276, 45298 (2001).

126. M. Grönholm et al., Merlin Links to the cAMP Neuronal Signaling Pathway by Anchoring the RIβ Subunit of Protein Kinase A. J Biol Chem 278, 41167 (2003).

127. J.L. Kissil et al., Merlin, the Product of the Nf2 Tumor Suppressor Gene, Is an Inhibitor of the p21-Activated Kinase, Pak1. Mol Cell 12, 841 (2003).

128. D.R. Scoles et al., Neurofibromatosis 2 tumour suppressor schwannomin interacts with [beta]II-spectrin. Nat Genet 18, 354 (1998).

129. A. Murthy et al., NHE-RF, a Regulatory Cofactor for Na^+-H+Exchange, Is a Common Interactor for Merlin and ERM (MERM) Proteins. J Biol Chem 273, 1273 (1998).

130. L. Goutebroze, E. Brault, C. Muchardt, J. Camonis, G. Thomas, Cloning and Characterization of SCHIP-1, a Novel Protein Interacting Specifically with Spliced Isoforms and Naturally Occurring Mutant NF2 Proteins. Mol Cell Biol 20, 1699 (2000).

131. D. Diviani, L.K. Langeberg, S.J. Doxsey, J.D. Scott, Pericentrin anchors protein kinase A at the centrosome through a newly identified RII-binding domain.Curr Biol 10, 417 (2000).

132. Q. Li et al., Kendrin/pericentrin-B, a centrosome protein with homology to pericentrin that complexes with PCM-1. J Cell Sci 114, 797 (2001).

133. M. Fabbro et al., Cdk1/Erk2- and Plk1-Dependent Phosphorylation of a Centrosome Protein, Cep55, Is Required for Its Recruitment to Midbody and Cytokinesis. Dev Cell 9, 477 (2005).

134. K. Miyoshi et al., DISC1 localizes to the centrosome by binding to kendrin. Biochem Biophys Res Commun 317, 1195 (2004).

135. J.E. Sillibourne, B. Delaval, S. Redick, M. Sinha, S.J. Doxsey, Chromatin Remodeling Proteins Interact with Pericentrin to Regulate Centrosome Integrity. Mol Biol Cell 18, 3667 (2007).

136. S.H. Tynan, A. Purohit, S.J. Doxsey, R.B. Vallee, Light Intermediate Chain 1 Defines a Functional Subfraction of Cytoplasmic Dynein Which Binds to Pericentrin. J Biol Chem 275, 32763 (2000).

137. R.A. Obar, J. Dingus, H. Bayley, R. B. Vallee, The RII subunit of camp-dependent protein kinase binds to a common amino-terminal domain in microtubule-associated proteins 2A, 2B, and 2C. Neuron 3, 639 (1989).

138. R.S. Ozer, S. Halpain, Phosphorylation-dependent Localization of Microtubule-associated Protein MAP2c to the Actin Cytoskeleton. Mol Biol Cell 11, 3573 (2000).

139. A.D. Roses et al., Morphological, Biochemical, and Genetic Support for an Apolipoprotein E Effect on Microtubular Metabolisma. Ann NY Acad Sci 777, 146 (1996).

140. S.P.Zamora-Leon, A. Bresnick, J. M. Backer, B. Shafit-Zagardo, Fyn Phosphorylates Human MAP-2c on Tyrosine 67. J Biol Chem 280, 1962 (2005).

141. R.W.L. Lim, S. Halpain, Regulated Association of Microtubule-associated Protein 2 (MAP2)with Src and Grb2: Evidence for MAP2 as a Scaffolding Protein. J Biol Chem 275, 20578 (2000).

142. P.T. Todorov, R.E. Hardisty, S.D. Brown, Myosin VIIA is specifically associated with calmodulin and microtubule-associated protein-2B (MAP-2B). Biochem. J. 354, 267 (2001).

143. H. Herrmann, G. Wiche, Plectin and IFAP-300K are homologous proteins binding to microtubule-associated proteins 1 and 2 and to the 240-kilodalton subunit of spectrin. J Biol Chem 262, 1320 (1987).

144. D. Cerecedo, B. Cisneros, R. Suárez-Sánchez, E. Hernández-González, I. Galván, β-Dystroglycan modulates the interplay between actin and microtubules in human-adhered platelets. Br J Haematol 141, 517 (2008).

145. N.M. Alto, J. Soderling, J.D. Scott, Rab32 is an A-kinase anchoring protein and participates in mitochondrial dynamics. J Cell Biol 158, 659 (2002).

146. M. Bui et al., Rab32 Modulates Apoptosis Onset and Mitochondria-associated Membrane (MAM) Properties. J Biol Chem 285, 31590 (2010).

147. K. Tamura et al., Varp Is a Novel Rab32/38-binding Protein That Regulates Tyrp1 Trafficking in Melanocytes. Mol Biol Cell 20, 2900 (2009).

148. J.J. Bultema, A.L. Ambrosio, C.L. Burek, S. M. Di Pietro, BLOC-2, AP-3, and AP-1 Proteins Function in Concert with Rab38 and Rab32 Proteins to Mediate Protein Trafficking to Lysosome-related Organelles. J Biol Chem 287, 19550 (2012).

149. H. Li, R. Adamik, G. Pacheco-Rodriguez, J. Moss, M. Vaughan, Protein kinase A-anchoring (AKAP) domains in brefeldin A-inhibited guanine nucleotide-exchange protein 2 (BIG2). Proc Natl Acad Sci U S A 100, 1627 (2003).

150. K.-F. Xu et al., Interaction of BIG2, a brefeldin A-inhibited guanine nucleotide-exchange protein, with exocyst protein Exo70. Proc Natl Acad Sci U S A 102, 2784 (2005).

151. E.I. Charych et al., The brefeldin A-inhibited GDP/GTP exchange factor 2, a protein involved in vesicular trafficking, interacts with the β subunits of the GABAA receptors. J Neurochem 90, 173 (2004).

152. R. Ishizaki, H.-W. Shin, S.M.M. Iguchi-Ariga, H. Ariga, K. Nakayama, AMY-1 (associate of Myc-1) localization to the trans-Golgi network through interacting with BIG2, a guanine-nucleotide exchange factor for ADP-ribosylation factors. Genes Cells 11, 949 (2006).

153. A. Islam et al., cAMP-dependent Protein Kinase A (PKA) Signaling Induces TNFR1 Exosome-like Vesicle Release via Anchoring of PKA Regulatory Subunit RIIβ to BIG2.J Biol Chem 283, 25364 (2008).

154. E. Puxeddu et al., Interaction of phosphodiesterase 3A with brefeldin A-inhibited guanine nucleotide-exchange proteins BIG1 and BIG2 and effect on ARF1 activity. Proc Natl Acad Sci USA 106, 6158 (2009).

155. F. Kuroda, J. Moss, M. Vaughan, Regulation of brefeldin A-inhibited guanine nucleotide-exchange protein 1 (BIG1) and BIG2 activity via PKA and protein phosphatase 1γ. Proc Natl Acad Sci USA 104, 3201 (February 2007).

156. J. Zhang et al., Brefeldin A-inhibited Guanine Exchange Factor 2 Regulates Filamin A Phosphorylation and Neuronal Migration. J Neurosci 32, 12619 (2012).

157. J. Sarparanta, Biology of myospryn: what's known? J Muscle Res Cell Motil 29, 177 (2008).

158. J.G. Reynolds, S.A. McCalmon, T. Tomczyk, F.J. Naya, Identification and mapping of protein kinase A binding sites in the costameric protein myospryn. Biochim Biophys Acta 1773, 891 (2007).

159. J. Sarparanta et al., Interactions with M-band Titin and Calpain 3 Link Myospryn (CMYA5) to Tibial and Limb-girdle Muscular Dystrophies. J Biol Chem 285, 30304 (2010).

160. M.A. Russell et al., The intermediate filament protein, synemin, is an AKAP in the heart. Arch Biochem Biophys 456, 204 (2006).

161. Y. Mizuno et al., Desmuslin, an intermediate filament protein that interacts with α-dystrobrevin and desmin. Proc Natl Acad Sci U S A 98, 6156 (2001).

162. R.C. Bhosle, D.E. Michele, K.P. Campbell, Z. Li, R. M. Robson, Interactions of intermediate filament protein synemin with dystrophin and utrophin. Biochem Biophys Res Commun 346, 768 (2006).

163. N. Sun, T.W. Huiatt, D. Paulin, Z. Li, R.M. Robson, Synemin interacts with the LIM domain protein zyxin and is essential for cell adhesion and migration. Exp Cell Res 316, 491 (2010).

164. A. Pitre, N. Davis, M. Paul, A. W. Orr, O. Skalli, Synemin promotes AKT-dependent glioblastoma cell proliferation by antagonizing PP2A. Mol Biol Cell 23, 1243 (2012).

165. G.M. Uys et al., Myomegalin is a novel A-kinase anchoring protein involved in the phosphorylation of cardiac myosin binding protein C. BMC Cell Biol 12, 18 (2011).

166. I. Verde et al., Myomegalin Is a Novel Protein of the Golgi/Centrosome That Interacts with a Cyclic Nucleotide Phosphodiesterase. J Biol Chem 276, 11189 (2001).

167. P. Küssel-Andermann et al., Unconventional Myosin VIIA Is a Novel A-kinase-anchoring Protein. J Biol Chem 275, 29654 (2000).

168. B. Boeda et al., Myosin VIIa, harmonin and cadherin 23, three Usher I gene products that cooperate to shape the sensory hair cell bundle. EMBO J 21, 6689 (2002).

169. M. Velichkova et al., A human homologue of Drosophila kelch associates with myosin-VIIa in specialized adhesion junctions. Cell Motil Cytoskeleton 51, 147 (2002).

170. M. Fukuda, T.S. Kuroda, Slac2-c (Synaptotagmin-like Protein HomologueLacking C2 Domains-c), a Novel Linker Protein that Interacts with Rab27, Myosin Va/VIIa, and Actin. J Biol Chem 277, 43096 (2002).

171. A. El-Amraoui et al., MyRIP, a novel Rab effector, enables myosin VIIa recruitment to retinal melanosomes. EMBO Rep 3, 463 (2002).

172. P.Kussel-Andermann et al., Vezatin, a novel transmembrane protein, bridges myosin VIIA to the cadherin-catenins complex. EMBO J 19, 6020 (2000).

173. S.E. Fiedler, R.V. Schillace, C.J. Daniels, S.F. Andrews, D.W. Carr, Myeloid translocation gene 16b is a dual A-kinase anchoring protein that interacts selectively with plexins in a phospho-regulated manner. FEBS Letters 584, 873 (2010).

174. C. Hundsrucker et al., Glycogen Synthase Kinase 3β Interaction Protein Functions as an A-kinase Anchoring Protein. J Biol Chem 285, 5507 (2010).

175. G. Pidoux et al., Optic atrophy 1 is an A-kinase anchoring protein on lipid droplets that mediates adrenergic control of lipolysis. EMBO J 30, 4371 (2011).

176. A. Scholten et al., Analysis of the cGMP/cAMP Interactome Using a Chemical Proteomics Approach in Mammalian Heart Tissue Validates Sphingosine Kinase Type 1-interacting Protein as a Genuine and Highly Abundant AKAP. J Proteome Res 5, 1435 (2006).

177. D. Kovanich et al., Sphingosine Kinase Interacting Protein is an A-Kinase Anchoring Protein Specific for Type I cAMP-Dependent Protein Kinase. ChemBioChem 11, 963 (2010).

178. C.K. Means et al., An entirely specific type I A-kinase anchoring protein that can sequester two molecules of protein kinase A at mitochondria. Proc Natl Acad Sci USA 108, E1227 (2011).

179. P.P. Burgers et al., A Small Novel A-Kinase Anchoring Protein (AKAP) That Localizes Specifically Protein Kinase A-Regulatory Subunit I (PKA-RI) to the Plasma Membrane. J Biol Chem 287, 40535 (2012).

180. L.J.-s. Huang, K. Durick, J.A. Weiner, J. Chun, S.S. Taylor, Identification of a Novel Protein Kinase A Anchoring Protein That Binds Both Type I and Type II Regulatory Subunits. J Biol Chem 272, 8057 (1997).

181. L.J.-s. Huang, K. Durick, J.A. Weiner, J. Chun, S.S. Taylor, D-AKAP2, a novel protein kinase A anchoring protein with a putative RGS domain. Proc Natl Acad Sci USA 94, 11184 (1997).

182. K. Miki, E.M. Eddy, Identification of Tethering Domains for Protein Kinase A Type Iα Regulatory Subunits on Sperm Fibrous Sheath Protein FSC1. J Biol Chem 273, 34384 (1998).

183. R. Angelo, C.S. Rubin, Molecular Characterization of an Anchor Protein (AKAPCE) That Binds the RI Subunit (RCE) of Type I Protein Kinase A from Caenorhabditis elegans. J Biol Chem 273, 14633 (1998).

184. H.M. Rubino, M. Dammerman, B. Shafit-Zagardo, J. Erlichman, Localization and characterization of the binding site for the regulatory subunit of type II cAMP-dependent protein kinase on MAP2. Neuron 3, 631 (1989).

185. D.W. Carr et al., Interaction of the regulatory subunit (RII) of cAMP-dependent protein kinase with RII-anchoring proteins occurs through an amphipathic helix binding motif. J Biol Chem 266, 14188 (1991).

186. N.M. Alto et al., Bioinformatic design of A-kinase anchoring protein-in silico: A potent and selective peptide antagonist of type II protein kinase A anchoring. Proc Natl Acad Sci USA 100, 4445 (2003).

187. L.L. Burns-Hamuro et al., Designing isoform-specific peptide disruptors of protein kinase A localization. Proc Natl Acad Sci USA 100, 4072 (2003).

188. C.R. Carlson et al., Delineation of Type I Protein Kinase A-selective Signaling Events Using an RI Anchoring Disruptor. J Biol Chem 281, 21535 (2006).

189. M.G. Gold et al., Molecular Basis of AKAP Specificity for PKA Regulatory Subunits. Mol Cell 24, 383 (2006).

190. L.L. Burns, J.M. Canaves, J.K. Pennypacker, D.K. Blumenthal, S.S. Taylor, Isoform Specific Differences in Binding of a Dual-Specificity A-Kinase Anchoring Protein to Type I and Type II Regulatory Subunits of PKA. Biochemistry 42, 5754 (2003).

191. P. Banky, L.J.-S. Huang, S.S. Taylor, Dimerization/Docking Domain of the Type Iα Regulatory Subunit of cAMP-dependent Protein Kinase. J Biol Chem 273, 35048 (1998).

192. P. Banky et al., Isoform-specific Differences between the Type Iα and IIα Cyclic AMP-dependent Protein Kinase Anchoring Domains Revealed by Solution NMR. J Biol Chem 275, 35146 (2000).

193. P. Banky et al., Related Protein–Protein Interaction Modules Present Drastically Different Surface Topographies Despite A Conserved Helical Platform. J Mol Biol 330, 1117 (2003).

194. F.S. Kinderman et al., A Dynamic Mechanism for AKAP Binding to RII Isoforms of cAMP-Dependent Protein Kinase. Mol Cell 24, 397 (2006).

195. D.A. León, F. W. Herberg, P. Banky, S.S. Taylor, A Stable α-Helical Domain at the N Terminus of the RIα Subunits of cAMP-dependent Protein Kinase Is a Novel Dimerization/Docking Motif. J Biol Chem 272, 28431 (1997).

196. M.G. Newlon et al., A novel mechanism of PKA anchoring revealed by solution structures of anchoring complexes. EMBO J 20, 1651 (2001).

197. M.G. Newlon et al., The molecular basis for protein kinase A anchoring revealed by solution NMR. Nat Struct Mol Biol 6, 222 (1999).

198. G.N. Sarma et al., Structure of D-AKAP2:PKA RI Complex: Insights into AKAP Specificity and Selectivity. Structure 18, 155 (2010).

199. M.L. Robinson, M.A. Wallert, C.A. Reinitz, J.B. Shabb, Association of the Type I Regulatory Subunit of cAMP-Dependent Protein Kinase with Cardiac Myocyte Sarcolemma. Arch Biochem Biophys 330, 181 (1996).

200. N. Aspres, N.R. Bleasel, K.M. Stapleton, Genetic testing of the family with a Carney-complex member leads to successful early removal of an asymptomatic atrial myxoma in the mother of the patient. Australas J Dermatol 44, 121 (2003).

201. J. Bertherat et al., Mutations in Regulatory Subunit Type 1A of Cyclic Adenosine 5′-Monophosphate-Dependent Protein Kinase (PRKAR1A): Phenotype Analysis in 353 Patients and 80 Different Genotypes. J Clin Endocrinol Metab 94, 2085 (2009).

202. J. Tröger, M.C. Moutty, P. Skroblin, E. Klussmann, A-kinase anchoring proteins as potential drug targets. Br J Pharmacol 166, 420 (2012).

203. G.K. Carnegie, C.K. Means, J.D. Scott, A-kinase anchoring proteins: From protein complexes to physiology and disease. IUBMB Life 61, 394 (2009).

204. J.D. Scott, L.F. Santana, A-Kinase Anchoring Proteins. Circulation 121, 1264 (2010).

205. P.C. Gray, V.C. Tibbs, W.A. Catterall, B.J. Murphy, Identification of a 15-kDa cAMP-dependent Protein Kinase-anchoring Protein Associated with Skeletal Muscle L-type Calcium Channels. J Biol Chem 272, 6297 (1997).

206. Y. Fu et al., Deletion of the Distal C Terminus of CaV1.2 Channels Leads to Loss of β-Adrenergic Regulation and Heart Failure in Vivo. J Biol Chem 286, 12617 (2011).

207. L. Chen, R.S. Kass, Dual roles of the A kinase-anchoring protein Yotiao in the modulation of a cardiac potassiumchannel: A passive adaptor versus an active regulator. Eur J Cell Biol 85, 623 (2006).

208. L. Chen et al., Mutation of an A-kinase-anchoring protein causes long-QT syndrome. Proc Natl Acad Sci USA 104, 20990 (, 2007).

209. S. Kammerer et al., Amino acid variant in the kinase binding domain of dual-specific A kinase-anchoring protein 2: A disease susceptibility polymorphism. Proc Natl Acad Sci USA 100, 4066 (2003).

210. W.G. Tingley et al., Gene-trapped mouse embryonic stem cell-derived cardiac myocytes and human genetics implicate AKAP10 in heart rhythm regulation. Proc Natl Acad Sci U S A 104, 8461 (2007).

211. C.M. Mayers et al., The Rho Guanine Nucleotide Exchange Factor AKAP13 (BRX) Is Essential for Cardiac Development in Mice. J Biol Chem 285, 12344 (2010).

212. R.S.Y. Wong, Apoptosis in cancer: from pathogenesis to treatment. J Exp Clin Canc Res 30, 87 (2011).

213. M.P. Mattson, Apoptosis in neurodegenerative disorders. Nat Rev Mol Cell Biol 1, 120 (2000).

214. H. Puthalakath, A. Strasser, Keeping killers on a tight leash: transcriptional and post-translational control of the pro-apoptotic activity of BH3-only proteins. Cell Death Differ 9, 505 (2002)

215. M.O. Hengartner, H.R. Horvitz, C. elegans cell survival gene ced-9 encodes a functional homolog of the mammalian proto-oncogene bcl-2. Cell 76, 665 (1994).

216. G. Lettre, M.O. Hengartner, Developmental apoptosis in C. elegans: a complex CEDnario. Nat Rev Mol Cell Biol 7, 97 (2006).

217. E. Lomonosova, G. Chinnadurai, BH3-only proteins in apoptosis and beyond: an overview. Oncogene 27, S2 (0000).

218. A.M. Petros, E.T. Olejniczak, S.W. Fesik, Structural biology of the Bcl-2 family of proteins. Biochim Biophys Acta 1644, 83 (2004).

219. T. Lindsten et al., The Combined Functions of Proapoptotic Bcl-2 Family Members Bak and Bax Are Essential for Normal Development of Multiple Tissues. Mol Cell 6, 1389 (2000).

220. M.C. Wei et al., Proapoptotic BAX and BAK: A Requisite Gateway to Mitochondrial Dysfunction and Death. Science 292, 727 (2001).

221. C.L. Day et al., Structure of the BH3 Domains from the p53-Inducible BH3-Only Proteins Noxa and Puma in Complex with Mcl-1. J Mol Biol 380, 958 (2008).

222. J.E. Chipuk, T. Moldoveanu, F. Llambi, M.J. Parsons, D.R. Green, The BCL-2 Family Reunion. Mol Cell 37, 299 (2010).

223. J.E. Chipuk, D.R. Green, PUMA cooperates with direct activator proteins to promote mitochondrial outer membrane permeabilization and apoptosis. Cell Cycle 8, 2692 (2009).

224. D. Ren et al., BID, BIM, and PUMA Are Essential for Activation of the BAX- and BAK-Dependent Cell Death Program. Science 330, 1390 (2010).

225. N. Inohara, L. Ding, S. Chen, G. Nunez, harakiri, a novel regulator of cell death, encodes a protein that activates apoptosis and interacts selectively with survival-promoting proteins Bcl-2 and Bcl-XL. EMBO J 16, 1686 (1997).

226. K. Nakano, K.H. Vousden, PUMA, a Novel Proapoptotic Gene, Is Induced by p53. Mol Cell 7, 683 (2001).

227. H. Puthalakath et al., Bmf: A Proapoptotic BH3-Only Protein Regulated by Interaction with the Myosin V Actin Motor Complex, Activated by Anoikis. Science 293, 1829 (2001).

228. E. Yang et al., Bad, a heterodimeric partner for Bcl-xL and Bcl-2, displaces bax and promotes cell death. Cell 80, 285 (1995).

229. J.E. Chipuk, D.R. Green, How do BCL-2 proteins induce mitochondrial outer membrane permeabilization? Trends Cell Biol 18, 157 (2008).

230. A. Scholten, T.A.B. van Veen, M.A. Vos, A.J.R. Heck, Diversity of cAMP-Dependent Protein Kinase Isoforms and Their Anchoring Proteins in Mouse Ventricular Tissue. J Proteome Res 6, 1705 (2007).

Chapter 2

Applications of Stable Isotope Dimethyl Labeling in Quantitative Proteomics

Duangnapa Kovanich
Salvatore Cappadona
Reinout Raijmakers
Shabaz Mohammed
Arjen Scholten
Albert J.R. Heck

Biomolecular Mass Spectrometry and Proteomics,
Utrecht Institute for Pharmaceutical Sciences and Bijvoet Center for Biomolecular Research,
Utrecht University, Padualaan 8, 3584 CH, Utrecht, The Netherlands

Based on Anal Bioanal Chem. 2012 , 404, 4, 991-1009

2.1 Abstract

Robust and accurate quantification of protein expression levels is essential for deciphering the dynamics of proteomes. Mass spectrometry provides an excellent platform for quantitative proteomics (1-4) with the most common and precise quantitative approaches using stable isotopes (5,6). In recent years several quantitative mass spectrometry based technologies have evolved to interrogate the complexity, interconnectivity and dynamic nature of proteomes. Isotope incorporation can occur either metabolically in cell culture (7,8), by labeling whole organisms (9), or via chemical labeling at the protein (10) or peptide level (11-13). A relative newcomer in the latter category is dimethyl labeling, sometimes also referred to as reductive dimethylation. In this review we focus solely on this method, and describe its history, mechanism, procedures and applications in the proteomics field.

2.2 Introduction

The chemical reaction employed for introducing dimethyl groups possessing heavy stable isotopes has been known for a long time, and was, for instance, already used more than 30 years ago for labeling of proteins to increase sensitivity for 13C NMR analysis (14). It was only in 2003 that stable isotope dimethyl labeling was first introduced as a quantitative proteomics technology by Hsu et al.(15). Highly selective dimethylation of primary amines (N termini and lysine residue side chain) is achieved through reductive amination using formaldehyde and cyanoborohydride (Figure 1). The reaction, which is optimally performed at near neutral pH, involves the formation of a Schiff base (reaction of formaldehyde with the amine), which is subsequently reduced by cyanoborohydride. The reaction is very fast and goes to completion in only a few minutes, does not give rise to any significant side products (14), and has no negative impact on tandem MS peptide identification. Using dimethylation all primary amines present in the sample are converted, with the only exception being an N-terminal proline, in which a monomethylamine is formed (16). This means that, when using trypsin to digest protein samples, peptides generated from cleavage after arginine will have a single label (at their N-terminus) and lysine cleaved peptides will have two labels (N-terminus and lysine side chain). If one prefers the same number of dimethyl groups per peptide then one can first protect the lysine side chains by guanidination, resulting in only N-terminal dimethylation, a method that has been termed 2MEGA (17).

The original setup used two labels and relied on the incorporation of only deuterium as a heavy isotope. The analysis of up to four different samples using only deuterium isotopes has been shown, but required the use of endoproteinase Lys-C instead of trypsin to ensure sufficient mass difference between the differentially labeled peptides, because the mass difference per labeling event in that setup was only 2 Dalton (18). Boersema et al. developed a labeling scheme that allowed the simultaneous analysis of three samples, while retaining a mass difference of 4 Dalton with the inclusion of formaldehyde containing also 13C (Figure 1). It was shown that such a scheme allowed reliable quantification of trypsin generated peptides that only contain a single labeling site (i.e. arginine cleaved peptides) (13). Although this triple labeling greatly reduced the amount of overlapping between isotopic peaks of different labels, it was shown very recently that the quantitation of such peptides can be further improved by in silico deconvolution of the isotope clusters (19).

Over the last couple of years, dimethyl labeling has been shown to be compatible with a variety of common peptide separation and enrichment strategies, including separation of peptides by regular C18 reversed phase liquid chromatography, high-pH reversed phase liquid chromatography, strong cation exchange (SCX), hydrophilic interaction chromatography (HILIC) (13, 20-22). The deuterium present in some of the labels has been shown to lead to a small shift in retention time for the deuterium containing peptides, but as long as quantification of the peptides is based on the entire extracted ion peaks of each of the three m/z values for a peptide, this has little to no effect on quantitation accuracy (23). In addition to generic separation strategies, dimethylation has also been used successfully in combination with specific enrichment methods, especially for phosphorylated peptides. These include combinations with immobilized metal ion affinity chromatography (IMAC) (24, 25) and titanium dioxide affinity chromatography (TiO2) (26) enrichment as well as the specific immunoprecipitation of peptides containing phosphorylated tyrosine residues (27).

Since most chemical labeling strategies for quantitative proteomics are sensitive to deviations in reaction efficiency and sample handling, efforts have been made towards the automation and robustness of the dimethylation procedure. In 2008, Raijmakers et al. showed that it was possible to perform reductive amination on peptides that were non-covalently bound to C18 solid phase material and that this could be performed online with LC-MS/MS analysis in an automated fashion (28). As this method placed restrictions on the size and complexity of the sample to be labeled and analyzed, this was later extended to automated labeling combined with SCX separation (29) and even automated labeling combined with online two dimensional separation (C18-SCX) (30). A very detailed protocol describing the original in-solution labeling as well as the solid phase labeling and automated online labeling is available (31).

Although most often performed at the peptide level, stable isotope dimethyl labeling can also be done on intact proteins, for example to aid the identification of protein N-termini (32,33). It is more difficult to force the reaction to completion and, if used for proteomics approaches, it places restraints on the proteases that can be used, as neither trypsin nor Lys-C cleave dimethylated lysine residues (34). The use of the dimethylation reaction has also been explored for other purposes than quantitative proteomics, like the improvement of peptide identification by ETD fragmentation (35) and as an aid in the de novo sequencing of peptides and proteins for which no genome sequences are available (35). While those applications might be more specialized, the stable isotope dimethylation procedure is now being applied widely for quantitative proteomics, especially for samples where metabolic labeling is not easily achievable, like for example patient material or other tissue samples, as described in more detail later in this review. In this review we will not further describe in detail protocols for stable isotope dimethyl labeling, as these do exist and are readily available (31,36), but instead focus on applications and data analysis.

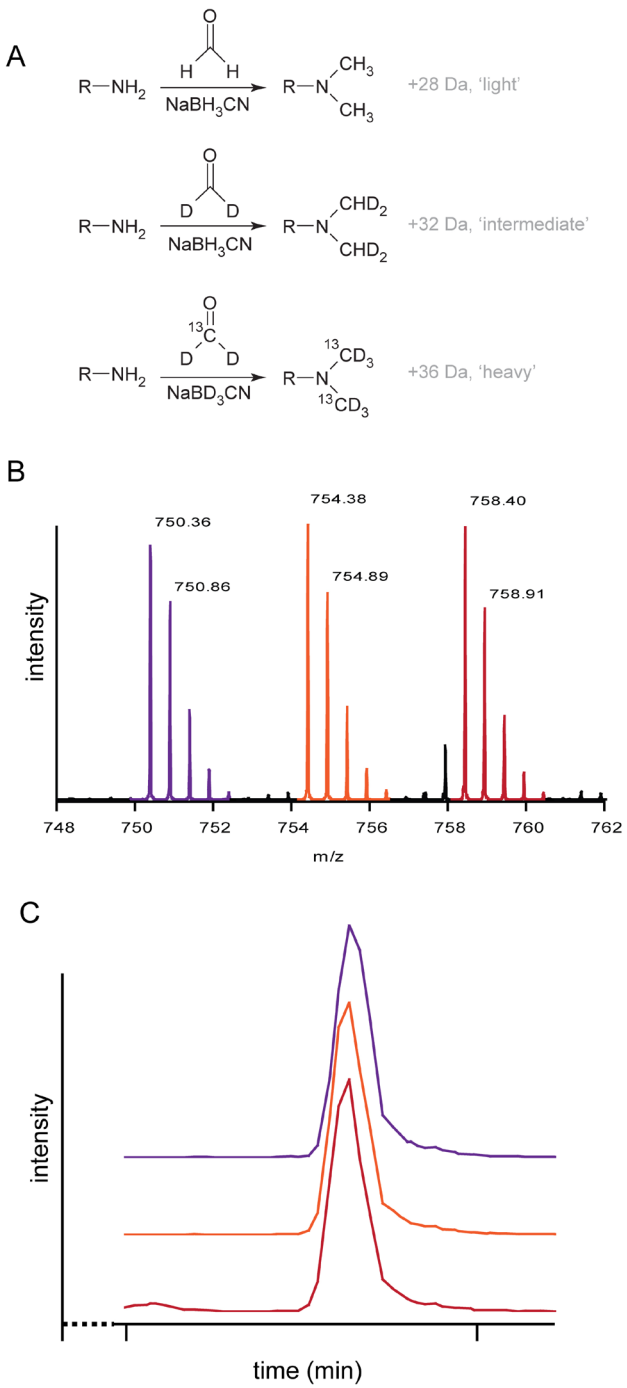

Figure 1 > Basic concepts of stable isotope dimethyl labeling.

A) *Labeling scheme for stable isotope dimethyl labeling. The reaction is performed at neutral pH, involves the formation of a Schiff base via the reaction of formaldehyde with the primary amines, which is then reduced by cyanoborohydride. Using different isotopomers of formaldehyde the mass added per labeling event can be varied.* **B)** *Mass spectrum and* **C)** *XIC of BSA peptide YICDNQDTISSK triple labeled with light (purple), intermediate (orange) and heavy (red) dimethyl labels. The labeled peptides are shifted by 28.03, 32.06 and 36.08 m/z respectively to the original m/z of 722.83 of the peptide, corresponding to two labeling events and the peptide ion being doubly charged. Within reason these three peptide isotopomers co-elute. Adapted from ref (31).*

2.3 Data Analysis

From a bioinformatics perspective, stable isotope dimethylation is a relatively straightforward technique. Quantification is performed at the MS level, by comparing the relative abundances of the differentially labeled peptides, while identification is achieved at the MS2 level, by setting N-terminal and lysine dimethylation as peptide modification. Two main threats frequently affecting stable isotope labeling (37) have been reported to possibly hamper the quantification of dimethylated peptides: retention time shifts between the labeled pairs and overlap of their isotopic clusters. Nevertheless, effective strategies to overcome both issues have been devised since the first studies introducing the procedure.

Retention time shifts can affect heavy deuterated peptides when using reverse phase chromatography, causing them to elute prior to the corresponding light ones (38). When labeled pairs are deemed chromatographically resolved, retention time shifts can simply be circumvented by quantifying peptides XICs (eXtracted Ion Chromatograms) rather than their intensities in one particular scan (31). A similar approach was originally described in the seminal publication by Hsu et al. (15), in which all spectra containing both the H4– and D4¬–labeled isotopologues of a given peptide were combined to produce a composite MS spectrum. The number of combined spectra was dependent on the peptide elution time and on the instrument duty cycle: at an acquisition rate of one scan per second, this typically meant combining 20 to 60 spectra, which was generally sufficient to span over the whole peptide elution profile and mathematically equivalent to performing whole XIC area integration. By this strategy, the inaccuracy in quantification caused by differential elution between the deuterated and the non-deuterated peptides, the so-called deuterium effect, was found to be minor. Peptide ratios were then calculated from the relative intensities of the monoisotopic peaks in the composite MS spectrum. Similar conclusions about a negligible deuterium effect were drawn by Ji et al. (23), who explicitly indicated the importance of summing up intensities over the entire elution profiles, in order to achieve accurate quantification. This group was also the first one to devise a dedicated strategy to tackle the overlapping issue (23), which occurs whenever the mass shift between the peptide pairs is smaller than their isotopic envelope and was found to become more critical as the mass of the original peptides increases, especially when approaching 3kDa (19). The problem can particularly affect dimethyl labeled peptides without a lysine residue, because they have a mass shift of only 4 Da between their isotopologues, resulting in the overlap of the fifth and consecutive peaks of the lighter peptide on the isotopic distribution of the heavier one. The overlap can clearly hamper quantification accuracy, with a typical upward bias for the heavy labeled peptides. In the proposed strategy, when overlapping occurred, the peptide sequences were submitted to the web-based tool MS–isotope, which is embedded in the Protein Prospector package (39), in order to model their theoretical isotopic distributions and to disentangle their relative contributions. In brief, the contribution of the lighter peptide was subtracted from the convoluted isotope pattern, in order to obtain the correct peak distribution of the heavier peptide. Correct peptide ratios were then determined by using the de-convoluted monoisotopic peak intensities.

In the first publications, quantification of the different peak intensities was performed manually, or by means of simple scripts that allowed for batch processing (40). At a later stage, when the technique started to gain popularity, many more software tools were adapted to allow for quantification of dimethyl-labeled peptides. Today, the most used tools include open source software, such as MSQuant (41), MaxQuant (42), PVIEW (43) and the XPRESS algorithm (44) embedded in the Trans Proteomics Pipeline (TPP) (45); vendors software, like Proteome Discoverer (Thermo Fisher Scientific); and commercial packages, like Mascot Distiller (http://www.matrixscience.com/distiller.html).

To our knowledge, no systematic study has been presented yet to compare the quantification performance of the different software packages on dimethyl labeling (as has been performed, for instance, for SILAC labeling (46)). For this reason, a few recommendations that can help driving the choice of the most appropriate tool will be given in the remainder of this introduction.

The initial consideration is purely pragmatic: the choice cannot prescind from the instruments and tools already present and commonly used in the laboratory. Proteome Discoverer and MaxQuant, for instance, can only analyze Thermo .raw data. Similarly, Mascot Distiller should be excluded a priori if Mascot is not the common or favorite database search for identification. The second consideration is merely economic: commercial packages like Mascot Distiller are quite expensive, but the cost can be justified when versatility is a prerequisite, in terms of supported instruments and labeling techniques. A third practical consideration regards software usability, which is often directly related to the presence of a good graphical user interface. To this extent, MSQuant has often been preferred to other tools that give a more 'black box' feeling and has become the most used tool for dimethyl labeling quantification. The software probably gained its popularity thanks to its interactive feedback during the quantification process, which allows for visual inspection of differentially expressed peptides and proper integration over their entire XICs, and because of the possibility to directly interface its output with post-processing tools like StatQuant (47) for normalization, outlier detection and further statistical analysis.

On a more technical note, the choice should also be based on the possibility to deal with the retention time shift and the overlapping issues introduced above. To overcome the deuterium effect, as already mentioned, simple strategies that calculate peptide ratios based on the area under the XIC peaks should be always preferred to more advanced algorithms like the one implemented in MaxQuant, which compares the intensities of the isotopologues in all scans across the XIC and fits a straight line through the origin of a their scatter plot. This algorithm was originally implemented for SILAC data and works very well for high quality data, but becomes unreliable in the presence of large retention time shifts. In this regard, Mascot Distiller gives the option to choose between the two quantification strategies. The second issue has been almost completely disregarded by quantification software, probably because it is known to only affect very large peaks. To our knowledge, Overlapping Peaks Finder (19) is still the only tool purposely devised for dimethyl labeling. The algorithm can be used in the form of a post-processing script and can correct quantitative results obtained by quantitation software that evaluate peptide ratios based on the XICs of their monoisotopic peaks ions, such as MSQuant and XPRESS.

The last consideration regards peptide identification. For most tools the quantification process is search-results driven, so only peptides identified by the database search are matched to the precursor signals for quantification. Recent algorithms, though, have proposed a multiplexed strategy for feature-driven quantification, in which feature detection is anticipated and drive database searches by better tailored constraints. When using MaxQuant, for instance, the labeling state of paired peptides is determined in advance, so as to allow separate database searches where each methylation state is set as a fixed modification. With a slightly different approach, PVIEW treats 'light' methylation as a fixed modification and 'intermediate' and 'heavy' methylations as modifications that are variable with respect to the 'light' one. These customized approaches should allow for a smaller search space than the one created by setting "light", "intermediate" and "heavy" methylations as variable modifications (as in Proteome Discoverer), thus reducing the probability to match false positive identifications.

As mentioned above, stable isotope dimethyl labeling has been incorporated into many types of experiments, albeit mostly for the purpose of relative quantification of protein expression. We have broadly sectioned these applications into global quantitative expression proteomics, quantitative analysis of post-translation modifications, and protein interaction studies. As more than 70 applications have been reported since 2003, we have made a selection and we highlight a few studies in more detail, but do also tabulate a more comprehensive list of published work using stable isotope dimethyl labeling.

2.4 Stable isotope dimethyl labeling for quantitative expression proteomics

The most widely used application of stable isotope dimethyl labeling in proteomics is as a quantification tool to determine globally the relative levels of protein expression between cellular or tissue states. A general strategy in an expression proteomics experiment using stable isotope dimethyl labeling can be illustrated by experiments performed by Munoz et al. to compare the proteomes of human embryonic stem cells (hSECs), human induced pluripotent stem cells (hiPSCs), and the fibroblast cells from which the latter originated (48). In order to characterize the differences and similarities in the protein content of hESC and hiPSC, an in-depth quantitative proteome profiling experiment was executed using two different hiPS cell lines, their two parental fibroblast cell lines and one hES cell line. Therefore, skin fibroblast (i.e. IMR90) and foreskin fibroblasts (4Skin) were reprogrammed into iPSc. A schematic of the experimental workflow is shown in Figure 2A. Cells were lysed and peptides were digested. hiPSC peptides were labeled with light, hESC peptides with intermediate, and parental fibroblast cell peptides with heavy isotopes. Labeled peptides were mixed in a 1:1:1 ratio based on total peptide amount determined by running an aliquot of the labeled samples on a regular LC-MS and comparing overall peptide signal intensity, fractionated by SCX and analyzed by LC-MS/MS. Independent biological replicates were performed, whereby the light and intermediate (hiPSC and hESC) isotope labels were swapped. Peptides appeared as a triplet in the mass spectra. Because the light, intermediate, and heavy peptides are nearly chemically identical, except for their mass difference (31), the ratio of peak intensities directly yields the ratio of the proteins in hiPSCs, hESCs, and fibroblasts, respectively.

Combining all the data from the 2 experiments and 2 replicates, more than 10,000 proteins were identified of which 7,000 proteins could be quantified. The comparative analysis focused on a smaller set of 2,683 proteins quantified in all experiments and replicates. The data revealed that protein expression of 98.7% of quantified proteins were alike in the hESC and hiPSC proteomes whereby only a small group of 58 proteins was found differentially expressed (figure 2B and 2C). These quantitative results indicate the reprogramming process remodeled the proteomes of both fibroblast cell lines to a proteome profile, which closely resembles the hESCs proteome making at the proteome level hiPSCs nearly indistinguishable from hESCs. In a comparable study Phanstiel et al. analyzed molecular differences between hESCs and hiPSCs at the proteome level, whereby they used iTRAQ isobaric tagging for quantification (49). Both studies came to the identical conclusion that at the proteome level hiPSCs are nearly indistinguishable from hESCs. Moreover, from a technical point of view it was also interesting to see that the depth of proteome coverage and accuracy and precision in protein quantification was alike, implying that stable isotope dimethyl labeling and iTRAQ can reach similar levels of depth and accuracy in quantification.

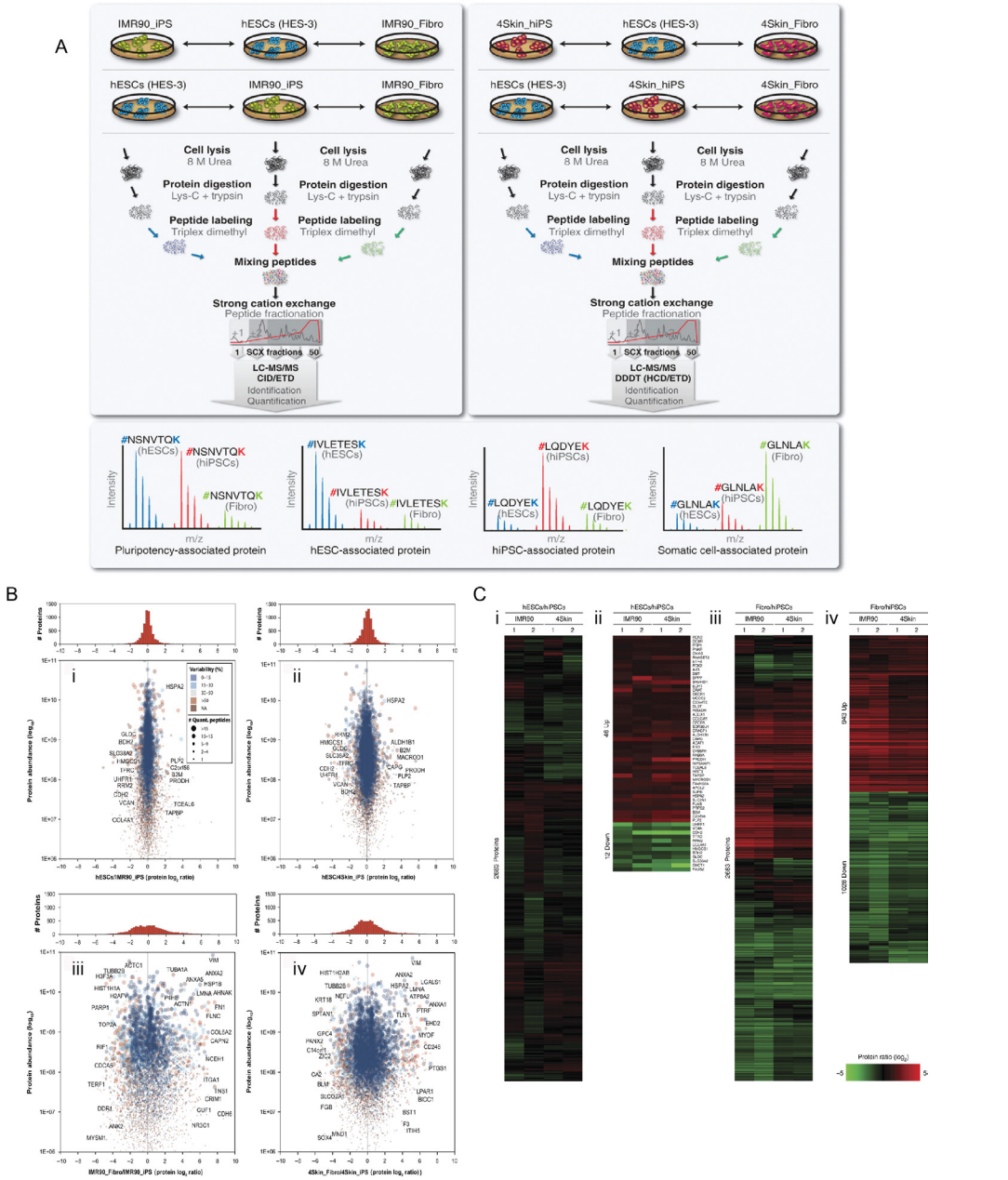

Figure 2 > Principle of a quantitative proteomics experiment and data analysis based on stable isotope dimethyl labeling, exemplified by quantitative proteome profiling of hiPSCs and hESCs.

A) Illustrative experimental design in a quantitative proteomics experiments based on stable isotope dimethyl labeling, as used for a quantitative proteome profiling of hiPSCs and hESCs. Quantitative proteomics experiments using two different hiPS cell lines were conducted, whereby in Experiment 1 (top left panel), IMR90_iPS were compared to hESCs (HES-3) and to the parental fibroblast cell line, IMR90_Fibro. In Experiment 2 (top right panel), 4Skin_iPS were compared to hESCs (HES-3) and the parental fibroblast cell line, 4Skin_Fibro. Cells were lysed, proteins were extracted and subsequently digested with Lys-C and trypsin. Peptides were labeled using triplex dimethyl chemistry, equally mixed and pre-fractionated by using strong cation exchange (SCX). Peptides originating from hESCs were labeled with light isotope (blue) while peptides originating from hiPSCs and its parental fibroblast cell line were labeled with intermediate (red) and heavy (green) isotopes respectively. Two biological replicates were performed for each experiment, where labels were swapped between hiPSCs and hESCs. SCX fractions were analyzed by high-resolution LC-MS/MS. The peak intensities of the identified peptides were proportional to their abundance.

B) Global quantitative proteomic comparisons of hESCs, two hiPSCs and their two precursor fibroblast cell lines. The absolute protein abundance (log10 scale) is plotted against the relative protein ratios (log2 scale) for the hESCs/IMR90_iPS (i), hESCs/4Skin_iPS (ii), IMR90_Fibro/IMR90_iPS (iii), and 4Skin_Fibro/4Skin_iPS (iv) comparisons. The number of peptides used for the quantification as well as the calculated variability or relative standard deviation of the peptide ratios is represented in the plots by the spot size and color scale respectively. In the plots between hESCs and hiPSCs, most of the proteins were quantified with close zero fold change, which indicates that hESC and hiPSC proteomes are very similar. By contrast, the plots between hiPSCs and their precursor fibroblast cells reveal large differences in their proteomes. On top, the histograms of frequencies show the density of proteins in each analysis using a bin size of 0.25 (log2). C) Proteome differences between hESCs, hiPSCs and their parental fibroblasts. 2683 proteins were consistently quantified in all the four data sets: i.e. two replicates (label-swaps) of the IMR90 and 4Skin experiments. Relative protein abundances are represented as heatmaps for hESCs/hiPSCs (i) and fibroblasts/hiPSCs (iii) comparisons. Using significance analysis of microarrays (SAM), 58 proteins (2.2%) were found significantly regulated between hESCs/hiPSCs (ii) and 1927 (73.4%) between fibroblasts/hiPSCs (iv). Red and green colors indicate upregulated and downregulated events, respectively. All data adapted from ref (48).

The broad potential and suitability of stable isotope dimethyl labeling for global quantitative expression proteomics has been demonstrated by several groups on diverse types of samples ranging from a variety of cells, tissues to body fluids. To illustrate this point we give an overview of recent studies in Table 1. Clearly the method is suitable for a wide range of samples, allowing deep coverage of the proteome and allowing adaptation to minute amounts of sample.

We finish this section by highlighting an interesting study using dimethyl labeling in population proteomics, highlighting that the method can also be used to probe large amounts of samples, as represented when proteomes need to be probed differentially across and within populations to define and better understand protein variation. With the massive amount of samples from several populations to be analyzed dimethyl labeling was used as it is cost-effective. Foster's group reported the differential proteomes of honey bees from geographically different bee farms with the aim to determine the diversity of protein expression in commercial honey bee populations and to identify the mechanisms used by the bees to adapt to different ecological conditions (50). They carried out a large-sale quantitative proteomics analysis of the mid-gut proteome from adult nurse bees from eight different locations. Between four to eleven colonies from each location were sampled and each colony was sampled in triplicate and each replicate comprised of mid-guts from five nurse bees. They applied a dimethyl triplex labeling and a random block experimental design to derive relative expression profiles for all proteins across all studied colonies. One block was a triplex analysis of bees from 3 different colonies. In total 58 blocks were analyzed. Overall, 578 proteins could be quantified from which 170 proteins showed differential expression in mid-guts correlating with distinct populations. Their dimethyl labeling based quantitative proteomics study revealed that bees indeed adapt to different climates. For example, the major energy-producing pathways of mitochondria were consistently higher in bees in colder climates whereas up-regulation of some proteins involved in metabolism was observed in bees originating from warmer climates (50).

Table 1 > Selected applications of stable isotope dimethyl labeling in quantitative expression proteomics.

Sample types	Dimethyl labels	Analysis	Quantification tool	Ref.
Human carcinoma cells	2xCH_3, CHD_2	SCX, LC-MALDI-MS	Ratios Manually calculated from monoisotopic signal intensities	(22)
Bovine photoreceptor cells	2xCH_3, 2xCHD_2	LC-MS	MSQuant	(51)
Human osteoprogenitor cells	2xCH_3, 2xCHD_2 (protein labeling)	LC-MS	XInteract (XPRESS) software (part of the Trans-Proteomic Pipeline)	(52)
Human uroepithelial cells	2xCH_3, 2xCHD_2	SCX, LC-MS	Ratios manually calculated from peak heights	(53)
Human carcinoma tissue	2xCH_3, 2xCHD_2	LC-MS	In-house adapted version of MSQuant	(54)
Honey bee abdominal tissue	2xCH_3, 2xCHD_2, 2x$^{13}CD_3$	LC-MS	MSQuant	(55)
Rat liver microsomes	2xCH_3, 2xCHD_2	LC-MS	In-house software PQ-SIDL (http://peptide.ce.ncu.edu.tw)	(56)
Human urine	2xCH_3, 2xCHD_2	LC-MS	In-house software	(57)
Arabidopsis plastoglobules	2xCH_3, 2xCHD_2	LC-MS	Ratios manually calculated from peak areas	(58)
Potatoes	2xCH_3, 2xCHD_2, 2x$^{13}CD_3$	SCX, LC-MS	In-house software	(59)
Pseudomonas putida S12	2xCH_3, 2xCHD_2	LC-MS	MSQuant	(60)
Clostridium phytofermentas	2xCH_3, 2xCHD_2	LC-MS	Ratios Manually calculated from peak areas	(61)

CH_3, labeled using CH_2O and $NaBH_3CN$; CHD_2, labeled using CD2O and NaBH3CN; $^{13}CD_3$, labeled using $^{13}CD_2O$ and $NaBD_3CN$

2.5 Dimethyl labeling for the analysis of protein post translational modifications

Next to the measurement of global protein expression profiles mass spectrometry has also become the tool of choice for the analysis of protein post-translational modifications (PTM). It can unravel PTMs without prior knowledge and it is typically much more comprehensive, specific and quantitative than antibody-based methods. Recent parallel developments in mass-spectrometry and chromatography, including new techniques for enriching peptides bearing a PTM, and concomitant improvements in bioinformatics software has facilitated the global analysis of PTMs, making it possible to pinpoint them with single amino acid resolution (62-64). However, identification of PTM sites by MS can be hindered by the low abundance of the modified peptides, especially in the case of signaling proteins, which are also often modified at substoichiometric levels. Luckily, this problem can largely be addressed by modification-specific enrichments. However, for functional annotation the goal of large scale PTM studies is not just to catalog many PTM sites but more importantly to determine how the identified PTMs change after a particular cell signaling pathway is activated or during disease development.

Stable isotope dimethyl labeling in combination with targeted enrichment provide a nice platform for the quantitative analysis of protein PTMs, and is still be cost-efficient when several milligrams of starting material are required to enable the detection of the low abundant modified peptides.

2.5.1 Dimethyl labeling application in quantitative phosphoproteomics

Phosphorylation is one of the most important and well-studied post-translational modifications as it plays a critical role in the regulation of several cellular processes including cell cycle, growth, apoptosis and differentiation. Several approaches have been developed to facilitate the enrichment of low abundant phosphopeptides, for example phosphotyrosine immunoprecipitation (pY IP), titanium dioxide (TiO2) affinity chromatography and immobilized metal ion affinity chromatography (IMAC) (63, 65). Dimethyl labeling is well suited to large-scale quantitative phosphoproteomics as it can easily incorporate with any kind of phosphoprotein or phosphopeptide enrichment approach even when started with milligrams of material (table 2). As an illustrative example we describe below how dimethyl labeling was incorporated in our laboratory with two important enrichment techniques in quantitative phosphoproteomics studies. We show examples for the targeted analysis of tyrosine phosphorylation using pY IP and the more global analysis of protein phosphorylation using SCX in combination with TiO2 to profile differential phosphorylation events in stem cells following stimulation leading to differentiation (27, 66).

Examining the Self-renewal Process in Human Embryonic Stem Cells (hESCs)

hESCs exhibit two exceptional properties which are the ability to self-renew and the ability to differentiate into all cell types of the human body (67). We were interested in how human embryonic stem self-renew and maintain their undifferentiated state. hESCs self-renewal are regulated by several factors and one of them is fibroblast growth factor-2 (FGF-2). FGFs execute their biological actions by activating cell surface FGF receptors (FGFRs) which are member of the receptor tyrosine kinases (RTKs) family, resulting in activation of further downstream signaling pathways including the mitogen activated protein kinase (MAPK) and phosphoinositide 3-kinase (PI3-K) pathways. To understand the role of FGF signaling in hESC, we performed two large-scale, targeted, quantitative phosphoproteomics experiments to investigate phosphorylation events following FGF-2 stimulation (27, 66).

Since FGF-2 signaling initiates via receptor tyrosine kinases, we initially performed an analysis of the early tyrosine phosphorylation events following FGF-2 stimulation. hESCs were treated with FGF-2 for 0, 5, and 15 mins. As tyrosine phosphorylation is less frequent in cells compared to serine and threonine, 6 mg lysate from each time point was digested and dimethyl labeled whereby the non-stimulated hESCs (0 min) were labeled with light dimethyl labels, the 5 min stimulation with intermediate labels and the 15 min with the heavy label. The differentially labeled samples were mixed 1:1:1 based on total peptide amount determined by running an aliquot of the labeled samples on a regular LC-MS and comparing overall peptide signal intensity and enriched for tyrosine phosphorylated peptides by pY immunoprecipitation. The enriched peptides were then analyzed by LC-MS/MS (figure 3). 300 unique tyrosine phosphorylation sites could be identified and quantified. As expected, an increase in tyrosine phosphorylation of all FGF receptors and their canonical downstream effectors (eg. MAPK and PI3-K) were identified. Interestingly, a large number of proteins not directly involved in the canonical FGF pathway, especially Src substrates were observed with increased phosphorylation upon FGF-2 stimulation, although only relatively small increases were observed for their Src family kinases (SFKs). Moreover, cluster analysis revealed that the identified Src substrates followed the same tyrosine phosphorylation profiles in response to FGF-2 as identified in all FGF receptors and their downstream targets. Our finding suggested for the first time the importance of Src kinase signaling in maintaining the undifferentiated hSEC phenotype, which could be confirmed by our Src kinase inhibition assays (68). From a technical point of view it is interesting to note that in these experiments we labeled 6 mg of material; however we only analyze ng of material acquired following pY IP, throwing the rest to waste. Similar experiments have been reported by the group of White et al. who used iTRAQ labeling for the quantitative readout (69). Compared to dimethyl labeling this increases the costs of the experiment tremendously, moreover the iTRAQ label may have a negative effect on the efficiency of the pY IP. In a comparison between iTRAQ and dimethyl labeling Boersema et al. reported quantitatively identical results following EGF stimulation in Hela cells, indicating that both methods can perform equally well (27).

To further understand the role of FGF-2 on hESCs, we extended our tyrosine phosphorylation profiling by performing a more global phosphoproteomics study under identical biological conditions aiming to include now also the vast majority of phosphorylation in cells that are on serine and threonine residues, albeit at the expense of detecting many tyrosine phosphorylations (66). Therefore, we performed a multi-dimension strategy combining SCX chromatography to reduce sample complexity, followed by TiO2 off-line to enrich for phosphopeptides, and dimethyl labeling for quantification. hESCs were stimulated with FGF-2 for 0, 1, 5, 15, and 60 mins. 1.5 mg lysate from each time point was digested and dimethyl labeled whereby for the first group, the non-stimulated hESCs (0 min) were labeled with light dimethyl labels, the 5 min stimulation with intermediate labels and the 15 min with heavy labels. For the second group the 1 min stimulation was labeled with light dimethyl labels, the 15 min stimulation with intermediate labels and the 60 min with heavy labels. Samples from each group were mixed 1:1:1 ratio and fractionated by SCX. The SCX fractions abundant in phosphopeptides were further enriched for phosphopeptides with TiO2 off-line and analyzed by LC-MS/MS (Figure 3). A total of 1653 phosphopeptides corresponding to 810 proteins could be quantified. In agreement with our study mentioned above, a rapid increase in phosphorylation was observed in all FGF receptors as well as downstream targets of the MAPK, PI3K, and Src family members. Complementing our previous analysis, we observed in this study that FGF-2 also regulated several other downstream signaling pathways including Wnt and actin/cytoskeletal pathways. The observed changes in phosphorylation emphasized that FGF-2 may directly regulate the pluripotency transcription factors to maintain the undifferentiated phenotype (66).

Technically similar applications of dimethyl labeling combined with a wide range of phosphoenrichment techniques are listed in Table 2). To end this section, we would like to highlight our recent study of a novel phosphopeptide enrichment approach based on a combination of low pH SCX and Ti4+ -IMAC. We have shown that the Ti4+ method can boost the number of phosphopeptide identification in dimethyl labeling based-quantitative proteomics. We were able to identify more than 9000 unique phosphorylation sites from a single experiment consisting of only 400µg triple dimethyl labeled lysate (25).

Overall all these studies combined reveal that stable isotope dimethyl labeling provides a versatile platform for quantitative phosphoproteomics studies as it can be incorporated in every workflow chosen to perform enrichment of phosphopeptides and phosphoproteins and applied to every kind of cell, tissue or organelles.

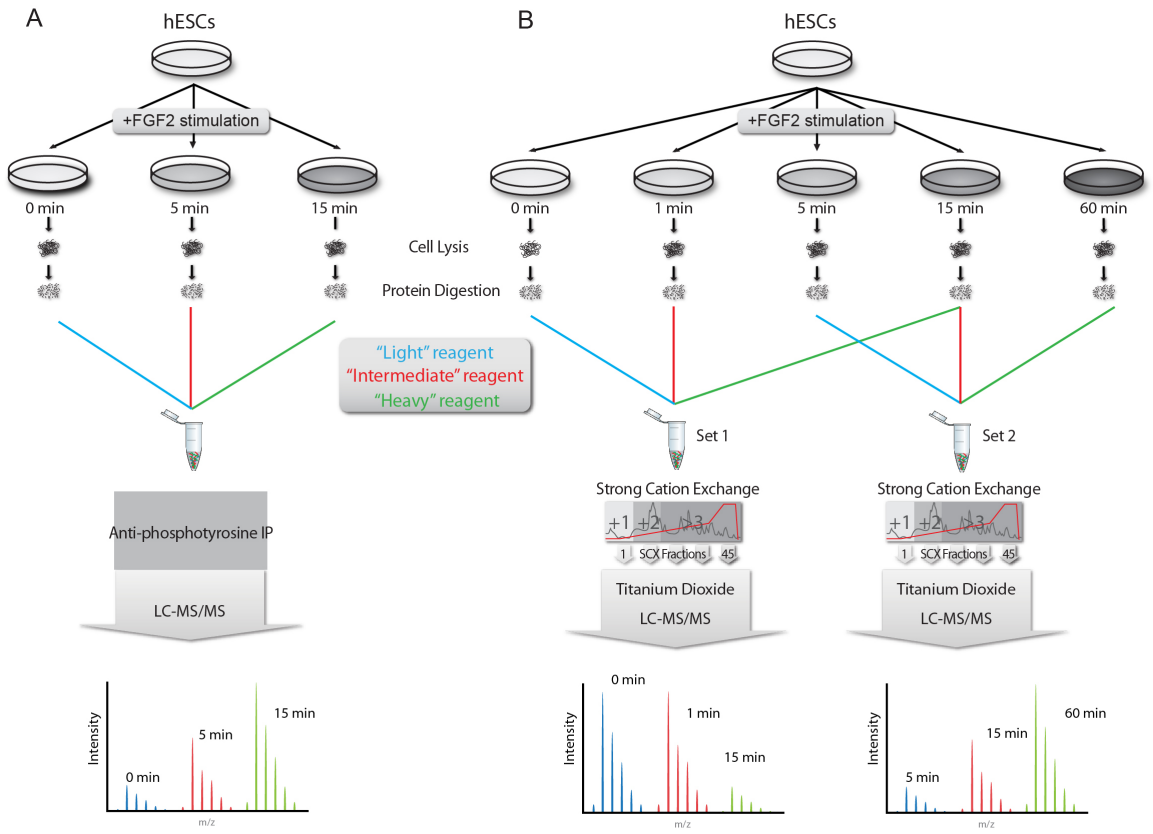

Figure 3 > Overview of the experimental design used in a quantitative phosphoproteomics study monitoring signaling responses in FGF-2 stimulated hESCs cells.

FGF-2-stimulated were harvested at different time points following stimulation and lysed, where after the extracted proteins were digested. The resulting peptides were stable isotope-labeled using triplex stable isotope dimethyl labeling. **A)** *Targeted phosphotyrosine profiling; The peptides extracted from hESCs stimulated for 0, 5, and 15 mins were mixed in a 1:1:1 ratio and pY IP was performed to enrich for pY peptides prior to LC-MS/MS.* **B)** *Global phosphopeptide profiling; The peptides from 0, 1, 5, 15, and 60 mins were mixed as depicted to create two sets of samples. SCX and TiO2 were used to enrich for phosphopeptides prior to LC-MS/MS. The two experiments combined provided global differential phosphorylation related signaling events during the early time course following FGF-2 stimulation. Adapetd from ref (67).*

Table 2 > Selected applications of stable isotope dimethyl labeling in quantitative phosphoproteomics.

Sample types	Dimethyl labels	Analysis	Quantification tool	Ref.
MCF-7 cells	2xCH_3, 2xCHD_2	IMAC-HILIC, LC-MS	MASCOT Distiller (used average peak area of the first 3 0r 4 isotopic peak across the elution profile)	(70)
Human lymphobastoid cells	2xCH_3, 2x$^{13}CHD_2$	TiO2, LC-MS	Ratios manually calculated from relative peak intensities	(71)
Human lymphoid cells	2xCH_3, 2xCHD_2, 2x$^{13}CD_3$	SCX, online TiO2, LC-MS	In-house dimethyl-adapted version of MSQuant	(72)
Mouse brain tissue	2xCH3, 2xCD_3	SCX, online IMAC, LC-MS	Ratios manually calculated from peak areas	(73)
Zebra fish embryos	2xCH_3, 2xCHD_2	SCX, online TiO2, LC-MS	In-house dimethyl-adapted version of MSQuant	(26)
Rat Uteri	2xCH_3, 2xCHD_2	IMAC, MALDI, LC-MS	Ratios manually calculated from relative peak heights	(24)
Arabidopsis	2xCH_3, 2xCHD_2	Zr4+-IMAC, LC-MS	Ratios manually calculated from relative intensities	(74)

CH_3, labeled using CH_2O and $NaBH_3CN$; CHD_2, labeled using CD_2O and $NaBH_3CN$; $^{13}CHD2$, labeled using $^{13}CD2O$ and NaBH3CN; CD_3, labeled using CD_2O and $NaBD_3CN$; $^{13}CD_3$, labeled using $^{13}CD_2O$ and $NaBD_3CN$

2.5.2 Dimethyl labeling applications in quantitative glycoproteomics

Glycosylation is one of the most frequent PTMs occurring often on cell surface and extracelllar proteins. The two main forms are O-linked oligosaccharides bound to serine or threonine residues and N-linked glycans attached to asparagine residues. Changes in the glycosylation profile have been reported to be associated with several diseases; therefore, quantitative glycoproteomics is rapidly gaining interest. Several enrichment strategies have been developed for the study of glycosylated proteins. The two major approaches are lectin affinity and hydrazide chemistry, which are mostly applied for the analysis of N-linked glycoproteins (75, 76). Alternative enrichment methods include HILIC and TiO2 chromatography for glycoproteins and peptides containing sialic acids (SA) (77, 78). Stable isotope labeling combined with different glycoprotein enrichment approaches has been utilized in several quantitative glycoproteomics studies (75, 76). Dimethyl labeling is well suited for quantitative glycoproteomics study for both N-linked and O-linked glycosylation as it can be combined with all these above mentioned enrichment strategies as described in more detail below.

Quantitatitive N-linked glycoproteomics profiling in cardiac remodeling

Parker et al. described a quantitative glycoproteomics strategy to profile the myocardial N-glycoproteome during cardiac modeling after I/R injury in a rat model (79). Their initial profiling used iTRAQ for quantification with 100 ug starting material. The starting material was sufficient only for one enrichment step and only 80 glycopeptides could be quantified with altered abundance. To increase the coverage of the glycopeptides, they performed dimethyl labeling for quantification so the amounts of starting material could be increased and therefore complementary glycopeptide enrichment methods based on different chemical properties of the attached glycans could be performed. 2mg of membrane proteins from control heart and those subjected to ischemia/reperfuison (I/R) injury were digested and dimethyl labeled. The labeled peptides were mixed and subjected to three different enrichment methods, TiO2 for SA-containing glycopeptides, ZIC-HILIC for neutral glycopeptides, and hydrazide capture. A total of 590 glycosylation sites were quantified and 123 glycopeptides were identified with abundance changes. Of these, 46 glycopeptides were in agreement with those obtained by the iTRAQ approach, whereas dimethyl labeling added another 62 glycopeptides with altered abundance. These glycosylation sites mapped to proteins from the three phases of cardiac remodeling ranging from extracellular matrix proteins, cell surface glycoproteins to proteins associated with sarcolemma and electrochemical signaling and solute transport (79).

Dimethyl labeling can also be combined with lectin affinity chromatography enrichment. Wei et al. established an analytical platform that can enrich, identify, and quantify glycoproteins in complex plasma samples for biomarker discovery in prion disease (80). Blood from mice inoculated with prion protein were collected 108, 158, and 198 days after inoculation. Plasma samples from 7 control and 7 infected mice from each time point were pooled and glycoproteins were enriched by lectin affinity chromatography. Glycoproteins were digested, differentially dimethyl labeled, and analyzed by 2D RP-RPLC-MS/MS. Dimethyl labeling revealed around 100 proteins with altered expression in the plasma collected from prion inoculated animals. As a consequence of the data they proposed serum amyloid P-component protein as a potential biomarker for the progression of prion disease (80).

Probing the dynamics of O-GlcNAc glycosylation in the brain

O-linked N-acetylglucosamine (O-GlcNAc) is an intracellular, reversible form of O-glycosylation that shares many features with phosphorylation. Khidekel et al. have reported a new quantitative proteomics strategy for monitoring the dynamics of O-GlcNAc glycosylation, in which a method is termed quantitative isotopic and chemo-enzymatic tagging (QUIC-Tag) (81). The method combines selective, chemo-enzymatic tagging of O-GlcNAc proteins, which allows selective biotinylation and avidin chromatography purification of the proteins using dimethyl labeling for quantification (Figure 4). The application of the QUIC-Tag method was shown in the study of O-GlcNAc glycosylation in neurons and brain where the modification is abundant. The QUIC-Tag method was used to probe global glycosylation changes as a response to extracellular stimuli. Interestingly, O-GlcNAc modification was identified on several proteins essential for synaptic function in neurons, suggesting a role of the modification in mediating the communication between neurons. Their data also showed for the first time that beside glucose concentration, extracellular stimuli can induce and regulate O-GlcNAc glycosylation in the brain (81).

2.5.3 Dimethyl labeling for identification of proteolytic products and natural N and C-termini

Endogenous proteolysis is a major, irreversible post-translational modification that can modify protein activity, function, localization and life span. Proteolysis generates proteins with neo N- and/or C-termini not originally present in the initially translated polypeptides. Proteases are one of the largest enzyme classes in mammalian organisms. However, for half of the proteases, substrates are relatively unknown and for the other half annotation of the substrate degradome is incomplete.

The group of Overall has developed two of the most powerful quantitative proteomics approaches for labeling and isolating N- or C-terminal peptides referred to as TAILS (terminal amine isotopic labeling of substrate) and C-TAILS (C-terminal amine-based isotope labeling of substrates) (82-87). The approaches are designed for comparison of protease-treated and control untreated proteomes as well as to compare proteolytic processing in different samples as shown in Figure 5A. The two methods combine an enrichment step for protein termini with stable isotope labeling, mostly with dimethyl labeling for quantification to 1) assign specific cleavage events to the protease of interest and 2) to distinguish the protease-induced proteolytic products from background proteolytic products in a control sample.

TAILS is developed to enrich, identify and quantify both natural and proteolysis-generated N-termini. As a critical step, at the protein level, dimethyl labeling is incorporated to modify natural and proteolysis-generated N-terminal and lysine amines, thus protecting the modified amines from trypsin and simultaneously labeling the proteins. As lysine dimethylation prevents trypsin cleavage after lysine, the resulting generation of longer peptides by trypsin aids the identification of the relatively short N-terminal peptides. After tryptic digestion, negative enrichment was performed by using amine-reactive, aldehyde-derivatized polymer to capture internal trypsin-generated N-termini in order to separate them from protected N-termini (Figure 5B). Quantification of the heavy and light ratios of peptides together with stringent bioinformatics search criteria enables discrimination of protease-cleaved neo N-terminal peptides from the background proteolysis products, therefore substrate repertoire of a specific protease can be identified and their accurate cleavage sites can be assigned (82-84).

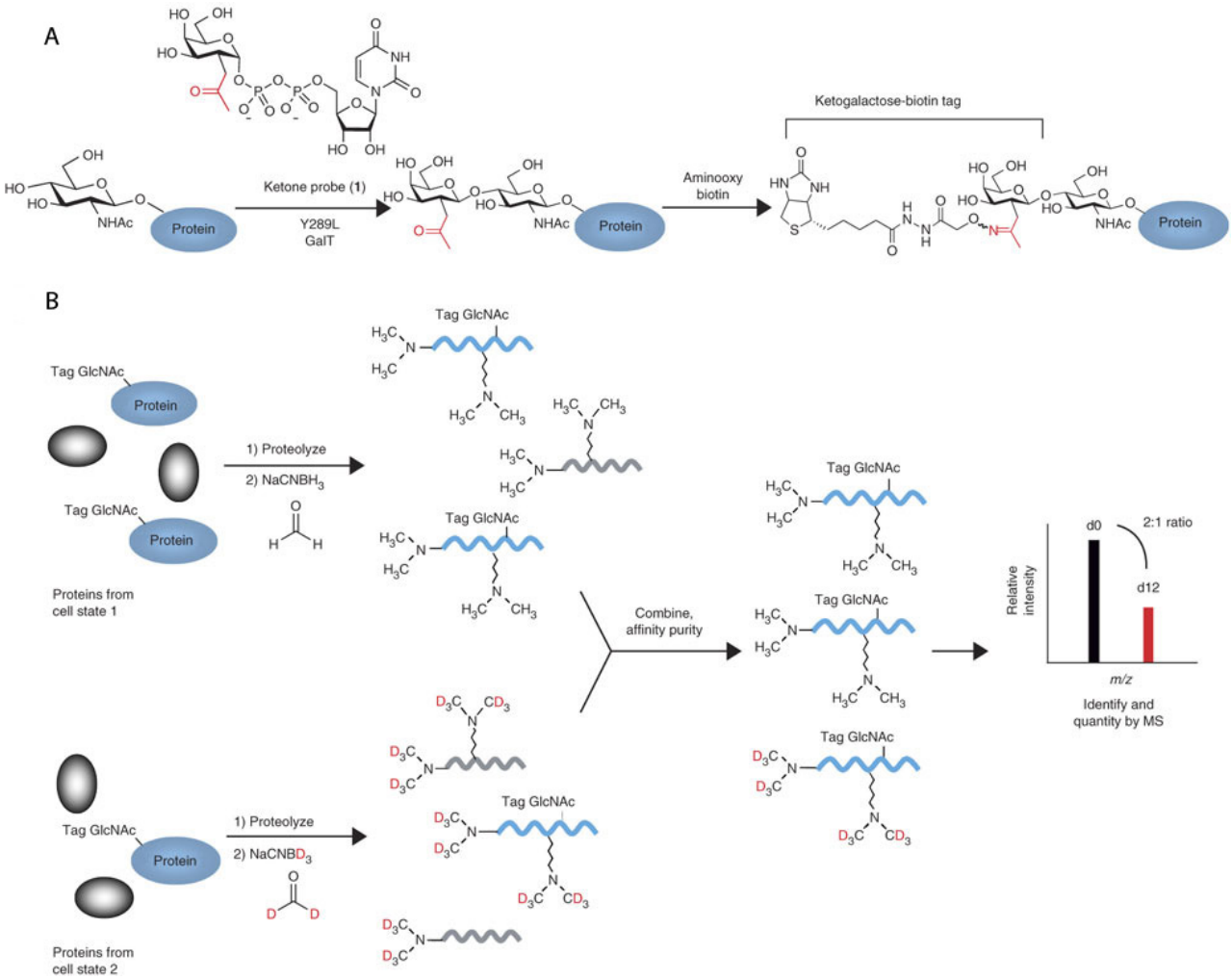

Figure 4 > Overview of the QUIC-tag approach including stable isotope dimethyl labeling.

A) *O-GlcNAc-glycosylated proteins are chemo-enzymatically tagged with a ketogalactose sugar, which allows selective biotinylation of the proteins.* **B)** *O-GlcNAc proteins from two different cell states are selectively tagged, digested and differentially labeled by stable isotope dimethyl labeling. The mixtures were subsequently combined, and O-GlcNAc peptides are selectively enriched by avidin chromatography prior to quantification by LC-MS. Adapted from ref (81).*

TAILS has been demonstrated in the study of broad-specificity metalloproteinase (MMP)-2 cleavages sites and substrates in mouse fibroblast secretomes. TAILS identified more than 200 cleavage sites from more than 100 substrates. TAILS has also been used to study mouse inflammatory bronchoalveolar fluid and revealed the substrates of the poorly defined breast cancer protease MMP-11 (82). Applications of TAILS have also been shown by Tholen et al., who were interested in the contribution of the endolysosomal cysteine endoprotease, cathepsin L (Cstl) to extracellular proteolysis of the mouse embryonic fibroblasts (MEFs). TAILS was used to determine changes in cleavage pattern of secreted proteins between wild-type and Cstl knockout MEFs and to identify the Cstl dependent cleavage sites. In total, TAILS identified more than 1500 protein termini, of which more than 300 were found reduced by Cstl deficiency (88).

A similar strategy was applied to study the protein C-terminome (85, 86). C-TAILS is currently one of the few methods that allow proteome-wide enrichment of C-terminal peptides. C-TAILS has been developed to enrich, identify and quantify both natural and proteolysis-generated C-termini. As an extra step from N-terminal TAILS, endogenous and protease-generated neo C-terminal together with aspartate and glutamate side chain carboxyl groups have to be chemically protected at the protein level. Dimethyl labeling is incorporated to label and protect amines at the protein and peptide level. Trypsin digestion yields the natural protein C-terminal peptides and neo-C terminal peptides, now with protected carboxyl groups. Original and neo C-terminal peptides which lack free carboxyl groups are isolated by negative enrichment (85, 86) (Figure 5B). A nice application of C-TAILs was reported by Schilling et al. who identified hundreds of C-terminal peptides in the Escherichia coli proteome (85).

2.6 Stable isotope dimethyl labeling applications in interaction proteomics

Rather than individual proteins themselves, protein complexes are the functional units of the cell. Indeed, signal transduction and cellular pathways require protein-protein interactions (PPIs) and the assemblies of proteins into large protein complexes. Therefore, mapping of PPIs and complex components are essential to understand regulatory mechanisms underlying biological processes. High-throughput yeast two-hybrid screens (Y2H) (89) and affinity purification followed by mass spectrometry (90) are two major techniques used to study PPIs. A major challenge in using affinity purification for interaction studies is that it is difficult to control/diminish false-positive interactions coming from the complex cellular background, regardless of the bait protein or protocol used. It has been shown that quantitative proteomics can assist in overcoming this problem performing pull-down and control pull-down in parallel and using incorporation of different stable isotopes to distinguish background proteins (equally abundant in both experiments) from specific interaction partners (absent in the control or at least two folds more abundant in the pull-down). Among the different quantitative proteomics strategies demonstrated in PPI studies, dimethyl labeling has proven to be quite successful in the mapping of protein-protein as well as protein-nucleic acid and protein-drug interactions (91-96).

One of the most useful applications of quantitative AP-MS has been the global elucidation of protein interaction networks (PINs) present in a cell or organism (97). Although, dimethyl labeling is still a relative newcomer in the field, it has been demonstrated as a tool to construct PINs in methicillin-resistant Staphylococcus aureus (MRSA-252) (93). 406 MRSA proteins were cloned and expressed as GST-fusion proteins and used as bait in high-throughput pull-down experiments, with each pull-down having an internal negative pull-down represented by the GST control. Di-

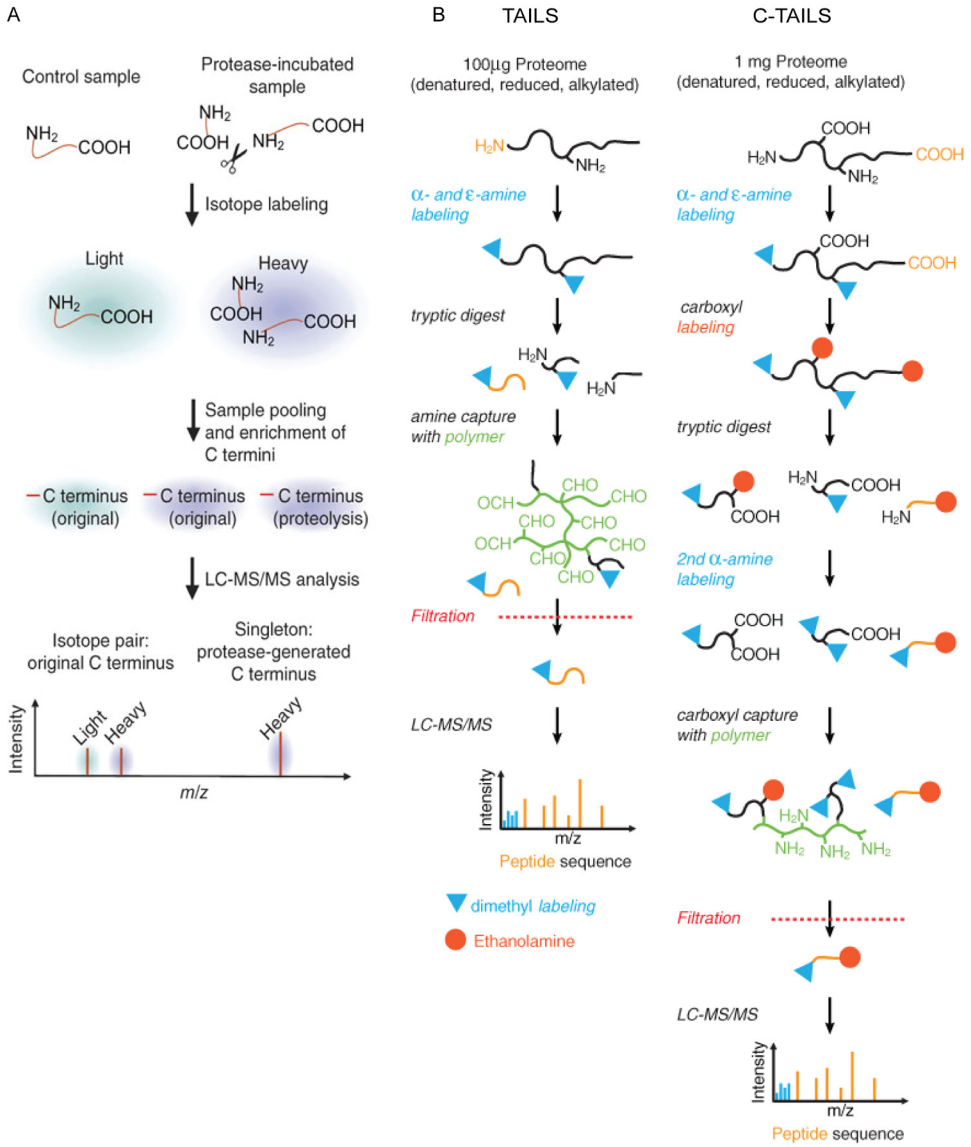

Figure 5 > Overview of N-terminal and C-terminal TAILS approaches including stable isotope dimethyl labeling.

A) Overview of the N-terminal and C-terminal TAILS approaches that can be used to identify protease-generated neo termini. The workflow depicts protease-generated C-termini as an example. A proteome sample is incubated with the targeted protease that generates neo–C protein termini. After proteolysis, the protease is inactivated and the samples are denatured and reduced. To distinguish induced proteolysis from background proteolysis, control and protease-treated samples are differentially labeled using dimethylation with light and heavy isotope, respectively. After trypsin digestion and labeling, both samples are mixed, and C-terminal peptides are isolated. In LC-MS/MS analysis, background proteolysis C-termini are present roughly equal in both samples and thus appear as heavy and light labeled peptides, whereas by the targeted protease generated C-termini appear exclusively in the heavy labeled form. B) Schematic representation of N- and C-terminal peptide enrichment strategies used in TAILS and C-TAILS. To enrich N-terminal peptides, protein amine groups are protected via dimethyl labeling (represented by blue triangles). After trypsin digestion, internal tryptic peptides are coupled to polymer via their free N-terminus. The original protein N-terminal peptides remain unbound and after separation by ultrafiltration are analyzed by LC-MS/MS. To enrich C-terminal peptides, protein amine groups are protected and simultaneously dimethyl labeled (represented by blue triangles). After that, carboxyl groups are chemically protected (represented by red circles). After trypsin digestion, peptide N termini are again protected and simultaneously dimethyl labeled (represented by blue triangles). N-terminal and internal tryptic peptides are coupled to polymer via their free C terminus. The original protein C-terminal peptides remain unbound and after separation by ultrafiltration are analyzed by LC-MS/MS. Adapted from refs (85, 87).

methyl labeling was incorporated into each pull-down pair to distinguish specific interactors from the nonspecific background by quantifying the amount of interactor bound to the GST-fused bait protein relative to the amount in the control GST alone pull down. Interactors with at least a 2-fold enrichment were considered bonafide. In total, 13,219 pairwise interactions involving 608 MRSA proteins were reconstructed into an MRSA PIN, which can serve as an important basis for investigation S.aureus biology and potential functions for previously uncharacterized proteins. Several proteins were identified as central hubs in the PIN, indicating that they may be essential for network integrity and stability, and thus essential and critical for MRSA viability and growth. The authors also suggested that some of the highly connected proteins can become prospective antimicrobial drug targets. Incorporating dimethyl labeling can be used to quantitatively assess the validity of the interaction and thus also pinpoint false-positive interactions, which is extremely difficult for the classical Y2H approach.

The dimethyl labeling approach outlined above to study PINs can be used to study any protein interaction as long as a bait and a proper control are available. Cheng et al. developed what they termed a quantitative nanoproteomics approach for charting protein complexes (QnanoPX) using gold nanoparticles as a probe for affinity purification (92). The approach was applied to globally map the transcriptional activation complex of estrogen response element (ERE) in MCF-7 cells. ERE is regulated by the estrogen receptor (ER). When activated with 17β-estradiol (E2), the ER is translocated to the nucleus where it binds to ERE, recruits other proteins to the complex to subsequently promote transcription of the target genes. In order to identify ER-ERE complex components, gold nanoparticle probes were functionalized with consensus sequences of 13-bp ERE (positive probes) and control negative probes were functionalized without ERE. The pull-down by the negative and the positive probes were differentially labeled to distinguish genuine ER-ERE complex components from nonspecific binding proteins. The same strategy was then extended to investigate E2-induced changes in protein expression after 24h E2 treatment (92). A pull-down in cells without E2 treatment was used as a control. Among the by E2 treatment affected proteins, they detected several proteins involved in transcriptional regulation by ER. For instance, c-Myc, suggesting it may play a significant role in E2-mediated transcription, which was further substantiated by western blot data. Both of these studies show powerful applications of dimethyl labeling to unravel biological pathways by tackling the generic problems of nonspecific binding and false positives in protein interaction studies.

Stable isotope dimethyl labeling can also be incorporated in the interaction study of small-immobilized molecules with proteins from a lysate to screen for drug targets and off-target binding, often referred to as chemical proteomics (98). We were interested in probing the interactome of cGMP specific phosphodiesterase 5 (PDE 5) inhibitors that resemble Sildenafil and Vardenafil. A quantitative chemical proteomics approach was performed to investigate whether proteins other than the clinically known target PDE5 could also interact with these drug analogues (94). We found that only three proteins displayed selective affinity for the PDE5 inhibitor, of which two were isoforms of PDE5, and only one new binder was observed, namely the Prenyl binding protein (PrBP). Follow-up experiments confirmed the specific interaction between the PDE5 inhibitor analogues and PrBP albeit in the lower micromolar range, much weaker than the interaction between the drug and PDE5 which is in lower nanomolar range (94). This approach was also used to assess the relative binding of chemically slightly different PDE5 inhibitors (figure 6). Their selectivity profiles were determined by differences in abundances of the proteins retrieved by PDE5 inhibitors pull-downs. Our data indicated that slight chemical modifications on the analogues can bias the inhibitor selectivity from PDE5 towards other interacting proteins (96).

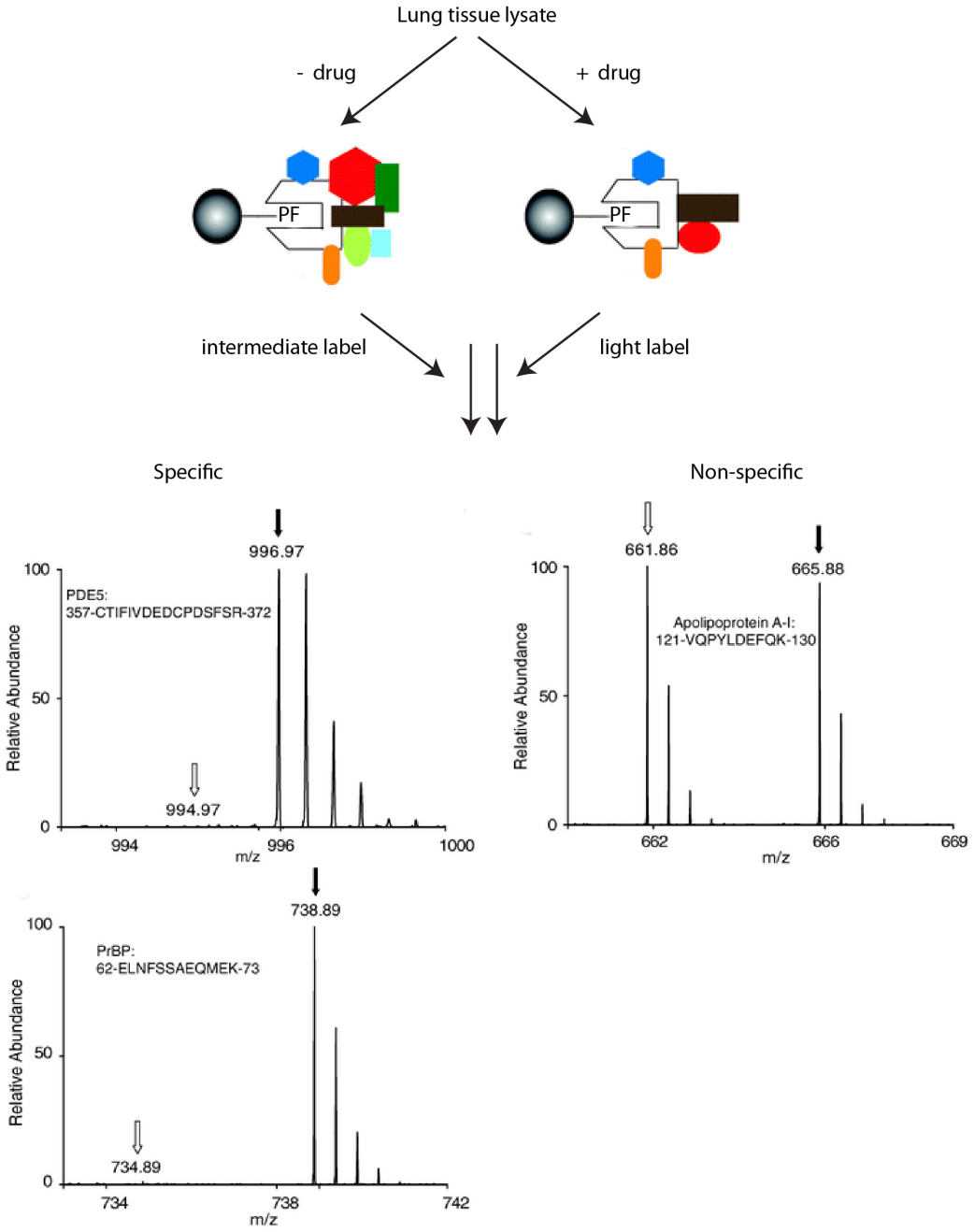

Figure 6 > Experimental strategy to identify binding partners of the PDE5 inhibitor (PF-4540124) using stable isotope dimethyl labeling.

The mouse lung tissue lysate was divided into two equal parts. The control lysate was supplemented with the free drug, at a concentration at which binding of interactors specific to the immobilized compound was blocked. After incubation with the beads, proteins were eluted and digested. Peptides originating from the control pull-down were labeled with light dimethyl labels whereas those originating from specific pull-down were labeled with the intermediate label. Each set of labeled samples were mixed in a 1:1 ratio and analyzed by LC-MS/MS. The absence of the light labeled peptides from PDE5 and PrBP (left) indicates that they are specific binding partners of the drug. The equal presence of the peptide pair (right) originating from Apolipoprotein A indicates that the protein is non-specifically bound to the matrix. Adapted from ref (94).

2.7 General Conclusions

Presently, there are many alternative ways to perform quantitative proteomics. The most robust forms require the use of stable isotope labeling. These stable isotopes can either be incorporated metabolically using popular methods such as 15N labeling (99) or SILAC (7, 8), or chemically using for instance ICAT (10), iTRAQ/TMT (11, 12) or 18O (100, 101). To this toolbox more recently stable isotope dimethyl labeling has been added. Although it is clear that all these different methods have their strengths and weaknesses the applications described in this review clearly show that stable isotope dimethyl labeling provides a very versatile method. Weakness of, but not unique to, stable isotope dimethyl labeling is that it cannot be easily multiplexed beyond four channels. Moreover, as quantification is based on MS spectra, and not on MS/MS fragments as in iTRAQ/TMT, overlapping ion signals originating from other peptides with similar masses can hamper quantification. In summary, strengths of stable isotope dimethyl labeling are that its low cost and high efficiency allow application on both large (mg) but also low (sub-µg) amounts of protein input. In addition, it can be used in both off-line and on-line methods and it can reach equal depth in protein quantitation as the alternative methods mentioned above. Another advantage of this chemical labeling strategy is that it can be applied to any sample including those originating from cells, tissue, body fluids and whole organisms. Therefore, we think the future of stable isotope dimethyl labeling in quantitative proteomics is bright.

2.8 Acknowledgements

We kindly acknowledge all members of the Heck-group for their contributions. This work was in parts supported by the PRIME-XS project, grant agreement number 262067, funded by the European Union 7th Framework Programme; the Netherlands Proteomics Centre, embedded in the Netherlands Genomics Initiative, the Centre for Biomedical Genetics; the Netherlands Organization for Scientific Research (NWO) with a VIDI grant (700.10.429) and the Netherlands Bioinformatics Centre. DK is funded by Utrecht Institute for Pharmaceutical Sciences (UIPS) and a Royal Thai Scholarship.

2.9 References

1. R. Aebersold, M. Mann, Mass spectrometry-based proteomics. Nature 422, 198 (2003).
2. J. Cox, M. Mann, Quantitative, high-resolution proteomics for data-driven systems biology. Annu Rev Biochem 80, 273 (2011).
3. P. Mallick, B. Kuster, Proteomics: a pragmatic perspective. Nat Biotech 28, 695 (2010).
4. M. Bantscheff, M. Schirle, G. Sweetman, J. Rick, B. Kuster, Quantitative mass spectrometry in proteomics: a critical review. Anal Bioanal Chem 389, 1017 (2007).
5. S. Julka, F. Regnier, Quantification in Proteomics through Stable Isotope Coding: A Review. J Proteome Res 3, 350 (2004).
6. A.J.R. Heck, J. Krijgsveld, Mass spectrometry-based quantitative proteomics. Expert Rev Proteomics 1, 317 (2004).
7. S.E. Ong et al., Stable Isotope Labeling by Amino Acids in Cell Culture, SILAC, as a Simple and Accurate Approach to Expression Proteomics. Mol Cell Proteomics 1, 376 (2002).
8. M. Mann, Functional and quantitative proteomics using SILAC. Nat Rev Mol Cell Biol 7, 952 (2006).
9. J.W. Gouw, J. Krijgsveld, A.J.R. Heck, Quantitative Proteomics by Metabolic Labeling of Model Organisms. Mol Cell Proteomics 9, 11 (2010).
10. S.P. Gygi et al., Quantitative analysis of complex protein mixtures using isotope-coded affinity tags. Nat Biotech 17, 994 (1999).
11. P.L. Ross et al., Multiplexed Protein Quantitation in Saccharomyces cerevisiae Using Amine-reactive Isobaric Tagging Reagents. Mol Cell Proteomics 3, 1154 (2004).
12. A. Thompson et al., Tandem Mass Tags: A Novel Quantification Strategy for Comparative Analysis of Complex Protein Mixtures by MS/MS. Anal Chem 75, 1895 (2003).
13. P.J. Boersema, T.T. Aye, T.A.B. van Veen, A.J.R. Heck, S. Mohammed, Triplex protein quantification based on stable isotope labeling by peptide dimethylation applied to cell and tissue lysates. Proteomics 8, 4624 (2008).
14. N. Jentoft, D. G. Dearborn, Labeling of proteins by reductive methylation using sodium cyanoborohydride. J Biol Chem 254, 4359 (1979).
15. J.L. Hsu, S.Y. Huang, N.H. Chow, S.H. Chen, Stable-Isotope Dimethyl Labeling for Quantitative Proteomics. Anal Chem 75, 6843 (2003).
16. J.L. Hsu, S.Y. Huang, J.T. Shiea, W.Y. Huang, S.-H. Chen, Beyond Quantitative Proteomics: Signal Enhancement of the a1 Ion as a Mass Tag for Peptide Sequencing Using Dimethyl Labeling. J Proteome Res 4, 101 (2005).
17. C. Ji, N. Guo, L. Li, Differential Dimethyl Labeling of N-Termini of Peptides after Guanidination for Proteome Analysis. J Proteome Res 4, 2099 (2005).
18. J.L. Hsu, S.Y. Huang, S.-H. Chen, Dimethyl multiplexed labeling combined with microcolumn separation and MS analysis for time course study in proteomics. Electrophoresis 27, 3652 (2006).
19. S. Cappadona et al., Deconvolution of overlapping isotopic clusters improves quantification of stable isotope–la beled peptides. J Proteomics 74, 2204 (2011).
20. K. Guo, C. Ji, L. Li, Stable-Isotope Dimethylation Labeling Combined with LC−ESI MS for Quantification of Amine-Containing Metabolites in Biological Samples. Anal Chem 79, 8631 (2007).
21. S. Di Palma, R. Raijmakers, A. J. R. Heck, S. Mohammed, Evaluation of the Deuterium Isotope Effect in Zwitterionic Hydrophilic Interaction Liquid Chromatography Separations for Implementation in a Quantitative Proteomic Approach. Anal Chem 83, 8352 (2011).
22. C.J. Ji, L.J. Li, M. Gebre, M. Pasdar, L. Li, Identification and quantification of differentially expressed proteins in E-cadherin deficient SCC9 cells and SCC9 transfectants expressing E-cadherin by dimethyl isotope labeling, LC-MALDI MS and MS/MS. J Proteome Res 4, 1419 (2005).
23. C. Ji, L. Li, Quantitative Proteome Analysis Using Differential Stable Isotopic Labeling and Microbore LC−MALDI MS and MS/MS. J Proteome Res 4, 734 (2005).
24. S.Y. Huang et al., Quantitation of protein phosphorylation in pregnant rat uteri using stable isotope dimethyl labeling coupled with IMAC. Proteomics 6, 1722 (2006).

25. H. Zhou et al., Enhancing the Identification of Phosphopeptides from Putative Basophilic Kinase Substrates Using Ti (IV) Based IMAC Enrichment. Mol Cell Proteomics 10, M110.006452 (2011).

26. S. Lemeer et al., Comparative Phosphoproteomics of Zebrafish Fyn/Yes Morpholino Knockdown Embryos. Mol Cell Proteomics 7, 2176 (2008).

27. P.J. Boersema et al., In-depth Qualitative and Quantitative Profiling of Tyrosine Phosphorylation Using a Combination of Phosphopeptide Immunoaffinity Purification and Stable Isotope Dimethyl Labeling. Mol Cell Proteomics 9, 84 (Jan, 2010).

28. R. Raijmakers et al., Automated Online Sequential Isotope Labeling for Protein Quantitation Applied to Proteasome Tissue-specific Diversity. Mol Cell Proteomics 7, 1755 (2008).

29. R. Raijmakers, A.J.R. Heck, S. Mohammed, Assessing biological variation and protein processing in primary human leukocytes by automated multiplex stable isotope labeling coupled to 2 dimensional peptide separation. Mol Biosyst 5, 992 (2009).

30. F. Wang et al., A Fully Automated System with Online Sample Loading, Isotope Dimethyl Labeling and Multidimensional Separation for High-Throughput Quantitative Proteome Analysis. Anal Chem 82, 3007 (2010).

31. P.J. Boersema, R. Raijmakers, S. Lemeer, S. Mohammed, A.J.R. Heck, Multiplex peptide stable isotope dimethyl labeling for quantitative proteomics. Nat Protocols 4, 484 (2009).

32. J.L. Hsu, S.H. Chen, D.T. Li, F. K. Shi, Enhanced a1 Fragmentation for Dimethylated Proteins and Its Applications for N-Terminal Identification and Comparative Protein Quantitation. J Proteome Res 6, 2376 (2007).

33. P.T. Shen, J.L. Hsu, S.H. Chen, Dimethyl Isotope-Coded Affinity Selection for the Analysis of Free and Blocked N-Termini of Proteins Using LC−MS/MS. Anal Chem 79, 9520 (2007).

34. N. Taouatas, A. J. R. Heck, S. Mohammed, Evaluation of Metalloendopeptidase Lys-N Protease Performance under Different Sample Handling Conditions. J Proteome Res 9, 4282 (2010).

35. M. Hennrich, S. Mohammed, A. Altelaar, A. Heck, Dimethyl isotope labeling assisted de novo peptide sequencing. J Am Soc Mass Spectrom 21, 1957 (2010).

36. D. Kovanich, T.T. Aye, A.J.R. Heck, A. Scholten, in Methods in Moleucular Biology: Chemical Proteomics. (2012), vol. 803, pp. 167-181.

37. S. Cappadona, P. Baker, P. Cutillas, A. Heck, B. van Breukelen, Current Challenges in Software Solutions for Mass Spectrometry-Based Quantitative Proteomics. Amino Acids 43, 1087 (2012).

38. K.C. Hansen et al., Mass Spectrometric Analysis of Protein Mixtures at Low Levels Using Cleavable 13C-Isotope-coded Affinity Tag and Multidimensional Chromatography. Mol Cell Proteomics 2, 299 (2003).

39. R.J. Chalkley et al., Comprehensive Analysis of a Multidimensional Liquid Chromatography Mass Spectrometry Dataset Acquired on a Quadrupole Selecting, Quadrupole Collision Cell, Time-of-flight Mass Spectrometer. Mol Cell Proteomics 4, 1194 (2005).

40. C. Ji et al., A study of reproducibility of guanidination–dimethylation labeling and liquid chromatography matrix-assisted laser desorption ionization mass spectrometry for relative proteome quantification. Analytica Chimica Acta 585, 219 (2007).

41. P. Mortensen et al., MSQuant, an Open Source Platform for Mass Spectrometry-Based Quantitative Proteomics. J Proteome Res 9, 393 (2009).

42. J. Cox, M. Mann, MaxQuant enables high peptide identification rates, individualized p.p.b.-range mass accuracies and proteome-wide protein quantification. Nat Biotech 26, 1367 (2008).

43. Z. Khan, J.S. Bloom, B.A. Garcia, M. Singh, L. Kruglyak, Protein quantification across hundreds of experimental conditions. Proc Natl Acad Sci 106, 15544 (2009).

44. D.K. Han, J. Eng, H. Zhou, R. Aebersold, Quantitative profiling of differentiation-induced microsomal proteins using isotope-coded affinity tags and mass spectrometry. Nat Biotech 19, 946 (2001).

45. E.W. Deutsch et al., A guided tour of the Trans-Proteomic Pipeline. Proteomics 10, 1150 (2010).

46. N. Colaert, J. Vandekerckhove, L. Martens, K. Gevaert, in Gel Free Proteomics: Methods and Protocols. (2011), vol. 753, pp. 373-398.

47. B. van Breukelen, H. W. P. van den Toorn, M. M. Drugan, A. J.R. Heck, StatQuant: a post-quantification analysis toolbox for improving quantitative mass spectrometry. Bioinformatics 25, 1472 (2009).

48. J. Munoz et al., The quantitative proteomes of human-induced pluripotent stem cells and embryonic stem cells. Mol Syst Biol 7 (2011).

49. D.H. Phanstiel et al., Proteomic and phosphoproteomic comparison of human ES and iPS cells. Nat Meth 8, 821 (2011).

50. R. Parker et al., Ecological Adaptation of Diverse Honey Bee (Apis mellifera) Populations. Plos One 5, e11096 (2010).

51. M.C.M. Kwok, J. M. Holopainen, L.L. Molday, L.J. Foster, R.S. Molday, Proteomics of photoreceptor outer segments identifies a subset of SNARE and Rab proteins implicated in membrane vesicle trafficking and fusion. Mol Cell Proteomics 7, 1053 (2008).

52. F. Kantawong et al., Whole proteome analysis of osteoprogenitor differentiation induced by disordered nanotopography and mediated by ERK signalling. Biomaterials 30, 4723 (2009).

53. S.H. Chen et al., Nucleophosmin in the pathogenesis of arsenic-related bladder carcinogenesis revealed by quantitative proteomics. Toxicol Appl Pharmacol 242, 126 (2010).

54. O.B. Bleijerveld et al., Protein signatures associated with tumor cell dissemination in head and neck cancer. J Proteomics 74, 558 (2011).

55. Q.W.T. Chan et al., The Worker Honeybee Fat Body Proteome Is Extensively Remodeled Preceding a Major Life-History Transition. Plos One 6, e24794 (2011).

56. H.J. Huang, M.L. Tsai, Y.-W. Chen, S.-H. Chen, Quantitative shot-gun proteomics and MS-based activity assay for revealing gender differences in enzyme contents for rat liver microsome. J Proteomics 74, 2734 (2011).

57. H.-L. Cheng et al., Urinary CD14 as a potential biomarker for benign prostatic hyperplasia - discovery by combining MALDI-TOF-based biostatistics and ESI-MS/MS-based stable-isotope labeling. Proteomics Clin Appl 5, 121 (2011).

58. A.J. Ytterberg, J.B. Peltier, K. J. van Wijk, Protein profiling of plastoglobules in chloroplasts and chromoplasts. A surprising site for differential accumulation of metabolic enzymes. Plant Physiol 140, 984 (2006).

59. J.P. Murphy, F. Kong, D.M. Pinto, G. Wang-Pruski, Relative quantitative proteomic analysis reveals wound response proteins correlated with after-cooking darkening. Proteomics 10, 4258 (2010).

60. D. Wijte, B. L.M. van Baar, A.J.R. Heck, A.F.M. Altelaar, Probing the Proteome Response to Toluene Exposure in the Solvent Tolerant Pseudomonas putida S12. J Proteome Res 10, 394 (2011).

61. A.C. Tolonen et al., Proteome-wide systems analysis of a cellulosic biofuel-producing microbe. Mol Syst Biol 7 (2011).

62. P.A. Grimsrud, D.L. Swaney, C.D. Wenger, N.A. Beauchene, J.J. Coon, Phosphoproteomics for the Masses. ACS Chem Biol 5, 105 (2010).

63. S. Lemeer, A. J. R. Heck, The phosphoproteomics data explosion. Curr Opin Chem Biol 13, 414 (2009).

64. B. Macek, M. Mann, J.V. Olsen, Global and Site-Specific Quantitative Phosphoproteomics: Principles and Applications. Annu Rev Pharmacol Toxicol 49, 199 (2009).

65. A. Leitner, M. Sturm, W. Lindner, Tools for analyzing the phosphoproteome and other phosphorylated biomolecules: A review. Anal Chim Acta 703, 19 (2011).

66. A.D. Zoumaro-Djayoon et al., Investigating the role of FGF-2 in stem cell maintenance by global phosphoproteomics profiling. Proteomics 11, 3962 (2011).

67. J.A. Thomson et al., Embryonic Stem Cell Lines Derived from Human Blastocysts. Science 282, 1145 (1998).

68. V.M.Y. Ding et al., Tyrosine Phosphorylation Profiling in FGF-2 Stimulated Human Embryonic Stem Cells. Plos One 6, e17538 (2011).

69. A. Wolf-Yadlin, S. Hautaniemi, D.A. Lauffenburger, F. M. White, Multiple reaction monitoring for robust quantitative proteomic analysis of cellular signaling networks. Proc Natl Acad Sci 104, 5860 (2007).

70. C.J. Wu, Y. W. Chen, J.H. Tai, S.H. Chen, Quantitative Phosphoproteomics Studies Using Stable Isotope Dimethyl Labeling Coupled with IMAC-HILIC-nanoLC−MS/MS for Estrogen-Induced Transcriptional Regulation. J Proteome Res 10, 1088 (2011).

71. S.V. Kozlov et al., Autophosphorylation and ATM Activation: additional sites add to the complexity. J Biol Chem 286, 9107 (2011).

72. N.G. Oberprieler et al., High-resolution mapping of prostaglandin E(2)-dependent signaling networks identifies a constitutively active PKA signaling node in CD8(+)CD45RO(+) T cells. Blood 116, 2253 (2010).

73. S. Ortega-Gutierrez, D. Leung, S. Ficarro, E.C. Peters, B.F. Cravatt, Targeted Disruption of the PME-1 Gene Causes Loss of Demethylated PP2A and Perinatal Lethality in Mice. Plos One 3, e2468 (2008).

74. J.L. Hsu et al., Functional phosphoproteomic profiling of phosphorylation sites in membrane fractions of salt-stressed Arabidopsis thaliana. Proteome Sci 7, (2009).

75. H. Kaji, Y. Yamauchi, N. Takahashi, T. Isobe, Mass spectrometric identification of N-linked glycopeptides using lectin-mediated affinity capture and glycosylation site-specific stable isotope tagging. Nat. Protocols 1, 3019 (2007).

76. H. Zhang, X. J. Li, D.B. Martin, R. Aebersold, Identification and quantification of N-linked glycoproteins using hydrazide chemistry, stable isotope labeling and mass spectrometry. Nat Biotech 21, 660 (2003).

77. P. Hägglund, J. Bunkenborg, F. Elortza, O.N. Jensen, P. Roepstorff, A New Strategy for Identification of N-Glycosylated Proteins and Unambiguous Assignment of Their Glycosylation Sites Using HILIC Enrichment and Partial Deglycosylation. J Proteome Res 3, 556 (2004).

78. M.R. Larsen, S.S. Jensen, L.A. Jakobsen, N.H.H. Heegaard, Exploring the Sialiome Using Titanium Dioxide Chromatography and Mass Spectrometry. Mol Cell Proteomics 6, 1778 (2007).

79. B.L. Parker et al., Quantitative N-linked Glycoproteomics of Myocardial Ischemia and Reperfusion Injury Reveals Early Remodeling in the Extracellular Environment. Mol Cell Proteomics 10, M110.006833 (2011).

80. X. Wei, A. Herbst, D. Ma, J. Aiken, L. Li, A Quantitative Proteomic Approach to Prion Disease Biomarker Research: Delving into the Glycoproteome. J Proteome Res 10, 2687 (2011).

81. N. Khidekel et al., Probing the dynamics of O-GlcNAc glycosylation in the brain using quantitative proteomics. Nature Chem Biol 3, 339 (2007).

82. O. Kleifeld et al., Isotopic labeling of terminal amines in complex samples identifies protein N-termini and protease cleavage products. Nat Biotech 28, 281 (2010).

83. O. Kleifeld et al., Identifying and quantifying proteolytic events and the natural N terminome by terminal amine isotopic labeling of substrates. Nat Protocols 6, 1578 (2011).

84. A. Doucet, O. Kleifeld, J.N. Kizhakkedathu, C.M. Overall, in Gel-Free Proteomics. (2011), vol. 753, pp. 273-287.

85. O. Schilling, O. Barré, P.F. Huesgen, C.M. Overall, Proteome-wide analysis of protein carboxy termini: C terminomics. Nat Methods 7, 508 (2010).

86. O. Schilling, P. F. Huesgen, O. Barré, C.M. Overall, in Network Biology : Methods and Applications. (2011), vol. 781, pp. 59-69.

87. P.F. Huesgen, C.M. Overall, N- and C-terminal degradomics: new approaches to reveal biological roles for plant proteases from substrate identification. Physiol Plantarum 145, 5 (2011).

88. S. Tholen et al., Contribution of cathepsin L to secretome composition and cleavage pattern of mouse embryonic fibroblasts. Biol Chem 392, 961 (2011).

89. N. Simonis et al., Empirically controlled mapping of the Caenorhabditis elegans protein-protein interactome network. Nat Meth 6, 47 (2008).

90. A.C. Gingras, M. Gstaiger, B. Raught, R. Aebersold, Analysis of protein complexes using mass spectrometry. Nat Rev Mol Cell Biol 8, 645 (2007).

91. T.T. Aye et al., Selectivity in Enrichment of cAMP-dependent Protein Kinase Regulatory Subunits Type I and Type II and Their Interactors Using Modified cAMP Affinity Resins. Mol Cell Proteomics 8, 1016 (2009).

92. P.C. Cheng, H.K. Chang, S.H. Chen, Quantitative Nanoproteomics for Protein Complexes (QNanoPX) Related to Estrogen Transcriptional Action. Mol Cell Proteomics 9, 209 (2009).

93. A. Cherkasov et al., Mapping the Protein Interaction Network in Methicillin-Resistant Staphylococcus aureus. J Proteome Res 10, 1139 (2010).

94. P. Dadvar, M. O'Flaherty, A. Scholten, K. Rumpel, A.J.R. Heck, A chemical proteomics based enrichment technique targeting the interactome of the PDE5 inhibitor PF-4540124. Mol Biosyst 5, 472 (2009).

95. D. Kovanich et al., Sphingosine Kinase Interacting Protein is an A-Kinase Anchoring Protein Specific for Type I cAMP-Dependent Protein Kinase. Chembiochem 11, 963 (2010).

96. R. Raijmakers et al., Target Profiling of a Small Library of Phosphodiesterase 5 (PDE5) Inhibitors using Chemical Proteomics. Chemmedchem 5, 1927 (2010).

97. R.M. Ewing et al., Large-scale mapping of human protein-protein interactions by mass spectrometry. Mol Syst Biol 3 (2007).

98. M. Bantscheff, A. Scholten, A.J.R. Heck, Revealing promiscuous drug–target interactions by chemical proteomics. Drug Discov Today 14, 1021 (2009).

99. J. W. Gouw, B.B.J. Tops, J. Krijgsveld, in Gel Free Proteomics: Methods and Protocols. (2011), vol. 753, pp. 29-42.

100. X. Yao, A. Freas, J. Ramirez, P. A. Demirev, C. Fenselau, Proteolytic 18O Labeling for Comparative Proteomics: Model Studies with Two Serotypes of Adenovirus. Anal Chem 73, 2836 (2001).

101. M. Bantscheff, B. Dümpelfeld, B. Kuster, Femtomol sensitivity post-digest 18O labeling for relative quantification of differential protein complex composition. Rapid Commun Mass Spectrom 18, 869 (2004).

Chapter 3

Probing the Specificity of Protein-Protein Interactions by Quantitative Chemical Proteomics

Duangnapa Kovanich
Thin Thin Aye
Albert J.R. Heck
Arjen Scholten

Biomolecular Mass Spectrometry and Proteomics,
Utrecht Institute for Pharmaceutical ciences and Bijvoet Center for Biomolecular Research,
Utrecht University, Padualaan 8, 3584 CH, Utrecht, The Netherlands

Based on Methods Mol Biol. 2012, 803, 167-81

3.1 Abstract

Chemical proteomics is a versatile tool to investigate protein-small molecule interactions, but can be extended to probe also secondary binding investigating small-molecule-protein 1-protein 2 interactions, providing insight into protein scaffolds. This application of chemical proteomics has in particular been applied extensively to cyclic nucleotide (cAMP, cGMP) signaling. cAMP regulates cellular functions primarily by activating cAMP-dependent protein kinase (PKA). Compartmentalization of PKA plays an important role in the specificity of cAMP signaling events and is mediated by interaction of the regulatory subunit (PKA-R) with A-kinase anchoring proteins (AKAPs), which often form the core of even larger protein machineries. To which AKAP the specific major isoforms PKA-R type I (PKA-RI) and PKA-R type II (PKA-RII) bind is not well established for most AKAPs, however, this specificity is an important feature of cAMP/PKA signaling. Here we describe the application of a chemical proteomics screening tool that combines cAMP-based affinity chromatography with quantitative mass spectrometry to investigate PKA-R isoform/AKAP specificity directly in lysates of cells and tissues of any origin. With this tool several novel PKA-R/AKAP specificities can be easily resolved.

3.2 Introduction

A large number of hormones and neurotransmitters utilize cyclic nucleotides, adenosine- and guanosine 3',5' cyclic monophosphate (cAMP, cGMP), as an intracellular second messenger (1). cAMP signaling plays an important role in a plethora of cellular processes and its principle intracellular target is cAMP-dependent protein kinase (PKA). Compartmentalization of PKA plays a key role in the specificity of cAMP mediated signaling events. This specificity is achieved by binding of PKA's regulatory subunit (PKA-R) to the large and diverse family of protein scaffolds, called A-kinase anchoring proteins (AKAPs). The binding affinities of PKA for AKAPs differ significantly for the two main classes of PKA-R isoforms, PKA-RI and PKA-RII. The AKAP family can roughly be divided into three groups on the basis of which PKA-R subunit(s) bind(s) to them. A first category is formed by AKAPs that bind rather specifically to PKA-RII (for a review see (2)). Also several dual-specificity AKAPs have been described, such as D-AKAP1 (3) and D-AKAP2 (4), which can anchor both PKA-RI and PKA-RII, although still with rather different affinities. Related to cAMP/PKA mediated signaling, also cGMP mediated signaling occurs in cells, mainly proceeding via the cGMP-dependent protein kinase (PKG), which as PKA also seems compartmentalized.

Most cAMP-mediated signaling proteins have a relative low abundance when compared to the abundant house-keeping proteins. Therefore specific enrichment techniques are required when these are to be studied by proteomics techniques. In recent years cAMP- and cGMP-based affinity enrichment techniques have been combined with sensitive mass spectrometric identification of the enriched proteins (5, 6) making a plethora of new information available on this important family of proteins. For instance, applied to heart tissue, these sort of analyses revealed the presence of at least 14 different AKAPs, but also other cyclic nucleotide based signaling proteins could be enriched for and identified, such as Epac, different phosphodiesterases, as well as different PKG isoforms.

Synthetic cAMP analogs have been developed as tools to unravel cAMP signal transduction pathways (7). A prime interest in PKA-RI and PKA-RII specific analogues exists; however, none have been discovered thus far. In addition, analogs that can differentiate between PKA and other cAMP-based signaling proteins have been described, of which 8pCPT-2'-OMe-cAMP is a prime

example as it only activates Epac, and not PKA (8). We recently screened the characteristics of the immobilized analog of the Epac-compound, 8-AHA-2'-OMe-cAMP, and found by quantitative mass spectrometry that it binds to PKA-RI about 3-4-fold better than to PKA-RII. Here we describe in detail how the binding characteristics of different immobilized cAMP-analogs can be utilized to investigate - PKA-AKAP interaction specificity directly in the lysate of cells and tissues. In a proof of principle study this method could enrich for more than 10 AKAPs and provide specificity information on all of them. Interestingly, for 3 of the enriched AKAPs their PKA-R specificity was established for the first time (9).

3.3 Materials

3.3.1 Cell and Tissue Lysis

1. Protease inhibitor cocktail (Complete mini) (Roche Diagnostics)

2. Phosphatase inhibitor cocktail II (Sigma)

3. Phosphate buffer saline (PBS): Prepare 10X stock with 1.37 M NaCl, 27mM KCl, 100mM Na2HPO4, 18 mM KH2PO4 and adjust to pH 7.4 with HCl if necessary. Prepare working solution by dilution of one part with nine parts Milli-Q water.

4. Lysis buffer: PBS buffer, 0.1% Tween 20, protease inhibitor cocktail (1 tablet per 15ml buffer) and 150µl of phosphatase inhibitor cocktail II (Sigma) (See Note 1).

3.3.2 cAMP-Affinity Pull-Down

1. 8AHA-cAMP-agarose beads (C8 beads) and 8AHA-2'-O-Me-cAMP-agarose beads (C8_OCH3 beads) (Biolog): Prepare 25% bead slurry in Milli-Q water containing 0.1% NaN3 and store at 4°C (See Note 2).

2. 100mM Adenosine 5′-diphosphate (ADP) sodium salt and Guanosine 5′-diphosphate (GDP) sodium salt (Sigma-Aldrich) are dissolved in Milli-Q water and stored at 4°C.

3. Washing buffer: 10mM ADP and GDP in PBS. Prepare for single use by dilution of 100mM to 10mM ADP, GDP with lysis buffer.

3.3.3 Dual-Protease In-Solution Digestion

1. 50mM Ammonium bicarbonate (ABC) in Milli-Q water.

2. 8M Urea in 50mM ABC (See Note 3).

3. LysC and Trypsin (Roche Diagnostics) are dissolved at 0.1 µg/µl in 50mM acetic acid and stored in single use aliquots at -80°C.

4. Dithiothreitol (DTT) and Iodoacetamide (IAA) are dissolved at 200mM in 50mM ABC and stored in single use aliquots at -20°C.

3.3.4 On-Column Isotopic Dimethyl Labeling

1. HPLC solvent A: 0.1 M acetic acid in Milli-Q water.

2. HPLC solvent B: 0.1 M acetic acid in 80% acetonitrile.

3. 50mM Sodium phosphate buffer pH 7.5: Prepare stock solutions of 50mM NaH2PO4 and 50mM Na2HPO4. Prepare Working solution by mixing 2ml of 50mM NaH2PO4 with 7ml of 50mM Na2HPO4 .

4. 250µl of 4% (V/V) formaldehyde (CH_2O, 37%, Sigma-Aldrich) in Milli-Q water (See Note 4).

5. 250µl of 4% (V/V) D-formaldehyde (CD_2O, 98%, Isotec) in Milli-Q water (See Note 4).

6. 600mM Sodium cyanoborohydride ($NaBH_3CN$, Fluka) in Milli-Q water (See Note 5).

7. Light labeling reagent: mix 4.5ml of 50mM sodium phosphate buffer (pH 7.5) with 250µl of 4% formaldehyde and 250µl of 600mM $NaBH_3CN$.

8. Intermediate labeling reagent: mix 4.5ml of 50mM sodium phosphate buffer (pH 7.5) with 250µl of 4% D-formaldehyde and 250µl of 600mM NaBH3CN.

9. Sep-Pak C18 cartridges (Waters).

3.3.5 Strong Cation Exchange (SCX) Fractionation

1. SCX Solvent A: 20 % acetonitrile, 0.05 % formic acid, pH 3.0 in Milli-Q water.

2. SCX Solvent B: 500mM KCl in 20 % acetonitrile and 0.05 % formic acid, pH 3.0 in Milli-Q water.

3.3.6 LC-MS/MS analysis

1. HPLC solvent A : 0.1M acetic acid in Milli-Q water.

2. HPLC solvent B: 0.1M acetic acid in 80% acetonitrile in Mill-Q water.

3.4 Methods

For the affinity purification of cAMP-interacting proteins, various synthetic cAMP analogs are available. These can be immobilized to beads using different coupling positions on the nucleotide and different linkers. For instance, here we used agarose beads on which cAMP is immobilized via an 1,6-diaminohexyl (AHA) spacer attached to the 8-position on the imidazole ring of the adenine moiety. Two types of beads are used 8AHA-cAMP-agarose beads, further referred to as C8 and 8AHA-2'-O-Me-cAMP-agarose beads, further referred to as C8_OCH_3, in which the hydroxyl group at the 2' position on the ribose is substituted by a methoxy group. The chemical structures of the two immobilized cAMP analogs beads are depicted in Figure 1. Initial chemical proteomics experiments showed that C8 has equal affinity for both PKA-RI and PKA-RII, whereas C8_OCH_3 has a 3-4-fold preference for PKA-RI. This difference in affinity is used as a discriminating factor to evaluate the specificity of enriched AKAPs. Following the affinity pull-downs with both beads,

all enriched proteins are digested and chemically labeled with stable isotopes using formaldehyde based chemical dimethylation of primary amines (10). Then both labeled samples are mixed in a 1:1 ratio and analyzed by mass spectrometry.

Stable isotope dimethyl labeling utilizes isotopomers of formaldehyde and sodium cyanoborohydride to incorporate dimethyl labels at the ε-amino groups of all lysines and at the N-terminus of all proteins and/or peptides. Using two different formaldehyde isotopomers, peptide doublets are generated that exhibit a mass difference of at least 4 Da, easily distinguishable in the mass spectrometer. Peptides which are enriched by C8 are ‘‘intermediate’’ isotope labeled and peptides which are enriched by C8-OCH_3 are ‘‘light’’ labeled. The intensity ratio between the ‘‘intermediate’’ and ‘‘light’’ peaks represents their relative abundance in each of the pull-downs. The ratios averaged over all peptides observed for each enriched AKAP are calculated and used as an indicator of its preference for PKA-RI and/or PKA-RII isoforms.

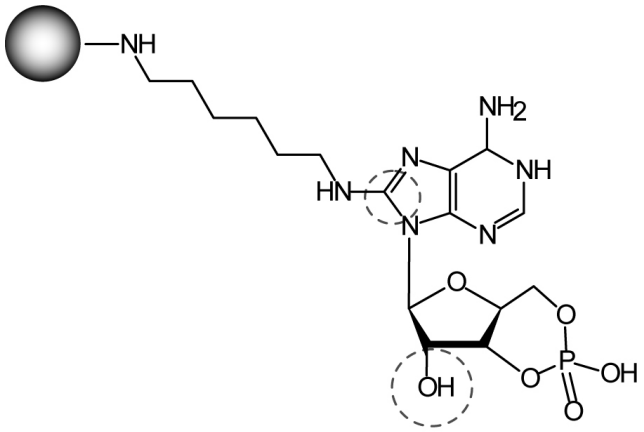

8AHA-cAMP (C8)

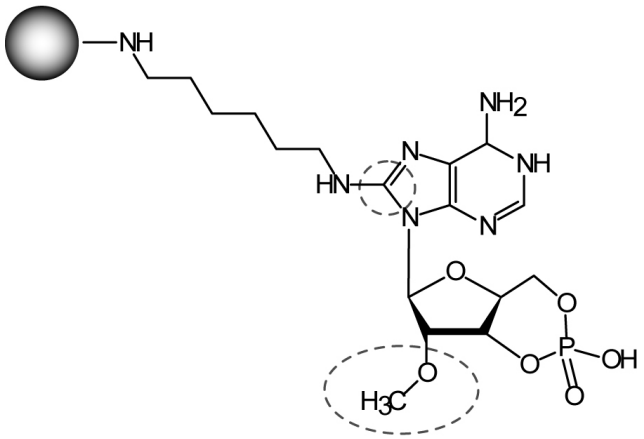

8AHA-2’OMe-cAMP(C8_OCH_3)

Figure 1 > Chemical structures of the immobilized cAMP beads C8 and C8_OCH_3.

cAMP derivatives are immobilized via an 1,6-diaminohexyl (AHA) spacer that is attached to the 8-position of the imidazole ring of the adenine moiety. The hydroxyl group at the 2’ position on the ribose of the C8 beads (left) is substituted with a methoxyl (OCH3) group to generate C8_OCH_3 beads (right).

3.4.1 Preparation of Cell and Tissue Lysate for cAMP Affinity Pull-Down

Cell Lysis

1. Harvest the cells at a density of 1.5 × 106 cells/ml by centrifugation (30 min, 1000 × g). Discard supernatant and wash the pellet once with ice-cold PBS (See Note 6).

2. Resuspend the pellet in 1ml ice-cold lysis buffer. Transfer the cell suspension to a pre-chilled glass homogenizer.

3. Lyse the cells using dounce homogenization on ice for 1-2 min. Transfer the lysate to a pre-chilled eppendorf tube.

4. Centrifuge the lysate at 20 000 × g at 4 °C. Carefully transfer a soluble fraction to a new pre-chilled falcon tube. Resuspend the pellet in 1ml ice-cold lysis buffer and repeat the dounce homogenization in step 3.

5. Repeat centrifugation in step 4. Combine both supernatants from step 3 and 4.

6. Wash the pellet from step 5 with 1ml ice-cold lysis buffer. Repeat centrifugation and combine the soluble fraction from this step to the one from step 5.

7. Measure the protein concentration of the soluble fraction.

Tissue Lysis

1. Pre-chill a steel mortar, pestle, and spoon in liquid nitrogen.

2. Ground about 1g of frozen tissue in the cold steel mortar with the cold pestle.

3. Use the cold spoon to transfer the pulverized tissue to a pre-chilled eppendorf tube.

4. Add 1 ml of ice-cold lysis buffer to the pulverized tissue, leave at room temperature for 5 min, and for another 10 min on ice.

5. Centrifuge the lysate at 20 000 × g at 4 °C. Carefully transfer the supernatant to a new pre-chilled falcon tube. The insoluble pallet can be washed several times as described in step 3, 4 and 5 of the cell lysis.

6. Measure the protein concentration of the soluble fraction. The lysate is now ready for pull-down assay (See Note 6).

3.4.2 cAMP affinity pull-down

1. C8 and C8_OCH3 pull-downs are performed separately. Use a lysate with 10mg total protein for each pull-down. The used amount depends somewhat on the abundance of PKA in the lysates and the number of washing steps incorporated.

2. Prior to the pull-down assay, supplement the lysate with 500µl of 100mM ADP and GDP to achieve a final concentration of 10mM ADP and GDP to the lysate. Then the lysate is topped up with ice-cold PBS to 5ml total volume to achieve a final protein concentration of 2mg/ml. Then incubate at 4 °C under agitation for at least 30 min (See Note 7).

3. Transfer 400µl bead slurry (100µl dry beads) to an eppendorf tube and wash the beads by adding 500µl lysis buffer to the slurry (See Note 8).

4. Centrifuge for 1 min at 1000 × g at 4 °C. Discard the supernatant and repeat the washing step (See Note 9).

5. Transfer the beads to the ADP,GDP treated lysate in a protein : beads ratio of 10mg protein:100ul of dry beads and incubate at 4 °C under agitation for at least 2 h.

6. Centrifuge the beads, remove the unbound fraction and wash the bead bound fraction for 2 times with 1ml of washing buffer.

7. Repeat the washing and centrifugation steps with 2ml lysis buffer for 4 times. (See Note 7).

8. Transfer the beads to a new eppendorf tube. Remove the last wash as much as possible by pipetting with a thin-bore gel-loader tip (Eppendorf). The bead bound fraction is now ready for dual-protease digestion, or if required for SDS-PAGE gel loading (See Note 9).

3.4.3 Dual-Protease In-Solution Digestion

1. Elute the bound proteins from the beads by adding 100µl 8M urea.

2. Reduce disulfide bonds in the protein digest with 2mM DTT by adding 4µl 200mM DTT to the digest and incubate at 56°C for 15 min.

3. Alkylate the protein digest with 4mM IAA by adding 8µl 200mM IAA to the digest and incubate at room temperature for 30 min in the dark.

4. Add 2µl LysC solution. Incubate the protein mixture at 37 °C for 4 h (See Note 10).

5. Dilute the LysC digested solution by adding 300µl of 50mM ABC to get a final concentration of 2M urea.

6. Repeat the 2nd-step digestion with trypsin by adding 2µl trypsin and incubate at 37 °C overnight.

7. Collect the supernatant (digested peptides) by centrifugation at 1000 × g and transfer to a new eppendorf tube. The digest is now ready for labeling.

3.4.4 On-Column Isotopic Dimethyl Labeling

1. These instructions assume the use of a Visiprep DL Vacuum manifold system (Sigma). The Visiprep system contains a valve system that allows for precise flow control. It is essential to achieve a stable flow at 0.5 ml/min during sample loading, labeling, and eluting steps (step 5, 7, and 9).

2. Wash two Sep-Pak columns with 2ml acetonitrile.

3. Equilibrate the Sep-Pak columns twice with 2ml of HPLC solvent A.

4. Acidify the digests from the C8 and C8_OCH3 pull-down experiments by adding 1ml of HPLC solvent A.

5. Load each sample on a separate Sep-Pak column.

6. Desalt the samples by washing the Sep-Pak columns with 2ml of HPLC solvent A.

7. Flush the Sep-Pak columns five times with 1ml of respective labeling reagent. Light labeling reagent is flushed though the sample that originated from C8_OCH3 pull-down whereas intermediate labeling reagent is flushed though the samples originated from C8 pull-down .

8. Wash the Sep-Pak columns with 2ml of HPLC solvent A to remove sodium phosphate buffer.

9. Elute and collect the labeled samples from the Sep-Pak columns with 500µl of HPLC solvent B.

10. Mix the differentially labeled samples (i.e. “intermediate labeled” C8 and “Light labeled” C8_OCH3) in 1:1 ratio.

11. Dry the mixed sample using a Speedvac (1500 RPM, room temperature) (See Note 11).

12. Reconstitute the labeled sample in 10µl of SCX solvent A. The sample is now ready for SCX fractionation.

3.4.5 Strong Cation Exchange (SCX) Fractionation

1. These instructions assume the use of Zorbax BioSCX-Series II columns (0.8 mm (i.d.) × 50 mm (l), 3.5 µm) (Agilent Technologies). SCX is performed using two in-line coupled Zorbax BioSCX-Series II columns, FAMOS autosampler (Dionex/ LC Packings), Shimadzu LC-9A binary pump and SPD-6A UV-detector (Shimadzu). SCX is performed at pH3 at which acidic residues (Asp and Glu) are uncharged to allow all the peptides to bind to the column.

2. Inject 10 µl labeled sample by FAMOS autosampler.

3. Load the injected sample to the column with SCX solvent A for 5 mins.

4. Elute with a 1% per minute linear gradient of SCX solvent B at a flow rate of 50uL/min for 45 min. Then equilibrate the column with SCX solvent A for 10min.

5. A total of 45 SCX fractions (1min each, 50ul elution volume) are collected using a fraction collector.

6. Dry all fractions using a SpeedVac (1500 RPM, room temperature) and resuspend in 20 µl 10% formic acid. The samples are now ready to subject to LC-MS/MS analysis.

3.4.6 LC-MS/MS analysis

1. These instructions assume the use of a nanoflow liquid chromatography setup, directly coupled to a LTQ-Orbitrap mass spectrometer equipped with an electrospray ion source (Thermo Electron) for MS analysis.

2. A volume of 10ul of resuspended SCX fractions is used for subsequent nanoLC-LTQ-Orbitrap-MS (Thermo).

3. An Agilent 1200 series LC system is equipped with a 20mm Aqua C18 (5µm, Phenomenex) trapping column (100µm (i.d.), packed in-house) and a 400mm ReproSil-Pur C18-AQ (3µm, Dr. Maisch GmBH) analytical column (50µm (i.d.), packed in-house).

4. Trapping is performed at 5µL/min for 10 min in solvent A, and elution is achieved with a gradient of 10−35% solvent B in 45 min in a total analysis time of 60 min. The flow rate is passively split to 100nL/min when performing the elution analysis. Nanospray is achieved using a distally coated fused-silica emitter (360µm (o.d.); 20µm (i.d.); tip inner diameter, 10µm) (New Objective) biased to 1.7 kV.

5. The LTQ-Orbitrap mass spectrometer is operated in data-dependent mode, automatically switching between MS and MS/MS. Full-scan MS spectra (350−1500 m/z) are acquired in the FT-Orbitrap with a resolution of R=60,000 at 350 m/z after accumulation to a target value of 500,000 ions in the linear ion trap. The two most intense peaks above a threshold of 500 are fragmented in the linear ion trap using normalized collision energy of 35 after accumulation to a target value of 30,000 ions.

3.4.7 Data analysis

1. Process MS/MS spectra collected from each LC-MS/MS run with Bioworks (Thermo Scientific). Combine the data of the individual LC-MS/MS run into a single mascot generic file using MGF combiner (MSQuant).

2. Perform Mascot searching on the generated MGF file against an appropriate database using MASCOT (Matrix Science) (See Note 12).

3. Searching criteria include carbamidomethylation on cysteine residues as a fixed modification. Oxidation (M), light-dimethyl (K- and N-term) and intermediate-dimethyl (K- and N-term) as variable modifications. Allow two missed cleavages and set a peptide mass tolerance to 10 ppm and the MS/MS mass tolerance to 0.9 Da.

4. The search result from Mascot is converted into .HTML file format. Use the .HTML file, in conjunction with the .RAW file generated by the mass spectrometer as an input for protein quantitation software MSQuant (11). MSQuant is an open-source software for quantitative proteomics and can be downloaded from http://msquant.alwaysdata.net/. MSQuant is needed to be customized for dimethyl labeling. An example of a screenshot of the quantitation window in MSQuant is shown in figure 2. Examples of MS spectra and extracted ion chromatograms of peptides enriched from pull-downs with two beads in HEK293 cell lysate are shown in figure 3.

5. Use MSQuant to extract and integrate ion chromatograms of all peptides. Area under the curve (AUC) between the monoisotopic peaks of "light" and "intermediate" is used to calculate a peptide ratio of the peptide pair. MSQuant does that for every charge state of a peptide pair. The constituted peptide ratio is calculated by averaging peptide ratios of all charge states and reported with their respective standard deviations. A protein ratio is calculated by averaging of all constituted peptide ratios originating from the protein. The protein ratio is used as a specificity ratio. An example of a summary of all specificity ratios obtained for each PKA isoform and all detected AKAPs is shown in figure 4.

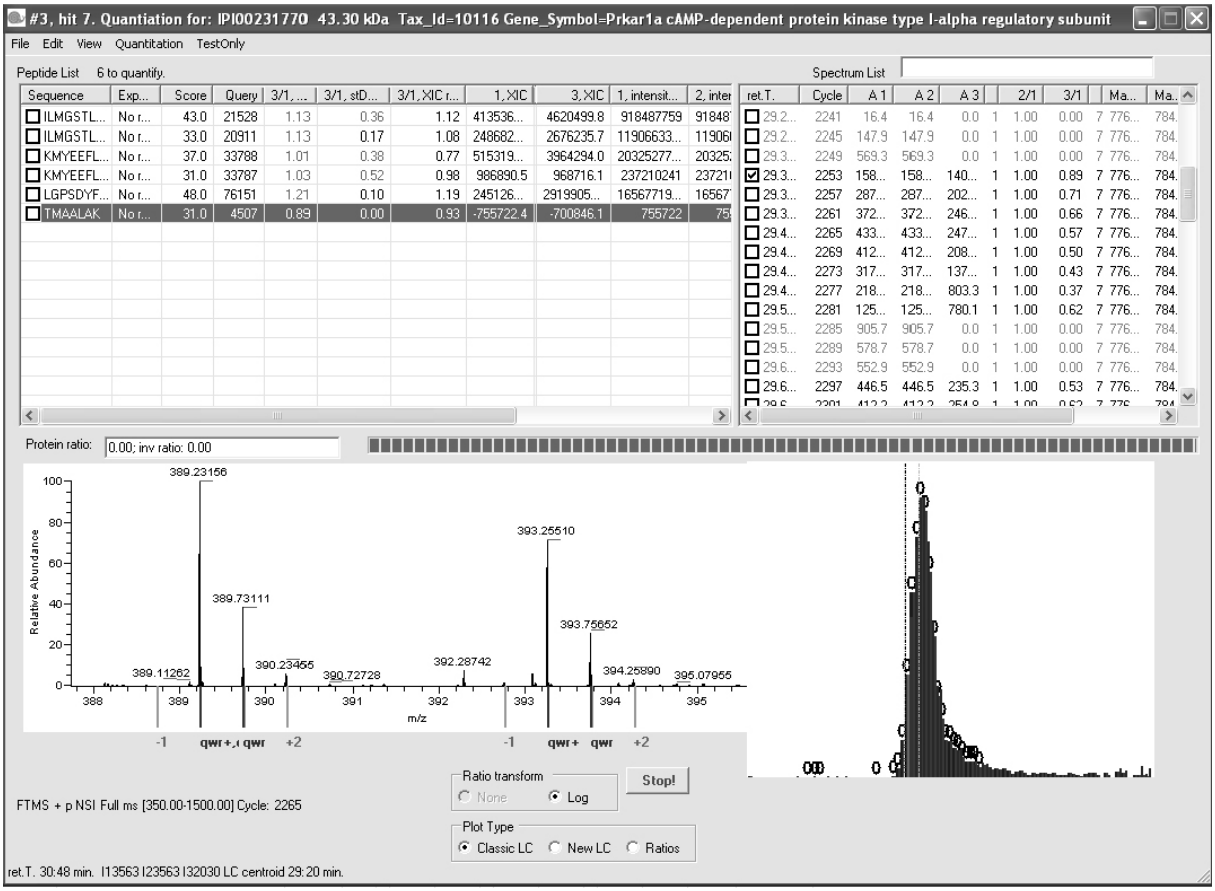

Figure 2 > Screenshot of the dimethyl-labeling quantitation window in MSQuant.

This window can be divided into four panels. A list of identified peptides of a protein that can be quantified is shown in the upper left panel and a list of MS scans with the retention time, scan number, intensities, and ratio indicated is shown in the upper right panel. A raw mass spectrum of each scan can be visualized in the lower left panel by activating (e.g. double clicking) a scan. The lower right panel shows a graph where the peak area of the peptides is plotted against the retention time.

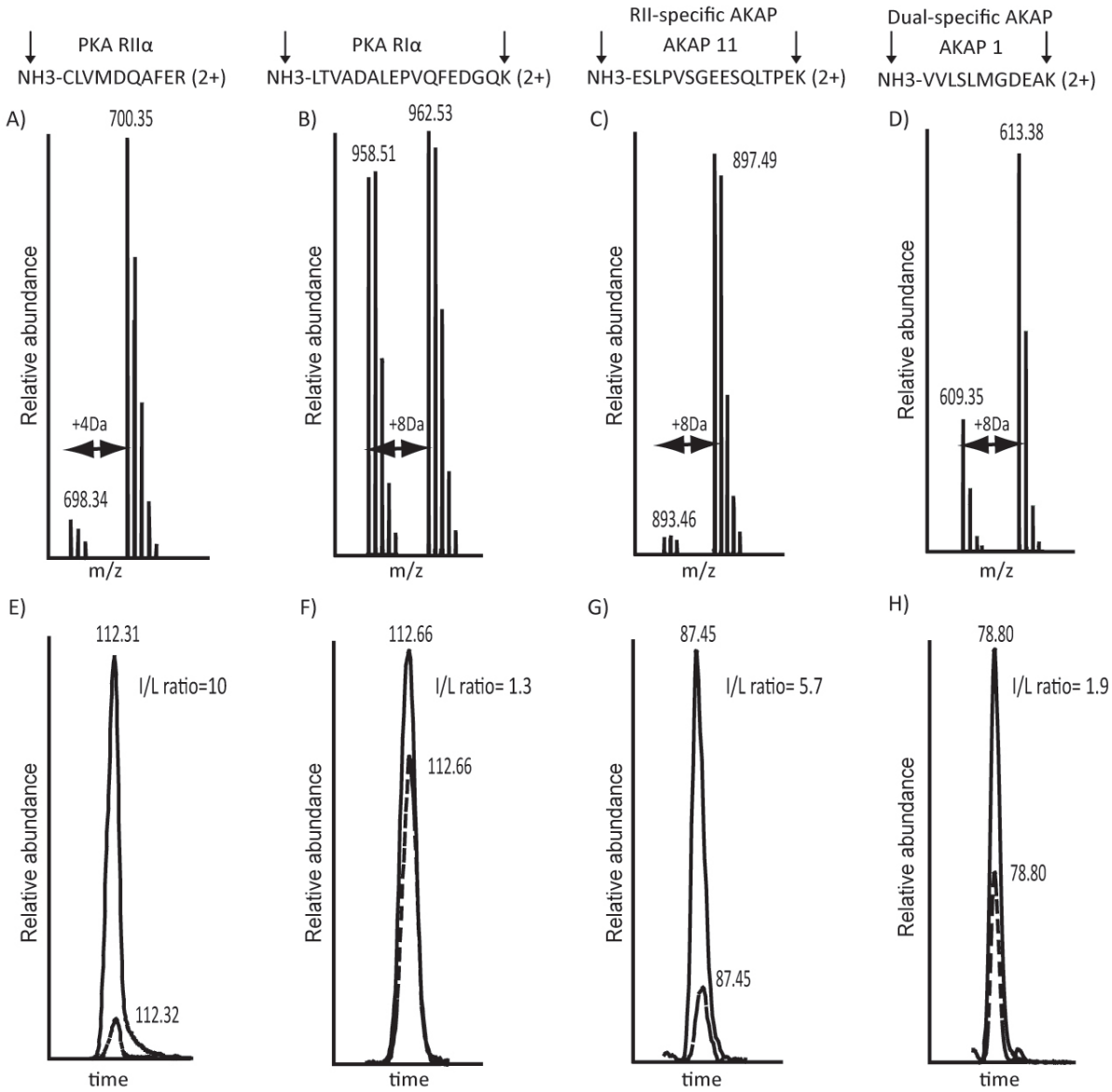

Figure 3 > An illustrative example of the subsequent quantitative MS-analysis.

MS spectra is shown in Upper panels, A–D) and extracted ion chromatograms (lower panels, E–H) of peptides originating from proteins in the affinity-enriched HEK293 cell lysate are depicted. MS spectra are presented in which "light" (C8_OCH_3, left) and "intermediate" (C8, right) peptides form peptide pairs that can be distinguished. Each dimethyl labeling event induces a typical 4 Da mass difference , so 4 Da (m/z difference of 2) for doubly charged peptides that have no lysine residues, and an 8 Da mass difference (4 Da m/z difference) is observed for doubly charged peptides with one lysine residue. Labeling sites are indicated by the arrows. In the lower panel, the extracted ion chromatograms of the intermediate-labeled peptides (peptides which are enriched by C8) are in solid line and light-labeled peptides (peptides which are enriched by C8_OCH3) are in dashed line. Each individual peptide pair is used for the assessment of differential binding affinities (Adapted from (9)).

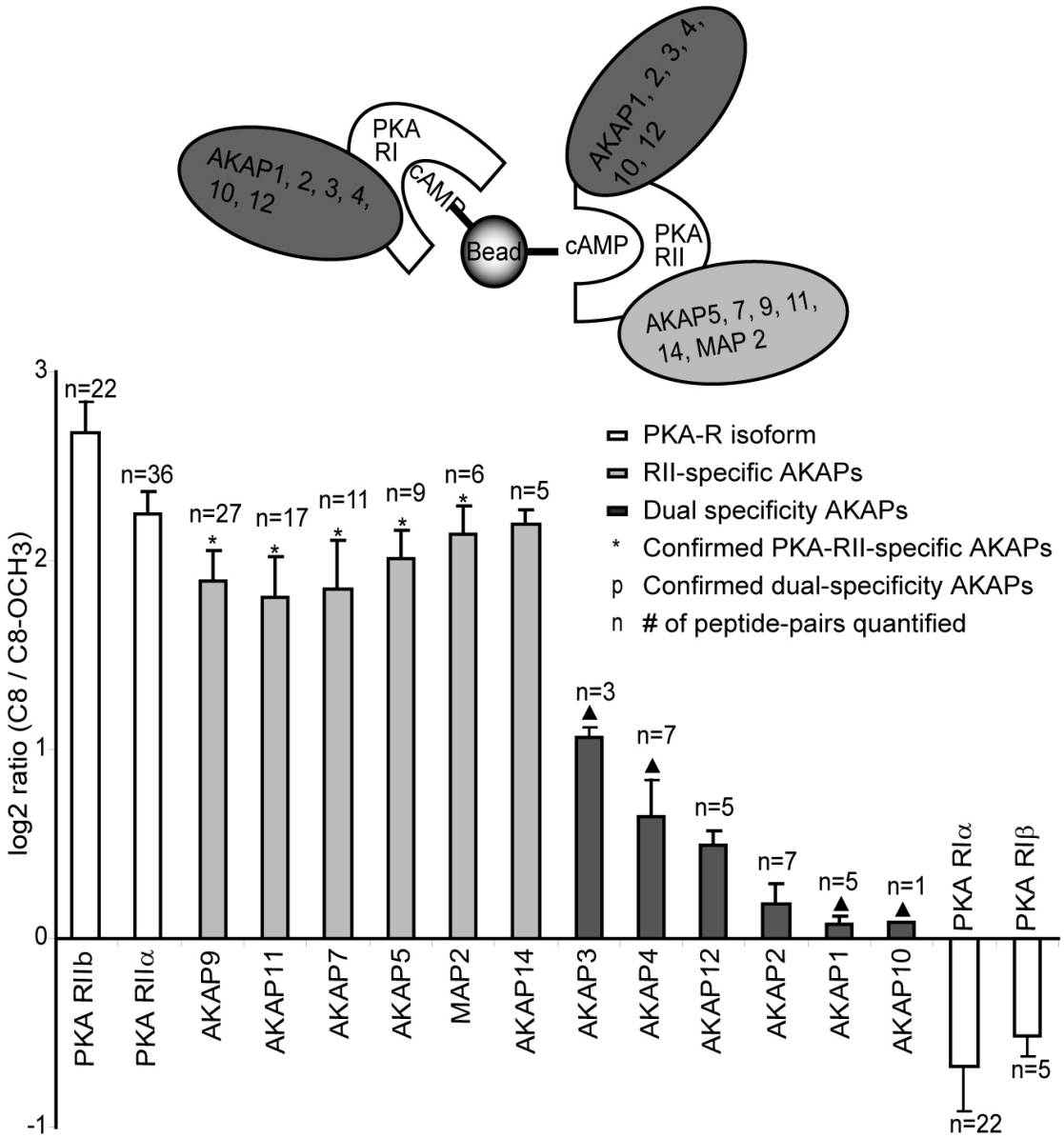

Figure 4 > Summary of all specificity ratios obtained for each PKA isoform and all detected AKAPs.

Overview of averaged binding specificity ratios of all AKAPs affinity purified from HEK293, and RCC10 cells, rat lung, and rat testis tissue. The protein ratios are calculated by pooling all peptide pairs detected in each tissue for a certain protein. The overall standard deviation is calculated over all spectra in the pool. For comparison, all averaged ratios are depicted on a ^{2}log scale. The number of spectra, which were used for the average ratios are shown. The PKA-RII isoforms show a clear positive C8 /C8-OCH3 ratio, indicative of their preference for the C8-resin, while PKA-RI isoforms show clear negative ratios, meaning they are more abundant in the C8-OCH3 pull down. As expected, the ratio of known PKA RII-specific AKAPs exactly follows the ratio of PKA-RII. In contrast, AKAP1, referred to as D-AKAP1 and AKAP10, referred to as D-AKAP2 for their dual specificity, have specificity ratio of approximately 1 (0 on the ^{2}log scale) which can be rationalized by their ability to bind to both PKA-RI and PKA-RII isoforms (Adapted from (9)).

3.5 Notes

1. PBS buffer with 0.1% Tween 20 can be prepared for multiple uses and stored at 4°C as the buffer should be cold when used. However, the lysis buffer should be prepared fresh for single use by adding protease and phosphatase inhibitor cocktails only very prior to use in order to keep 100% efficiency of the inhibitors.

2. 0.1% NaN3 is necessary for preventing the bacterial and fungus growth in the beads slurry.

3. It is recommended to prepare 8M urea in 50mM ABC fresh for single use to avoid urea precipitation. It is possible to store the rest of the solution at RT under agitation.

4. Try to avoid putting the pipette tip or the poly pipette directly into a formaldehyde stock bottle. It is recommended to use a glass pipette to transfer the desired amount from the stock bottle into an eppendorf for single use .

5. Labeling reagent mixtures should be kept at 4 °C and not stored longer than 24 h to ensure labeling efficiency. It is recommended to prepare fresh sodium cyanoborohydride for single use as it is very water reactive and easy to decompose on exposure to moist air or water. Excess sodium cyanoborohydride can be discarded by neutralizing with NaOH.

6. Cell pellet can be stored at -80°C for future use. To avoid dissociation of protein complexes, tissue lysate should be stored at high protein concentration in 50% glycerol at -20°C until use. Before pull-down, dilute the lysate to get a protein concentration at 2mg/ml and a glycerol concentration at 10% or below.

7. It is necessary to supplement the lysate prior to the pull-down as well as the washing buffer of the first two washes after the pull-down with 10mM ADP and GDP to reduce interactions of non-cyclic nucleotide binding proteins to the resin (5, 6). It is also essential to further wash the immobilized fraction at least 3-4 times with a large volume of lysis buffer. We recommend to use at least 1-2ml buffer per 100µl of beads for each washing step.

8. Cut off the end of a pipette tip when handling cAMP agarose beads to avoid disruption of the beads and to assist in measuring out the correct volume of beads. It is also important to centrifuge cAMP beads at maximally 1000 × g to avoid loss of binding.

9. An alternative to in-solution digestion is SDS-PAGE gel loading. The enriched proteins can be eluted from the beads by boiling the beads at 95°C in an equal volume of SDS-PAGE loading buffer for 5 mins. After that, the eluate can be subjected to an SDS-PAGE gel , followed by in-gel digestion and LC-MS/MS analysis or Western blot analysis.

10. For a single cAMP pull-down with 10 mg protein, expected bound fraction is 20 µg. A protease: protein ratio of 1:50 to 1:100 (w/w) is recommended for digestion..

11. The labeled sample should not dry completely as it is difficult to reconstitute. The best thing is to dry the sample until 1-2 µl are left. After that the sample can be stored at -20°C until MS analysis.

12. For samples of human origin, it is recommended to use the Swiss-Prot/ Uniprot database as its current annotation of ~23.000 entries is the most non-redundant. For rat and mouse samples, no clear preference for a database to be used can be stated.

3.6 Conclusion

Here we describe a chemical proteomics approach targeting proteins involved in cAMP mediated signaling, whereby both primary nucleotide interactors and secondary binders can be enriched for. This approach is highly relevant as the specificity of cAMP signaling is mediated by interaction of the regulatory subunit (PKA-R) with A-kinase anchoring proteins (AKAPs), which often form the core of even larger protein machineries. As a proof of the potential, we utilized this technique in chapter 4 to monitor the specificity of SPHKAP in mammalian heart and spleen tissue.

3.7 Acknowledgements

The authors would like to thank Toon A.B. van Veen for lysate preparation. This work was supported by the Netherlands Proteomics Centre (DK, TA, AJRH and AS), the Utrecht Institute of Pharmaceutical Sciences (DK, AS) and a Focus and Massa grant from Utrecht University (AS).

3.8 References

1. H.P. Bar, O. Hechter, Adenyl cyclase and hormone action. I. Effects of adrenocorticotropic hormone, glucagon, and epinephrine on the plasma membrane of rat fat cells. Proc Natl Acad Sci U S A 63, 350 (1969).
2. W. Wong, J.D. Scott, AKAP signalling complexes: focal points in space and time. Nat Rev Mol Cell Biol 5, 959 (2004).
3. L.J. Huang, K. Durick, J.A. Weiner, J. Chun, S.S. Taylor, Identification of a novel protein kinase A anchoring protein that binds both type I and type II regulatory subunits. J Biol Chem 272, 8057 (1997).
4. L. Wang et al., Cloning and mitochondrial localization of full-length D-AKAP2, a protein kinase A anchoring protein. Proc Natl Acad Sci USA 98, 3220 (2001).
5. A. Scholten et al., Analysis of the cGMP/cAMP interactome using a chemical proteomics approach in mammalian heart tissue validates sphingosine kinase type 1-interacting protein as a genuine and highly abundant AKAP. J Proteome Res 5, 1435 (2006).
6. A. Scholten, T. A. van Veen, M.A. Vos, A.J. Heck, Diversity of cAMP-dependent protein kinase isoforms and their anchoring proteins in mouse ventricular tissue. J Proteome Res 6, 1705 (2007).
7. H. Poppe et al., Cyclic nucleotide analogs as probes of signaling pathways. Nat Methods 5, 277 (2008).
8. M.J. Vliem et al., 8-pCPT-2'-O-Me-cAMP-AM: an improved Epac-selective cAMP analogue. Chembiochem 9, 2052 (2008).
9. T.T. Aye et al., Selectivity in enrichment of cAMP-dependent protein kinase regulatory subunits type I and type II and their interactors using modified cAMP affinity resins. Mol Cell Proteomics 8, 1016 (2009).
10. P.J. Boersema, R. Raijmakers, S. Lemeer, S. Mohammed, A.J. Heck, Multiplex peptide stable isotope dimethyl labeling for quantitative proteomics. Nat Protoc 4, 484 (2009).
11. P. Mortensen et al., MSQuant, an open source platform for mass spectrometry-based quantitative proteomics. J Proteome Res 9, 393 (2010).

Chapter 4

Sphingosine kinase interacting protein is an A-kinase anchoring protein specific for type I cAMP-dependent protein kinase

Duangnapa Kovanich[1]
Marcel A.G. van der Heyden[2]
Thin Thin Aye[1]
Toon A.B. van Veen[2]
Albert J.R. Heck[2]
Arjen Scholten[2]

[1]Biomolecular Mass Spectrometry and Proteomics,
Utrecht Institute for Pharmaceutical Sciences and Bijvoet Center for Biomolecular Research,
Utrecht University, Padualaan 8, 3584 CH, Utrecht, The Netherlands

[2]Department of Medical Physiology, Division Heart & Lungs,
University Medical Centre Utrecht, Yalelaan 50, 3584 CM, Utrecht ,The Netherlands

Based on Chembiochem. 2010, 11, 7, 963-71

4.1 Abstract

Compartmentalization of kinases and phosphatases plays an important role in the specificity of second messenger mediated signaling events. Localization of the cAMP-dependent protein kinase is mediated by interaction of its regulatory subunit (PKA-R) with the versatile family of A-kinase anchoring proteins (AKAPs). Most AKAPs bind avidly to PKA-RII, while some have dual specificity for both PKA-RI and PKA-RII, however, no mammalian PKA-RI specific AKAPs have thus far been assigned. This was mainly attributed to the observation that PKA-RI is more cytosolic, as compared to the more heavily compartmentalized PKA-RII. Chemical proteomics screens of the cAMP interactome in mammalian heart tissue recently identified sphingosine kinase type 1-interacting protein (SKIP, SPHKAP) as a putative novel AKAP. Biochemical characterization now shows that SPHKAP can be considered as the first mammalian AKAP that preferentially binds to PKA-RIα. Recombinant human SPHKAP functions as an RI-specific AKAP that utilizes the for AKAPs characteristic amphipathic helix for interaction. Further chemical proteomic screening utilizing differential binding characteristics of specific cAMP-resins confirms SPHKAPs endogenous specificity for PKA-RI directly in mammalian heart and spleen tissue. Immunolocalization studies revealed recombinant SPHKAP is expressed in the cytoplasm where PKA-RIα also mainly resides. Alignment of SPHKAPs amphipathic helix with peptide models of PKA-RI or PKA-RII specific anchoring domains shows that it has largely only PKA-RIα characteristics . Being the first mammalian PKA-RI specific AKAP with cytosolic localization, SPHKAP is a very promising model to study the function of the less explored cytosolic PKA-RI signaling nodes.

4.2 Introduction

Several hormones influence cellular functions by inducing receptor activation, resulting in cAMP (3'-5'-cyclic adenosine monophosphate) production and subsequent intracellular propagation of the hormone signal (1). cAMP is a second messenger molecule that mediates a plethora of physiological responses downstream of the receptor activated signal. The cAMP-dependent protein kinase (PKA) is one of the principal intracellular targets of cAMP. The PKA holoenzyme is a tetramer consisting of two catalytic subunits (PKA-C) that are held in an inactive conformation by a regulatory subunit (PKA-R) dimer. The two PKA-R subtype dimers can form a tetramer with all three PKA-C isoforms (Cα, Cβ and Cγ), thereby generating the type-I and type II holoenzymes. For both PKA holoenzymes, binding of cAMP to the PKA-R subunits results in dissociation of the PKA-C subunits which then become active and are able to phosphorylate nearby substrates. As PKA and many of its substrates are ubiquitously present throughout the cell and in a plethora of tissues, tight regulation of its function through compartmentalization of the PKA holoenzyme(s) is required to achieve signaling specificity. Compartmentalization of PKA is mediated by proteins referred to as A-kinase anchoring proteins (AKAPs). AKAPs target PKA to distinct subcellular compartments, thereby providing a mechanism that positions PKA to respond to localized changes in cAMP and to confine phosphorylation to only a subset of potential substrates (for a review see (2-4)). Anchored PKA has been shown to be important in various cellular processes including hormone-mediated insulin secretion from pancreatic islet B-cells (5), vasopressin-induced aquaporin shuttle in renal principal cells (6), and regulation of pre-mRNA splicing (7). It is also heavily involved in the proper functioning of cardiomyocytes (8).

To date, over 70 different AKAPs have been described in a large number of organisms and cell types (2). The AKAP family consists of structurally highly diverse, but functionally very related members. AKAPs share three characteristics: (i) all AKAPs contain a PKA-anchoring domain, an amphipathic helix motif of 14–18 residues, which binds to the N-terminal dimerization and docking domain (D/D-domain) of PKA-R; (ii) all AKAPs have unique localization signals to tether them to specific cellular locations , and (iii) AKAPs have the ability to assemble into multiprotein signaling nodes that include other kinases, phosphatases, phosphodiesterases and various other regulatory proteins (4). The AKAP family can be divided into three groups on the basis of which PKA-R subunit binds to them. The large majority of AKAPs bind to PKA-RII. Also several dual-specificity AKAPs have been described, such as D-AKAP1 (9) and D-AKAP2 (10), which can anchor both PKA-RI and PKA-RII. Relatively little RI-specific AKAPs have been identified. Two examples include AKAP-CE which was identified in C. elegans (11) and α4-integrin, which does not contain the typical amphipathic helix for interaction with PKA-R but a distinct, non-classical type of PKA binding site (12). In mammalians, no PKA-RI specific AKAP has been identified to date.

The interaction between PKA-R and AKAPs occurs mainly through hydrophobic interactions. For this, the antiparallel X-type four-helix bundle in the D/D-domain, binds tightly to the before mentioned amphipathic helix of the AKAPs. NMR studies revealed that the hydrophobic face of the amphipathic helix lies across the D/D-domain, allowing extensive hydrophobic interactions between both proteins (13, 14). Besides interaction, the sequence of the D/D-domain determines PKA-R isoform-specificity and therefore different PKA-R isoforms interact with AKAPs with different affinities.

On the basis of the different amphipathic helices identified in the now extensive family of AKAPs, a number of anchoring inhibitor peptides have been designed. A classical prototype of such peptides is Ht31, which encompasses the minimum region required for RII binding of human AKAP-Lbc or AKAP13 (15) and non-selectively inhibits binding to PKA-R isoforms, although it is more effective in disrupting PKA-RII interactions (16, 17). New peptides with nearly exclusive affinities to just one PKA-R isoform have been designed in silico and through extensive peptide arrays, such as AKAP-IS (18) and SuperAKAP-IS (19) which bind to PKA-RII with much greater affinity than Ht31, and are also selective towards PKA-RII, over PKA-RI. A more selective disruptor of PKA-RI interactions is the so-called RIAD-peptide (20).

The sphingosine kinase type 1-interacting protein (SKIP, in the Swissprot database referred to as SPHKAP), was characterized by yeast-2-hybrid screening as an anchoring protein for sphingosine kinase 1 (SPHK1) and its regulatory role in the modulation of SPHK1 was shown (21). According to Northern blot analysis, SPHKAP is expressed in spleen, ovary, brain and most prominently in heart (21). Recently, we have identified SPHKAP as a putative novel AKAP, which is highly abundant in heart ventricular tissue using a chemical proteomics screen of the cAMP interactome directly in heart tissue lysate (22). Additional evidence for SPHKAP being a genuine AKAP was provided by Hidden Markov based motif searches on the SPHKAP sequence that predicted the presence of the required amphipathic helix in SPHKAPs to interact with PKA (22).

Here, we evaluate several specific characteristics of SPHKAP by using a variety of biochemical and proteomics methods. These complementary methods show for the first time that SPHKAP behaves as a genuine PKA-RI specific AKAP both in vitro and in vivo, which is unique as thus far only RI specific binding regions on dual specific AKAPs were identified (7, 23). SPHKAP can therefore pose as a model protein for the thus far unexplored RI-specific AKAPs and their function.

4.3 Materials and Methods

Materials

2-AHA-cAMP, 8-AHA-cAMP and 8-AHA-2'-OMe-cAMP coupled agarose beads (~6 µmol/mL) were purchased from Biolog. The HA Tag IP/Co-IP Kit was from Fisher Scientific. GFP-Trap agarose beads for GFP immune-precipitation were obtained from Chromotek. Protease inhibitor cocktail was from Roche Diagnostics. Anti-PKA-RIα (ab60064) and anti-PKA-RII (ab57414) were purchased from Abcam. Anti-HA (H9658) were obtained from Sigma. Goat anti-mouse HRP (172-1011) and goat anti-rabbit HRP (170-6515) were purchased from Biorad. Anti-GFP (SC-9996) and Western blotting luminol reagent (SC-2048) were obtained from Santa Cruz. Fluorescein isothiocyanate (FITC)-conjugated donkey anti-mouse was from Jackson Immunoresearch. Isotope labeled CD2O formaldehyde (20% solution in D2O) was from Sigma. High purity water, obtained from a Milli-Q system (Millipore, Bedford, MA USA), was used for all experiments. All other chemicals were purchased from commercial sources and were of analysis grade, unless stated otherwise.

Molecular Biology

A cDNA construct encoding Human SPHKAP (pCR-XL-TOPO SPHKAP) (cDNA clone MGC:132614 IMAGE:8143957) was obtained from imaGENES. SPHKAP was cloned into the pcDNA3 expression vector (Invitrogen) containing an N-terminal HAHIS6-Tag at the EcoRI restriction site to generate pcDNA3 HAHIS6-SPHKAP. For generating a plasmid encoding a fusion protein consisting of the full-length SPHKAP and C-tagged GFP, SPHKAP stop codon was mutated by PCR (sense 5'-CTGTGCTGGGGAACCTGAACCCTTC-3', antisense 5'-TTGGATCCAATCCCAGTTCCAAGAGCCAGTCA-3') . SPHKAP with a mutated stop codon was cloned into pEGFP-N1 (Clontech, Saint-Germain-en-Laye, France) with C-terminal EGFP at the ApaI and BamHI sites to generate SPHKAP-GFP. All constructs were confirmed by sequencing.

Cell culture and transfection

HEK-293 cells (ATCC) were cultured at 37°C and 5% CO_2 in DMEM supplemented with 10% fetal calf serum, 2 mM l-glutamine, and 50 µg/ml streptomycin. Cells were transfected with pcDNA3 HAhis_6-SPHKAP or pEGFP-SPHKAP using lipofectamin 2000 (InVitrogen) according to the manufacturer's instructions.

RT-PCR

Total RNA was isolated from human left ventricular heart tissue using Trizol (Invitrogen) according to the manufacturer recommendations, and treated with DNAse. cDNA was made using oligo-dT and Superscript II (Invitrogen). Subsequently, SPHKAP cDNA was amplified by 35 rounds of PCR at an annealing temperature of 56°C, using primers located on exon 7 and exon 11 respectively (sense 5'-CTCCTAGAGGAAGCAGAAGGGC-3'; antisense 5'-GTTGATCACCAGCAGGCTCCTC-3'). PCR products were run on a 1.5% ethidium bromide stained gel.

Sequence analysis and phylogeny

Alignment and phylogenetic tree reconstruction was performed with MEGA version 4.0 software (24) operating with ClustalW and Neighbor-Joining algorithms. Support for each node was determined by interior-branch test (1000 replicates; seed=64238). Accession numbers of protein sequences are as follows: Homo sapiens NP_001136116 and NP_085126; Pan troglodytes XP_001137841 and XP_001137938; Macaca mullata XP_001111587 and -XP_001111626; Rattus norvegicus NP_001120964; Mus musculus Q6NSW3 and NP_766018; Monodelphis domestica XP_001373368 ; Taeniopygia guttata XP_002194884; Gallus gallus XP_422607; Danio rerio NP_001076514.

Tissues

Human left ventricular tissue samples were obtained from explanted male hearts suffering from late stage dilated cardiomyopathy (classified as NYHA IV). Rat ventricular tissue was obtained as described previously (25). All investigations conform to the principles outlined in the Declaration of Helsinki (Cardiovascular Research 1997, 35:2 to 35:4) and experimental protocols were approved by the Ethical Review Board of the University Medical Center Utrecht (The Netherlands).

Tissue and cell lysis prior to cAMP pull-down experiments

For cAMP-pull-down experiments directly in tissue, the tissue was pulverized in a custom made steel mortar which was pre-cooled with liquid nitrogen. Subsequently, 1 mL of ice-cold lysis buffer (50mM K2HPO4, pH 7.0, 150mM NaCl. 0.1% Tween 20, protease Inhibitor cocktail) was added and the sample was left at room temperature for 5 min and subsequently on ice for another 10 minutes. The soluble fraction was taken after centrifugation at 20,800g for 10 minutes. HEK293 cells were lysed in lysis buffer (PBS, 0.1% Tween-20, protease inhibitor cocktail) by dounce homogenization, followed by the same procedure as that for tissue.

cAMP pull-down in human heart lysate

10mg of four different human LV tissue lysates was incubated with 2-AHA-cAMP agarose (100µl dry volume). Prior to pull-down, the lysis buffer was supplemented with 10mM ADP and GDP in order to reduce non-specific and less-specific binding of high abundant ADP and GDP binding proteins (25, 26). After pull-down and washing, bound proteins were eluted with 90µl of 8M urea under denaturing conditions. Subsequently, digestion to peptides for mass spectrometric analysis was performed with Lys-C (Roche Dignostics) for 4hr at 37°C, followed by reduction with 2 µM dithiothreitol for 15 min at 65°C and alkylation with 4 µM iodoacetamide in the dark for 30 min at room temperature. Further digestion was performed after dilution to 2M urea with trypsin (Roche Diagnostics) for 16hr at 37°C.

cAMP pull-downs in HEK293 expressing HAHIS6-SPHKAP

Lysates from control HEK293 or HEK293 cells expressing SPHKAP-HAHIS$_6$ were, supplemented with ADP and GDP as described above and where applicable, different concentrations of anchoring inhibitor peptide, Ht31 (DLIEEAASRIVDAVIEQVKAAGA) or control peptide Ht31P (DLIEEAASRIVDAPIEQVKAAGA) for 2 hr. Then the cAMP agarose beads (25µL 8-AHA-cAMP) were added to the lysate and the suspension was incubated by rotary shaking (4 °C, overnight). Beads were washed two times with 10mM ADP and GDP in lysis buffer and another 2 times with regular lysis buffer. Then the bound fraction was eluted with Leammli sample buffer (95 °C). The bound and unbound fractions were analyzed by Western blot using the different antibodies described above.

cAMP pull-down in rat heart and spleen tissue lysate

Pulldowns with 8-AHA-cAMP (C8) and 8AHA-2'-O-Me-cAMP (C8-OCH_3), both 50µl dry volume, in rat heart and spleen tissue lysate were performed as described previously (26). Prior to the pull-down assays, the lysates were treated as described above. The bound fractions were combined, eluted in 8M urea and digested as mentioned above. The peptides originating from the C8 pull-down were labelled with CH2O (light labelling) whereas the peptides originating from C8-OCH3-cAMP pulldown were labelled with CD_2O (intermediate labelling) directly on a C18-Sep Pak column (Waters) according to (27). Subsequently, the two labelled samples (intermediate and light) were mixed in a 1:1 ratio and dried. Subsequently, the dried samples were fractionated by Strong Cation Exchange (SCX) as described previously (28). A total of 45 SCX fractions were manually collected and dried in a vacuum centrifuge prior to LC-MS analysis.

Mass spectrometry and Data analysis

LC-MS/MS was performed by coupling an Agilent 1100 HPLC system (Agilent Technologies) to a LTQ-Orbitrap mass spectrometer (Thermo) as described previously (26). Resulting spectra were processed with Bioworks 3.3 (Thermo), and the subsequent data analysis was carried out using Mascot (version 2.1.0) against the IPI_Rat database version 3.36 (42688 sequences; 22370098 residues) allowing 2 missed cleavages, carbamidomethylation on cysteine residues as fixed modification and oxidation of methionine as variable modification. The search space was limited with a peptide mass tolerance of 10 ppm and the MS/MS mass tolerance to 0.9 Da. Quantitation of peptides was performed using an in-house dimethyl-adapted version of MSQuant (29). Briefly, peptide ratios were obtained by calculating the intensities of the extracted ion chromatograms (XIC) of the "light" and "intermediate" forms of the peptide. The quantified protein ratios were calculated by averaging all quantified peptide pairs in individual proteins. Differential binding ratios between C8-OCH3 and C8 (C8-OCH3/C8) of each protein was obtained by averaging over all peptide pairs measured for that particular protein on a 2log scale.

Immunoprecipitation

HEK-293 cells transiently expressing HAHIS6-SPHKAPor SPHKAP-EGFP were lysed in lysis buffer (20mM HEPES pH 7.6, 125 mM NaCl, 1 mM EDTA, 1mM EGTA, 1 mM DTT, 10% glycerol, 1% Triton X-100, protease inhibitor cocktail) and cleared by centrifugation (20800g, 4 °C, 15 min). For anti-HA immunoprecipitation, 4 mg total cell lysate was incubated with 20 µl anti-HA agarose beads (~30 µg of anti-HA antibody) with constant rotation at 4°C overnight. Beads were washed five times with lysis buffer. The obtained bound fraction was eluted with 2X non-reducing sample buffer (0.12 M Tris-HCl, pH 6.8, 2% SDS, 20% glycerol, lane marker tracking dye) (95 °C). For GFP immunoprecipitation, 30 µl anti-GFP beads were equilibrated in dilution buffer (10 mM Tris-HCl, pH7.5, 150 mM NaCl, 0.5 mM EDTA). 4 mg lysate was added to the beads and incubated with constant rotation at 4°C overnight. Beads were washed 5 times with lysis buffer. The bound fraction was eluted with 2X Leammli sample buffer (95 °C). The bound and unbound fractions and input lysates were analysed by Western blot analysis.

Immunofluorescence microscopy

Cells were cultured on glass cover slips. Cells were washed with PBS, fixed for 25 min with 4% paraformaldehyde, quenched with 50mM glycine 2 times 10 min each, and permeabilized with 0.5% Triton X-100 for 5 min. Primary and secondary antibodies were diluted with NET-gel (50mM Tris pH 8.0, 150mM NaCl, 1mM EDTA, 0.2% gelatine) to appropriate concentration and incubated Antibodies used were anti-HA as the primary antibody and FITC-conjugated donkey anti-mouse. After nuclei DAPI-staining, cover slips were mounted with citiflour (Agar Scientific) and imaged (40X objective) using a Nikon eclipse 801 microscope equipped for epifluorescence.

4.4 Results

SPHKAP is abundantly present in human left ventricle

We previously reported the presence of SPHKAP in the cAMP pull-down fraction of rat heart tissue lysate, and provided bioinformatics evidence for the classification of SPHKAP as a potential novel AKAP in heart (22). To confirm these data in human tissue, we performed four individual cAMP pull-downs in male human left ventricle tissue lysates. Subsequent LC-MS/MS analyses of these PKA/AKAP enriched protein fractions showed the abundant presence of SPHKAP with 55% sequence coverage (Figure 1A). In the human Swissprot database, two protein annotations for SPHKAP are present. The first annotated as a 1700 amino-acid SPHKAP (Q2M3C7-1, SPHKAP isoform 1, SPHKAP1) with a calculated mass of 186kDa and the second annotated as a 1671 amino-acid SPHKAP (Q2M3C7-2, SPHKAP isoform 2, SPHKAP2) with a calculated mass of 183 kDa. Both sequences were aligned using ClustalW and it became clear that the sequence of SPHKAP2 lacked 29 amino acids 1545-1574 according to SPHKAP1 numbering (Figure 1A). Comparing the 29 amino-acid sequence with the genomic organization indicated alternative splicing of exon 9. In the MS data, we found a unique peptide that only exists in SPHKAP2, also depicted in Figure 1A, thereby providing crucial evidence for the existence of this splice variant at the protein level in human heart. Unfortunately, by LC-MS/MS we were unable to prove the presence of SPHKAP1 in this tissue, as the 1545-1574 region lacks lysine and arginine residues. A list of all SPHKAP peptides identified is shown in supplemental table S1. RT-PCR experiments using primers located in exon 7 and 11 coded sequences respectively generated two products of different size thereby confirming the presence of two splice variants at mRNA level in human left ventricle tissue (Figure 1B). Screening (predicted protein) databases obtained from vertebrate genome projects revealed the presence of SPHKAP1 and SPHKAP2 variants in primates, rodents and fish, while no SPHKAP1 variants are annotated for birds and marsupials. However, given the phylogenetic relationships as depicted in Figure 1C, we expect both variants to be present in all vertebrate species from fish to man.

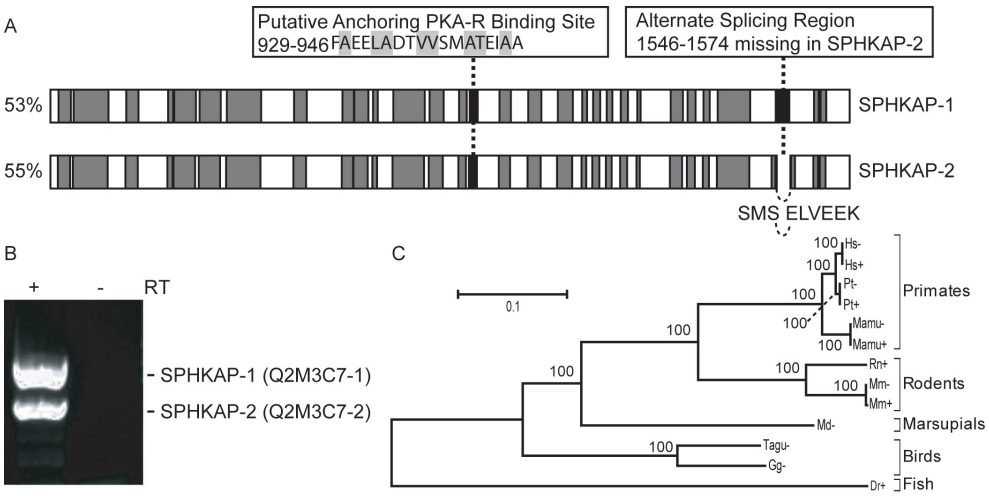

Figure 1 > Initial characterization of SPHKAP. A) Schematic alignment of SPHKAP-1 and SPHKAP-2.

A) *Observed sequence coverage of SPHKAP1 and SPHKAP2 in human heart. Shared peptides are depicted in gray. Peptide SMSELVEEK (1543–1551), which is unique to SPHKAP-2 as it bridges the exon 9 splice site, is shown separately. The predicted amphipathic helix for PKA-R binding22 is depicted in black.* ***B)*** *RT-PCR products of two SPHKAP isoforms (lane 1) in human heart. Lane 2 is the RT-free control. The primers used were designed to encompass the alternative spliced exon 9 region yielding differentially sized cDNA products for each isoform.* ***C)*** *Phylogenetic relationships of vertebrate SPHKAP amino acid sequences. Abbreviations: Hs: Homo sapiens, human; Pt: Pan troglodytes, chimpanzee; Mamu: Macaca mullata; rhesus monkey; Rn: Rattus norvegicus, Norwegian rat; Mm: Mus musculus, house mouse; Md: Monodelphis domestica, gray short tailed opossum; Tagu: Taeniopygia guttata, zebra finch; Gg: Gallus gallus, chicken; Dr: Danio rerio, zebrafish. The scale bar indicates the number of substitutions per amino-acid residue.*

Identification of SPHKAP as an AKAP in vitro

To further explore the properties of SPHKAP and to further validate it being an AKAP, we generated a full-length human recombinant SPHKAP1 construct and fused it to a HAHIS6 tag, as well as to GFP ($HAHIS_6$-SPHKAP and SPHKAP-GFP) and expressed them in HEK 293 cells. First, we examined whether the recombinant $HAHIS_6$-SPHKAP could be retrieved in a cAMP pull down. As shown in Figure 2A, both PKA-RIα and PKA-RIIα were efficiently pulled down from HEK293 cell lysate. $HAHIS_6$ -SPHKAP was also efficiently enriched from these cells, whereas from the control cell line, no HA signal was retrieved. We further investigated whether SPHKAP binding to PKA isoforms could be disrupted by the prototypic non-selective PKA-AKAP anchoring inhibitor peptide, Ht31. Ht31P, an inactive analogue of Ht31, in which a proline residue is introduced to disrupt the anchoring helix (15) was used as a control. As shown in Figure 2B, the interaction between the cAMP-resin and its primary binder PKA was not disrupted by Ht31, however the interaction between recombinant SPHKAP and PKA-R was efficiently competed by Ht31 (Figure 2B, lane 1), but not by control peptide Ht31P (Figure 2B, lane 2), suggesting that the interaction of SPHKAP with the resin relies on interaction with PKA-R through an amphipathic helix, thereby establishing SPHKAP as a genuine AKAP. Furthermore in Figure 2C, we show that the effect of Ht31 is dose-dependent as increasing concentrations (10, 100, and 500 μM) of Ht31 compete for binding to PKA-R more efficiently.

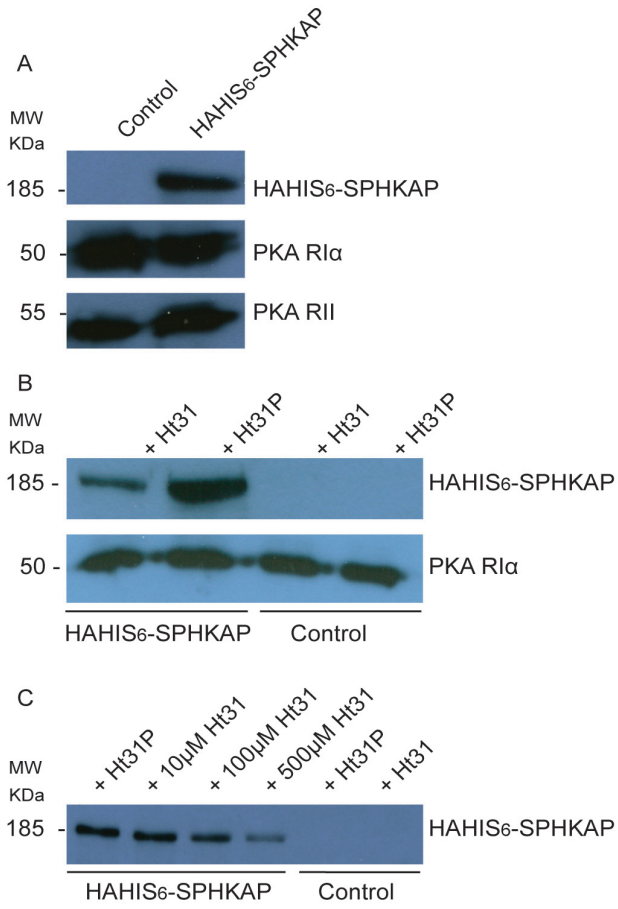

Figure 2 > Classification of SPHKAP as an AKAP in vitro.

A) *Western blot analysis of 8-AHA-cAMP pull-down from HAHIS6-SPHKAP expressing (lane 2) and control HEK 293 cells.* ***B)*** *Western blot analysis of 8-AHA-cAMP pull-down from HAHIS6-SPHKAP-expressing and control HEK293 cells in the presence of 100 μM Ht31 (lanes 1 and 3) or 100 μM Ht31P (lanes 2 and 4).* ***C)*** *Western blot analysis of 8-AHA-cAMP-agarose pull-down from HAHIS6-SPHKAP -expressing HEK293 cells with Ht31P (500 μM) compared to an increasing dose of Ht31 (lanes 2–4).*

Classification of SPHKAP as a PKA-RI-specific AKAP

Having established that SPHKAP is an AKAP in vitro, that requires its amphipathic helix for interaction with PKA-R, we then studied its interaction characteristics with PKA-R in more detail by investigating its preference for either PKA-RIα or PKA-RIIα, the predominant PKA-R isoforms in the mammalian ventricle (22). For this, we immunoprecipitated both HAHIS6-SPHKAP and SPHKAP-GFP from HEK293 cells and investigated the immunoprecipitates (IPs) for the presence of these different PKA-R isoforms. As shown in lane 1 of Figure 3A and 3B, both SPHKAP constructs were effectively immunoprecipitated by their consecutive immobilized specific antigens, anti-HA-agarose and anti-GFP-magnetic beads. Both specific tags were not detected in their respective control IPs. The anti-HA IP contained PKA-RIα but not PKA-RIIα (Figure 3A, lane 1) while both were present in the unbound fraction and input lysate (lane 2 and lane 3). PKA-RIα and PKA-RIIα were not detected in control IPs (lane 4). The anti-GFP IP (Figure 3B) result shows this is consistent when swapping the tag on SPHKAP from HA to GFP. These data indicate that SPHKAP has a very strong preference for binding to PKA- RIα since no detectable amounts of PKA-RIIα could be retrieved from the IPs.

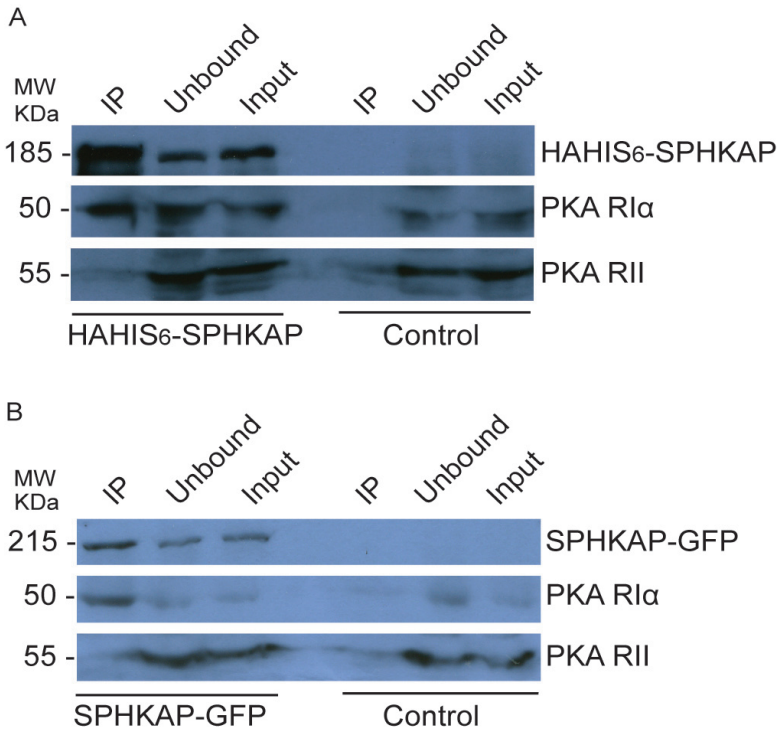

Figure 3 > Classification of SPHKAP as a PKA RI-specific AKAP.

A) *Western blot analysis of immunoprecipitates (IPs), unbound fractions, and input lysates from anti-HA pull-down in HAHIS6-SPHKAP-expressing HEK293 (lanes 1–3) and control (lanes 4–6) cells.* ***B)*** *Western blot analysis of IPs, unbound fractions, and input lysates from anti-GFP immunoprecipitations in SPHKAP-GFP-expressing HEK293 (lanes 1–3) and control (lanes 4–6) cells.*

SPHKAP interacts with PKA-RIα in vivo

To further authenticate the high preference of SPHKAP for PKA-RIα over PKA-RIIα we performed our recently established screening method for PKA RI/RII specificity of AKAPs using chemical proteomics directly in tissue (30). This allows us to evaluate the in vivo specificity of endogenous, non-tagged, SPHKAP. Next to heart tissue, spleen was chosen as SPHKAP is also expressed in this tissue (21). Our method exploits differential pull down experiments with two dif-

ferent cAMP analogues; 8-AHA-cAMP (C8) and 8-AHA-2'-OMe-cAMP (C8-OCH3). The first has about equal affinity for both PKA-RI and PKA-RII, whereas the latter has a ~3-4-fold preference for PKA-RI (30). The differences in affinity for the two PKA-R isoforms can thus be used as a discriminating factor to monitor the specificity of SPHKAP. Following the affinity pull-downs with both resins, all enriched proteins were digested and chemically labeled with stable-isotope dimethyl labelling (27). In Figure 4A, an illustrative example of the subsequent quantitative MS-analysis is shown. MS spectra are presented in which "light" (C8, left) and "intermediate" (C8-OCH3, right) forms of peptide pairs can be distinguished. For instance, the peak pair of a doubly-charged PKA-RIα peptide (NVLFSHLDDNER) bears a single label on the N-terminus and as a consequence an m/z difference of 2Da is observed. This corresponds to a mass difference of 4 Da between the light- and intermediate-labeled peptides. The intensity ratio between the peaks represents their relative abundance in each of the pull-downs. The ratios averaged over all peptides observed for either PKA-RI , PKA-RII isoforms, or several AKAPs pulled down from heart and spleen tissue lysates are summarized in figure 4B and C, respectively. A List of peptides used for quantitation is shown in supplemental table S2. PKA-RII isoforms show a clear negative C8-OCH3/C8 ratio, indicative of their preference for the C8-resin, while PKA-RIα, has a positive ratio, meaning it is more abundant in the C8-OCH3-pull down. The ratio of known PKA RII-specific AKAPs , AKAP11 (31) and AKAP13 (32) from the heart pull-down (black bars, Figure 4B) and AKAP5 (33) and AKAP 9 (34) from the spleen pull-down (black bars, Figure 4C) exactly follow, as expected, the ratio of PKA-RII. In contrast, AKAP1, also referred to as D-AKAP1, for dual-specificity AKAP1 (9), has an intermediate ratio of 1 (0 on the 2log scale, black bar, Figure 4B), which can be rationalized by its ability to bind to both PKA-RI and PKA-RII. Uniquely amongst the pulled-down AKAPs, SPHKAP, consistent with our in vitro data, displays similar ratios as PKA-RIα (grey bars, Figure 4B and C) in both heart and spleen tissue, reiterating its preference.

Intracellular localization of SPHKAP

As data from in vitro and in vivo studies indicate that SPHKAP preferentially binds to PKA-RIα, which predominantly resides in the cytoplasm (35-37), we examined the localization of SPHKAP. Therefore, HEK293 cells were transiently transfected with HAHIS6-SPHKAP and analyzed by immunofluorescence microscopy. These results indicate that recombinant SPHKAP was diffusely expressed throughout the cytoplasm but not in the nucleus. In cells displaying strong recombinant SPHKAP expression, some clustering could be observed (Figure 5, lower panels), presumably resulting from improperly folded protein accumulation in the ER or Golgi.

Rationale in the protein sequence of SPHKAP predicting specific PKA-RIα interaction

We previously predicted an 18 amino acid stretch in SPHKAP as the putative anchoring domain (929-946, Figure 1) for PKA-R binding and showed that the predicted domain was highly conserved throughout species. To investigate whether this region in SPHKAP could potentially accommodate PKA-RI binding, we aligned it with PKA-RI specific, PKA-RII specific, and dual-specificity anchoring sequences known from the literature; RIAD (20) , AKAP-CE (11), FCS1 domain B (FCS1-B), (23), AKAP-IS (18), SuperAKAP-IS (19), AKAP13 (15), D-AKAP2 (38). When combining all sequences in a single alignment, as done previously by Gold et al. (19) and Kinderman et al. (39) (Figure 6A) SPHKAP aligns in agreement with these studies . However, when the SPHKAP anchoring domains are separately aligned with PKA-RI specific and PKA-RII specific anchoring domains, it becomes apparent that it aligns much better with RIAD and AKAP-CE (figure 6B) than with AKAP13 and superAKAP-IS (figure 6C), as measured by the amount of identical (grey), and similar (pink), amino acids. Interestingly, SPHKAPs amphipathic helix alignment shifts when aligned with PKA-RII-specific anchoring domains (figure 6C vs. Figure 6A). In Figure 6A, Ile5 of AKAP13 aligns with Ile5 of SPHKAPs but in Figure 6C, it aligns better when Ile5 of AKAP13 is aligned with Ala9 of SPHKAP. In other words, the interaction seems to move one helix turn over on the so-called D/D-domain.

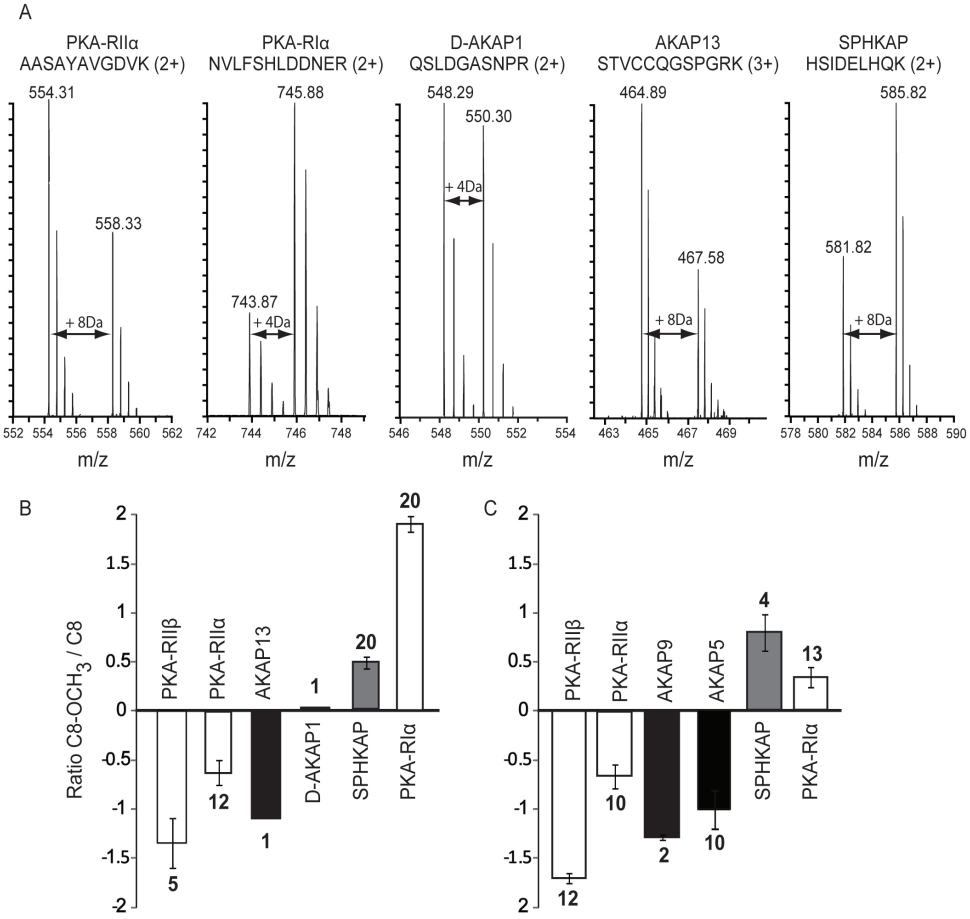

Figure 4 > SPHKAP is a PKA-RI-specific AKAP in the heart and spleen.

A) Mass spectra of typical peptide pairs observed following differential pull downs with cAMP analogues (C8-OCH3/C8) with either similar affinities to PKA-RII and -RI, or higher affinity for RI. Peptides originating from the pulled-down proteins were isotopically dimethyl labeled (light or intermediate). Representative MS spectra of peptide pairs originating from the primary binders PKA-RIα, PKA-RIIα, and the secondary binders AKAP13, D-AKAP1, and SPHKAP are shown. The numbers in parentheses indicate the charge state of the peptides. The upper panel shows that each detected peptide exists as a pair with a typical 4 Da mass difference (2 Da m/z difference) for doubly charged peptides that have no lysine residues, whereas an 8 Da mass difference (4 Da m/z difference) is observed for doubly charged peptides with one lysine residue. 2log C8-OCH3/C8 ratios obtained for each PKA isoform and all pulled-down AKAPs in B) rat heart and C) rat spleen, including the overall standard deviation over all peptides. The number indicates the number of peptide pairs used for quantitation.

4.5 Discussion

Using cAMP pull-downs and immunoprecipitations of tagged versions of SPHKAP transfected into HEK293 cells, we were able to show that SPHKAP is an AKAP (Figure 2), and furthermore that it binds preferentially to PKA-RI as no PKA-RII could be retrieved from the specific tag based immunoprecipitations (Figure 3). This striking result was confirmed by a chemical proteomics assay, that employs two different cAMP derivatives to differentiate binding specificity of AKAPs for PKA-RI and PKA-RII (30). This experiment showed that endogenous, untagged, SPHKAP behaves as an RI-specific AKAP in heart and spleen tissue. In the same experiments other AKAPs also co-purified, whereby the quantitative MS-based approach confirmed their known PKA-R (dual) specificity, validating this more unconventional method to establish the PKA-R specificity of SPHKAP in vivo. Moreover, immunofluorescence analyses of tagged versions of SPHKAP shows that it resides mainly in the cytoplasm, where PKA-RIα also predominantly resides (35-37).

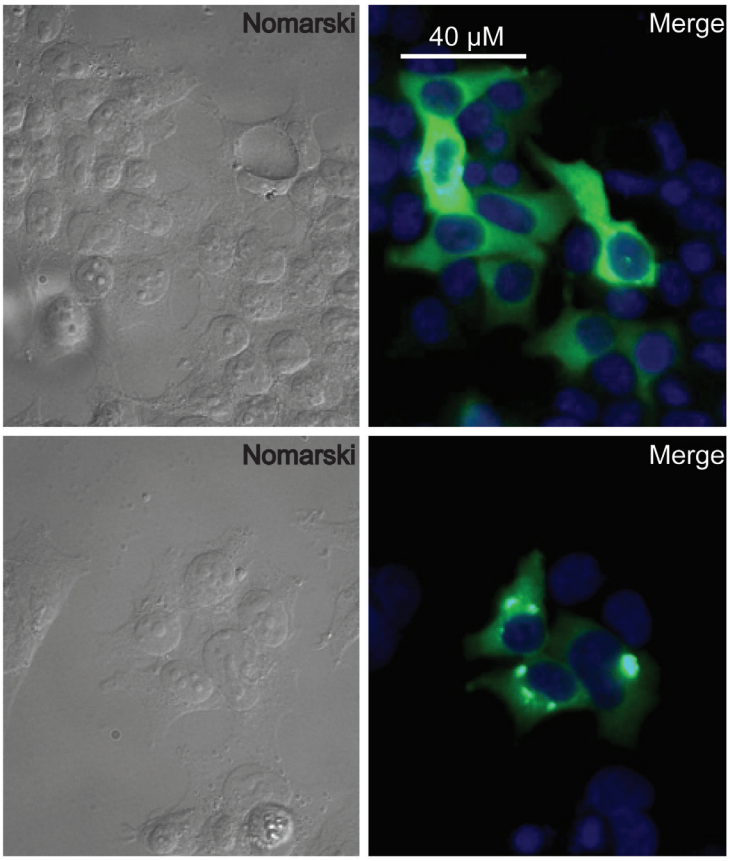

Figure 5 > SPHKAP is a cytosolic protein.

Immunofluorescence microscopy (right) on HEK293 cells transiently transfected with HA-His6-SPHKAP by using HA-antibody (green). Nuclei were stained with DAPI (blue). Nomarski microscopy was used to visualize all cells in a field (left). Cells expressing moderate levels of HA-His6-SPHKAP protein display diffuse cytosolic staining (top). Strongly expressing cells display diffuse cytosolic and aggregate-like staining patterns (bottom).

The specificity to anchor to PKA-RI, PKA-RII or both, of the more than 70 members of the AKAP family has been the object of many studies (19, 20, 39). Early on, the 14-18 amino acid amphiphatic helix motif, which is present in all AKAPs, was identified as the site of interaction to the N-terminal D/D domain of PKA-R, (15). With this motif as basis, PKA-AKAP disrupting peptides that mimic the anchoring domain of known AKAPs have been developed as a tool to study PKA signaling events (8). Amongst these is the classical Ht31 peptide, which sequence is based on the anchoring domain of PKA-RII binding AKAP13 (AKAP-Lbc) (15). Ht31 is however not really selective, and can compete for binding of both PKA-RI and PKA-RII to dual specific D-AKAP1, albeit with a better IC50 for PKA-RII disruption (16, 17). Here we used Ht31 to confirm that the PKA-AKAP-type interaction between SPHKAP and PKA is indeed based on the putative amphipathic helix of SPHKAP (Figure 2). Binding between SPHKAP and PKA-R could be disrupted by the Ht31 peptide, and not by its control counterpart Ht31P. The competition was dose-dependent.

The structural basis for the AKAP-PKA-R interaction has been addressed in most detail by NMR aiming to identify the specific sequence determinants on both PKA-R and the anchoring proteins (40, 41). Despite the conserved X-type four-helix bundle structure, structural differences between the PKA-R isoforms in the N-terminal domain lead to differences in surface topography. While PKA-RIIα presents a shallow hydrophobic groove for AKAP binding across the D/D-domain, The PKA-RIα D/D-domain presents a less hydrophobic, deeper cleft for AKAP binding (41). In addition, PKA-RIα contains an abundance of charges on its AKAP binding surface while PKA-RIIα

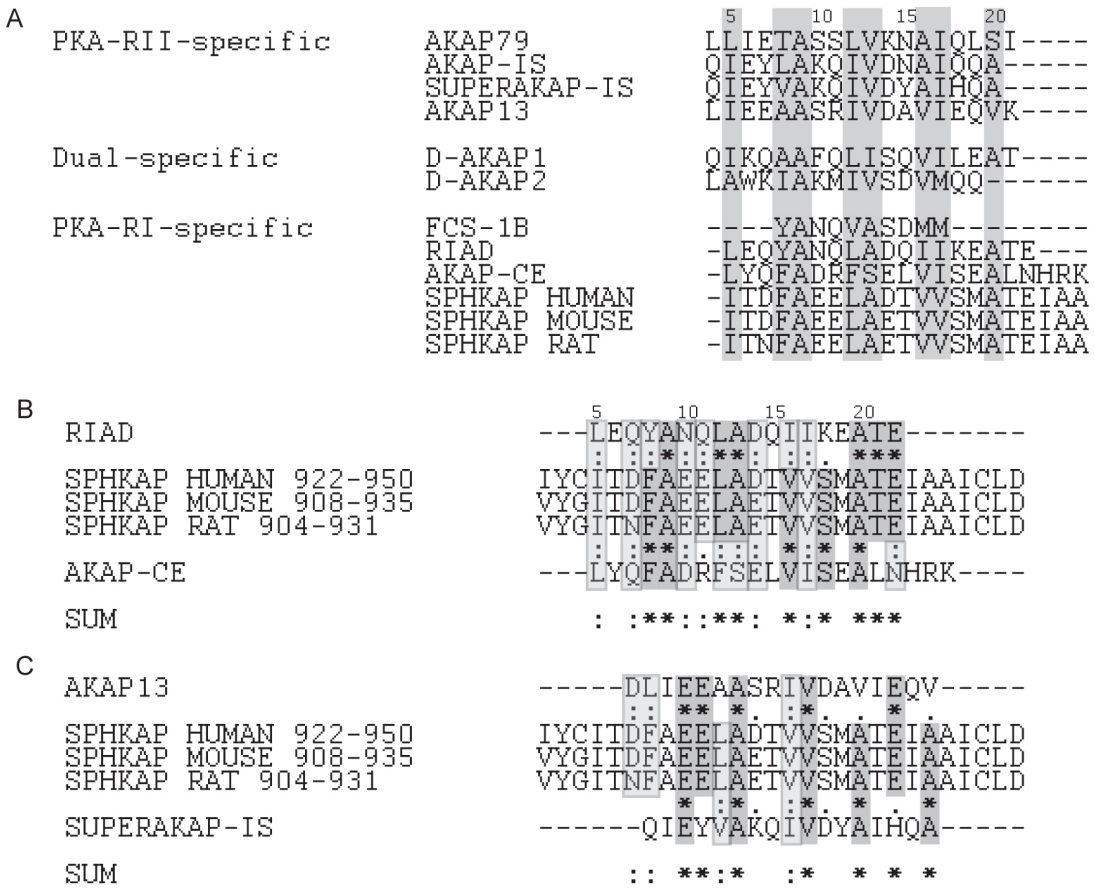

Figure 6 > The SPHKAP anchoring sequence aligns well with known PKA-RI-specific amphipathic helices.

*A) ClustalW alignment of SPHKAP anchoring sequences from human, rat, and mouse with PKA-RI-specific, PKA-RII-specific, and dual-specificity anchoring sequences. Repeats of hydrophobic residues, which are a general characteristic of amphipathic helices are boxed in gray. B) ClustalW alignments of SPHKAP anchoring sequences from human, rat, and mouse with PKA RI-specific anchoring sequences RIAD and AKAP-CE. C) ClustalW alignments of SPHKAP anchoring sequences with PKA-RII-specific anchoring sequences Ht31 and SuperAKAP-IS. Identical amino acids are marked with * and boxed in grey, while similar amino acids are marked with : and boxed in light gray.*

is less charged and more hydrophobic (41). Another difference between PKA-RIα and PKA-RIIα interaction with D-AKAP2, is the enlarged interaction surface that PKA-RI requires, as revealed by extensive peptide arrays (38).

The A-kinase anchoring domain of D-AKAP2 has been used (38, 39, 42) as a model to study the differences in AKAP binding to PKA-R isoforms as it binds with high affinity to both PKA-RIα and PKA-RIIα (KD = 2 and 48 nM, respectively) (42). The crystal structure of the PKA-RIIα D/D-domain bound to the 22-residue anchoring domain of D-AKAP2 has largely revealed the atomic determinants for PKA-RII, but also PKA-RI, specificity of AKAP docking (39). Non-polar aliphatic hydrophobic residues at position 8, 9, 12 and 13 (Figure 6) are required to form a hydrophobic ridge running along the AKAP helix axis whereby their side chains are essential to make multiple interactions with the hydrophobic surface of the PKA-RIIα D/D domain.

The D-AKAP2 domain has also been used as the starting point to optimize PKA-AKAP binding disruption peptides using peptide binding arrays. A specific peptide disruptor is now available to disrupt PKA-RI (RIAD, specificity >1000-fold, (20)) binding. Peptide substitution arrays within the anchoring domain of D-AKAP2 by Burns-Hamuro et. al. (38) revealed the importance of bulky residues in selectively reducing the affinity to PKA RIIα (Ile8Tyr, Met17Tyr) (residues are numbered as assigned in figure 6A) and in some cases these bulky amino acids completely abolish the affinity to PKA RIIα (Val13Trp, Val13Phe). Burns-Hamuro et. al. also confirmed by in vivo experiments that the anchoring domain with bulky residue substitutions failed to recruit PKA-RIIα but as expected was able to recruit PKA-RIα. The mentioned critical residues at position 8, 9, 12, and 13, are all at the center of the hydrophobic ridge of the anchoring domain that docks to the hydrophobic surface of the D/D domain, becoming completely buried inside the hydrophobic groove. By alignment with the NMR structure of the PKA-RIα D/D domain (41), it became clear that a bulky residue is too big to fit in the shallow hydrophobic groove of PKA-RIIα causing steric clashing and disruption of PKA-RIIα docking. The homologous surface of PKA-RIα contains in that particular region a deeper cavity which is sufficient to accommodate such bulky residues(39). This is in agreement with extensive peptide substitution screening data when generating SuperAKAP-IS from AKAP-IS, which confirmed the importance of negating the bulky amino acids at positions 8, 12, 20 (Leu8Phe, Leu8Tyr, ILe12Tyr, Ala20Phe, Ala20Tyr) in selecting for PKA-RII binding (19, 38). The importance of a bulky residue at position 8 for PKA RIα-binding was also shown in the dual-specificity AKAP, FCS1 (23). Tyr8Val and Tyr8Ala mutations (Figure 6A) in the PKA-RI specific anchoring domain B of FCS1 revealed that the bulky tyrosine is crucial for PKA-RI selectivity.

Classical RII-specific AKAPs contain hydrophobic amino acids with aliphatic side-chains composed exclusively of Ala, Leu, Val, or Ile that are crucial for binding to PKA-RII (19, 39).In support of this, it has been shown for AKAP-CE, a C.elegans AKAP for the PKA-RI-like regulatory subunit in this organism. It stringently discriminates against mammalian PKA-RII. This selectivity is relieved when Phe-12 and Ser-13 are mutated to Leu and Val respectively, thereby switching selectivity to PKA-RII entirely (43). Although in figure 6B, Phe8 of SPHKAP does not align with Phe12 of AKAP-CE, one could imagine that the binding could shift one helix turn over by aligning Phe8 of SPHKAP with Phe12 of AKAP-CE. If such a shift would occur, the amphipathic character of the helix would be retained.

Besides bulky residues, acidic residues (Asp, Glu) have been claimed to play a role in PKA-RI-AKAP binding as well. Biochemical studies, again of D-AKAP2 showed that the charge contribution is different for binding to different PKA-R isoforms. In line with the more charged surface of PKA-RIα compared to the more hydrophobic surface of PKA-RIIα (41) we observed that the SPHKAP anchoring domain contains 5 acidic residues (Asp-7, Glu-10, Glu-11, Asp/Glu-14, Glu-22). Acidic mutations in the D-AKAP2 anchoring domain affected binding to PKA-RIα but not to PKA-RIIα (42). Similar observations were done while optimizing the RIAD-peptide using peptide screens (20), where introduction of Glu6 and Asp14 provided higher specificity for PKA-RIα. Similarly in this optimization study, substitution of Asn-10/Gln-11 to Glu-10/Glu-11, significantly increased PKA-RIα binding. SPHKAP also contains Asp-14, and although it seems to lack Glu-6, it contains an aspartic acid at position 7 in some species. The double Glu at position 10 and 11 is also present in SPHKAP. After our work had been published, the structure of D-AKAP2:PKA RI complex was solved (44). These data confirmed our structural predictions based on the alignments and previously published peptide arrays presented here. By performing structural alignments of the D-AKAP2 sequence bound to RI and RII (39), it became clear that the D-AKAP2 peptide bound to the RIIα structure is indeed shifted towards the N terminus of the D/D domain by a single helical turn. Moreover, it was predicted from structural alignments and peptide arrays that the various acidic residues in the anchoring domain could contribute to the more specific binding with RI through helix-stabilizing interactions while it would disrupt the interaction with the RII subunit. The structure also demonstrated

that the conserved Ala-9 (figure 6B) is the only unique fit and extremely required for binding to PKA-RI. Taken together, the structure of the D-AKAP2/PKA-RI complex predicts that the anchoring region of SPHKAP has all the earlier predicted ingredients required for a PKA-RI specific AKAP.

It was described recently that dual specificity AKAPs may contain an additional PKA binding determinant called the RI Specifier Region (RISR), which is located just in front of the amphipathic helix (45). RISR itself binds to PKA-RIα with low affinity but it has the ability to form a helical configuration that can enhance binding of PKA-RIα to the conventional amphipathic helix. Mutations in the Erzin RISR were shown to reduce binding to PKA-RI in vivo and in vitro. We questioned whether a RISR domain is also present in SPHKAP, however we could not find such a domain in SPHKAP.

4.6 Concluding Remarks

Here we demonstrate that SPHKAP can be genuinely qualified as the first mammalian PKA-RI-specific AKAP using the classical amphipathic helix for interaction. Several structural studies on PKA RII-AKAP complexes have established the crucial role of hydrophobic residues on the PKA RII-AKAP binding surface. Whereas information on PKA-RI specificity can solely be extracted from extensive peptide arrays based on the D-AKAP2 amphipathic helix and modelling studies. To date, structural studies on PKA RI-AKAP interactions are currently missing. Taking into account that SPHKAP is thus far the only natural RI-Specific AKAP, structural determination of PKA RI-SPHKAP complexes will be important to reveal in more detail the differences in AKAP binding for PKA-RI versus PKA-RII and to address the role of bulky and acidic residues in selectivity towards PKA-RI. In addition, establishment of its physiological role in for instance heart, wherein it is one of the most abundant AKAPs, will undoubtedly reveal interesting features on the thus far underexplored functionality of anchored PKA-RI signaling modules.

4.7 Acknowledgements

We would like to thank Pepijn Burgers and Christian Preisinger for helpful comments. We especially thank Bart Kok for technical assistance. This work was funded in part by The Netherlands Proteomics Centre. Duangnapa Kovanich is partially funded by a Royal Thai scholarship.

4.8 References

1. H.P. Bar, O. Hechter, Adenyl cyclase and hormone action. I. Effects of adrenocorticotropic hormone, glucagon, and epinephrine on the plasma membrane of rat fat cells. Proc Natl Acad Sci U S A 63, 350 (1969).
2. A. Scholten, T.T. Aye, A.J. Heck, A multi-angular mass spectrometric view at cyclic nucleotide dependent protein kinases: in vivo characterization and structure/function relationships. Mass Spectrom Rev 27, 331 (2008).
3. K. Tasken, E. M. Aandahl, Localized Effects of cAMP Mediated by Distinct Routes of Protein Kinase A. Physiol. Rev. 84, 137 (2004).
4. W. Wong, J.D. Scott, AKAP signalling complexes: focal points in space and time. Nat Rev Mol Cell Biol 5, 959 (2004).
5. L.B. Lester, L.K. Langeberg, J.D. Scott, Anchoring of protein kinase A facilitates hormone-mediated insulin secretion. Proc Natl Acad Sci USA 94, 14942 (1997).
6. V. Henn et al., Identification of a novel A-kinase anchoring protein 18 isoform and evidence for its role in the vasopressin-induced aquaporin-2 shuttle in renal principal cells. J Biol Chem 279, 26654 (Jun 18, 2004).
7. E. Jarnaess et al., Splicing factor arginine/serine-rich 17A (SFRS17A) is an A-kinase anchoring protein that targets protein kinase A to splicing factor compartments. J Biol Chem 284, 35154 (2009).
8. M.A. Fink et al., AKAP-Mediated Targeting of Protein Kinase A Regulates Contractility in Cardiac Myocytes. Circ Res 88, 291 (2001).
9. L.J. Huang, K. Durick, J.A. Weiner, J. Chun, S.S. Taylor, Identification of a novel protein kinase A anchoring protein that binds both type I and type II regulatory subunits. J Biol Chem 272, 8057 (1997).
10. L. Wang et al., Cloning and mitochondrial localization of full-length D-AKAP2, a protein kinase A anchoring protein. Proc Natl Acad Sci U S A 98, 3220 (2001).
11. R. Angelo, C.S. Rubin, Molecular characterization of an anchor protein (AKAPCE) that binds the RI subunit (RCE) of type I protein kinase A from Caenorhabditis elegans. J Biol Chem 273, 14633 (1998).
12. C.J. Lim et al., α4 Integrins are Type I cAMP-dependent protein kinase-anchoring proteins. Nat Cell Biol 9, 415 (2007).
13. M.G. Newlon et al., The molecular basis for protein kinase A anchoring revealed by solution NMR. Nat Struct Mol Biol 6, 222 (1999).
14. P. Banky et al., Isoform-specific differences between the type Ialpha and IIalpha cyclic AMP-dependent protein kinase anchoring domains revealed by solution NMR. J Biol Chem 275, 35146 (2000).
15. D.W. Carr et al., Interaction of the regulatory subunit (RII) of cAMP-dependent protein kinase with RII-anchoring proteins occurs through an amphipathic helix binding motif. J Biol Chem 266, 14188 (1991).
16. F.W. Herberg, A. Maleszka, T. Eide, L. Vossebein, K. Tasken, Analysis of A-kinase anchoring protein (AKAP) interaction with protein kinase A (PKA) regulatory subunits: PKA isoform specificity in AKAP binding. J Mol Biol 298, 329 (2000).
17. A.J. Stokka et al., Characterization of A-kinase-anchoring disruptors using a solution-based assay. Biochem J 400, 493 (2006).
18. N.M. Alto et al., Bioinformatic design of A-kinase anchoring protein-in silico: a potent and selective peptide antagonist of type II protein kinase A anchoring. Proc Natl Acad Sci U S A 100, 4445 (2003).
19. M.G. Gold et al., Molecular basis of AKAP specificity for PKA regulatory subunits. Mol Cell 24, 383 (2006).
20. C.R. Carlson et al., Delineation of type I protein kinase A-selective signaling events using an RI anchoring disruptor. J Biol Chem 281, 21535 (2006).
21. E. Lacana, M. Maceyka, S. Milstien, S. Spiegel, Cloning and characterization of a protein kinase A anchoring protein (AKAP)-related protein that interacts with and regulates sphingosine kinase 1 activity. J Biol Chem 277, 32947 (2002).
22. A. Scholten et al., Analysis of the cGMP/cAMP interactome using a chemical proteomics approach in mammalian heart tissue validates sphingosine kinase type 1-interacting protein as a genuine and highly abundant AKAP. J Proteome Res 5, 1435 (2006).
23. K. Miki, E.M. Eddy, Single amino acids determine specificity of binding of protein kinase A regulatory subunits by protein kinase A anchoring proteins. J Biol Chem 274, 29057 (1999).
24. K. Tamura, J. Dudley, M. Nei, S. Kumar, MEGA4: Molecular Evolutionary Genetics Analysis (MEGA) Software Version 4.0. Mol Biol Evol 24, 1596 (2007).

25. A. Scholten et al., Analysis of the cGMP/cAMP Interactome Using a Chemical Proteomics Approach in Mammalian Heart Tissue Validates Sphingosine Kinase Type 1-interacting Protein as a Genuine and Highly Abundant AKAP. J Proteome Res 5, 1435 (2006).

26. T.T. Aye et al., Selectivity in Enrichment of cAMP-dependent Protein Kinase Regulatory Subunits Type I and Type II and Their Interactors Using Modified cAMP Affinity Resins. Mol Cell Proteomics 8, 1016 (2009).

27. P.J. Boersema, R. Raijmakers, S. Lemeer, S. Mohammed, A.J.R. Heck, Multiplex peptide stable isotope dimethyl labeling for quantitative proteomics. Nat. Protocols 4, 484 (2009).

28. J.W. Gouw, B.B.J. Tops, P. Mortensen, A.J.R. Heck, J. Krijgsveld, Optimizing Identification and Quantitation of 15N-Labeled Proteins in Comparative Proteomics. Anal Chem 80, 7796 (2008).

29. P. Mortensen et al., MSQuant, an Open Source Platform for Mass Spectrometry-Based Quantitative Proteomics. J Proteome Res 9, 393 (2009).

30. T.T. Aye et al., Selectivity in enrichment of cAMP-dependent protein kinase regulatory subunits type I and type II and their interactors using modified cAMP affinity resins. Mol Cell Proteomics 8, 1016 (2009).

31. L.B. Lester, V.M. Coghlan, B. Nauert, J.D. Scott, Cloning and characterization of a novel A-kinase anchoring protein. AKAP 220, association with testicular peroxisomes. J Biol Chem 271, 9460 (1996).

32. D.W. Carr, Z.E. Hausken, I.D. Fraser, R.E. Stofko-Hahn, J.D. Scott, Association of the type II cAMP-dependent protein kinase with a human thyroid RII-anchoring protein. Cloning and characterization of the RII-binding domain. J Biol Chem 267, 13376 (1992).

33. H.B. Landsverk et al., Regulation of anchoring of the RIIα regulatory subunit of PKA to AKAP95 by threonine phosphorylation of RIIα: implications for chromosome dynamics at mitosis. J Cell Sci 114, 3255 (2001).

34. A. Feliciello et al., Yotiao protein, a ligand for the NMDA receptor, binds and targets cAMP-dependent protein kinase II(1). FEBS Lett 464, 174 (1999).

35. J.D. Corbin, S.L. Keely, C.R. Park, The distribution and dissociation of cyclic adenosine 3':5'-monophosphate-dependent protein kinases in adipose, cardiac, and other tissues. J Biol Chem 250, 218 (1975).

36. C.S. Rubin, R. Rangel-Aldao, D. Sarkar, J. Erlichman, N. Fleischer, Characterization and comparison of membrane-associated and cytosolic cAMP-dependent protein kinases. Physicochemical and immunological studies on bovine cerebral cortex protein kinases. J Biol Chem 254, 3797 (1979).

37. G. Di Benedetto et al., Protein kinase A type I and type II define distinct intracellular signaling compartments. Circ Res 103, 836 (2008).

38. L.L. Burns-Hamuro et al., Designing isoform-specific peptide disruptors of protein kinase A localization. Proc Natl Acad Sci U S A 100, 4072 (2003).

39. F.S. Kinderman et al., A dynamic mechanism for AKAP binding to RII isoforms of cAMP-dependent protein kinase. Mol Cell 24, 397 (2006).

40. M.G. Newlon et al., A novel mechanism of PKA anchoring revealed by solution structures of anchoring complexes. EMBO J 20, 1651 (2001).

41. P. Banky et al., Related protein-protein interaction modules present drastically different surface topographies despite a conserved helical platform. J Mol Biol 330, 1117 (2003).

42. L.L. Burns, J.M. Canaves, J.K. Pennypacker, D.K. Blumenthal, S.S. Taylor, Isoform specific differences in binding of a dual-specificity A-kinase anchoring protein to type I and type II regulatory subunits of PKA. Biochemistry 42, 5754 (2003).

43. R.G. Angelo, C.S. Rubin, Characterization of structural features that mediate the tethering of Caenorhabditis elegans protein kinase A to a novel A kinase anchor protein. Insights into the anchoring of PKAI isoforms. J Biol Chem 275, 4351 (2000).

44. G.N. Sarma et al., Structure of D-AKAP2:PKA RI Complex: Insights into AKAP Specificity and Selectivity. Structure 18, 155 (2010).

45. E. Jarnæss et al., Dual Specificity A-kinase Anchoring Proteins (AKAPs) Contain an Additional Binding Region That Enhances Targeting of Protein Kinase A Type I. J Biol Chem 283, 33708 (2008).

Chapter 5

A BH3 domain in the A-kinase anchoring protein SPHKAP provides a link between cAMP signaling and mitochondrial-mediated apoptosis

Duangnapa Kovanich[1]
Marcel A.G. van der Heyden[2]
Yuliang Ma[3]
Manjula Darshi[3]
Mira Sastri[3]
Susan S. Taylor[3,4,5]
Albert J.R. Heck[1]
Arjen Scholten[1]

[1] Biomolecular Mass Spectrometry and Proteomics,
Utrecht Institute for Pharmaceutical Sciences and Bijvoet Center for Biomolecular Research,
Utrecht University, Padualaan 8, 3584 CH, Utrecht, The Netherlands

[2] Department of Medical Physiology, Division Heart & Lungs,
University Medical Centre Utrecht, Yalelaan 50, 3584 CM, Utrecht ,The Netherlands

[3] Department of Chemistry and Biochemistry,
University of California San Diego, La Jolla, CA, 92093, United States of America

[4] Department of Pharmacology,
University of California San Diego, La Jolla, CA, 92093, United States of America

[5] The Howard Hughes Medical Institute,
University of California San Diego, La Jolla, CA, 92093, United States of America

Based on Chembiochem. 2010, 11, 7, 963-71

5.1 Abstract

We recently characterized the abundant cardiac AKAP, sphingosine kinase interacting protein (SPHKAP) as the first PKA-RI specific AKAP. To further investigate the role of the protein, we combined subcellular fractionation, confocal microscopy and LC-MS/MS analysis to study its subcellular localization and exact molecular environment. We found that SPHKAP localizes to the cytoplasm as well as to the mitochondrial inner membrane space and matrix. Here, it colocalizes with PKA-RIα and associates with a mitochondrial inner membrane organizing system (MINOS) complex that is responsible for maintaining crista structure. Additionally, SPHKAP associates with apoptosis-inducing factor (AIF) and the phosphatase PGAM5. We found that the protein N-terminus is required for its mitochondrial localization and overexpression of SPHKAP results in abnormal mitochondria. We show that SPHKAP is a substrate of PKA and that phosphorylation regulates the interaction between SPHKAP and AIF upon cAMP and apoptosis stimulation. Sequence analysis revealed that SPHKAP contains a 13-amino acid motif similar to the BH3 domain present in BCL-2 family proteins. As with other BH3-only proteins, co-immunoprecipitation and deletion of BH3 core amino acids demonstrated that SPHKAP interacts with the anti-apoptotic BCL-2 and BCL-xL through its BH3 domain. Taken together, The data suggest a putative role for the mitochondrial SPHKAP-PKA type I complex in regulating mitochondrial crista structure and mitochondrial-mediated apoptosis.

5.2 Introduction

Pathways signaling through cAMP mediate a multitude of biological processes and physiological responses which are ubiquitously present in every mammalian cell type. When an extracellular cue binds and activates a G protein-coupled receptor, this often results in the activation of adenylyl cyclase and subsequent cAMP generation from ATP. In this way the signal is transferred over the cell membrane and amplified. One of the principle targets of cAMP is the highly abundant cAMP-dependent protein kinase (PKA). This hetero-tetrameric PKA holoenzyme consists of a regulatory subunit dimer (PKA-R) and two catalytic (PKA-C) subunits. Once the PKA-R dimer binds up to four cAMP molecules, the PKA-C's are released and thus activated to phosphorylate nearby substrates. Dedicated scaffold proteins; A-kinase anchoring proteins (AKAPs), provide important temporal and spatial specificity by recruiting PKA holo-enzymes close to their local substrates in specific compartments in the cells.

PKA activity has been described in nearly all cellular organelles (1-3). In mitochondria, cAMP and PKA are involved in several processes such as respiration, fusion/fission, and apoptosis (as reviewed in (3, 4)). In recent years, numerous studies have also implicated a role of cAMP signaling in mitochondrial-mediated apoptosis. However, conflicting results have suggested that cAMP either promotes or blocks apoptosis (5). The fact that different cell lines derived from the same tissue respond differently to cAMP may partly explain this discrepancy (5). Also, PKA mediated phosphorylation has been reported to regulate mitochondrial-mediated apoptosis (6). Several AKAPs recruit PKA isoforms to the cytoplasmic side of the mitochondrial outer membrane (7-11), of which AKAP121's (AKAP1, dAKAP1) function has been characterized with most detail. AKAP 121 recruits PKA to phosphorylate the mitochondrial pro-apoptotic BCL-2 family protein BAD. This subsequently blocks the association of BAD with the anti-apoptotic BCL-2 protein and hence prevents apoptosis (6). Another example is the role of the mitochondrial AKAP, Rab32, of which its activity and expression level has been shown to determine the speed of apoptosis onset. Apoptosis onset is delayed with by a high Rab32 level and accelerated by a low Rab32 level (11).

We recently identified sphingosine kinase interacting protein (SPHKAP), as an abundant cardiac AKAP, which anchors specifically type I PKA holo-enzymes and found it to localize to the cytoplasm (12, 13). Later Means et al. showed that SPHKAP also localizes to mitochondria to facilitate phosphorylation of ChChd3, a component of the mitochondrial inner membrane organizing system (MINOS) (14). To further investigate the role of this intriguing, in heart quite abundant, 180 kDa large AKAP without any conserved domains, we combined subcellular fractionation, confocal microscopy, and LC-MS/MS analysis to characterize its exact molecular environment and function. The data suggest a putative role for the mitochondrial SPHKAP-PKA type I complex in regulating mitochondrial crista structure and mitochondrial-mediated apoptosis.

5.3 Material and Methods

Antibodies and Plasmids

HEK 293 and HeLa S3 cells were obtained from ATCC and cultured at 37 °C and 5 % CO2 in Dulbecco's Modified Eagle Medium supplemented with 10 % fetal calf serum, L-glutamine (2 mM), and streptomycin (50 µg/ mL). Mitotracker Red CMH2-XRos was obtained from Invitrogen. Anti-SPHKAP (GTX101952) was obtained from GeneTex. Anti-mitofilin (ab110329), anti-AIF (ab32516), and anti-GAPDH (ab8245) were obtained from Abcam. Anti- PGAM5 (sc-161156) was obtained from Santa Cruz. Anti-Flag (2368) and anti-phospho PKA substrate (100G7E) were obtained from Cell Signaling. Anti-HA (H9658) was obtained from Sigma-Aldrich. Anti-PKA RIα (610166) and anti-Hsp90 (610418) was obtained from BD Transduction. Anti-PKA RIβ (AF4177) was obtained from R&D Systems. DyLight 488-donkey anti-mouse was obtained from Jackson Immunoresearch. GFP-Trap agarose beads for GFP immune-precipitation were obtained from Chromotek. The SPHKAP-GFP construct was described previously (13) and deletion of residue 801-807 from this SPHKAP-GFP construct to generate SPHKAP Δ BH3 was performed at BaseClear (The Netherlands). The cDNA clones for Flag-BCL-2, Flag-BCL-xL, and Flag-BCL-W (15) were received as gifts from Dr. Nesrin Özören at Boğaziçi University, Turkey.

Mitochondrial Isolation and Fractionation

Soluble/cytoplasmic and insoluble/particulate fractions were isolated from rat H9C2, human HEK 293 and HeLa S3 cells using a commercial Qproteome Cell Compartment Kit (Qiagen). The supernatant (cytoplasmic fraction) and the membrane pellet containing mitochondria (particulate fraction) were probed by Western blot analysis for presence of SPHKAP, Hsp90 and AIF using the immune reagents listed above. Rat ventricular tissue was used for mitochondria isolation and fractionation. Mitochondria from rat heart were purified using a Histodenze/ Percoll gradient as described previously (16, 17). Briefly, the tissue was minced and subsequently disrupted with a polytron (IKA Works) at 4°C in mitochondrial isolation buffer(MSHE) (70 mM sucrose, 210 mM mannitol, 5 mM HEPES, 1 mM EGTA, pH 7.2) containing 0.5% (w/v) fatty acid-free BSA. The homogenate was centrifuged at 600 g for 10 min to remove unbroken cells and nuclei. The post-nuclear supernatant (PNS) was filtered through cheesecloth and subsequently centrifuged at 15,000 g for 10 min to pellet crude mitochondria (dark brown in color). The pellet was gently dispersed into a minimal amount of MSHE+BSA using a fine-tipped paintbrush and washed twice in MSHE with BSA followed by one wash in BSA free MSHE. The pellet was resuspended in minimal amount of MSHE and layered over a gradient of 35% Histodenz (Sigma), 17.5% Histodenz, and 6% Percoll (Sigma) and centrifuged at 45,000g for 45 minutes at 4°C. Pure Mitochondria were collected from the 17.5-35% interface, centrifuged at 15,000g for 15 min, and resuspended in a small volume of MSHE buffer.

Mitochondrial subfractions (outer membrane (OM), inter membrane space (IMS), inner membrane (IM) and matrix) were obtained by a swell-shrink procedure and further purified by using a sucrose gradient ultracentrifugation method (16, 17). Pure mitochondria were resuspended in hypotonic buffer (10 mM KCl, 2 mM HEPES, pH 7.2) at 5 mg/mL for 10 minutes on ice to swell mitochondria. One-third volume of hypertonic buffer (1.8 mM sucrose, 2 mM ATP, 2 mM MgSO4, 2 mM HEPES, pH 7.2) was then added and allowed to incubate for an additional 5 min. Subsequently mitochondria were sonicated for 15 seconds and layered on a sucrose gradient containing 0.76, 1 and 1.32 M sucrose and centrifuged at 75,000g for 3 hours at 4°C. The IMS soluble fraction was collected from the uppermost supernatant. The OM fraction was collected from the 0.76 and 1 M sucrose interface, washed with MSHE, and pelleted by centrifugation at 120,000 g. Mitoplasts (MP) (IM and matrix) were collected from the pellet, washed with MSHE, and centrifuged at 15,000g. MP were sonicated 6-7 times for 15sec on ice with brief intervals. The solution was centrifuged at 15,000 g to remove intact MP, and the resulting supernatant was centrifuged at 140,000g for 45 min at 4°C to pellet IM. The soluble matrix fraction was collected from the supernatant. Each subfraction was immunoblotted for SPHKAP, PKA-RIα, PKA-RIβ and GAPDH and AIF as controls.

Immunostaining and Confocal Microscopy

For confocal microscopy experiments, HeLa S3 cells maintained in DMEM supplemented with 10% fetal bovine serum (FBS) were grown to 70-80% confluency on 35mm glass bottom dishes (Mattek) and transfected using Polyfect (Qiagen) according to the manufacturer's protocol. Approximately 16 h after transfection, Mitotracker was incubated with the cells for 30 min before fixation. Cells were fixed with 4% paraformaldehyde for 10 mins and washed twice with PBS. For immunostaining, cells were permeabilized with 0.3% Triton X-100 and blocked with 1% normal donkey serum, 0.5% BSA, and 50 mM glycine. Cells were incubated with primary antibodies for 2h at 37 °C and secondary antibodies for 1h at room temperature. Images were acquired using FluoView 1000 confocal laser scanning microscope on a 60x objective lens with an NA of 1.2 (Olympus). Stacks of 10–15 slices were acquired (0.4 µm) using sequential scanning method to prevent bleach through between the channels. The images were processed on a customized ImageJ macro by maximum intensity projection method.

GFP Immunoprecipitation and Mass spectrometry analysis

For immune-precipitation of SPHKAP-GFP or GFP alone (control) HEK293 cells were transiently transfected with Polyfect (Qiagen) according to the manufacturer's protocol. Approximately 24 h post-transfection, cells were harvested in lysis buffer (50mM HEPES, 150mM NaCl, 1mM EGTA, 10% glycerol and 0.5% Triton X-100 with a protease inhibitor cocktail (Roche Diagnostics)) and the cell lysates were incubated with GFP-trap agarose beads (Chromotek) for 2 h at 4 °C. The resins were washed with lysis buffer 5 times and 50 mM ammonium bicarbonate 5 times. Enriched proteins were eluted with 150µl 8 M urea in 50 mM ammonium bicarbonate and subjected to in-solution digestion. In brief, proteins were reduced (2 mM dithiothreitol, 1h at 56°)/alkylated (4 mM iodoacetamide, 30 min at room temperature in the dark) and digested for 4 h with Lys-C (Wako Chemicals). The digests were then diluted with 450µl 50 mM ammonium bicarbonate to 2 M urea and digested overnight with trypsin (Promega). Digestion was quenched by acidification with formic acid (final concentration 2%). Resulting peptides were desalted and chemically labeled with stable isotope dimethyl labels as described previously (18). Briefly, peptides were loaded on 50mg Sep-Pak Vac C18 1cc cartridges (Waters) and washed twice with 1mL of 0.1 M acetic acid. Subsequently peptides from control IP were labeled with a mixture of formaldehyde and sodium cyanoborohydride ('light' reagent) and peptides from SPHKAP-GFP IP were labeled with a mixture of D-formaldehyde and sodium cyanoborohydride ('intermediate' reagent). Labeled peptides were eluted with 80% ACN and lyophilized. In a second biological replicate experiment, the labeling reagents were swapped. The 'light' and 'intermediate' dimethyl-labeled samples were resuspended in 5% formic acid, mixed in equal amounts and subjected to mass spectrometric analysis.

Nanoflow LC-MS/MS was carried out by coupling a Thermo Scientific EASY-nLC 1000 to an LTQ-Orbitrap Elite mass spectrometer (Thermo Scientific). The trap (200 mm × 100 µm I.D.) and the analytical column (40 cm × 75 µm I.D.) were packed in-house using Zorbax SB-C18, 1.8 µm (Agilent Technologies). The flow rate was set to 150 nl/min. Mobile-phase solvent A consisted of 0.1 M acetic acid in water and mobile-phase solvent B consisted of 0.1 M acetic acid in 80% acetonitrile. The FT survey scan was set from 350 to 1500 m/z at a resolution of 30,000. After the survey scan, the 10 most intense precursor ions were selected for subsequent fragmentation in a data-dependent decision tree using CID, ETD-IT and ETD-FT activation techniques, similarly to Frese et al. (19).

MS data were processed and quantified using Proteome Discoverer (version 1.3, Thermo Electron). In brief, peptide identification was performed with Mascot 2.3 (Matrix Science) against the Swissprot database (06/2012) whereby Homo sapiens was the selected taxonomy. Trypsin was set as the enzyme and up to two missed cleavages were allowed. Carbamidomethyl cysteine was set as fixed modification and oxidized methionine together with 'light' and 'intermediate' dimethyl labels were set as variable modifications. The dimethyl-based quantitation method was chosen in Proteome Discoverer and only unique peptides were used for quantification. After identification and quantification, the results were filtered with stringent peptide acceptance criteria, which include (i) Mascot ion score of at least 20, (ii) a minimum length of 7 amino-acids and (iii) only Mascot rank 1. Every quantified peptide was manually scrutinized and the proteins, of which all peptides used for quantification were absent completely from the control IP were given an infinite ratio.

Immunoprecipitation and Western blot analysis

HEK293 cells were co-transfected with SPHAKP-GFP and one of the three Flag-BCL 2 family proteins, Flag-BCL-2, Flag-BCL-xL, and Flag-BCL-W using Polyfect (Qiagen). Co-transfection with a vector containing only GFP was used for control experiments. The IP was performed as mentioned above and proteins were eluted with Laemmli sample buffer, and analyzed on SDS-PAGE followed by immunoblot using anti-GFP and anti-Flag antibodies. For mitofilin, AIF, and PGAM5 IPs, HEK293 cells overexpressing SPHKAP-GFP were lysed and the lysate was pre-cleared with protein A-agarose beads for 1h at 4 °C. Pre-cleared samples were incubated with the antibody against the target protein or the corresponding control IgG for 4h and captured with protein A-agarose beads. After overnight incubation, the beads were washed 5 times with lysis buffer and eluted with Laemmli sample buffer. For the PKA phosphorylation study, HEK293 cells overexpressing SPHKAP-GFP were treated with 1mM 8-Br-cAMP or DMSO (control) for 4h and subjected to GFP-IP. For the apoptosis study, HEK293 cells overexpressing SPHKAP-GFP were treated with 1µM staurosporine or DMSO (control) for 4h and subjected to GFP-IP.

5.4 Results

A distinct fraction of SPHKAP Localizes to Mitochondria

We previously reported that overexpressed N-terminally tagged HAHIS6-SPHKAP localizes to the cytosol (13). In contrast, later Means et al. reported mitochondrial localization of C-terminally FLAG-tagged SPHKAP (14). To better understand this discrepancy, we further analyzed the intracellular localization of SPHKAP by both subcellular protein fractionation and confocal fluorescence microscopy (Figure 1). Since SPHKAP is avidly expressed in heart we used rat cardiomyocyte derived H9C2 cells as SPHKAP positive cells and HEK293 and HeLa S3 cells were used as negative controls. An initial crude cell fractionation demonstrates that SPHKAP is present in both the cyto-

solic and particulate fraction (plasma membrane and organelles) of H9C2 cells, while the control markers (Hsp90) (cytosolic) and AIF (mitochondria) are mainly present in their appropriate fractions (Figure 1A). With the reported mitochondrial localization in cardiac myocytes as rationale (14), the distribution of SPHKAP in mitochondrial compartments was further studied in a rat ventricular lysate. A Histodenze/ Percoll gradient centrifugation of post-nuclear supernatants was used, (Figure 1B). Starting from a membrane fraction and multiple centrifugation steps (see materials and methods for details), a pure mitochondrial fraction was obtained, which still contained SPHKAP. Putative contamination was monitored using GAPDH (cytosolic) and AIF (mitochondrial) as markers. These data further prove that a small portion of SPHKAP localizes to mitochondria while the majority localizes to the cytoplasm. To gain more detail, a mitochondrial sub-fractionation was performed (Figure 1C), which revealed that SPHKAP was mainly enriched in the soluble parts of the mitochondria, i.e. the inter membrane space (IMS), and the mitochondrial matrix. Probing these fractions for PKA RIα and RIβ, which were both found in mitochondria, revealed that SPHKAP co-localizes in the same mitochondrial compartments as PKA-RIα, but not PKA-RIβ. This suggests mitochondrial SPHKAP forms a complex uniquely with PKA-RIα in the IMS and perhaps with both RIα and RIβ in the matrix. The cellular localization of SPHKAP was also (re)-analyzed in HEK293 cells by confocal fluorescence microscopy (Figure 1D) using two differently tagged SPHKAP constructs. We observed that the N-terminally tagged HAHIS6-SPHKAP and the C-terminally tagged SPHKAP-GFP showed differential localization. SPHKAP-GFP was observed in the cytoplasm and mitochondria, in line with the C-terminally tagged SPHKAP-FLAG of Means et al. (14) whereas the N-terminally tagged HAHIS6-SPHKAP did not localize to mitochondria. These observations and the presence of endogenous SPHKAP in cardiac mitochondria suggests that the N-terminal tag interferes with mitochondrial targeting of SPHKAP. We have evaluated the SPHKAP sequence for a known mitochondrial targeting sequence (MTS) using MITOPROT (20), however, none could be detected. Upon closer inspection, figure 1D also shows a differential mitochondrial morphology in the SPHKAP-GFP expressing cells. In comparison to the apparent normal mitochondrial morphology in HA-HIS6-SPHKAP expressing cells, the SPHKAP-GFP mitochondria were small and fragmented and lacked the expected Mitotracker red staining of tubular mitochondrial networks. This suggests overexpression of mitochondrial SPHKAP has a detrimental effect on mitochondrial morphology.

The protein interaction network of SPHKAP

To further understand the role of SPHKAP in regulating mitochondrial structure and function, we sought to identify potential binding partners beyond PKA RI. For this purpose, we performed duplicate parallel GFP immunoprecipitations in total cell lysates obtained from SPHKAP-GFP and GFP expressing control HEK 293 cells. Enriched proteins from the SPHKAP-GFP and control GFP immunoprecipitations were digested to peptides and the peptides were labeled using different stable isotope dimethyl labels (light and intermediate) and analyzed by mass spectrometry (figure 2A). All proteins confidently identified in these pull-downs and their enrichment ratios are presented in supplemental table 1. Proteins specifically present in the SPHKAP-GFP experiment were selected as based on an infinite SPHKAP-GFP/GFP ratio and only proteins quantified with two or more unique peptides were considered. Amongst these proteins were PKA-RIα, PKA-RIβ, PKA-C and the protein ChChD3, all previously described as SPHKAP interacting proteins (13, 14). Also many novel putative interactors were identified, such as PGAM5, a protein phosphatase and AIF, a caspase-independent apoptosis-inducing factor. As expected, many SPHKAP enriched proteins are mitochondrial and a STRING interaction analysis (21) supplemented with recent literature shows that they form a well-connected network (14, 16, 22-25) (figure 2B). This subset of proteins may represent the mitochondrial environment of SPHKAP. Interestingly, components of the cytosolic proteasome and chaperone machinery were also enriched and those may represent the cytosolic environment of SPHKAP. Here, we decided to focus on some of the novel putative mitochondrial interactors.

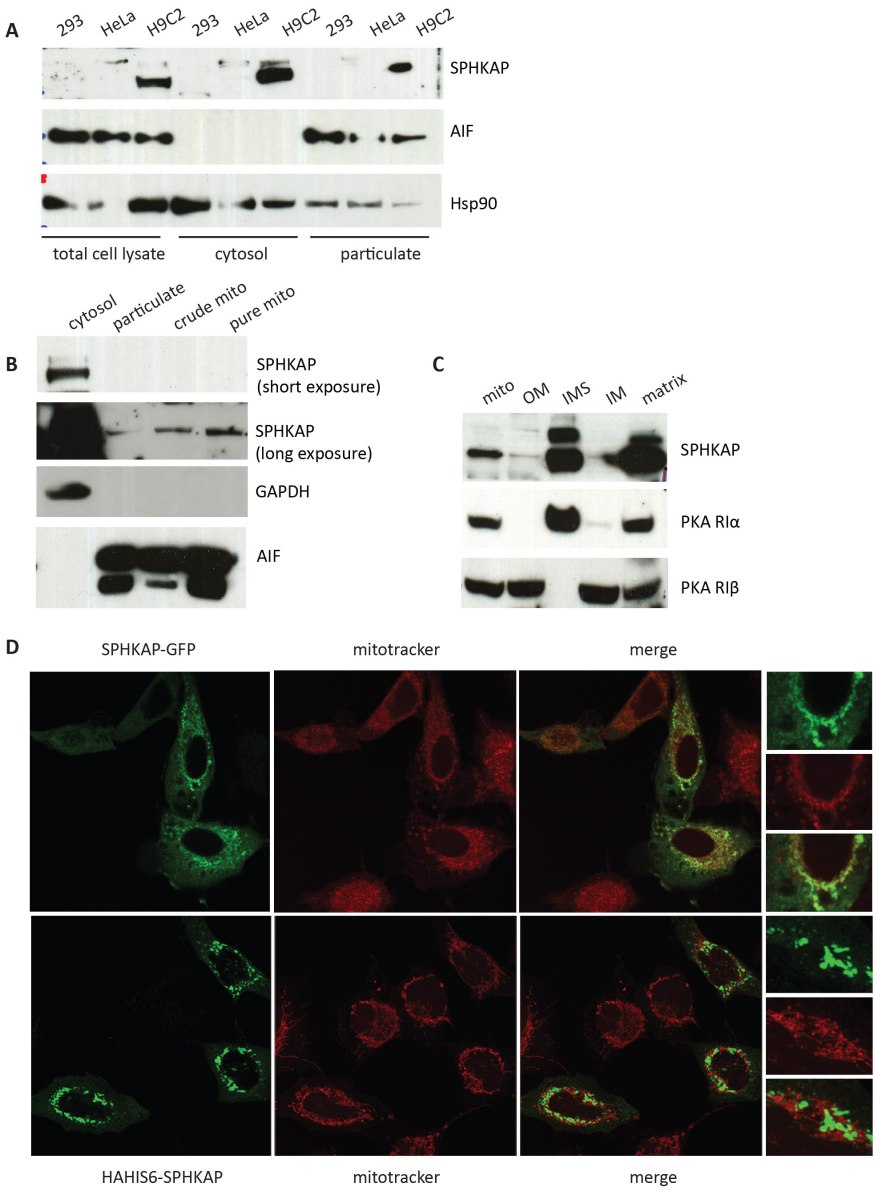

Figure 1 > SPHKAP subcellular localization to mitochondria.

A) *SPHKAP is localized to both the cytosolic as well as the particulate fraction. Three cell lines, HEK293, HeLa S3, and H9C2 were fractionated into a cytosolic, a particulate (plasma membrane and compartmentalized organelles), and a nuclear fraction. Cytosolic and particulate fractions were analyzed by immunoblotting using antibodies against SPHKAP, Hsp90 (cytosolic marker), and AIF (mitochondrial marker). SPHKAP was detected only in cardiac H9C2 cells in both fractions.* ***B)*** *SPHKAP is localized to the cytosol as well as to mitochondria. The post-nuclear supernatant of a rat heart lysate was fractionated to obtain a pure mitochondrial pellet as described in the Materials and Methods. Samples collected from each step were analyzed by immunoblotting with antibodies against SPHKAP, GAPDH (cytosolic marker), and AIF (mitochondrial marker). SPHKAP was exposed for a longer time as well.* ***C)*** *Sub-fractionation of mitochondria purified from rat ventricular tissue. SPHKAP, PKA-RIα and PKA-RIß Western blots were performed on the outer membrane (OM), inter membrane space (IMS), inner membrane (IM) and matrix fraction.* ***D)*** *SPHKAP's N-terminus is required for mitochondrial targeting. HeLa S3 cells were transfected with SPHKAP-GFP or HA-HIS6-SPHKAP and before fixing, cells were stained for mitochondria with Mitotracker. For HA-HIS6-SPHKAP, cells were stained with anti-HA and DyLight 488-donkey anti-mouse. Images were captured sequentially for GFP or DyLight 488 and Mitotracker. The image shown represents composite images of Z sections captured using a ×100 objective with oil. Co-localization between SPHKAP-GFP and Mitotracker is evident (upper panel, while N-terminally tagged HA-HIS6-SPHKAP failed to co-localize with Mitotracker (bottom panel).*

To further verify the interaction between SPHKAP and the proteins identified by mass spectrometry, we performed reciprocal immuno-precipitations in the SPHKAP-GFP lysate targeting three of the novel identified endogenous interacting proteins, mitofilin (IMMT), AIF and PGAM5. Mitofilin was selected as it is known to associate with ChChD3 and several other mitochondrial proteins identified in our SPHKAP enrichment (16, 23-26). Immunoblots of co-immunoprecipitated SPHKAP with endogeneous mitofilin, AIF, and PGAM5 did confirm in all these cases the association of these proteins with SPHKAP-GFP (figure 2C).

AKAPs recruit PKA holo-enzymes to defined locations in the cell to facilitate PKA phosphorylation of local substrates in response to cAMP. Besides this, they can also be substrates of PKA themselves and these phosphorylation events may influence AKAP-complex composition (27-29). Here we explore the role of PKA in the mitochondrial SPHKAP complex. Based on the minimal PKA consensus motif ([R/K]XX[pS/pT][noP]), SPHKAP contains 5 putative PKA sites (http://scansite.mit.edu) of which one was already observed in human and mouse high-throughput phosphoproteomics experiments (www.phosphosite.org and (30)) (figure 2E). To investigate possible SPHKAP phosphorylation by PKA-C, in parallel, SPHKAP-GFP expressing cells were treated with 8-bromo-cAMP (8-Br-cAMP) or a vehicle control. SPHKAP-GFP was immunoprecipitated and phosphorylation was monitored by immunoblot using an antibody recognizing the mentioned substrate motif of PKA. When probing the total lysate, PKA activation through 8-Br-cAMP promoted a large increase in signal over control on many different proteins (Figure 2D). When probing the GFP immunoprecipated fraction, the antibody detected a band migrating at the same molecular weight as SPHKAP in both control and 8-Br-cAMP treated SPHKAP-GFP cells. However, the signal in the 8-Br-cAMP treated sample was much stronger, suggesting SPHKAP is phosphorylated phosphorylated in a cAMP dependent manner. The lower signal in the vehicle treated cells likely represents basal phosphorylation of SPHKAP.

We then explored the possibility that SPHKAP phosphorylation by PKA may change complex composition. Cells were treated with 8-Br-cAMP and from the lysate we immuno-precipitated SPHKAP-GFP and probed these for IMMT and AIF. Interestingly, the amount of AIF co-purified is elevated upon cAMP treatment while that of IMMT remained unchanged (Figure 2F). Taken together these data indicate that SPHKAP is a substrate of PKA and that phosphorylation regulates at least part of the protein interaction network of SPHKAP.

AIF is a mitochondrial flavoprotein that plays a role in apoptosis (31). As indicated above, the interaction between SPHKAP and AIF is increased in response to PKA activation. We then investigated the possibility that the interaction between SPHKAP and AIF might also change upon apoptosis induction for which it is known that AIF migrates from mitochondria towards the nucleus (31). HEK293 cells overexpressing SPHKAP were treated with the apoptosis-inducing reagent, staurosporine. Apoptosis was assessed by cell shrinkage and nuclear condensation (data not shown). Lysates were subjected to GFP-IP and AIF was detected by immunoblotting. Although the amount of SPHKAP is slightly reduced after staurosporine treatment, the amount of AIF co-purified is increased compared to that from the unstimulated condition (figure 2G). This and the change in morphology observed in SPHKAP-GFP overexpressing cells (Figure 1D) suggest a putative role for the mitochondrial SPHKAP-PKA complex in apoptosis.

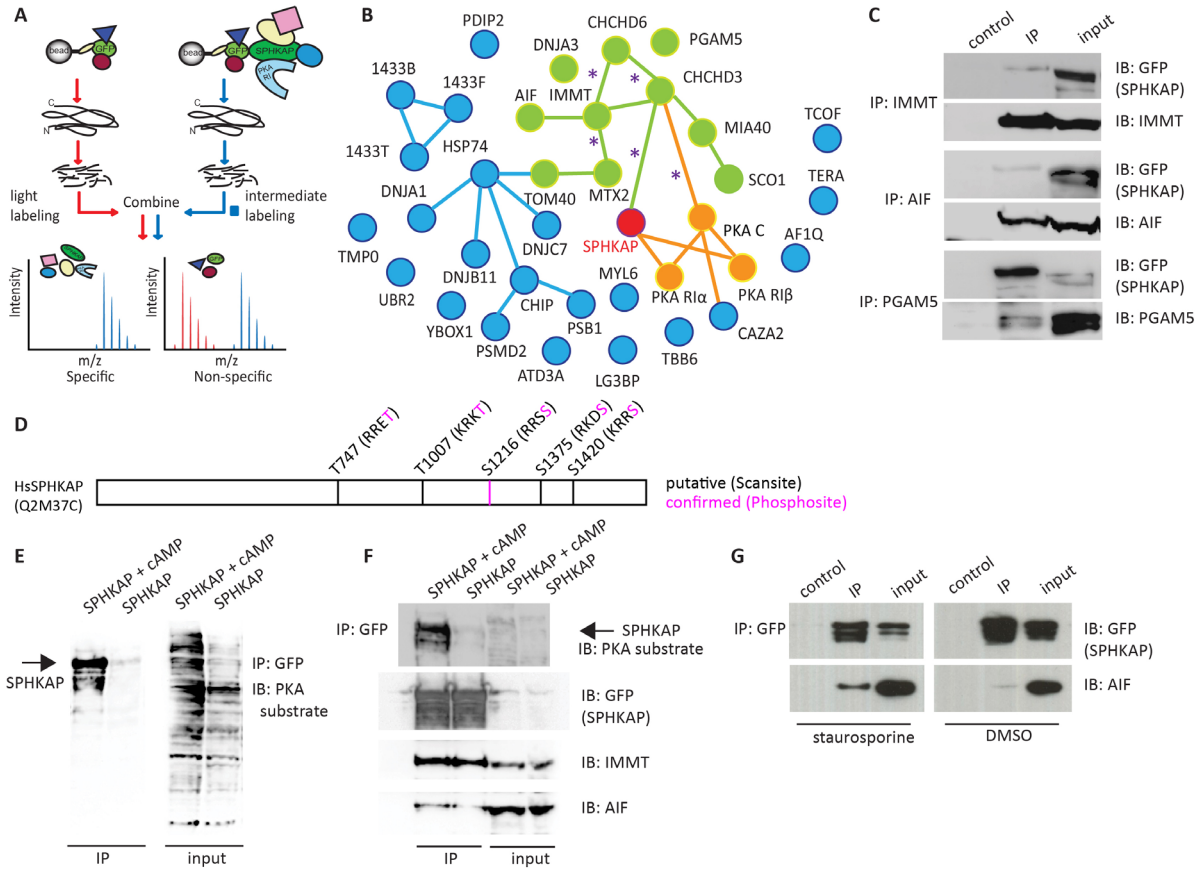

Figure 2 > The SPHKAP interactome captured by GFP immune-precipitation and quantitative mass spectrometry.

A) *Overview of the strategy. GFP immunoprecipitation was performed in a lysate from HEK293 cells overexpressing SPHKAP-GFP or GFP alone as control. Enriched proteins were digested and the peptides from the SPHKAP-GFP and GFP IPs were differentially labeled using dimethyl labeling. The two labeled digests were combined, subsequently analyzed by LC-MS/MS and peptide pairs quantified. In a biological replicate experiment, the labels were swapped. The absence of the light labeled peptide results in an infinite ratio indicating a specific interacting partner of SPHKAP.* ***B)*** *Specific interactors of SPHKAP were subjected to STRING analysis to reveal an interaction network based on prior knowledge. Mitochondrial proteins are green color-coded, PKA subunits orange and other proteins are blue. Proteins connected by lines are known interactors whereby the lines with an asterisk represent additional confirmed interactions from literature review not available in STRING yet (14, 16, 22-25).* ***C)*** *Verification of SPHKAP interaction with mitofilin (IMMT), AIF, and PGAM5. Immuno-precipitations of endogenous IMMT, AIF and PGAM5 from SPHKAP-GFP expressing HEK293 cells were probed with anti-GFP D) SPHKAP is a substrate of PKA. SPHKAP-GFP was immune-precipitated from HEK293 cells treated with 8-Br-cAMP to induce PKA activity or by just the vehicle as a control. Phosphorylated SPHKAP was detected by using an antibody against PKA substrates.* ***E)*** *Schematic representation of putative and confirmed PKA phosphorylation sites identified on human SPHKAP (Q2M37C). Five putative PKA motifs were identified by Scansite (http://scansite.mit.edu), among which, phosphorylated Ser1216 (depicted in pink) was confirmed by high-throughput phosphoproteomics screens (www.phosphosite.org).* ***F)*** *The interaction between SPHKAP and AIF is up-regulated after cAMP treatment. SPHKAP-GFP was immunoprecipitated from cAMP-treated SPHKAP-GFP expressing cells as mentioned in D. Immunoblots for anti-phospho PKA substrate confirmed that PKA was activated and SPHKAP was phosphorylated in 8-Br-cAMP-treated cells. Mitofilin and AIF were detected in cAMP-treated and control IPs. While the level of interaction between SPHKAP and mitofilin remained unchanged, the interaction with AIF was increased.* ***G)*** *Interaction between SPHKAP and AIF also increases after induction of apoptosis by staurosporine. GFP-IP was performed in staurosporine-treated SPHKAP-GFP overexpressing cells and probed for AIF. The amount of AIF co-precipitated with SPHKAP from apoptotic cells is increased.*

SPHKAP is a putative BH3-only protein

Circumstantial evidence linking SPHKAP with apoptosis comes from its interaction partners: apoptosis-inducing factor (AIF) and the phosphatase PGAM5. The latter is a known interactor of the anti-apoptotic BCL-xL protein (32, 33). Pro-apoptotic Bcl-2 family proteins are divided into two groups, which are (1) the multi-domain pro-apoptotic proteins that contain three BCL-2 homology (BH) domains, BH4, BH3 and BH1 and (2) the BH3-only pro-apoptotic proteins that contain only the BH3 domain. In both groups, the BH3 domain is required for interaction with anti-apoptotic BCL-2 family proteins. A BH3 domain is characterized as a four-turn amphiphatic α-helix, bearing the variable 13-residue sequence motif, Φ1ΣXXΦ2XXΦ3ΣDZΦ4Γ, that typically contains a highly conserved leucine (L) at hydrophobic position Φ2 and an aspartic acid residue (D) at position D (Figure 3A). The domain identification is often difficult by sequence analysis alone, as the pattern of residues is relatively poorly conserved. Thus, combined evidence of putative BH3 domains and binding to one of the anti-apoptotic BCL-2 family proteins is essential to identify proteins as BH3-only proteins.

To rationalize whether the mitochondrial disruption caused by SPHKAP-GFP overexpression, could be caused by the fact that SPHKAP induces apoptosis, we initially interrogated the SPHKAP sequence for putative BH3 domains. Sequence analysis revealed that both human, mouse, and rat SPHKAP contain a highly conserved 13-amino acid sequence reminiscent of the BH3 domains from known BCL-2 family proteins (Figure 3A). To study if the putative BH3 domain on SPHKAP is functional, we next screened for the interaction between SPHKAP and three representative anti-apoptotic BCL-2 family proteins, BCL-2, BCL-xL, and BCL W. We found that SPHKAP-GFP co-purified with co-expressed FLAG-BCL-2 and FLAG-BCL-xL, but not FLAG-BCL-W (figure 3B). We then investigated whether the interaction was through the putative BH3 domain. 7 amino acids starting from the highly conserved leucine at posistion Φ2 to the aspartic acid at position D were deleted from the SPHKAP BH3 domain (Figure3C). As shown in figure 3D, the mutation destroyed the interaction between SPHKAP and BCL-xL. This data provides clear evidence that SPHKAP may be regarded as a novel BH3-protein as it also interacts with the anti-apoptotic BCL-2 and BCL-xL.

5.5 Discussion

SPHKAP was first described by us as one of the most abundant AKAPs in the mammalian heart (12) and subsequently characterized as the first entirely PKA-RI specific AKAP (13). We confirm here that, based on subcellular fractionation, mitochondrial isolation and confocal fluorescence microscopy, SPHKAP is localized to mitochondria as well as to the cytosol (14). Submitochondrial fractionation reveals that the protein localizes to the two soluble fractions of mitochondria, the inner membrane space (IMS) and the matrix, where it uniquely co-localizes with PKA-RIα. Several AKAPs have been characterized to associate with mitochondria at the cytoplasmic side of the mitochondrial outer membrane (7-11). To our knowledge, SPHKAP is the first AKAP identified to localize inside mitochondria. Furthermore, our data indicates that the N-terminus of the protein is required for mitochondrial targeting although a clear conserved mitochondrial targeting sequence is missing.

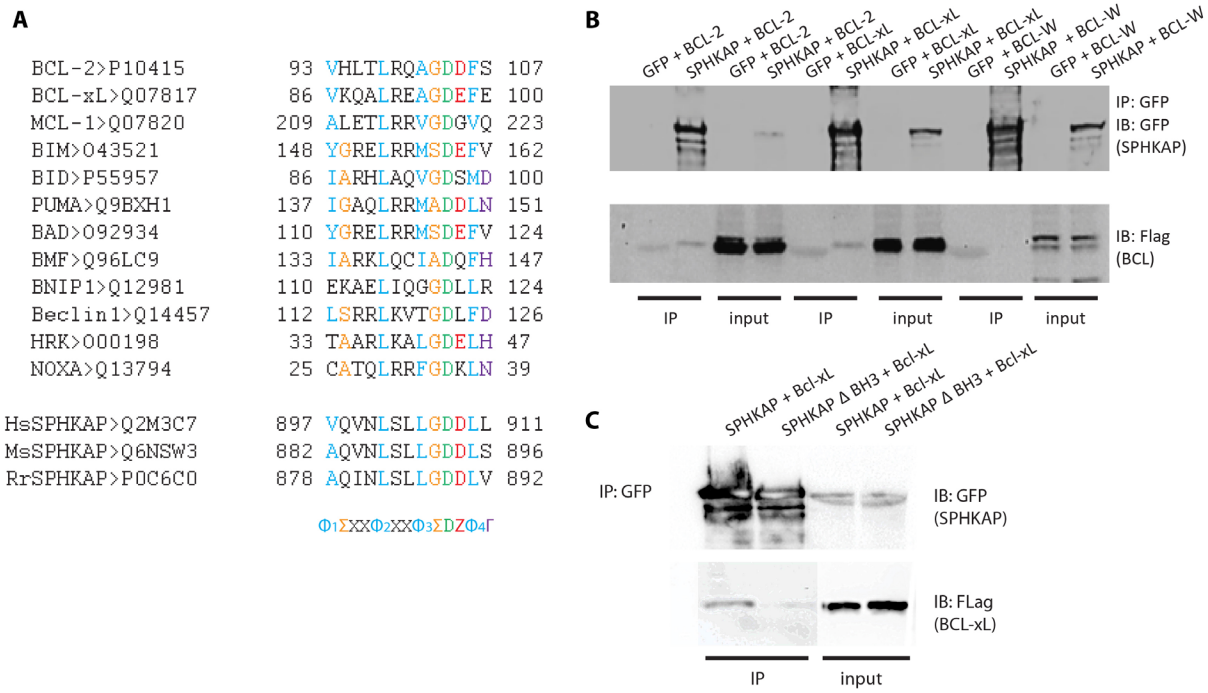

Figure 3 > SPHKAP is a novel BH3-only protein.

A) *Alignment of BCL-homology 3 (BH3) domains from human, mouse and rat SPHKAPs with those of various well-characterized members of the BCL-2 protein family. Their accession numbers are indicated. Numbers before and after the sequences denote amino acid positions in the context of full-length protein. The consensus sequence of the BH3 domain is shown at the bottom. Φ represents a hydrophobic residue (Φ2 is usually leucine). Σ is a small residue (G, A, S, C) and Z represents an acidic residue. Γ is a hydrophilic residue (N, H, D or Y).* ***B)*** *SPHKAP interacts with BCL-2 and BCL-xL, but not BCL-W. GFP-IPs were performed in the lysates obtained from HEK293 co-transfected with SPHKAP and Flag-BCL-2 or Flag-BCL-xL or Flag-BCL-W. Co-precipitated Flag-BCL2 and Flag-BCL-xL were detected by immoblotting using anti-Flag.* ***C)*** *SPHKAP interacts with BCL-xL through its BH3 domain. 7 core residues (901-907) were removed from SPHKAP-GFP to create SPHKAP Δ BH3. BCL-xL co-precipitated with SPHKAP-GFP but not SPHKAP Δ BH3, indicating that the BH3 domain is required to interact with BCL-xL.*

The distinct abnormal mitochondrial morphology observed in cells overexpressing SPHKAP suggests that SPHKAP has a function in this organelle. Our quantitative SPHKAP-GFP IP reveals that the molecular environment of SPHKAP consists of mitochondrial as well as cytosolic proteins. The two most abundant proteins identified in our IP are the IMS-facing inner membrane proteins, mitofilin and ChChD3. The two proteins are central components of the mitochondrial inner membrane organizing system (MINOS) complex which is very essential to preserve the connections between the inner and cristae membranes (15). Disruption of either core protein resulted in fragmentation of the mitochondrial network and cristae disorganization (14, 22), which is the exact phenotype we observed upon overexpression of SPHKAP (34). To place SPHKAP's mitochondrial environment in perspective, we also enriched for ChChD6, metaxin-2 and Mia40, proteins previously characterized to associate with IMMT, ChChD3 and other MINOS proteins. This puts forward an interesting conundrum since the MINOS-components and their associated proteins are expressed abundantly in almost all kind of tissues, while SPHKAP's tissue distribution seems limited to heart, brain, ovary and spleen (35). Also taking into account that ChChD3 from mouse brain was previously identified as a substrate of PKA (22), hint at SPHKAP being a novel, but not a critical component of the MINOS complex. We propose that SPHKAP rather facilitates another level of regulation to the MINOS complex in the tissues where it is expressed. This still leaves the question whether SPHKAP is also crucial for the reported phosphorylation of ChChD3 (22).

Interestingly, we also found that SPHKAP interacts with the apoptosis inducing factor (AIF). AIF is a mitochondrial restricted caspase-independent apoptotic effector, which is loosely associated with the inner mitochondrial membrane. Upon apoptotic stimulation, AIF is cleaved from the inner membrane and translocated to the nucleus, where it triggers chromatin condensation and DNA degradation (31). Up to date, the mechanism underlying apoptotic processing and translocation of mitochondrial AIF into the cytoplasm is complex and not fully understood (31). According to our data, AIF interacts with SPHKAP and the interaction is up-regulated upon apoptotic as well as cAMP stimulation providing an extra level for regulation of AIF.

Besides the PKA holoenzyme, AKAPs also scaffold phosphatases to their signaling complexes to mediate the level of phosphorylation events on PKA substrates (36). In our study, we identified the serine/threonine phosphatase PGAM5 as a novel interacting partner of SPHKAP. PGAM5 localizes to the cytoplasmic side of the mitochondrial outer membrane and its role in regulating necrosis and apoptosis have been described recently (32, 33, 37). PGAM5 was identified as an interacting partner of the anti-apoptotic BCL-xL and later shown to mediate apoptosis by facilitating degradation of BCL-xL (33). In our study we also found that SPHKAP is a BH3-only protein that interacts with BCL-xL as well as BCL-2 via a here identified novel BH3 domain.

Summarizing, our study provides novel information on the mitochondrial molecular environment of the unexplored SPHKAP/PKA-RI complex. The data suggest a potential role of SPHKAP in regulating the mitochondrial MINOS complex and thereby crista structure. SPHKAP is phosphorylated by PKA and the phosphorylation regulates its interaction with AIF. Moreover, we also show that SPHKAP is a novel BH3-only protein. Taken together, the data reveals a potential role for SPHKAP as a link between cAMP signaling and apoptosis.

5.6 Acknowledgements

We thank Dr. Nesrin Özören from Boğaziçi University, Turkey for providing us cDNA clones for Flag-BCL-2, Flag-BCL-xL, and Flag-BCL-W and Susanna Petrosyan for mitochondria isolation and fractionation. Kristofer Haushalter is kindly acknowledged for providing the PKA-RIβ antibody, and Pepijn P. Burgers for confocal images and discussion. This work was in part supported by the PRIME-XS project, Grant Agreement Number 262067, funded by the European Union Seventh Framework Program. The Netherlands Proteomics Centre, embedded in The Netherlands Genomics Initiative is acknowledged for funding.

5.7 References

1. M.D. Kritzer, J. Li, K. Dodge-Kafka, M.S. Kapiloff, AKAPs: The architectural underpinnings of local cAMP signaling. J Mol Cell Cardiol 52, 351 (2012).
2. F. Mavillard, J. Hidalgo, D. Megias, K.L. Levitsky, A. Velasco, PKA-Mediated Golgi Remodeling During cAMP Signal Transmission. Traffic 11, 90 (2010).
3. A. Feliciello, M.E. Gottesman, E.V. Avvedimento, cAMP-PKA signaling to the mitochondria: protein scaffolds, mRNA and phosphatases. Cellular Signalling 17, 279 (2005).
4. A. Carlucci, L. Lignitto, A. Feliciello, Control of mitochondria dynamics and oxidative metabolism by cAMP, AKAPs and the proteasome. Trends Cell Biol 18, 604 (2008).
5. P. A. Insel, L. Zhang, F. Murray, H. Yokouchi, A.C. Zambon, Cyclic AMP is both a pro-apoptotic and anti-apoptotic second messenger. Acta Physiol 204, 277 (2012).
6. A. Affaitati et al., Essential Role of A-kinase Anchor Protein 121 for cAMP Signaling to Mitochondria. J Biol Chem 278, 4286 (2003).
7. Q. Chen, R.Y. Lin, C.S. Rubin, Organelle-specific targeting of protein kinase AII (PKAII): Molecular and in situ characterization of murine A kinase anchor proteins that recruit regulatory subunits of PKAII to the cytoplasmic surface of mitochondria. J Biol Chem 272, 15247 (1997).
8. L. Cardone et al., A-Kinase Anchor Protein 84/121 are Targeted to Mitochondria and Mitotic Spindles by Overlapping Amino-terminal Motifs. J Mol Biol 320, 663 (2002).
9. J. Liu et al., Protein-protein interactions mediate mitochondrial cholesterol transport and steroid biosynthesis. J Biol Chem 281, 38879 (2006)
10. Y. Ma, S.S. Taylor, A Molecular Switch for Targeting between Endoplasmic Reticulum (ER) and Mitochondria: conversion of a mitochondria-targeting element into an ER-targeting signal in D-AKAP1. J Biol Chem 283, 11743 (2008).
11. M. Bui et al., Rab32 Modulates Apoptosis Onset and Mitochondria-associated Membrane (MAM) Properties. J Biol Chem 285, 31590 (2010).
12. A. Scholten et al., Analysis of the cGMP/cAMP Interactome Using a Chemical Proteomics Approach in Mammalian Heart Tissue Validates Sphingosine Kinase Type 1-interacting Protein as a Genuine and Highly Abundant AKAP. J Proteome Res 5, 1435 (2006).
13. D. Kovanich et al., Sphingosine Kinase Interacting Protein is an A-Kinase Anchoring Protein Specific for Type I cAMP-Dependent Protein Kinase. ChemBioChem 11, 963 (2010).
14. C.K. Means et al., An entirely specific type I A-kinase anchoring protein that can sequester two molecules of protein kinase A at mitochondria. Proc Natl Acad Sci U S A 108, E1227 (2011).
15. N. Özören, N. Inohara, G. Núñez, A putative role for human BFK in DNA damage-induced apoptosis. Biotechnol J 4, 1046 (2009).
16. M. Darshi et al., ChChd3, an Inner Mitochondrial Membrane Protein, Is Essential for Maintaining Crista Integrity and Mitochondrial Function. J Biol Chem 286, 2918 (2011).
17. M.T. Radin, G.S. Taylor, J.E. Dixon, in Methods in Enzymology : Mitochondrial Function, part B: Mitochondrial Protein Kinases, Protein Phosphatases and Mitochondrial Diseases. (2009), vol. 457, pp 275-287
18. P.J. Boersema, R. Raijmakers, S. Lemeer, S. Mohammed, A.J.R. Heck, Multiplex peptide stable isotope dimethyl labeling for quantitative proteomics. Nat Protocols 4, 484 (2009).
19. C. K. Frese et al., Improved Peptide Identification by Targeted Fragmentation Using CID, HCD and ETD on an LTQ-Orbitrap Velos. J Proteome Res 10, 2377 (2011).
20. M.G. Claros, P. Vincens, Computational Method to Predict Mitochondrially Imported Proteins and their Targeting Sequences. Eur J Biochem 241, 779 (1996).
21. D. Szklarczyk et al., The STRING database in 2011: functional interaction networks of proteins, globally integrated and scored. Nucleic Acids Research 39, D561 (2011).
22. S. Schauble et al., Identification of ChChd3 as a Novel Substrate of the cAMP-dependent Protein Kinase (PKA) Using an Analog-sensitive Catalytic Subunit. J Biol Chem 282, 14952 (2007).

23. J. Xie, M. F. Marusich, P. Souda, J. Whitelegge, R.A. Capaldi, The mitochondrial inner membrane protein Mitofilin exists as a complex with SAM50, metaxins 1 and 2, coiled-coil-helix coiled-coil-helix domain-containing protein 3 and 6 and DnaJC11. FEBS Letters 581, 3545 (2007).

24. J. An et al., CHCM1/CHCHD6, Novel Mitochondrial Protein Linked to Regulation of Mitofilin and Mitochondrial Cristae Morphology. J Biol Chem 287, 7411 (2012).

25. M. Darshi, K.N. Trinh, A. N. Murphy, S.S. Taylor, Targeting and Import Mechanism of Coiled-coil Helix Coiled-coil Helix Domain-containing Protein 3 (ChChd3) into the Mitochondrial Intermembrane Space. J Biol Chem 287, 39480 (2012).

26. R.M. Zerbes et al., Mitofilin complexes: conserved organizers of mitochondrial membrane architecture. Biol Chem 393, 1247 (2012).

27. J. Tao, H.-y. Wang, C.C. Malbon, Protein kinase A regulates AKAP250 (gravin) scaffold binding to the β2-adrenergic receptor. EMBO J 22, 6419 (2003).

28. G.K. Carnegie, F.D. Smith, G. McConnachie, L.K. Langeberg, J.D. Scott, AKAP-Lbc Nucleates a Protein Kinase D Activation Scaffold. Mol Cell 15, 889 (2004).

29. L. Chen, J. Kurokawa, R. S. Kass, Phosphorylation of the A-kinase-anchoring Protein Yotiao Contributes to Protein Kinase A Regulation of a Heart Potassium Channel. J Biol Chem 280, 31347 (2005).

30. E.L. Huttlin et al., A Tissue-Specific Atlas of Mouse Protein Phosphorylation and Expression. Cell 143, 1174 (2010).

31. I.F. Sevrioukova, Apoptosis-inducing factor: structure, function, and redox regulation. Antioxid Redox Signal 14, 2545 (2011)

32. S.-C. Lo, M. Hannink, PGAM5 tethers a ternary complex containing Keap1 and Nrf2 to mitochondria. Exp Cell Res 314, 1789 (2008).

33. S.K. Niture, A.K. Jaiswal, Inhibitor of Nrf2 (INrf2 or Keap1) Protein Degrades Bcl-xL via Phosphoglycerate Mutase 5 and Controls Cellular Apoptosis. J Biol Chem 286, 44542 (2011).

34. R.F. Yang et al., Mitofilin regulates cytochrome c release during apoptosis by controlling mitochondrial cristae remodeling. Biochem Biophys Res Commun 428, 93 (2012).

35. E. Lacaná, M. Maceyka, S. Milstien, S. Spiegel, Cloning and Characterization of a Protein Kinase A Anchoring Protein (AKAP)-related Protein That Interacts with and Regulates Sphingosine Kinase 1 Activity. J Biol Chem 277, 32947 (2002).

36. J.M. Redden, K.L. Dodge-Kafka, AKAP phosphatase complexes in the heart. J Cardiovasc Pharmacol 58, 345 (2011)

37. Z. Wang, H. Jiang, S. Chen, F. Du, X. Wang, The Mitochondrial Phosphatase PGAM5 Functions at the Convergence Point of Multiple Necrotic Death Pathways. Cell 148, 228 (2012).

Supplemental table 1 > List of identified proteins with their enrichment ratios from the two SPHKAP-GFP-IP experiments.

Accession number	Description	Official symbol	Experiment 1			Experiment 2		
			Ratio SPHKAP/ GFP	Area	No. of peptides used for quantification	Ratio SPHKAP/ GFP	Area	No. of peptides used for quantification
P31946	14-3-3 protein beta/alpha GN=YWHAB	1433B	infinite	4.829E8	1	infinite	1.206E9	3
Q04917	14-3-3 protein eta GN=YWHAH	1433F	infinite	2.326E8	3	infinite	8.100E8	4
P27348	14-3-3 protein theta GN=YWHAQ	1433T	infinite	4.069E8	1	infinite	1.356E9	6
Q13015	Protein AF1q GN=MLLT11	AF1Q	infinite	9.279E7	1	infinite	1.084E8	2
O95831	Apoptosis-inducing factor 1, mitochondrial GN=AIFM1	AIFM1	infinite	1.108E8	2	infinite	1.940E8	7
Q9NVI7	ATPase family AAA domain-containing protein 3A GN=ATAD3A	ATD3A	infinite	1.120E8	1	infinite	9.963E8	4
P47755	F-actin-capping protein subunit alpha-2 GN=CAPZA2	CAZA2	infinite	4.640E7	1	infinite	1.205E8	2
Q9NX63	Coiled-coil-helix-coiled-coil-helix domain-containing protein 3, mitochondrial GN=CHCHD3	CHCH3	infinite	3.797E9	8	infinite	5.361E9	16

Accession number	Description	Official symbol	Experiment 1			Experiment 2		
			Ratio SPHKAP/ GFP	Area	No. of peptides used for quantification	Ratio SPHKAP/ GFP	Area	No. of peptides used for quantification
Q9BRQ6	Coiled-coil-helix-coiled-coil-helix domain-containing protein 6 GN=CHCHD6	CHCH6	infinite	6.745E8	1	infinite	5.726E8	2
Q9UNE7	E3 ubiquitin-protein ligase CHIP GN=STUB1	CHIP	infinite	4.766E7	2	infinite	5.828E7	1
Q9UBS4	DnaJ homolog subfamily B member 11 GN=DNAJB11	DJB11	infinite	1.197E8	2	infinite	9.239E7	2
P31689	DnaJ homolog subfamily A member 1 GN=DNAJA1	DNJA1	infinite	7.330E8	1	infinite	1.073E9	1.073E9
Q96EY1	DnaJ homolog subfamily A member 3, mitochondrial GN=DNAJA3	DNJA3	infinite	8.571E8	4	infinite	1.561E9	6
P34932	Heat shock 70 kDa protein 4 GN=HSPA4	HSP74	infinite	7.453E6	1	infinite	1.538E8	4
Q16891	Mitochondrial inner membrane protein GN=IMMT	IMMT	infinite	3.298E9	15	infinite	4.465E9	36
P10644	cAMP-dependent protein kinase type I-alpha regulatory subunit GN=PRKAR1A	KAP0	infinite	1.330E9	4	infinite	2.578E9	10

Accession number	Description	Official symbol	Experiment 1			Experiment 2		
			Ratio SPHKAP/ GFP	Area	No. of peptides used for quantification	Ratio SPHKAP/ GFP	Area	No. of peptides used for quantification
P31321	cAMP-dependent protein kinase type I-beta regulatory subunit GN=PRKAR1B	KAP1	infinite	2.798E8	1	infinite	3.651E8	1
P42166	Lamina-associated polypeptide 2, isoform alpha GN=TMPO	LAP2A	infinite	3.265E7	1	infinite	6.833E7	2
Q08380	Galectin-3-binding protein GN=LGALS3BP	LG3BP	infinite	1.513E8	1	infinite	4.182E8	4
Q8N4Q1	Mitochondrial intermembrane space import and assembly protein 40 GN=CHCHD4	MIA40	infinite	1.216E8	1	infinite	1.706E8	1
O75431	Metaxin-2 GN=MTX2	MTX2	infinite	1.795E8	3	infinite	5.394E8	5
P60660	Myosin light polypeptide 6 GN=MYL6	MYL6	infinite	1.871E7	1	infinite	6.938E6	1
Q9Y2S7	Polymerase delta-interacting protein 2 GN=POLDIP2	PDIP2	infinite	5.566E7	1	infinite	1.275E8	2
Q96HS1	Serine/threonine-protein phosphatase PGAM5, mitochondrial GN=PGAM5	PGAM5	infinite	5.222E8	4	infinite	3.862E8	2
P20618	Proteasome subunit beta type-1 GN=PSMB1	PSB1	infinite	4.108E7	1	infinite	4.828E7	1

Accession number	Description	Official symbol	Experiment 1			Experiment 2		
			Ratio SPHKAP/ GFP	Area	No. of peptides used for quantification	Ratio SPHKAP/ GFP	Area	No. of peptides used for quantification
Q13200	26S proteasome non-ATPase regulatory subunit 2 GN=PSMD2	PSMD2	infinite	5.076E7	1	infinite	1.028E8	1
O75880	Protein SCO1 homolog, mitochondrial GN=SCO1	SCO1	infinite	3.313E8	1	infinite	5.172E8	1
Q2M3C7	A-kinase anchor protein SPHKAP GN=SPHKAP	SPKAP	infinite	4.257E9	29	infinite	6.243E9	46
Q9BUF5	Tubulin beta-6 chain GN=TUBB6	TBB6	infinite	1.715E8	1	infinite	7.772E8	4
Q13428	Treacle protein GN=TCOF1	TCOF	infinite	6.652E7	1	infinite	7.160E7	2
P55072	Transitional endoplasmic reticulum ATPase GN=VCP	TERA	infinite	2.830E7	1	infinite	3.170E7	3
O96008	Mitochondrial import receptor subunit TOM40 homolog GN=TOMM40	TOM40	infinite	8.043E7	1	infinite	6.337E8	1
Q8IWV8	E3 ubiquitin-protein ligase UBR2 GN=UBR2	UBR2	infinite	5.597E7	1	infinite	1.328E8	4

Accession number	Description	Official symbol	Experiment 1			Experiment 2		
			Ratio SPHKAP/ GFP	Area	No. of peptides used for quantification	Ratio SPHKAP/ GFP	Area	No. of peptides used for quantification
P67809	Nuclease-sensitive element-binding protein 1 GN=YBX1	YBOX1	infinite	4.718E7	1	infinite	7.425E7	2
Q14257	Reticulocalbin-2 GN=RCN2	RCN2	infinite	1.955E8	2	100.000	8.405E8	4
Q9Y265	RuvB-like 1 GN=RUVBL1	RUVB1	infinite	8.827E7	1	100.000	2.970E8	6
Q9Y230	RuvB-like 2 GN=RUVBL2	RUVB2	infinite	2.573E8	5	100.000	4.932E8	7
P50990	T-complex protein 1 subunit theta GN=CCT8	TCPQ	infinite	7.716E7	1	100.000	2.574E8	6
P40227	T-complex protein 1 subunit zeta GN=CCT6A	TCPZ	infinite	4.466E7	1	100.000	2.226E8	5
Q9UMS4	Pre-mRNA-processing factor 19 GN=PRPF19	PRP19	infinite	1.385E8	1	4.687	3.452E8	2
O15069	NAC-alpha domain-containing protein 1 GN=NACAD	NACAD	infinite	1.336E8	1	1.000	1.306E8	2
O95816	BAG family molecular chaperone regulator 2 GN=BAG2	BAG2	100.000	2.388E9	5	infinite	4.324E9	11

Accession number	Description	Official symbol	Experiment 1			Experiment 2		
			Ratio SPHKAP/ GFP	Area	No. of peptides used for quantification	Ratio SPHKAP/ GFP	Area	No. of peptides used for quantification
P07196	Neurofilament light polypeptide GN=NEFL	NFL	100.000	7.621E8	5	infinite	1.388E9	14
P07197	Neurofilament medium polypeptide GN=NEFM	NFM	100.000	9.226E8	9	100.000	1.613E9	15
O60884	DnaJ homolog subfamily A member 2 GN=DNAJA2	DNJA2	56.982	3.664E8	2	infinite	5.249E8	7
P62258	14-3-3 protein epsilon GN=YWHAE	1433E	41.361	2.623E9	6	100.000	3.344E9	9
P08670	Vimentin GN=VIM	VIME	35.521	8.648E8	2	100.000	1.198E9	6
P63104	14-3-3	1433Z	26.039	2.633E8	2	infinite	9.080E8	8
Q2TAA2	Iso amyl acetate-hydrolyzing esterase 1 homolog GN=IAH1	IAH1	23.305	2.497E8	2	infinite	6.717E7	1
P20700	Lamin-B1 GN=LMNB1	LMNB1	22.837	1.213E8	4	28.767	2.262E8	6
O43852	Calumenin GN=CALU	CALU	22.719	2.908E8	4	60.841	3.074E8	3
Q16531	DNA damage-binding protein 1 GN=DDB1	DDB1	21.029	7.044E7	2	100.000	3.444E8	6
P48643	T-complex protein 1 subunit epsilon GN=CCT5	TCPE	19.889	6.865E7	2	100.000	2.427E8	3

Accession number	Description	Official symbol	Experiment 1			Experiment 2		
			Ratio SPHKAP/ GFP	Area	No. of peptides used for quantification	Ratio SPHKAP/ GFP	Area	No. of peptides used for quantification
P61981	14-3-3 protein gamma GN=YWHAG	1433G	18.290	8.439E8	4	100.000	1.409E9	5
P05387	60S acidic ribosomal protein P2 GN=RPLP2	RLA2	14.640	6.413E8	4	44.057	1.236E9	4
O00193	Small acidic protein GN=SMAP	SMAP	12.197	1.973E8	2	infinite	5.208E7	2
P11142	Heat shock cognate 71 kDa protein GN=HSPA8	HSP7C	10.749	7.803E9	12	100.000	1.027E10	16
Q5T9A4	ATPase family AAA domain-containing protein 3B GN=ATAD3B	ATD3B	9.278	8.506E8	1	46.205	1.142E9	1
P49411	Elongation factor Tu, mitochondrial GN=TUFM	EFTU	8.418	1.062E8	3	infinite	2.868E8	4
P07900	Heat shock protein HSP 90-alpha GN=HSP90AA1	HS90A	8.362	5.179E8	1	infinite	3.189E8	4
P68363	Tubulin alpha-1B chain GN=TUBA1B	TBA1B	8.186	3.322E9	11	100.000	6.640E9	3
Q04837	Single-stranded DNA-binding protein, mitochondrial GN=SSBP1	SSBP	7.543	1.990E8	1	27.739	1.191E8	2
P42677	40S ribosomal protein S27 GN=RPS27	RS27	6.990	2.785E8	1	infinite	4.532E8	2

Accession number	Description	Official symbol	Experiment 1			Experiment 2		
			Ratio SPHKAP/ GFP	Area	No. of peptides used for quantification	Ratio SPHKAP/ GFP	Area	No. of peptides used for quantification
Q9UHB6	LIM domain and actin-binding protein 1 GN=LIMA1	LIMA1	6.950	9.061E7	2	100.000	8.696E7	3
Q15293	Reticulocalbin-1 GN=RCN1	RCN1	6.842	5.051E8	4	43.313	1.113E9	3
P17987	T-complex protein 1 subunit alpha GN=TCP1	TCPA	6.834	1.032E8	1	infinite	2.194E8	4
P08238	Heat shock protein HSP 90-beta GN=HSP90AB1	HS90B	6.562	5.179E8	2	100.000	4.065E8	5
Q13263	Transcription intermediary factor 1-beta GN=TRIM28	TIF1B	6.365	7.470E8	1	100.000	9.211E8	9
Q14103	Heterogeneous nuclear ribonucleoprotein D0 GN=HNRNPD	HNRPD	5.988	1.067E8	1	2.102	7.941E7	1
P50991	T-complex protein 1 subunit delta GN=CCT4	TCPD	5.340	8.481E7	2	100.000	7.321E7	2
P10809	60 kDa heat shock protein, mitochondrial GN=HSPD1	CH60	5.020	8.271E8	12	100.000	1.464E9	13

Accession number	Description	Official symbol	Experiment 1			Experiment 2		
			Ratio SPHKAP/ GFP	Area	No. of peptides used for quantification	Ratio SPHKAP/ GFP	Area	No. of peptides used for quantification
P38646	Stress-70 protein, mitochondrial GN=HSPA9	GRP75	4.762	1.950E9	17	100.000	2.540E9	30
P08107	Heat shock 70 kDa protein 1A/1B GN=HSPA1A	HSP71	4.574	1.892E10	13	54.104	3.337E10	21
Q13439	Golgin subfamily A member 4 GN=GOLGA4	GOGA4	4.043	6.797E7	1	infinite	8.022E7	4
P22626	Heterogeneous nuclear ribonucleoproteins A2/B1 GN=HNRNPA2B1	ROA2	4.031	1.813E8	1	1.523	1.775E8	3
P35268	60S ribosomal protein L22 GN=RPL22	RL22	3.965	1.380E8	1	3.937	2.250E8	1
P11021	78 kDa glucose-regulated protein GN=HSPA5	GRP78	3.804	2.437E9	7	100.000	1.259E9	13
P55735	Protein SEC13 homolog GN=SEC13	SEC13	3.515	1.244E7	1	infinite	1.289E8	1
Q16576	Histone-binding protein RBBP7 GN=RBBP7	RBBP7	3.420	1.691E8	1	infinite	4.955E8	1
P84090	Enhancer of rudimentary homolog GN=ERH	ERH	3.308	1.321E8	1	infinite	1.357E8	2

Accession number	Description	Official symbol	Experiment 1			Experiment 2		
			Ratio SPHKAP/ GFP	Area	No. of peptides used for quantification	Ratio SPHKAP/ GFP	Area	No. of peptides used for quantification
Q15369	Transcription elongation factor B polypeptide 1 GN=TCEB1	ELOC	3.213	2.353E8	3	100.000	4.175E8	3
P06748	Nucleophosmin GN=NPM1	NPM	2.957	5.834E8	1	17.092	1.509E8	2
Q15029	116 kDa U5 small nuclear ribonucleoprotein component GN=EFTUD2	U5S1	2.884	6.699E7	1	infinite	5.443E7	3
P68104	Elongation factor 1-alpha 1 GN=EEF1A1	EF1A1	2.673	6.279E8	5	8.518	1.580E9	7
Q14061	Cytochrome c oxidase copper chaperone GN=COX17	COX17	2.672	4.460E8	1	2.783	4.798E8	1
P19338	Nucleolin GN=NCL	NUCL	2.668	6.336E8	10	100.000	6.856E8	7
P10599	Thioredoxin GN=TXN	THIO	2.539	4.324E9	1	3.113	3.874E9	2
P78371	T-complex protein 1 subunit beta GN=CCT2	TCPB	2.529	8.261E7	1	100.000	4.498E8	8
P30048	Thioredoxin-dependent peroxide reductase, mitochondrial GN=PRDX3	PRDX3	2.520	1.602E8	1	infinite	3.440E7	1
P63208	S-phase kinase-associated protein 1 GN=SKP1	SKP1	2.476	7.300E8	1	100.000	5.496E8	3

Accession number	Description	Official symbol	Experiment 1			Experiment 2		
			Ratio SPHKAP/ GFP	Area	No. of peptides used for quantification	Ratio SPHKAP/ GFP	Area	No. of peptides used for quantification
P61289	Proteasome activator complex subunit 3 GN=PSME3	PSME3	2.366	9.690E7	1	19.651	4.861E7	2
P07437	Tubulin beta chain GN=TUBB	TBB5	2.178	3.625E9	4	infinite	7.528E9	6
P61978	Heterogeneous nuclear ribonucleoprotein K GN=HNRNPK	HNRPK	2.050	1.090E8	1	36.920	1.439E8	4
P31943	Heterogeneous nuclear ribonucleoprotein H GN=HNRNPH1	HNRH1	2.029	1.064E8	2	31.025	1.416E8	2
P63167	Dynein light chain 1, cytoplasmic GN=DYNLL1	DYL1	2.019	2.100E8	1	infinite	4.216E8	2
P63151	Serine/threonine-protein phosphatase 2A 55 kDa regulatory subunit B alpha isoform GN=PPP2R2A	2ABA	1.995	8.472E7	1	infinite	5.126E7	3
P31040	Succinate dehydrogenase [ubiquinone] flavoprotein subunit, mitochondrial GN=SDHA	DHSA	1.982	1.904E8	1	43.049	1.706E8	2

Accession number	Description	Official symbol	Experiment 1			Experiment 2		
			Ratio SPHKAP/ GFP	Area	No. of peptides used for quantification	Ratio SPHKAP/ GFP	Area	No. of peptides used for quantification
P53396	ATP-citrate synthase GN=ACLY	ACLY	1.961	4.835E7	1	infinite	2.801E7	1
P15531	diphosphate kinase A GN=NME1	NDKA	1.918	1.899E8	2	18.230	5.359E8	2
P67870	Casein kinase II subunit beta GN=CSNK2B	CSK2B	1.830	2.886E7	2	infinite	6.328E7	1
P32119	Peroxiredoxin-2 GN=PRDX2	PRDX2	1.754	1.815E9	1	infinite	1.817E9	1
P05388	60S acidic ribosomal protein P0 GN=RPLP0	RLA0	1.698	3.592E7	3	100.000	1.457E8	4
P67936	Tropomyosin alpha-4 chain GN=TPM4	TPM4	1.626	31.248	1	31.248	1.019E8	2
P40222	Alpha-taxilin GN=TXLNA	TXLNA	1.555	7.007E7	2	2.707	1.537E8	1
Q9Y5K6	CD2-associated protein GN=CD2AP	CD2AP	1.520	6.570E7	2	5.888	3.052E8	7
Q9UMS0	NFU1 iron-sulfur cluster scaffold homolog, mitochondrial GN=NFU1	NFU1	1.482	1.694E8	2	3.279	1.796E8	2
Q99873	Protein arginine N-methyltransferase 1 GN=PRMT1	ANM1	1.450	2.766E8	4	28.105	6.490E8	8

Accession number	Description	Official symbol	Experiment 1			Experiment 2		
			Ratio SPHKAP/ GFP	Area	No. of peptides used for quantification	Ratio SPHKAP/ GFP	Area	No. of peptides used for quantification
P00390	Glutathione reductase, mitochondrial GN=GSR	GSHR	1.438	2.640E8	1	2.172	3.401E8	3
P30084	Enoyl-CoA hydratase, mitochondrial GN=ECHS1	ECHM	1.405	6.756E7	4	78.649	2.067E8	6
O00410	Importin-5 GN=IPO5	IPO5	1.359	9.881E7	3	100.000	2.093E8	9
Q9HA64	Ketosamine-3-kinase GN=FN3KRP	KT3K	1.357	6.064E8	1	2.864	3.005E8	2
Q99714	3-hydroxyacyl-CoA dehydrogenase type-2 GN=HSD17B10	HCD2	1.353	2.430E8	3	100.000	7.790E7	3
Q06830	Peroxiredoxin-1 GN=PRDX1	PRDX1	1.321	3.302E9	9	2.678	4.282E9	6
P0CG48	Polyubiquitin-C GN=UBC	UBC	1.309	6.668E8	5	5.719	6.013E8	4
Q15185	Prostaglandin E synthase 3 GN=PTGES3	TEBP	1.286	1.146E8	1	4.407	1.979E8	1
Q15181	Inorganic pyrophosphatase GN=PPA1	IPYR	1.270	3.253E7	1	infinite	8.491E7	2
P00813	Adenosine deaminase GN=ADA	ADA	1.248	7.695E7	1	2.356	1.322E8	4

Accession number	Description	Official symbol	Experiment 1			Experiment 2		
			Ratio SPHKAP/ GFP	Area	No. of peptides used for quantification	Ratio SPHKAP/ GFP	Area	No. of peptides used for quantification
P63220	40S ribosomal protein S21 GN=RPS21	RS21	1.232	1.116E8	1	23.316	1.203E8	2
P00492	Hypoxanthine-guanine phosphoribosyltransferase GN=HPRT1	HPRT	1.219	1.876E8	2	14.770	2.953E8	2
P52907	F-actin-capping protein subunit alpha-1 GN=CAPZA1	CAZA1	1.195	3.064E8	1	100.000	3.903E8	3
Q9NSD9	Phenylalanine-tRNA ligase beta subunit GN=FARSB	SYFB	1.181	1.344E8	3	14.743	1.657E8	2
Q9NS86	LanC-like protein 2 GN=LANCL2	LANC2	1.117	2.048E8	4	4.113	6.155E8	2
Q16527	Cysteine and glycine-rich protein 2 GN=CSRP2	CSRP2	1.115	9.666E8	4	2.575	8.555E8	6
Q9P258	Protein RCC2 GN=RCC2	RCC2	1.107	4.070E8	2	2.610	8.580E8	2
P25398	40S ribosomal protein S12 GN=RPS12	RS12	1.100	3.219E8	1	5.622	6.443E8	1
P33316	Deoxyuridine 5'-triphosphate nucleotidohydrolase, mitochondrial GN=DUT	DUT	1.074	3.512E8	2	19.300	5.376E8	4
P04080	Cystatin-B GN=CSTB	CYTB	1.027	1.128E9	1	17.202	2.545E9	2

Accession number	Description	Official symbol	Experiment 1			Experiment 2		
			Ratio SPHKAP/ GFP	Area	No. of peptides used for quantification	Ratio SPHKAP/ GFP	Area	No. of peptides used for quantification
Q07021	Complement component 1 Q subcomponent-binding protein, mitochondrial GN=C1QBP	C1QBP	1.025	5.261E8	3	25.063	1.911E9	9
P49368	T-complex protein 1 subunit gamma GN=CCT3	TCPG	1.022	6.233E7	1	100.000	1.437E8	5
P19388	DNA-directed RNA polymerases I, II, and III subunit RPABC1 GN=POLR2E	RPAB1	0.993	1.844E8	1	2.638	3.326E8	2
P13797	Plastin-3 GN=PLS3	PLST	0.981	1.490E8	3	4.615	1.687E8	3
Q9Y266	Nuclear migration protein nudC GN=NUDC	NUDC	0.961	1.838E8	2	2.759	1.124E8	2
O75340	Programmed cell death protein 6 GN=PDCD6	PDCD6	0.919	3.370E8	4	21.412	7.472E8	4
Q8IYB5	Stromal membrane-associated protein 1 GN=SMAP1	SMAP1	0.918	2.756E8	1	1.895	2.525E8	1
P49589	Cysteine-tRNA ligase, cytoplasmic GN=CARS	SYCC	0.914	3.193E7	1	infinite	4.098E7	1
Q9H3K6	BolA-like protein 2 GN=BOLA2	BOLA2	0.914	6.192E8	2	2.623	1.613E9	3

Accession number	Description	Official symbol	Experiment 1			Experiment 2		
			Ratio SPHKAP/ GFP	Area	No. of peptides used for quantification	Ratio SPHKAP/ GFP	Area	No. of peptides used for quantification
P25205	DNA replication licensing factor MCM3 GN=MCM3	MCM3	0.883	1.285E7	3	17.553	1.655E8	4
P46109	Crk-like protein GN=CRKL	CRKL	0.872	1.007E9	10	3.777	2.237E9	7
O60313	Dynamin-like 120 kDa protein, mitochondrial GN=OPA1	OPA1	0.846	2.102E8	4	4.909	6.681E8	5
P62158	Calmodulin GN=CALM1	CALM	0.822	2.086E9	4	2.810	1.344E9	4
P62937	Peptidyl-prolyl cis-trans isomerase A GN=PPIA	PPIA	0.806	3.355E8	1	2.375	3.404E8	1
P17812	CTP synthase 1 GN=CTPS	PYRG1	0.804	3.019E8	3	3.464	5.236E8	2
Q96CN7	Isochorismatase domain-containing protein 1 GN=ISOC1	ISOC1	0.789	4.938E7	1	3.318	1.163E8	1
P35080	Profilin-2 GN=PFN2	PROF2	0.757	2.099E8	4	infinite	7.249E7	2
P49327	Fatty acid synthase GN=FASN	FAS	0.755	1.742E8	10	12.781	4.495E8	23
Q9NZL9	Methionine adenosyltransferase 2 subunit beta GN=MAT2B PE=1 SV=1	MAT2B	0.734	2.176E8	2	5.896	1.511E8	3

Accession number	Description	Official symbol	Experiment 1			Experiment 2		
			Ratio SPHKAP/ GFP	Area	No. of peptides used for quantification	Ratio SPHKAP/ GFP	Area	No. of peptides used for quantification
P14174	Macrophage migration inhibitory factor GN=MIF	MIF	0.719	4.436E9	1	15.384	5.454E9	2
P23526	Adenosylhomocysteinase GN=AHCY	SAHH	0.715	9.256E7	2	36.924	9.416E7	2
P52272	Heterogeneous nuclear ribonucleoprotein M GN=HNRNPM	HNRPM	0.702	1.693E7	1	infinite	1.937E8	5
P60709	Actin, cytoplasmic 1 GN=ACTB	ACTB	0.654	5.682E9	5	30.853	6.512E9	6
O43837	Isocitrate dehydrogenase [NAD] subunit beta, mitochondrial GN=IDH3B	IDH3B	0.563	2.255E7	1	infinite	5.860E7	1
Q16643	Drebrin GN=DBN1	DREB	0.541	3.750E8	1	3.729	3.885E8	1
Q9ULA0	Aspartyl aminopeptidase GN=DNPEP	DNPEP	0.538	2.500E8	2	14.978	3.759E8	2
P24534	Elongation factor 1-beta GN=EEF1B2	EF1B	0.519	4.207E7	1	infinite	1.171E8	1
P23528	Cofilin-1 GN=CFL1	COF1	0.509	2.566E8	4	40.560	1.177E9	7
Q99497	Protein DJ-1 GN=PARK7	PARK7	0.502	2.960E8	4	6.937	5.117E8	5

Accession number	Description	Official symbol	Experiment 1			Experiment 2		
			Ratio SPHKAP/ GFP	Area	No. of peptides used for quantification	Ratio SPHKAP/ GFP	Area	No. of peptides used for quantification
P31153	S-adenosylmethionine synthase isoform type-2 GN=MAT2A	METK2	0.488	2.383E8	2	9.415	2.043E8	1
P30042	ES1 protein homolog, mitochondrial GN=C21orf33	ES1	0.448	7.882E7	2	1.659	1.085E8	1
Q15366	Poly(rC)-binding protein 2 GN=PCBP2	PCBP2	0.334	3.590E8	1	4.161	2.440E8	2
P08865	40S ribosomal protein SA GN=RPSA	RSSA	0.144	2.108E7	2	infinite	6.735E7	2
Q15084	Protein disulfide-isomerase A6 GN=PDIA6	PDIA6	0.133	1.292E7	2	16.405	4.418E7	2
Q9BUI4	DNA-directed RNA polymerase III subunit RPC3 GN=POLR3C	RPC3	0.089	5.779E7	2	100.000	5.950E7	4
Q96CX2	BTB/POZ domain-containing protein KCTD12 GN=KCTD12	KCD12	0.085	6.619E6	2	infinite	5.625E7	1
Q96AB3	Isochorismatase domain-containing protein 2, mitochondrial GN=ISOC2	ISOC2	0.061	2.196E8	4	8.912	5.231E8	1
O00170	AH receptor-interacting protein GN=AIP	AIP	0.010	2.842E7	1	infinite	3.287E7	1

Accession number	Description	Official symbol	Experiment 1			Experiment 2		
			Ratio SPHKAP/ GFP	Area	No. of peptides used for quantification	Ratio SPHKAP/ GFP	Area	No. of peptides used for quantification
Q15370	Transcription elongation factor B polypeptide 2 GN=TCEB2	ELOB	0.010	4.636E9	1	infinite	7.169E8	1
P55209	Nucleosome assembly protein 1-like 1 GN=NAP1L1	NP1L1	0.010	8.273E6	1	infinite	5.400E7	2
Q99471	Prefoldin subunit 5 GN=PFDN5	PFD5	0.010	1.763E7	1	infinite	4.327E7	1
P22061	Protein-L-isoaspartate(D-aspartate) O-methyltransferase GN=PCMT1	PIMT	0.010	1.094E8	1	infinite	7.646E7	2
Q9H9H4	Vacuolar protein sorting-associated protein 37B GN=VPS37B	VP37B	0.010	1.102E7	1	infinite	2.154E7	1
P30153	Serine/threonine-protein phosphatase 2A 65 kDa regulatory subunit A alpha isoform GN=PPP2R1A	2AAA	0.010	1.718E7	1	4.407	4.396E7	1
Q06323	Proteasome activator complex subunit 1 GN=PSME1	PSME1	0.010	7.641E7	1	2.685	1.148E8	2

Chapter 6
Summary, Outlook, and Samenvatting

6.1 Summary

The primary focus of this thesis is the functional characterization of the novel A-kinase anchoring protein (AKAP), sphingosine kinase interacting protein (SPHKAP) and its associated type I cAMP-dependent protein kinase holoenzyme (PKA). As an introduction to this topic, Chapter 1 starts with a general overview of cAMP (3'-5'cyclic adenosine monophosphate) signaling at the cellular level. cAMP regulates cellular functions primarily by activating a single kinase, PKA. Therefore, compartmentalization of PKA plays a key role in the spatial and temporal specificity of parallel cAMP signaling events that occur in the same cell. This is mediated through the interaction of PKA's regulatory subunits (PKA-R) with many different AKAPs. AKAPs often form highly efficient, compact signalosomes by harboring other signaling proteins such as phosphatases and phosphodiesterases alongside PKA. The selective binding of AKAPs to one of the major isoforms of PKA-R (type I (PKA-RI) and PKA-R type II (PKA-RII)) is an important feature of specific cAMP signaling. Therefore, chapter 1 continues to discuss in detail the key differences in structural features between the relatively well characterized PKA-RII and the largely unexplored PKA-RI, which may explain why PKA-RI is more selective towards a small subset of AKAPs and why RII-specific AKAPs are likely more abundantly identified thus far. Then, a systematic overview of all mammalian AKAPs identified thus far is provided. Since SPHKAP was abundantly identified in ventricular tissue, chapter 1 continues with a short functional focus on AKAPs functioning in cardiac physiology and pathophysiology. In the light of SPHKAPs putative role in mitochondrial induced apoptosis (chapter 5), chapter 1 continues with the general basics of apoptosis with a focus on intrinsic or mitochondrial-mediated pathways. The intrinsic pathway proceeds through the coordinated regulation of multiple anti- and pro-apoptotic BCL-2 family proteins that ultimately induce the discontinuity of the outer mitochondrial membrane and the release of cytochrome C. Within the BCL-2 protein family a subclass of pro-apoptotic members termed the BH3-only proteins exists, which directly and/or indirectly regulate other anti- and pro-apoptotic BCL-2 family proteins to engage apoptosis. The focus of this review is to discuss the characteristics of the BH3 domain and the two mutual models by which BH3-only proteins mediate apoptosis.

Chemical proteomics has proven to be a versatile tool to investigate cyclic nucleotide (cAMP and cGMP (3', 5'-cyclic guanosine monophosphate)) signaling by providing insight into the variety of signalosomes present in cells and tissues. In this approach cAMP-based affinity chromatography is combined with (quantitative) proteomics to identify PKA-R/AKAP complexes, including novel AKAPs, in lysates of any origin.

Over the past decade, several approaches of stable isotope labeling have been developed to allow MS-based quantification. Among these, dimethyl labeling has developed as the most simple and cost-effective method. By using the cheap and readily available reagents, which are different isotopomers of formaldehyde and cyanoborohydride, three different dimethyl labels can be generated to simultaneously label peptides from three different samples. In chapter 2, we briefly introduce the basic concepts of dimethyl labeling and how the reaction is performed. Several commercial and freeware quantification softwares were adapted for dimethyl labeling, which are discussed. Major technical challenges encountered included retention time shifts between the labeled pairs and the overlap of their isotopic clusters. The main aim of chapter 2 is to provide a comprehensive overview of reported applications using dimethyl labeling in the analysis of differential protein expression, posttranslational modifications, and protein interactions. Two examples of dimethyl labeling combined with cAMP-affinity purification and GFP immunoprecipitation to characterize SPHKAP interactors are also described in this thesis (chapter 4 and 5 respectively).

Chapter 3 describes in detail a further maturation of our chemical proteomics protocol in which two synthetic immobilized cAMP analogs (8-AHA-cAMP and 2'OMe-8-AHA-cAMP) were utilized. The former has equal affinity for PKA-RI and RII while the latter one displayed a significant binding preference towards PKA-RI. When a parallel cAMP pull-down is performed with these two immobilized compounds and combined with stable-isotope labeling and LC-MS/MS read-out, a PKA-R specificity profiling tool is generated. This tool is based on the principle of quantifying the differential enrichment of the PKA-R isoforms and thus their interacting AKAPs. In a proof of principle study, the approach was applied to reveal the unique PKA-RI binding characteristics of SPHKAP in chapter 4.

At the start of this thesis project, SPHKAP was identified from cAMP-based chemical proteomics screening in mammalian ventricular tissues as a putative novel AKAP (1, 2). In chapter 4 we describe the initial studies on several characteristics of SPHKAP by using a variety of molecular biology and proteomics approaches. We show by immunoprecipitation that SPHKAP utilizes the hypothesized amphipathic helix for the interaction with PKA-RI. Further chemical proteomics screening using the novel approach described in chapter 2 revealed SPHKAP's specificity for solely PKA-RI in mammalian heart and spleen tissues, thus making SPHKAP the first PKA RI-specific AKAP ever identified in mammalians. Based on sequence analysis, the proposed PKA anchoring domain on SPHKAP matched perfectly with synthetically derived PKA-RI-specific anchoring domains as well as predicted structural determinants based on dual-specific AKAPs as reviewed in chapter 1.

Our initial immunolocalization study in chapter 4 revealed that HAHIS6-tagged SPHKAP resides extensively in the cytoplasm. Later work by Means et al. (3) confirmed SPHKAP's specificity for PKA-RI and the cytosolic localization, however additionally they revealed a putative mitochondrial localization. Therefore, in chapter 5, we aimed to continue evaluating SPHKAP's localization. By utilizing confocal microscopy with two recombinant SPHKAPs, HAHIS6-SPHKAP and SPHKAP-GFP, subcellular fractionation and mitochondrial isolation we concluded that SPHKAP localizes both to mitochondria and the cytoplasm. Interestingly we have found that the protein N-terminus is required for mitochondrial targeting. Unexpectedly, overexpression of SPHKAP-GFP which partially localized to mitochondria has a serious effect on mitochondrial morphology. The mitochondria from SPHKAP-GFP cells are fragmented and fail to form a tubular network. Further submitochondrial fractionation revealed that SPHKAP resides in the mitochondrial inner membrane space and matrix. Subsequently, we characterize SPHKAP's molecular environment through identification of its interacting partners. Dimethyl labeling based-quantitative GFP immunoprecipitation using SPHKAP-GFP revealed Mitofilin and coiled-coil-helix-coiled-coil-helix domain containing 3 (ChChD3) and other members of the mitochondrial inner membrane organizing system (MINOS) complex, which is responsible to maintain crista (folded mitochondrial inner membrane) structure. We also confirmed the interactions between SPHKAP and apoptosis inducing factor (AIF) and the mitochondrial phosphatase phosphoglycerate mutase 5 (PGAM5) and that several of SPHKAP's interactions are altered by PKA phosphorylation of SPHKAP. With this information in mind, we continued to study the possible link between SPHKAP, PKA-RI and apoptosis. Sequence analysis and functional binding assays identified a BH3 domain on SPHKAP which proved to interact with the pro-survival proteins BCL-2 and BCL-xL. Taken together, these data suggest a putative role of SPHKAP and anchored PKA type I in regulating mitochondrial crista structure as well as mitochondrial-mediated apoptosis. To complete these studies, several future experiments are suggested in the outlook section below.

6.2 Outlook

In the late 1950s, cAMP was discovered as a secondary messenger produced in response to ephinephrine and glucagon (4, 5). Today, the variety of hormones, neurotransmitters, and effectors that stimulate the production of cAMP is extensive. However it is the different expression of cAMP signaling components such as GPCRs, ACs, PDEs, PKAs, and AKAPs that create each unique cAMP response within different tissues, cell types and cellular compartments. For example, there are 4 isoforms of the PKA regulatory (RIα, RIβ, RIIα, and RIIβ) and 2 isoforms of catalytic (Cα and Cβ) subunit. Subcellular localization of PKA holoenzymes is obtained through the interaction between PKA-R and the wide variety of AKAPs. Since the key discovery of AKAPs in 1980s, cAMP signaling research has moved forward to focus on localized PKA activities. Up to date, more than 50 AKAPs including isoforms have been described (chapter 1). Interestingly, the majority of them are RII-specific and few are described as dual-specificity, while an entirely RI-specific AKAP was never been observed. The widely accepted paradigm for this observation was that PKA-RI was preferentially cytoplasmic while PKA-RII was exclusively particulate (6). Therefore, the subcellular localization and functional characterization of RI has received less attention .

In contrast, the function of PKA-RI is essential for life, since only knockout of PKA-RIα, not the other 3 isoforms, results in early embryonic lethality in mice. This is caused by failure in cardiac morphogenesis. Moreover, PKA-RIα is the only PKA-R isoform that can compensate for the functions of the other three PKA-R isoforms (7). Down-regulation or overexpression of PKA-RIα has been shown to disrupt normal cell cycle (8) and inactivating mutations result in severe reduction in fertility (9). Moreover, mutations in the RIα gene is the underlying cause of familial neoplasia Carney complex syndrome (9). On the other hand, deletion of PKA-RIβ results in defects in brain hippocampal function (10). In light of these findings, the data suggest a pivotal role of PKA-RI. However, our knowledge of PKA-RI is still limited at present.

Our discovery of SPHKAP as the first PKA-RI specific AKAP has brought new light in the field of cAMP/PKA research. In the final section of this thesis, I would like to give an overview of several future experiments that could be entertained to further complete our knowledge, of course in the hypothetical case of unlimited resources and time.

SPHKAP is the first PKA-RI specific AKAP identified in mammalians

First, it became obvious that the PKA anchoring domain of SPHKAP, as well as of the other RI-specific smAKAP identified by us in 2012 (11), is different from those of dual and RII-specific AKAPs. Computational models based on known RII and dual-anchoring domains has been used as a method to search for novel AKAPs from human databases (12, 13). The RI-specific anchoring domains of SPHKAP and smAKAP will definitely improve the model to search for more RI-specific AKAPs. Recently the structure of PKA-RIα in complex with the D-AKAP2 anchoring domain has been solved, which provided surprising new insights into molecular determinants of PKA-RI and PKA-RII binding to AKAP. However, since we now have entirely RI-specific AKAPs, further structure analysis of PKA-RI in complex with RI-specific anchoring domains is now possible. This will definitely improve the current structural model on how RI-specific AKAPs dock on PKA-RI isoforms. This could also highlight putative differences between PKA-RIα and PKA-RIβ.

Over the past few years, high affinity peptides mimicking the PKA-AKAP anchoring domain that can disrupt PKA-AKAP interactions and inhibit signaling by delocalization of PKA have been developed as a tool to study cellular processes regulated by PKA (14-17). The SPHKAP anchoring domain can definitely be used as a template to re-design RI-specific disrupting peptides. When

introduced into cells , the peptide may reveal primary and secondary effects executed by anchored PKA type I and identify novel downstream targets and relationships to other signaling pathways. For example, in the heart, PKA RIα is believed to play a role in cardiac function as it is the predominant isoform associated with the cardiomyocyte plasma membrane (18), however, as mentioned earlier, the function of PKA-RI in the heart remains unclear. SPHKAP-based disrupting peptides could be used to elucidate cellular processes regulated by anchored PKA type I in cardiomyocytes. Furthermore, as perturbed PKA signaling has been shown to play an important role in many diseases, SPHKAP-based disrupting peptides may potentially be used to elucidate whether those effects are dependent on anchored PKA type I.

cAMP-based quantitative chemical proteomics as a tool to study AKAP characteristics

Over the past years, cAMP based enrichment followed by mass spectrometric analysis has allowed us to identify 2 novel AKAPs (SPHKAP, and more recently also smAKAP (11)). Both turn out to be PKA-RI specific, indicative of the complementarity of this approach compared to more classical approaches. This, and the method (19) described in Chapter 2 provides a good starting point to embark on a more extensive screen for novel AKAPs in a large variety of tissues and cell lines. The method allows for the enrichment of these low abundant signaling proteins and also allows the immediate elucidation of their specificity towards PKA-RI or PKA-RII species. Besides discovering new AKAPs, also the different expression profile of cAMP signaling components which is key to understand the unique cAMP response of different tissues and cell types, will be generated. Further developments at the method level could lead us to build enrichment tools for related proteins such as phosphodiesterases (PDEs), which break down cAMP, or Epac, another cAMP responsive protein (20). Another interesting application to entertain is to combine the cAMP enrichment strategy with a blue-native polyacrylamide gel (BN-PAGE) for separation of enriched intact PKA/AKAP complexes. After that, a protein migration profile can be created for each protein by plotting the number of identified peptide spectra in the mass spectrometer versus the migration distance along the BN-PAGE and correlation analysis can be used to reveal additional PKA-AKAP complex members (figure 1A). This BN-PAGE method has been utilized successfully to characterize the composition of yeast mitochondrial complexes under aerobic and anaerobic conditions (21). According to our preliminary work, this approach can resolve several PKA-AKAP complexes isolated from rat heart. An example of a megadalton SPHKAP-PKA-RIα complex is shown in figure 1B. However, further improvement of the method is needed to allow more efficient enrichment and putatively the identification of other AKAP complex members. In this way, the results of the GFP-SPHKAP immunoprecipitation in chapter 5 could be supplemented with SPHKAP interaction data directly in cardiac tissue. Moreover, the application of such a method can also be extended to probe differences in cAMP-signaling-complex compositions under different physiological/ pathophysiological conditions.

SPHKAP and anchored PKA type I are novel members of MINOS complex and regulate crista structure

The data in chapter 5 suggests that SPHKAP and anchored PKA type I are associated with the mitochondrial MINOS complex. Knock down of MINOS component ChChd3 leads to an almost complete loss of its binding partner mitofilin (22) . It would be interesting to study whether SPHKAP localization and perhaps expression also requires ChChD3 and mitofilin . Abnormal and fragmented mitochondria were observed upon SPHKAP overexpression. The MINOS complex is crucial for maintenance of proper crista structure and knockdown of either mitofilin or ChChD3 results in reduction and remodeling of crista as probed by transmission electron microscopy and finally cytochrome C release from mitochondria (22, 23) . Performing similar studies in SPHKAP overexpressed cells would be ideal to confirm whether the SPHKAP mitochondrial phenotype is identical. Extending these studies to a PKA anchoring domain deficient SPHKAP mutant could then shed light on the respective role of PKA localization to the MINOS complex.

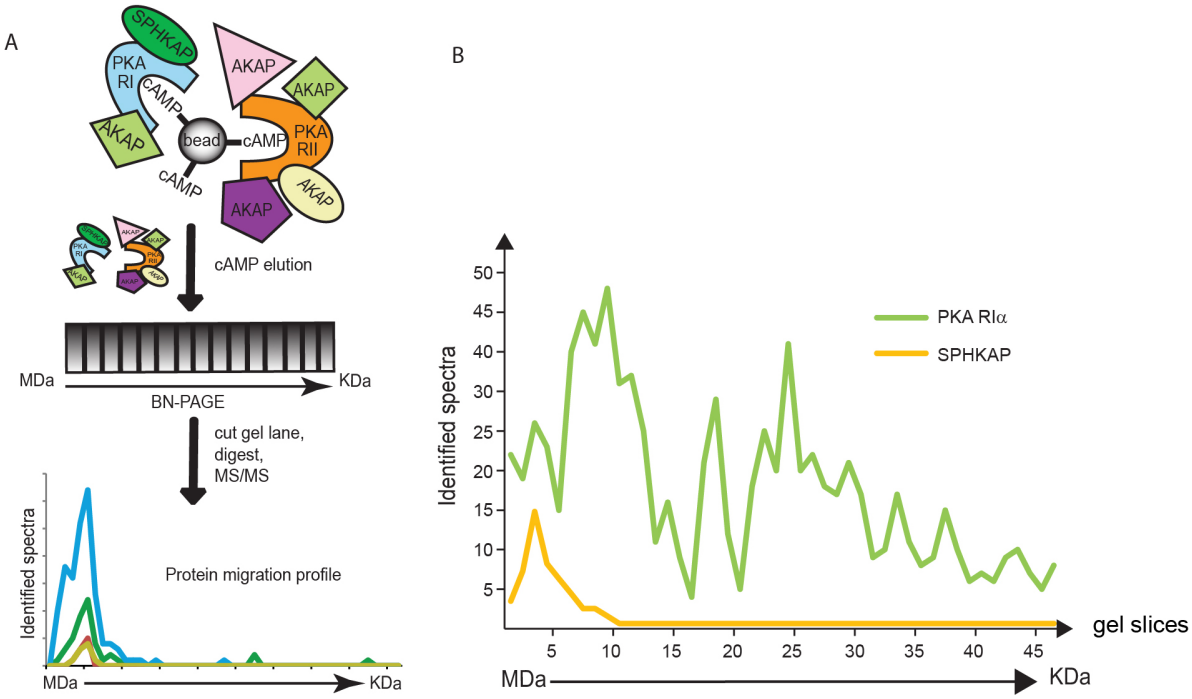

Figure 1 > cAMP-based chemical proteomics in combination with BN-PAGE as a tool to study PKA/AKAP complex.

A) *An overview of BN-PAGE based cAMP chemical proteomics. cAMP resin was used to enrich for PKA-AKAP complexes. Subsequently, protein complexes were eluted from cAMP resins by free excess of cAMP and seperated by BN-PAGE. The gel was cut into 45 slices, and the proteins therein identified by LC-MS/MS. A protein migration profile was generated for each protein by plotting the number of identified spectra versus the migration distance (gel slice 1-45) along the BN-PAGE. The proteins from the same complex result in the same migration pattern, which roughly indicates the molecular weight of the complex.* ***B)*** *A megadalton PKA-RIα-SPHKAP complex revealed by BN-PAGE based cAMP chemical proteomics.*

Mitochondrial SPHKAP and its anchored PKA-RI are functionally associated with the MINOS complex which likely harbors more substrates than the confirmed ChChD3 (3, 24) and SPHKAP (chapter 5). It is also possible that mitofilin is a substrate of PKA as mitofilin also contains a putative PKA site (http://scansite.mit.edu). Further quantitative LC-MS/MS studies on the immunoprecipitated complex from cAMP-stimulated and mock treated cells in combination with phospho-peptide enrichment could provide insight into the exact phosphorylation sites targeted by PKA in this context.

SPHKAP and anchored PKA type I provide another level of regulation to AIF

AIF is a dynamic protein. During apoptosis, it is cleaved from mitochondrial inner membrane and subsequently released from mitochondria and translocated to the nucleus where it might associate with an unknown endonuclease to cleave DNA (25). We show that the novel interaction between SPHKAP and AIF increases when PKA is activated or when apoptosis is induced. This makes it tempting to speculate that AIF and its apoptotic role are, at least in part, regulated by cAMP via SPHKAP and anchored PKA type I. Immunoprecipitation in separate cytosolic and mitochondrial fractions under apoptotic conditions and/or cAMP stimulation would be ideal to investigate if the change in SPHKAP-AIF interaction is due to AIF translocation. H9C2 cells would be an ideal cell line for the study as it expresses endogeneous SPHKAP and responds well to apoptotic drugs (26).

AIF is localized to the inner membrane (25) where mitofilin and ChChD3 reside. Since it is enriched in the SPHKAP IP along with components of MINOS complex, another possibility is that AIF is a novel component of the MINOS complex. An AIF-IP in H9C2 cells or heart lysates could answer this. In the context of heart, the AIF-SPHKAP interaction is interesting. Knock-down of AIF was shown to induce severe dilated cardiomyopathy and heart failure (27) , while in our own studies we observed a severe increase in the PKA-RI/SPHKAP interaction at the end stage of the human failing heart (28) .

SPHKAP is a novel BH3-only protein

Our observation that SPHKAP contains a functional BH3 domain hints us to a pro-apoptotic role of SPHKAP. We postulate that it is the cytoplasmic pool of SPHKAP that interacts with the anti-apoptotic BCL-xL and possibly BCL-2. The identification of PGAM5 as an interacting partner also correlates BCL-xL with SPHKAP. Further investigations on apoptotic hallmarks, for example cytochrome C release, caspase cleavage, and DNA laddering in SPHKAP overexpressing cells, would be required to consolidate the pro-apoptotic role of SPHKAP. Another question is whether cAMP stimulation/PKA activation can alter the interaction between SPHKAP, BCL-xL, and PGAM5? Immunoprecipitation in the lysates from cells overexpressing SPHKAP treated with cAMP and from cells treated with staurosporine would be obvious experiments to do.

In conclusion, our study provides data on the mitochondrial molecular environment of the unexplored SPHKAP/PKA-RI complex, but it also reveals a potential role for SPHKAP as a link between cAMP signaling and apoptosis. Furthermore, as severe increase in the PKA-RI/SPHKAP interaction in the human failing heart has been observed (28) and apoptosis has been causally linked to the pathogenesis of heart failure (29), it will be interesting to investigate whether SPHKAP and anchored PKA-RI contribute to the development of heart failure by apoptosis.

6.3 References

1. A. Scholten et al., Analysis of the cGMP/cAMP Interactome Using a Chemical Proteomics Approach in Mammalian Heart Tissue Validates Sphingosine Kinase Type 1-interacting Protein as a Genuine and Highly Abundant AKAP. J Proteome Res 5, 1435 (2006).
2. A. Scholten, T.A.B. van Veen, M.A. Vos, A.J.R. Heck, Diversity of cAMP-Dependent Protein Kinase Isoforms and Their Anchoring Proteins in Mouse Ventricular Tissue. J Proteome Res 6, 1705 (2007).
3. C.K. Means et al., An entirely specific type I A-kinase anchoring protein that can sequester two molecules of protein kinase A at mitochondria. Proc. Natl. Acad. Sci. USA. 108, E1227 (2011).
4. J. Berthet, T.W. Rall, E.W. Sutherland, The relationship of epinephrine and glucagon to liver phosphorylase. IV. Effect of epinephrine and glucagon on the reactivation of phosphorylase in liver homogenates. J Biol Chem 224, 463 (1957).
5. T.W. Rall, E.W. Sutherland, Formation of a cyclic adenine ribonucleotide by tissue particles. J Biol Chem 232, 1065 (1958).
6. L.L. Brunton, J.S. Hayes, S.E. Mayer, Functional compartmentation of cyclic AMP and protein kinase in heart. Adv Cyclic Nucleotide Res 14, 391 (1981).
7. P.S. Amieux, G.S. McKnight, The Essential Role of RIα in the Maintenance of Regulated PKA Activity. Ann NY Acad Sci 968, 75 (2002).
8. G. Tortora et al., The RI alpha subunit of protein kinase A controls serum dependency and entry into cell cycle of human mammary epithelial cells. Oncogene 9, 3233 (1994).
9. K.A. Burton et al., Haploinsufficiency at the Protein Kinase A RIα Gene Locus Leads to Fertility Defects in Male Mice and Men. Mol Endocrinol 20, 2504 (2006).
10. E.P. Brandon et al., Hippocampal long-term depression and depotentiation are defective in mice carrying a targeted disruption of the gene encoding the RI beta subunit of cAMP-dependent protein kinase. Proc Natl Acad Sci U S A 92, 881 (1995).
11. P.P. Burgers et al., A Small Novel A-Kinase Anchoring Protein (AKAP) That Localizes Specifically Protein Kinase A-Regulatory Subunit I (PKA-RI) to the Plasma Membrane. J Biol Chem 287, 43789 (2012).
12. M.A. Russell et al., The intermediate filament protein, synemin, is an AKAP in the heart. Arch Biochem Biophys 456, 204 (2006).
13. W.A. McLaughlin, T. Hou, S.S. Taylor, W. Wang, The identification of novel cyclic AMP-dependent protein kinase anchoring proteins using bioinformatic filters and peptide arrays. Protein Eng Des Sel 24, 333 (2011).
14. L.L. Burns-Hamuro et al., Designing isoform-specific peptide disruptors of protein kinase A localization. Proc. Natl. Acad. Sci. USA. 100, 4072 (2003).
15. C.R. Carlson et al., Delineation of Type I Protein Kinase A-selective Signaling Events Using an RI Anchoring Disruptor. J Biol Chem 281, 21535 (2006).
16. M.G. Gold et al., Molecular Basis of AKAP Specificity for PKA Regulatory Subunits. Mol Cell 24, 383 (2006).
17. O.M. Faruque et al., Cell-permeable peptide-based disruption of endogenous PKA-AKAP complexes: a tool for studying the molecular roles of AKAP-mediated PKA subcellular anchoring. Am J Physiol Cell Physiol 296, C306 (2009).
18. M.L. Robinson, M.A. Wallert, C.A. Reinitz, J.B. Shabb, Association of the Type I Regulatory Subunit of cAMP-Dependent Protein Kinase with Cardiac Myocyte Sarcolemma. Arch Biochem Biophys 330, 181 (1996).
19. D. Kovanich, T.T. Aye, A.J.R. Heck, A. Scholten, in Methods in Moleucular Biology: Chemical Proteomics. (2012), vol. 803, pp. 167-181.
20. H. Poppe et al., Cyclic nucleotide analogs as probes of signaling pathways. Nat Meth 5, 277 (2008).
21. A.O. Helbig et al., A three-way proteomics strategy allows differential analysis of yeast mitochondrial membrane protein complexes under anaerobic and aerobic conditions. Proteomics 9, 4787 (2009).
22. M. Darshi et al., ChChd3, an Inner Mitochondrial Membrane Protein, Is Essential for Maintaining Crista Integrity and Mitochondrial Function. J Biol Chem 286, 2918 (2011).
23. R.F. Yang et al., Mitofilin regulates cytochrome c release during apoptosis by controlling mitochondrial cristae remodeling. Biochem Biophys Res Commun 428, 93 (2012).
24. S. Schauble et al., Identification of ChChd3 as a Novel Substrate of the cAMP-dependent Protein Kinase (PKA) Using an Analog-sensitive Catalytic Subunit. J Biol Chem 282, 14952 (2007).

25. I.F. Sevrioukova, Apoptosis-inducing factor: structure, function, and redox regulation. Antioxid Redox Signal 14, 2545 (2011).

26. A. Lax, F. Soler, F. Fernández-Belda, Mitochondrial damage as death inducer in heart-derived H9C2 cells: more than one way for an early demise. J Bioenerg Biomembr 41, 369 (2009).

27. N. Joza et al., Muscle-Specific Loss of Apoptosis-Inducing Factor Leads to Mitochondrial Dysfunction, Skeletal Muscle Atrophy, and Dilated Cardiomyopathy. Mol Cell Biol 25, 10261 (2005).

28. T.T. Aye et al., Reorganized PKA-AKAP associations in the failing human heart. J Mol Cell Cardiol 52, 511 (2012).

29. S.S. Singh, P.M. Kang, Mechanisms and inhibitors of apoptosis in cardiovascular diseases. Curr Pharm Des 17, 1783 (2011).

6.4 Samenvatting

Dit proefschrift draait om de twee eiwitten sphingosine kinase bindend eiwit (SPHKAP) en cAMP-afhankelijk kinase (PKA). PKA is een kinase, wat betekent dat het aan andere eiwitten een fosfaatgroep zet. Dit noemen we fosforylering. De fosfaatgroepen veranderen de eigenschappen van dat eiwit: het wordt actief of inactief, het bindt aan een ander eiwit, of laat juist los, het verplaatst zich naar een ander gedeelte van de cel, etc. PKA wordt actief als het bindt met het signaalmolecuul cAMP wat weer wordt aangemaakt als de cel daar een externe opdracht voor krijgt via hormonen in het bloed. Bijvoorbeeld adrenaline dat door de hersenen eropuit wordt gestuurd om pijlsnel de hartslag te verhogen, zal uiteindelijk in de hartspiercellen zorgen voor de aanmaak van cAMP en de activatie van PKA. PKA kan dan andere eiwitten fosforyleren om uiteindelijk het beoogde effect van adrenaline te induceren in het hart.

SPHKAP werd in hoge mate door ons aangetoond in hartweefsel en initieel gekarakteriseerd als een A-kinase bindend eiwit (AKAP). Dit betekent dat het PKA bindt en naar een specifieke plaats in de cel brengt waar de actie van PKA is vereist. Dit is de functie van alle AKAP eiwitten. Er bestaan vele verschillende AKAPs, die elk PKA naar een andere specifieke plek in de cel brengen. Zo is de cel in staat om onder invloed van één signaal (cAMP) met één gereedschap (PKA), heel veel verschillende functies te vervullen. Zo wordt ook specificiteit gecreëerd, omdat PKA populaties met verschillende functies fysiek van elkaar gescheiden worden en daardoor niet elkaars substraten kunnen beïnvloeden. Om alle functies van het belangrijke eiwit PKA te begrijpen, moeten we dus de locatie en rol van alle AKAPs te weten komen. Toen SPHKAP door ons werd getypeerd als AKAP, was er niets bekend over waar SPHKAP PKA brengt in de cel en wat daarvan de functie is. Het doel van dit proefschrift was om dit nader in te vullen.

Ter introductie start **hoofdstuk 1** met een algemene beschouwing van cAMP signalen in cellen via de activatie van PKA. PKA bestaat eigenlijk uit twee eiwitten, het regulatoire deel dat bindt aan cAMP (PKA-R) en aan AKAPs, en het katalytische deel (PKA-C), de eigenlijke kinase. Samen vormen deze het PKA holo-enzym bestaande uit twee PKA-R en twee PKA-C eenheden. PKA-R houdt PKA-C inactief, maar zodra cAMP bindt aan PKA-R, zal het PKA-C laten gaan om substraten te activeren of deactiveren. De interactie van PKA met verschillende AKAPs vindt plaats via een klein gedeelte op PKA-R genoemd het dimerisatie/docking domein. Er zijn vier verschillende PKA-R varianten bekend (PKA-RIα, PKA-RIβ, PKA-RIIα en PKA-RIIβ). Tot dit proefschrift waren er gek genoeg alleen AKAPs bekend die aan PKA-RII varianten binden en een handjevol die zowel PKA-RI als RII varianten kunnen binden, terwijl specifieke PKA-RI AKAPs niet bekend waren. Wel was bekend dat de binding van AKAPs aan PKA-RI anders is dan bij PKA-RII. Deze verschillen worden in detail beschreven in hoofdstuk 1. Ter verduidelijking geven we een overzicht van alle tot nog toe bekende AKAPs en de eiwitten waaraan ze binden naast PKA. Omdat SPHKAP sterk aanwezig is in hart, beschrijft hoofdstuk 1 verder de functie van een aantal andere AKAPs in het hart. Met betrekking tot de door ons gevonden betrokkenheid van SPHKAP in geprogrammeerde celdood, apoptose, is ook een introductie voor dit onderwerp geschreven.

Het gebruik van massaspectrometrie voor de identificering van eiwitten heeft een enorme vlucht genomen de afgelopen 15 jaar. Voor deze analyse worden de eiwitten in korte stukjes geknipt, genaamd peptiden. Van deze peptiden kunnen we met de massaspectrometer uiteindelijk de aminozuurvolgorde (sequentie) bepalen en aan de hand daarvan de identiteit van het eiwit, omdat alle eiwitten unieke sequenties bevatten. Zoals beschreven in de vorige paragraaf is het gebruik van kwantitatieve massaspectrometrie een zeer krachtige methode . De laatste 10 jaar is er veel gebeurd op dit gebied. Een massaspectrometer is heel goed in het bepalen van het gewicht van een molecuul, maar minder goed in het vaststellen van de hoeveelheid van veel verschillende mol-

eculen in een complex monster. Daarom moeten we voor kwantitatieve methoden gebruik maken van relatieve kwantificering: het meten van de verschillen in hoeveelheid in plaats van de absolute hoeveelheid. Relatieve kwantificering gaat het eenvoudigst als beide te vergelijken waarden tegelijk gemeten worden door de massaspectrometer. Echter, de peptiden van de eiwitten uit monster A en monster B die vergeleken worden, hebben exact dezelfde massa. Daarom is het handig gebruik te maken van labels met daarin verschillende isotopen van koolstof, stikstof of zuurstof, de veel voorkomende atomen in eiwitten. Isotopen verschillen chemisch gezien niet van elkaar, terwijl ze wel een verschil in massa hebben. Dit verschil in massa is eenvoudig te onderscheiden voor een massaspectrometer. Een van dergelijke methoden, genaamd dimethyl labelen, is in ons lab verder ontwikkeld. In hoofdstuk 2 is een overzicht gegeven van deze ontwikkelingen. Dimethyl labelen maakt gebruik van een eenvoudige en efficiënte chemische reactie die aan alle primaire aminegroepen in een peptide twee methylgroepen zet. De reagentia zijn formaldehyde en cyanoborohydride. Wanneer we gebruik maken van 'normaal' formaldehyde, formaldehyde met twee zware waterstofisotopen (deuterium), of formaldehyde met een zware koolstofisotoop en twee deuteriums in combinatie met cyanoborodeuteride verkrijgen we drie labels met elk een afwijking van 4 atomaire massaeenheden. Door het gebruik van deze basale chemicaliën en de snelheid en eenvoud van de reactie onstaat een zeer efficiënt label reagens tegen een zeer gunstige prijs. **Hoofdstuk 2** beschrijft de basale concepten van deze methode, maar ook technische uitdagingen die overwonnen moesten worden op zowel analytisch als software vlak. Ook beschrijven we velerlei applicaties van deze techniek.

De bestudering van de interacties van 'kleine moleculen', zoals cAMP, met de grote eiwitten wordt onder andere bestudeerd in het veld van 'chemical proteomics'. Zo hebben we in het verleden een zeer efficiënte methode ontwikkeld om PKA en AKAPs uit een complex eiwitsysteem als het hart te isoleren en in meer detail te bestuderen. Deze methode maakt gebruik van een vaste matrix met chemisch verankerd cAMP. Op deze wijze hebben we SPHKAP en nog een aantal nieuwe AKAPs ontdekt. Hoofdstuk 3 beschrijft een verdere ontwikkeling op dit gebied. Hier staat een methode beschreven die tegelijkertijd PKA met daaraan allerhande AKAPs opzuivert, maar ook tegelijkertijd kan aangeven of deze AKAPs specifiek zijn voor PKA-RI, RII of beide. Dit doen we door gebruik te maken van 2 verankerde cAMP varianten genaamd 8-AHA-cAMP en 2'OMe-8-AHA-cAMP. De eerste bindt even sterk aan beide PKA varianten, terwijl de tweede een sterke voorkeur heeft voor PKA-RI. Allereerst binden we met beide materialen PKA en AKAPs uit hetzelfde systeem. Vervolgens worden de twee gebonden PKA/AKAP fracties elk met een verschillend chemisch label gemarkeerd, bij elkaar gestopt, en als één monster met een massaspectrometer geanalyseerd (zie **hoofdstuk 3** voor details over deze methode). Zo zien we gelijke hoeveelheden PKA-RI in beide verrijkingen, terwijl er meer PKA-RII geïsoleerd wordt met 8-AHA-cAMP. Alle AKAPs die we zien volgen het verrijkingspatroon van de PKA-R vorm waaraan ze binden en zo kunnen we dus in één oogopslag zien met welke PKA-R vorm de AKAP verrijkt is. Zo konden we ook de preferentie van SPHKAP bekijken (zie hoofdstuk 4).

Bij de start van het onderzoek beschreven in dit proefschrift was het verhaal van SPHKAP een onbeschreven blad. In **hoofdstuk 4** staat onze eerste karakterisering van SPHKAP in detail beschreven. Daarvoor zijn een variëteit aan technieken gebruikt. Allereerst hebben we bevestigd dat SPHKAP inderdaad een AKAP is en met de methode uit hoofdstuk 3 konden we vaststellen dat het een zeer speciale is. SPHKAP bleek de eerste PKA-RI specifieke AKAP. Gedetailleerde analyse van de interactielocatie liet voor het eerst zien dat SPHKAP inderdaad een andere interactie aangaat met PKA dan RII specifieke AKAPs zoals reeds in hoofdstuk 1 beschreven. Celstudies lieten zien dat SPHKAP voornamelijk in het cytosol van de cel aanwezig is.

In **hoofdstuk 5** hebben we ons gefocust op de rol van SPHKAP in de cel. Tijdens deze experimenten publiceerde een andere groep dat SPHKAP mogelijk ook in het mitochondrium aanwezig kon zijn en dit hebben wij in dit hoofdstuk daarna ook bevestigd en verder onderzocht door de mitochondriën van het rattenhart verder te ontleden. Hieruit bleek dat SPHKAP aanwezig is tussen het buiten en binnenmembraan (inner membrane space) en de oplosbare fractie binnen het binnenmembraan, de matrix. Ondanks dat PKA-RIα en PKA-RIß beiden aanwezig zijn, bleek de verdeling van SPHKAP over de mitochondriale compartimenten overeenkomstig met PKA-RIα. Bij bestudering van de mitochondriën die SPHKAP bevatten, bleken deze niet meer integer. Ze leken sterk op de mitochondriën van cellen die in apoptose zijn, leidende tot de aanname dat SPHKAP wellicht bij apoptose betrokken is. Tegelijkertijd hebben we via moleculaire biologie een biochemisch anker aan SPHKAP gezet door het te fuseren met GFP (green fluorescent protein). Middels dit anker konden we met behulp van massaspectrometrie onderzoeken aan welke eiwitten SPHKAP bindt. We vonden PKA-RIα, PKA-RIß en PKA-C, maar ook een aantal mitochondriale eiwitten. Enkelen hiervan hebben ook een rol in apoptose. Verdere analyse van de SPHKAP sequentie bracht nog een link naar apoptose naar voren. SPHKAP bevat een geconserveerd BH3 domein en kwalificeert SPHKAP bij de BH3-only eiwitten die allen apoptose mediëren. Samenvattend suggereren deze vindingen dat mitochondriaal SPHKAP een rol speelt bij apoptose.

Dit proefschrift laat zien dat de toepassing van massaspectrometrie om fundamentele biologische vraagstukken te beantwoorden zeer krachtig kan zijn. Zowel in hoofdstuk 3, 4 als 5 bracht dit nieuwe, onverwachte vindingen naar voren.

Acknowledgements

During 6 years of my stay at Heck's lab at Utrecht University to obtain an MSc and a PhD, I have received constant support and enormous contributions from a large number of people. This thesis would not have been possible without all the support and encouragement. I like to end this thesis acknowledging all the people, colleagues, and friends. Hopefully, I did not leave out any name…

First and foremost, I would like to acknowledge and thank my promoter and supervisor, Albert for so many opportunities that I have received from you. Starting in 2007, you gave me the first opportunity to participate in a proteomics project with Natasja for 9 months. During my first internship, I was shy to speak English and did not talk much. You were trying to encourage me to talk more. You proposed that I could talk to you everyday to improve my English. This was a very sweet of you and yes my English has improved! and I am more confident than 6 years ago. During my first internship, you suggested that I worked with Poupak for my second internship. It was not common for my master's programme to do two internships in one research group. However, with your support, I continued with the second project in the field of chemical proteomics and got a chance to spend few months with our collaboration at NMR group. I then proposed to you that I was very interested in learning more on mass spectrometry and you again gave me another opportunity to write my master thesis in the topic of top-down proteomics with Shabaz. Just before I finished with my master study, you and Arjen were looking for a PhD student to do a chemical proteomics project and this was the start of a real adventure for me. You always come up with great ideas. It has been a real pleasure to work in your laboratory. I thank you for all these.

Arjen, it is difficult to overstate my gratitude to you and I especially would like to thank you for being my supervisor and co-promoter during my PhD. You have encouraged me from my first day to propose what I want to do, to have my own plans and work independently and very importantly, to take some vacations when appropriate. You have been very open minded and welcome new ideas. You have changed my attitude from "I have a problem" to " I have a challenge". You were always there when I had "a challenge" in my project, especially during the thesis-writing period. I remember that you worked until late to correct my first paper as we needed to submit it ASAP. Even for my master's graduation, you were there to give a speech. This was a very sweet of you and and I really appreciated that. You have provided me with ongoing encouragement and with your support, I got a job that I like in Oxford. I want to thank you for believing in my capabilities and giving me the freedom during my PhD study. I have to admit that my thesis couldn't have been possible without your guidance and endless support. I thank you for everything.

I am also in debt to my co-promoter Marcel. You have helped me a lot especially with all your tips and tricks in basic molecular biology. I thank you for the time we spent together in front of the microscope and the time you spent to listen to my concerns and the challenges from my project.

I also have to thank Corine for being so available and helpful to everybody in the lab. You have been helping me with all the paperwork since my very first days in the group. You always have to time to read dutch letters for me and more importantly to fill in my tax form. I thank you for being so kind and helpful.

I would like to acknowledge the following people in Arjen's group. I first thank Pepijn for critical and helpful comments during my study. You have helped me several times (actually every time I asked) to process confocal images, to make figures for publications, to survive in UCSD and many mores. Eleonora, my good friend and my paranymp, for helping me with mass spectrometry and dimethyl labeling. It was fun to spend a day in Milan with you! and thank for your support during my first time rafting. My friend Thin Thin for help and support since I was a master student in pull-down experiments and also outside the lab. I thank you for being very kind and sweet to me. Christian senior for sharing a great dealt of knowledge and tips and tricks to make the experiments work.

Thanks to the mass spec team of the lab. Special thanks for Shabaz and Teck Yew for training me on mass spec. Thanks for helping me to design my experiments and for troubleshooting. Many of you have helped me many times to run my samples: Harm, Mirjam, Vincent Halim, Soenita, Lucrece, Houjiang, Marco, Maarten, Gianluca, Alba, Erik, Christian junior, Nadine, Fabio, Nikolas, Arjan, and Benji.

Thanks to the bioinformatics team of the lab: Bas, Henk for helping me to restore my presentation from the server, Salvo for the review paper, Mao, and Geert for helping me in many occasions on my laptop and my PC. Thanks to Andreas, Renske, and Monique for helping me with native gels. Thanks to Natasja, Poupak, Reinout, and Martina for supervision during my master internship. Adja and Nadia for being so sweet and helpful. It was quiet in the office without you. And still, Onno, Patrick, Sara, Ayse, Natalie, Jess, and Joost.

I also would like to acknowledge colleagues at department of medical physiology, UMCU. First, I thank Bart for being so helpful during my time at UMCU. You have taught me basic techniques in cloning, western blot, cell culture, PCR and many mores. Marien, for helping me with cell culture, Toon and Siddarth for providing rat heart lysate, Marti for stable cell line generation, Teun for cardiomyocytes, Tonni , Shirley, Hiroki, Martin, Magda , previous members of the group, Joost and Leonie, and all lab members that helped me during my stay.

I cannot forget to thank all the people in Taylor's group who mentored me during stay at UCSD. First of all, I would like to thank Susan for accepting me to work in your group. I have learned a lot in your lab. Thank for your very useful and critical comments and also for my farewell lunch. Frank for being so sweet and teaching me almost every experiment for the whole 6 months ! I have learned so much from you. Mira and Manjula for confocal microscope and apoptosis assays, and also for indian lunch and dinner. I really enjoyed spending time with you after work. I thank you for being so nice to me. Kris for mitochondrial prep and RIbeta antibody and also for the ride !, Phil and Eric for all the help and the ride during my stay, Jeff, Ronit, Jon, Mike, Jessica, Grace and all members of Taylor's lab. I really enjoyed my stay there !

สุดท้ายนี้คงต้องขอขอบคุณบรรดาเพื่อนๆ นักเรียนไทยในฮอลแลนด์และในยุโรปที่ให้ความช่วยเหลือและเพิ่มเติมสีสันทำให้ชีวิตการเรียนหกปีในฮอลแลนด์นี้ไม่น่าเบื่อ เริ่มจากท้อปที่ได้รู้จักตั้งแต่ก่อนมา พอมาถึงวันแรกก็มีสารพัดเรื่องไหว้วาน ท้อปก็พึ่งพาได้และดอนน่าก็พึ่งพาท้อปมาตลอดหกปีคงจะบรรยายไม่หมดว่ามีเรื่องอะไรบ้าง เอาเป็นว่าถ้าไม่มีท้อปคงจะแย่เหมือนกัน ขอบคุณมากจริงๆ ขอบคุณยัยอ้นเพื่อนพึ่งพายามยากทางใจ เสียดายที่เจอกันแค่ปีเดียวได้ไปเที่ยวด้วยกันไม่กี่ครั้ง แต่ว่าถึงดอนน่าย้ายไปออกฟอร์ดแล้วก็ยังชวนได้อยู่นะ ขอบคุณพี่จูน สำหรับอาหาร เจ๊มิ้น เจ๊อิ๋ว หาญ ขอบคุณมากสำหรับภาพพรีเวดดิ้ง จ๋า ปัทและเพื่อนๆ นักเรียนไทยคนอื่นๆ และต้องขอบคุณพี่ๆ ที่จบไปแล้ว พี่ฉ่าง พี่โอ้ย กิ๊บ ที่ช่วยเหลือตอนมาถึงฮอลแลนด์ใหม่ๆ

ขอบคุณยัยแป้มนะจ๊ะ ทิปดีซีสนุกมาก ขอบคุณน้องๆ นักเรียนไทยในซานดิเอโก้มากๆๆๆๆๆ ที่ช่วยเหลือ เริ่มจากนอ ขอบคุณมากๆ เลยจ้ะ ช่วยตั้งแต่วันแรกยันวันสุดท้าย ทุกเรื่องทุกเวลา ขอบคุณปอยสำหรับบ้านพัก ขุน โต๊ด ไมค์ น้องคิม และน้องๆ คนอื่นๆ ที่ช่วยสร้างสีสันให้หลังจากเพลียจากการทำแลบที่ไม่มีวันจบสิ้น ขอบคุณเพื่อนๆ พสวท สำหรับมิตรภาพอันยาวนาน อิ๋ว เปิ้ล ฝน เทป อันนี้ต้องขอบคุณเป็นพิเศษเพราะช่วยเหลือกันมาตั้งแต่เริ่มสมัครเรียนทริปแอลเอสนุกมาก ขอบคุณเพื่อนๆ จุฬา ยศเวทกับยัยเต้ย ขอบคุณน้องๆ จุฬา โอ๊ค ย้วย เจี๊ยบ ขอบคุณจ้ะที่พาไปดูนกพัฟฟิน กริช พี่ ๆ เพื่อน ๆ ทุนสกอ พี่ปิง พี่หยู อาร์ต เพื่อนๆ โรงเรียนเซนต์ปอล ขอบคุณเพื่อนนักเรียนไทยในยุโรปที่ไปท่องเที่ยวด้วยกัน ดอนน่าจึงไม่ต้องไปคนเดียว โอ๊ค กิ่งแก้ว พี่เอ๋ เจ๊ดิว

ขอบคุณน้องไนท์สถามฑูตที่ช่วยติดต่อประสานงานกันกพ ขอบคุณพี่เพ้งที่มาช่วยถ่ายรูปแต่งงานและทำเลย์เอาท์ทีสิซเล่มนี้ (ราคามิตรภาพ สนใจติดต่อได้ค่ะ) ท้ายที่สุดขอขอบคุณครอบครัวและพี่ตั๋งที่ช่วยเหลือช่วงหกปีที่อยู่ในฮอลแลนด์ ช่วยเหลือในทุกๆ ด้านทำให้จบจนได้ในที่สุด ถ้าลืมกล่าวถึงใครไปคงต้อขอโทษด้วย u know I love you xoxo

DONNA

Curriculum Vitae

About the author

The author was born on 26th June, 1982 in Chonburi province, Thailand. She was funded during her Bachelor study by a Royal Thai government under the project of Development and Promotion of Science and Technology Talents (DPST). She received her Bachelor's degree in Botany in 2004 from the Faculty of Science, Chulalongkorn University, Thailand. Then, supported by a Higher Educational Strategic Scholarship for Frontier Research Network (SFR) grant, she studied Master's degree in Biomolecular Sciences at Utrecht University, The Netherlands.

After receiving the degree in 2008, she continued in Prof. Dr. Albert Heck's lab as a PhD student under supervision of Dr. Arjen Scholten. Her PhD project involved functional characterization of the novel cAMP signaling component, sphingosine-kinase interacting protein (SPHKAP, SKIP). As a part of her PhD project, she spent 6 months at Prof. Dr. Susan Taylor's lab at UCSD for the training in confocal microscopy and mitochondrial studies.

After her PhD, she will be joining Prof. Dr. Manuela Zaccolo's lab as a post-doctoral researcher, focusing on cyclic nucleotide signalling in the heart at Oxford University, UK. Subsequently, she will return to Thailand to take up a position as a lecturer at Institute of Molecular Biosciences, Mahidol University.

Contact address in UK:

Department of Physiology, Anatomy and Genetics

Le Gros Clark Building, South Parks Road, Oxford OX1 3QX

Tel: +441865272169

Fax: +441865272420

Contact address in Thailand:

Institute of Molecular Biosciences, Mahidol University

25/25 Phuttamonthon 4 Road, Salaya, Nakhon Pathom, Thailand, 73170

Tel: +6624419003

Fax. +6624411013

kovanich@hotmail.com